The Dissertation Committee for Chao Wang Certifies that this is the approved version of the following dissertation:

Mass Transfer Coefficients and Effective Area of Packing

Committee:

Gary Rochelle, Supervisor

Frank Seibert, Co-Supervisor

Roger Bonnecaze

Jennifer Maynard

Bruce Eldridge

Richard Corsi

Mass Transfer Coefficients and Effective Area of Packing

by

Chao Wang, M.S. CH.E.

Dissertation

Presented to the Faculty of the Graduate School of

The University of Texas at Austin

in Partial Fulfillment

of the Requirements

for the Degree of

Doctor of Philosophy

The University of Texas at Austin

March 2015

Dedication

To my family

Acknowledgements

Firstly I would like to acknowledge my advisors, Dr. Gary Rochelle and Dr. Frank Seibert. Dr. Rochelle is one of the greatest professors I have met. His broad knowledge and enthusiasm for teaching always inspires me in my academic career. Dr. Rochelle is always willing to help his students, making time to meet with each student every week. I would also like to thank him for his tremendous help in my search for post-graduate careers. Dr. Seibert has been both a friend and teacher for me. As an expert in separations and mass transfer, he offered lots of help and advice to me on experiments, data analysis, and model development. I also appreciate his arrangement of project time at Separations Research Program (SRP), so I could get access to my experiments. I am so lucky to have my two advisors; I truly learned a lot from them.

I want to thank all my committee members, Dr. Bruce Eldridge, Dr. Jennifer Maynard, Dr. Roger Bonnecaze, and Dr. Richard Corsi, for their valuable time and insightful inputs to my research work.

For the financial support of my research, I would like to thank the Texas Carbon Management Program, Process Science and Technology Center, Separations Research Program, and all sponsors participating these programs. Sulzer Chemtech, Raschig, GTC Technology deserve special recognition for providing the packings that were used in this work.

I want to express my special thanks to our assistant Maeve Cooney, who spent tremendous time and efforts on editing my quarterly reports and papers, arranging my appointments with Dr. Rochelle, and taking care of my tuition payments.

I would also like to acknowledge former Rochelle group student, Dr. Robert E Tsai, who offered great help and experimental training when I first came to the group. I continuously get help from him and keep learning from him in the area of packing characterization. I want to thank all members of the Rochelle group, Xi Chen, Qing Xu, Peter Frailie, Alex Voice, Stephanie Freeman, Fred Closmann, Di Song, Yue Zhang, June Ding, Jorge Plaza, Steven Folk, Lynn Li, Brent Sherman, Darshan Sachde, Yu-Jeng Lin, Thu Nguyen, Nathan Fine, Yang Du, Matt Walters and Omkar Namjoshi. I would also like to thank the staff in the Separations Research Program, Micah Perry, Steve Briggs, and Robert Montgomery.

I am also very grateful to my close friends: Wei Xie, Yuqun Zhang, Yingying Jiang, Yuxuan Chen and many of other friends. I really appreciate the fun moments we spent together in Austin and all the help for me. I wish you all have a bright future.

Most of all, I would like to thank my family, who has always been the greatest support to me. My parents always have the deepest trust in me, and give me the biggest love I could have. I am so blessed to be born in this family. My family will always be the most important thing in my life.

Mass Transfer Coefficients and Effective Area of Packing

Chao Wang, Ph.D.

The University of Texas at Austin, 2015

Supervisor: Gary Rochelle

Co-Supervisor: Frank Seibert

The effective mass transfer area (a_e), liquid film mass transfer coefficient (k_L), and gas film mass transfer coefficient (k_G) of eleven structured packings and three random packings were measured consistently in a 0.428 m packed column. Absorption of CO_2 with 0.1 gmol/L NaOH with 3.05 m packing was used to measure a_e, while air stripping of toluene from water with 1.83 m packing was used to measure k_L, and absorption of SO_2 with 0.1 gmol/L NaOH with 0.51 m packing was used to measure k_G. The experiments were conducted with liquid load changing from 2.5 to 75 $m^3/(m^2*h)$ and gas flow rate from 0.6 to 2.3 m/s. Packings with surface area from 125 to 500 m^2/m^3 and corrugation angle from 45 to 70 degree were tested to explore the effect of packing geometries on mass transfer.

The effective area increases with packing surface area and liquid flow rate, and is independent of gas velocity. The packing corrugation angle has an insignificant effect on mass transfer area. The ratio of effective area to surface area decreases as surface area increases due to the limit of packing wettability. A correlation has been developed to predict the mass transfer area with an average deviation of 11%.

$$\frac{a_e}{a_P} = 1.41[(\frac{\rho_L}{\sigma})g^{1/3}(\frac{u_L}{a_P})^{4/3}]^{0.116}$$

The liquid film mass transfer coefficient is only a function of liquid velocity while the gas film mass transfer coefficient is only a function of gas velocity. Both k_L and k_G increase with packing surface area, and decrease with corrugation angle. A new concept, Mixing Point Density, was introduced to account for the packing geometry effect on k_L and k_G. Mixing points are the joint points of packing corrugated sheets where liquid and gas flows mix with each other, change directions, and create turbulence. The mixing point density can be calculated by either packing characteristic length or by surface area and corrugation angle:

$$M = \frac{6}{B * h * B \tan\theta}$$

$$M' = \frac{3 * a_P^3 \sin\theta\cos\theta}{16(\sin^2\theta + 1)^{3/2}}$$

The dimensionless k_L and k_G models can then be developed based on the effects of liquid/gas velocity, mixing point density, packing surface area:

$$Sh_L = 1.79 * \mathrm{Re}_L^{0.74} Mi^{0.42} Sc_L^{0.5},\ k_L = Sh_L a_P D_L$$

$$Sh_G = 0.83 * \mathrm{Re}_G^{0.58} Mi^{0.3} Sc_G^{0.5},\ k_G = Sh_G a_P D_G$$

An economic analysis of the absorber was conducted for a 250 MW coal-fired power plant. The optimum operating condition is between 50 to 80 % of flooding, and the optimum design is to use packing with 200 to 250 m^2/m^3 surface area and high corrugation angle (60 to 70 degree). The minimum total cost ranges from \$4.04 to \$5.83 per tonne CO_2 removed with 8 m PZ.

Table of Contents

List of Tables

List of Figures

Chapter 1: Introduction

1.1 Global warming and CO_2 Capture

Greenhouse gas (GHG) emissions due to human activities are believed to be the major cause of global warming. CO_2 is the most important anthropogenic GHG. There are three major systems for CO_2 capture: pre-combustion, oxy-combustion and post-combustion.

Pre-combustion capture refers to removing CO_2 from fossil fuels before combustion is completed. A widely used approach for pre-combustion is the Integrated Gas Combined Cycle (IGCC). Currently, pre-combustion can only be applied to new power plants and lack of short-term flexibility, and construction cost is relatively high.

Oxy-fuel combustion uses oxygen instead of air, thus eliminating nitrogen from the oxidant gas stream and producing a CO_2-enriched flue gas. This flue gas is ready for sequestration after water has been condensed and other impurities have been separated out. However, a significant cost is to separate O_2 from air and recycle the flue gas. To dramatically reduce the cost of oxy-combustion, more efficient technologies for oxygen production need to be developed.

Post-combustion technology captures CO_2 directly from flue gas emitted from power plants. It can be readily retro-fitted to the existing power plants. Therefore post-combustion provides the greatest near-term potential to reduce CO_2 emission, especially those from coal-fired power plants. In particular, post-combustion CO_2 capture with amines is the most mature and readily employable technology.

Figure 1.1 shows CO_2 capture by amine scrubbing. Flue gas from power plant usually has a temperature above 100 ℃ and is cooled down to about 40 ℃ at the direct contact cooler (DCC). Then the flue gas stream is fed to the bottom of the absorber, where it is brought into counter-current contact with lean amine solvent flowing down from the top. Most of CO_2 in the gas stream is picked up by amine with exothermic chemical reactions. The mass transfer in the absorber is controlled by the chemical reaction. Before the gas stream exits the top of the absorber, it goes through a water wash unit to reduce loss of volatile amine components. At the water wash and the DCC, the mass transfer is controlled by gas film diffusion. The rich amine solution exits the bottom and is heated by a heat exchanger. As it goes to the stripper, the temperature is further elevated by heat from the reboiler. As a result, the amine-CO_2 reaction is reversed. In the stripper, the temperature is usually 100 to 150 ℃, and the mass transfer is liquid film controlled. The released CO_2 is then collected from the top

of the stripper and compressed for transportation and sequestration; the lean amine solvent is cooled by the heat exchanger and pumped back to the absorber for next cycle of CO_2 absorption. Since the mass transfer in different parts of the process is controlled by different mechanisms, a comprehensive understanding of the mass transfer coefficients and the effective area is important. As the focus of this work, the mass transfer in the process will be further discussed in Section 1.3.

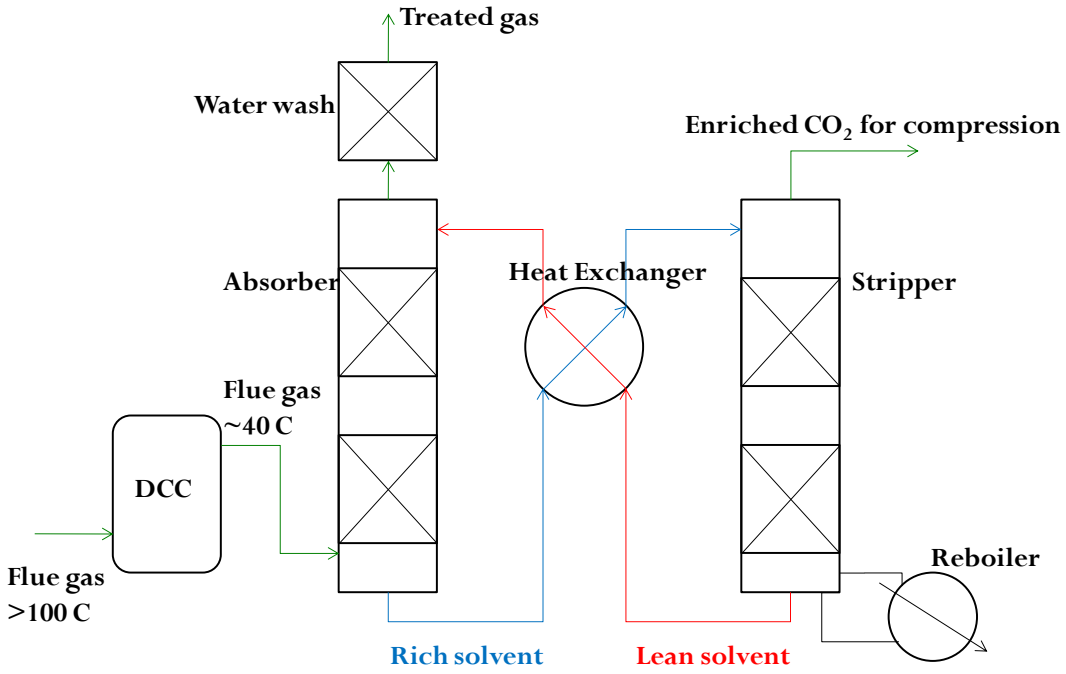

Figure 1.1. Process flow diagram for a CO_2 absorption/stripping process

1.2 Packing applied in Post Combustion CO_2 Capture

Packing is widely used in distillation, stripping, and scrubbing processes because of its relatively low pressure drop, good mass transfer efficiency, and ease of installation. As a result, packing is being investigated for the post-combustion carbon capture process. In most cases, the absorber, stripper and water wash section are filled with packing.

Packing can be made of stainless steel, plastic (PP, PVC etc.), or ceramics. In the post combustion CO_2 capture, stainless steel packing is widely used considering the operating temperature, corrosion and the costs. Thus, in this paper, studies are focused on stainless steel packing.

Packing is classified as random or structured. Random packing consists of uniquely shaped fragments, with nominal sizes ranging from 3 to 75 mm, which are randomly dumped into a column. Random packing has the advantage of low price and high mechanical strength. Structured packing consists of corrugated sheets and is manufactured in modular form to permit stacking in an ordered array. Structured

packing is generally more expensive and requires good initial liquid distribution, but also offers lower pressure drop and more efficient mass transfer.

Random and structured packings have their own advantages and disadvantages which make them favorable for different situations. Research continues to focus on development of high performance packing, especially on minimizing pressure drop, maximizing mass transfer efficiency and minimizing costs.

1.3 Mass Transfer in Packed Columns

Mass transfer in CO_2 absorption by amines can be described by Figure 1.2 (Cullinane, 2005). CO_2 transfers from the bulk gas phase to the bulk liquid phase through three films: the gas film, the reaction film, and the diffusion (liquid) film. The total mass transfer resistance is the sum of the resistances from these three films, represented by the following equation:

$$\frac{1}{K_{OG}} = \frac{1}{k_G} + \frac{H_{CO2}}{\sqrt{k_2[Am]D_{CO2}}} + \frac{1}{k_L}\left(\frac{\Delta C_{CO2,G}}{\Delta C_{CO2,L}}\right) \qquad (1.31)$$

Where k_G and k_L are the gas and liquid film mass transfer coefficients. $\sqrt{k_2[Am]D_{CO2}} / H_{CO2}$, also referred to as k_g', is the reaction film mass transfer coefficient.

Thus, in the CO_2 absorption column, mass transfer performance can be characterized in terms of two parameters: the mass transfer coefficients (k_G, k_L, k_g') and the gas-liquid mass transfer area (a_e). In the amine scrubbing CO_2 capture process, k_G is the dominant mass transfer coefficient in the DCC and water wash; k_g' and k_L are the dominant mass transfer coefficients for the absorber and stripper respectively; and a_e is important for all parts. The scope of this work will be focused on measurements and modeling of k_G, k_L, and a_e.

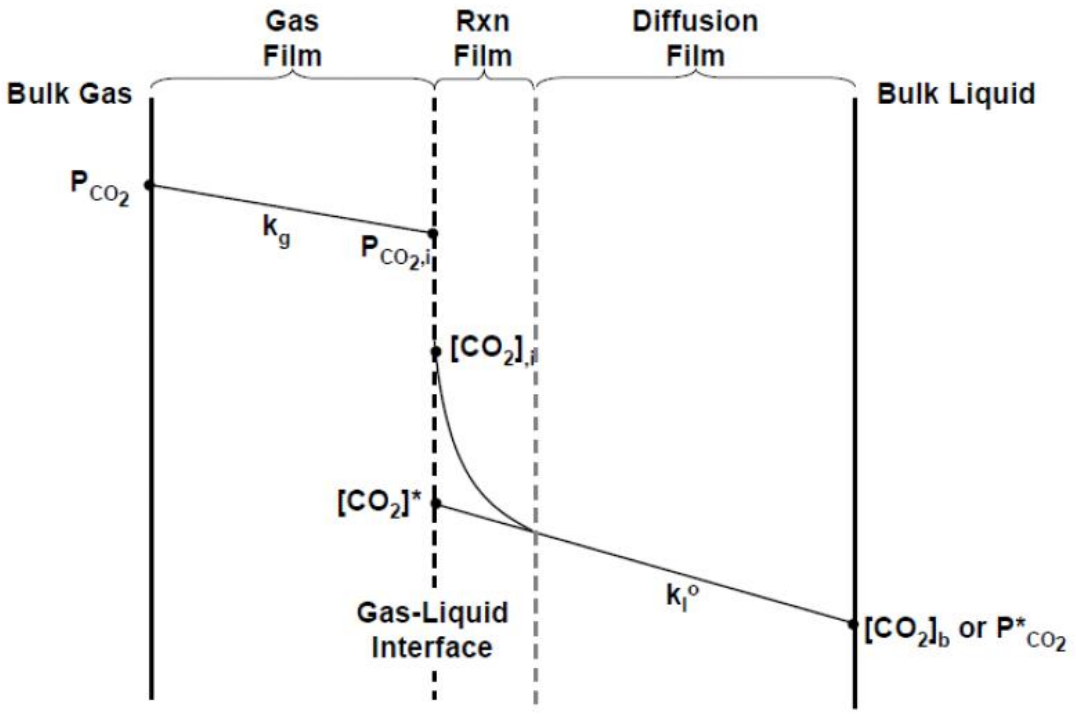

Figure 1.2. Mass transfer of CO_2 into bulk liquid with fast chemical reaction.

1.4 Previous work

Numerous mass transfer models for packings have been developed and proposed in the literature. Onda (1968) developed the first and still widely used mass transfer area models based on database from the absorption of CO_2 by NaOH. However, the packings measured were mostly random packings. Rocha et al. (1996) developed a model for effective area based on an extensive experimental database, mostly for structured packing. In this model, the gas film mass transfer coefficient is based on earlier investigations of wetted-wall columns while the liquid film is based on the penetration theory. Widely used mass transfer correlations for random packings were developed by Billet and Schultes (1993). The correlations for the gas and liquid mass-transfer coefficients were developed from the original formulation of Higbie (1935). Detailed features of various mass transfer correlations will be discussed in Chapter 2.

In general, these previous mass transfer models have a common ground. The combination of mass transfer coefficient and area (Ka) was measured. However, to separate K and a, either a theoretical assumption of area or proposed K models from other work were used. In other words, none of the mass transfer values (k_G, k_L, a_e) were independently validated. In distillation systems, most cases only required the combination (Ka) values, where these models were acceptable. However, the design and optimization of different parts of the amine scrubbing CO_2 capture system needs

to know validated separate values of k_G, k_L, and a_e. Therefore, a consistent measurement of k_G, k_L, a_e at the same condition is required.

1.4 Research Objectives and Scope

The primary goal of this work is to develop models for effective area (a_e) and gas and liquid film mass transfer coefficients (k_G and k_L) based on consistent measurements. All the experiments were made in a pilot-scale column in the Separations Research Program (SRP) at the University of Texas at Austin. By applying a direct methodology to obtain the area and the mass transfer coefficients, the shortcoming of the previous discussed models are addressed. The general objectives are to:

- Determine suitable systems to measure a_e, k_G and k_L consistently. Measure k_G and k_L directly.
- Explore influence of gas and liquid flow rate on a_e, k_G and k_L. Characterize the exponent of gas and liquid flow rate on a_e, k_G and k_L.
- Explore the influence of packing geometry, such as the effect of corrugation angle and packing surface area on hydraulic and mass transfer properties.
- Combine experimental data and theory into a_e, k_G and k_L models for structured packings.
- Conduct an economic optimization for the absorber based on mass transfer models from this work. Determine the optimal absorber size, packing type and operating conditions to achieve the lowest total costs.

Chapter 2: Literature Review

2.1 Effective Area Measurements and Models

2.1.1 Methods of measuring Effective Area

There are several methods for measuring the effective area of packing. Danckwerts (1967, 1970) provides the most widely used method for CO_2-amine systems. This method is based on systems where mass transfer is controlled by a fast chemical reaction in the liquid phase. Thus, the overall mass transfer coefficient is independent of the gas and liquid phase hydrodynamics, and it is determined by the chemical reaction. It can be calculated using the equation:

$$k_r = (r_I D)^{0.5} \tag{2-1}$$

Where

k_r is the mass transfer coefficient in case of absorption, controlled by a first or pseudo-first order fast chemical reaction, (m/s);

r_I is the rate constant of the reaction, (1/s);

D is the diffusivity of the absorbed component (CO_2) in the liquid phase, (m^2/s).

The conditions that determine if the rate of the absorption is independent from the hydrodynamics of the gas and of the liquid phase are given by the equations:

$$k_r >> k_L \tag{2-2}$$

and

$$k_r << mk_G \tag{2-3}$$

Where

k_L is the liquid side controlled mass transfer coefficient, (1/s);

k_G is gas side controlled mass transfer coefficient, (1/s);

m is the slope of the equilibrium line.

CO_2 absorption by amines is a fast reaction in the liquid phase. The system fulfills conditions (2-2) and (2-3) so the Danckwerts method can be used to measure the effective area. Variants of the Danckwerts method use different types of chemical reactions such as the absorption of CO_2 from air into NaOH solution, a commonly studied test system. It has the advantage of low cost and ease of operation, low toxicity and volatility compared with amine systems. An additional advantage is that

this method has been used to compare areas of different packings (Perry, 1999). Because of these advantages and ease of operation by this method, previous SRP researchers (Wilson, 2004; Tsai 2008) applied this method to measure gas-liquid contact area. In this work, absorption of atmospheric CO_2 with 0.1 gmol/L NaOH solution was used to measure effective area of packings.

2.1.2 Previous Effective Area Models

2.1.2.1 Onda et al.

The correlation of Onda and co-workers (Onda et al., 1968) is recognized as the first powerful, most-accepted predictive equation for the effective interfacial area of random packing. The system used was absorption of CO_2 with aqueous NaOH, which is a pseudo first-order reaction. The effective area was calculated:

$$a = \frac{k_L^o a}{\sqrt{k_r C_B D_L}} \tag{2-4}$$

Where

k_L^0 is the liquid-phase coefficient for chemical absorption, (m/hr);

k_r is the reaction rate constant for second-order reaction, (m^3/kg-mole*hr);

C_B is the average concentration of the reactant, (kg-moles/m^3).

The model accounts for the effects of hydrodynamics and liquid physical properties on the wetted surface area of random packing. An empirical relation was developed from the results:

$$\frac{a_e}{a_P} = 1 - \exp[-1.45(\frac{\sigma_C}{\sigma_L})^{0.75} \mathrm{Re}_L^{0.1} Fr_L^{-0.05} We_L^{0.2}] \tag{2-5}$$

Where

Re_L, Fr_L, and We_L are the liquid phase Reynolds number, Froude number, and Weber number;

σ_C is the critical surface tension, (N/m);

σ_L is the liquid phase surface tension, (N/m).

However, this correlation was developed mainly based on random packing with nominal size of 12.5 and 15 mm, which had a relatively large surface area. For packing with smaller surface area, this correlation would under predict the effective area. It should also be noted that, based on the data of Raschig Rings, Berl Saddle, spheres and rod packing, and ceramic Pall Rings, this model is not applicable to new-type random packings. This model predicts that the maximum wetted area is a_p.

Data from Tsai and Wilson frequently give values of wetted area greater thatn a_p with random packing.

2.1.2.2 Billet and Schultes

Billet and Schultes (1993) analyzed the mass transfer results from a large data bank including 31 different systems and 67 different types and sizes of packings. A dimensionless analysis of the influencing parameters on effective area was performed. The fractional effective area correlation was given by Equation (2-6a) and (2-6b):

$$\frac{a_e}{a_P} = 1.5(a_P d_h)^{-0.5}\left(\frac{u_L d_h}{\nu_L}\right)^{-0.2}\left(\frac{u_L^2 \rho_L d_h}{\sigma}\right)^{0.75}\left(\frac{u_L^2}{g d_h}\right)^{-0.45} \quad (2\text{-}6a)$$

$$\frac{a_e}{a_P} = 1.5(a_P d_h)^{-0.5}\,\mathrm{Re}_L^{-0.2}\,We_L^{0.75}Fr_L^{-0.45} \quad (2\text{-}6b)$$

Where d_h is the hydraulic diameter and can be expressed by Equation (2-7):

$$d_h = 4\frac{\varepsilon}{a_P} \quad (2\text{-}7)$$

This correlation, the general form originating from a dimensional analysis of the influencing parameters, reflected well the results of the experiments if the surface tension increases from top to bottom. When applied to negative systems, the Marangoni effect, a phenomenon involving the flow of liquid away from regions of low surface tension, would need to be considered. The authors then multiplied a correction factor to account for this effect:

$$\left(\frac{a_e}{a_P}\right)_{negative} = \left(\frac{a_e}{a_P}\right)_{Eq(2-5)}\left(1 - 2.4\times10^{-4}\left|Ma_L\right|^{0.5}\right) \quad (2\text{-}8)$$

Where Ma_L is the Marangoni number and can be expressed by:

$$Ma_L = \frac{d\sigma_L}{dx}\frac{\Delta x}{D_L \mu_L a_P} \quad (2\text{-}9)$$

Where x is the mole fraction of the more volatile component in the liquid phase.

2.1.2.3 Rocha-Bravo-Fair model

The first overall investigation for structured packing was conducted by Bravo et al (1982) based on data from a commercial-scale packed distillation column. The effective interfacial area correlation was obtained by correlating the extensive experimental data bank included in paper by Bolles and Fair (Bolles et al., 1979)

which involved a wide range of packings, column size, and systems. This model was called the Bravo-Rocha-Fair (BRF) model. In this model, gas phase mass transfer coefficient (k_G) was based on earlier investigation of wetted wall column results, where Sherwood (1975) concluded that the relationship of Johnstone and Pigford (1942) should be used for the gas side coefficient:

$$\frac{k_G d_{eq}}{D_G} = 0.0328[\frac{d_{eq}\rho_G(u_{G,eff} + u_{L,eff})}{\mu_G}]^{0.77}(\frac{\mu_G}{\rho_G D_G})^{0.33} \quad (2\text{-}10)$$

The liquid phase mass transfer coefficient (k_L) was based on penetration theory, as first expounded by Higbie (1935):

$$k_L = 2\sqrt{\frac{D_L u_{L,eff}}{\pi S}} \quad (2\text{-}11)$$

Therefore, the effective area can then be separated from ka values:

$$\frac{a_e}{a_P} = 0.498(\frac{\sigma^{0.5}}{Z^{0.4}})(Ca_L\ \mathrm{Re}_G)^{0.392} \quad (2\text{-}12)$$

Where

Z is the height of the packed bed, (m);

σ is surface tension, (dyn/cm);

Ca_L and Re_G are dimensionless liquid capillary number and gas Reynolds number.

Compared with previous correlations, the BRF model introduced the concept "effective" gas and liquid velocities to account for the interaction between the two phases.

Rocha et al. (1993, 1996) updated the BRF model with some new results. In the k_G model, the experimental constant and the exponent were slightly changed. In the k_L model, a correction factor (C_E) was introduced to account for regions in packed bed not conducive to rapid surface renewal. The updated correlations were recognized as the Rocha-Bravo-Fair (RBF) model:

$$\frac{k_G S}{D_G} = 0.054[\frac{\rho_G S(u_{Ge} + u_{Le})}{\mu_G}]^{0.8}(\frac{\mu_G}{D_G\rho_G})^{0.33} \quad (2\text{-}13)$$

$$k_L = 2\sqrt{\frac{D_L C_E u_{Le}}{\pi S}} \quad (2\text{-}14)$$

The effective area correlation for the RBF model was based on area model of Shi and Mersmann (1985) by introducing a factor F_{SE} to account for packing variations in surface texture:

$$\frac{a_e}{a_P} = F_{SE}\frac{29.12u_L^{0.4}\nu_L^{0.2}S^{0.359}}{(1-0.93\cos\gamma)(\sin\alpha)^{0.3}\varepsilon^{0.6}}(\frac{\rho_L}{\sigma g})^{0.15} \quad (2\text{-}15)$$

Where cosγ was the contact angle and can be calculated by (2-16a) and (2-16b):

$$\cos\gamma = 5.211\times10^{-16.835\sigma}, \quad \sigma > 55mN/m \quad (2\text{-}16a)$$

$$\cos\gamma = 0.9, \quad \sigma < 55mN/m \quad (2\text{-}16b)$$

Both models utilized correlations or assumptions from others work either for the area model or for the $k_{G/L}$ model. Therefore, the area model and k model should be used together to get the ka values instead of using them separately.

2.1.2.4 Tsai model

Tsai et al. (2010) measured the mass transfer contact areas of nine structured packings using the absorption of CO_2 from air into 0.1 gmol/L NaOH. The mass transfer was controlled by the chemical reaction in the liquid phase. The overall mass transfer coefficient K_{OG} can be assumed as the liquid phase mass transfer coefficient with chemical reactions (k_g'). It can be calculated by (2-16):

$$k_g^{'} = \frac{\sqrt{k_{OH^-}[OH^-]D_{CO2,L}}}{H_{CO2}} \quad (2\text{-}17)$$

Therefore, Tsai was able to separate k and a to obtain the effective area.

A global mass transfer contact area model (2-18) was developed as a function of the liquid Weber and Froude numbers. According to Tsai, the contact area is a function of liquid flow rate, surface tension, liquid density, structured packing geometry and is not a function of gas flow rate and liquid viscosity. The model satisfactorily represented the entire database (±13%).

$$\frac{a_e}{a_P} = 1.34[(\frac{\rho_L}{\sigma})g^{1/3}(\frac{Q}{L_P})^{4/3}]^{0.116} \quad (2\text{-}18)$$

Where L_P is the wetted parameter specified in terms of packing geometry:

$$L_P = \frac{4S}{Bh}A \quad (2\text{-}19)$$

2.1.2.5 Delft

Another important correlation to predict packing effective area was proposed by Olujic (1999) called the Delft model (2-20). In this model, the effective area was

correlated as a function of liquid velocity and packing perforation factor (Ω), which represents the ratio of packing surface area occupied by the holes to the total surface area.

$$\frac{a_e}{a_P} = \frac{1-\Omega}{1+A/u_{Ls}^B} \tag{2-20}$$

Where A and B are the packing type and size dependent constants.

2.2 Gas Film Mass Transfer Coefficient Measurements and Models

2.2.1 Methods of measuring gas film mass transfer coefficient

Mehta and Sharma (1966) measured the volumetric gas side coefficient $k_G a$ and the contact area a_e separately. They determined the true gas-side film coefficient k_G from the overall coefficient $k_G a$ and area. The systems chosen were such that the liquid side resistance was absent and that the gas-side resistance controlled the mass transfer rate. The systems were sulfur dioxide, chlorine, Freon-22 (monochlorodifluorominethane), or Freon-114 (dichlorotetrafluoroethane)) absorbed by aqueous sodium hydroxide solutions (2 gmol/L NaOH). Another potential system was ammonia or triethylamine in different carrier gases absorbed by dilute sulfuric acid (1 to 2 gmol/L H_2SO_4).

The $k_G a$ was calculated by the equation

$$k_G a = \frac{u_G \ln(\frac{y_{in}}{y_{out}})}{ZRT} \tag{2-21}$$

Where

u_G = gas superficial velocity, (m/s);

y_{in}, y_{out} = inlet and outlet gas mole fraction of the transferring solute;

R= gas constant, 8.314 J/(K*mole);

T = absolute temperature, (K);

Z = packed height, (m).

Yaici and Laurent (1988) used the method of absorption of dilute SO_2 into NaOH and into an organic medium (N, N-dimethylaniline) to determine the value of $k_G a$. For an irreversible, instantaneous chemical reaction at a surface the rate which is controlled by the gas phase resistance, the absorptive flux per unit reactor volume can be written as follows:

$$\phi = k_G a * P \tag{2-22}$$

Then the volumetric gas film mass transfer coefficient can be calculated:

$$k_G a = \frac{G_m}{PZ} \ln \frac{P_{in}}{P_{out}} \qquad (2\text{-}23)$$

Where

G_m is the gas flow rate, (kg/s);

P_{in} and P_{out} are the partial pressures of the gaseous solute at the inlet and the outlet, (Pa);

Z is the reactor of a packed height, (m).

Moucha and Linek (2005) measured the $k_G a$ for new types of Intalox metal saddles (IMTP) 25, 40 and 50. The volumetric gas phase mass transfer coefficient, $k_G a$, was determined by absorption of dilute SO_2 (0.02 vol% in air) into 1 M NaOH aqueous solution. The height of the measuring section was 0.5 m. Experiments were performed at liquid flow rates from 3 to 100 $m^3/(m^2h)$. The temperature of the liquid and gas phases was kept at 20 ± 1C in all experiments.

Considering all the methods and systems used for measuring gas phase mass transfer coefficient, sulfur dioxide absorbed in aqueous sodium hydroxide solutions was chosen as our test system. The advantage of this system is that the reaction between SO_2 and NaOH is an instantaneous reaction so the liquid side mass transfer resistance can be neglected. The gas side mass transfer coefficient $k_G a$, which equals the overall mass transfer $K_{OG}a$ coefficient at this condition, can be measured directly. Since the effective area a_e was already measured from the previous experiment, k_G can be obtained by dividing $k_G a$ by a_e. In this method, both the $k_G a$ and a_e were measured directly, so the k_G obtained was validated. Another advantage of this system is that the properties of SO_2 are similar to CO_2 which is used for area measurement, which will keep the measurement consistent.

2.2.2 Previous Gas Film Mass Transfer Coefficient Models

2.2.2.1 Onda et al

Onda (1967) developed k_G model based on his effective area model (Equation 2-5). The packings measured in this work were all random packings (Raschig rings, Berl saddles, Spheres). The correlation is:

$$Sh_G = 5.23 \,\mathrm{Re}_G^{0.7} \, Sc_G^{1/3} (a_P + D_P)^{-2.0} \qquad (2\text{-}24a)$$

Where D_P is the nominal size of packing, m.

For Raschig rings and Berl saddles smaller than 15mm, the constant in Equation (2-23a) was changed from 5.23 to 2.00 to better fit the data (Equation 2-23b).

$$Sh_G = 2.00 \,\mathrm{Re}_G^{0.7} \, Sc_G^{1/3} (a_P + D_P)^{-2.0} \qquad (2\text{-}24b)$$

Onda also measured the rate of vaporization for air-water system under adiabatic conditions to validate the k_G model. Equations (2-24a) and (2-24b) can correlate most of the vaporization data as well. However, Onda's k_G model was mostly based on 1st and 2nd generation random packings. There will be deviations when apply to structured packings and recently developed high performance random packings.

2.2.2.2 Mehta and Sharma

Mehta and Sharma (1966) performed a study of diffusivity effect on the gas film mass transfer coefficient in a liquid continuous or bubble column. The carrier gases were hydrogen, nitrogen, Freon-12 and Freon-114. The solute gases were chlorine, SO_2, ammonia, n-butylamine, di-n-propylamine, triethylamine, methyl ethyl ketone, n-butyl formate and ethyl propionate. By matching different solute gases and different carrier gases, 17 absorption systems and 18 vaporization systems with different diffusivities were tested. The log-log plot of k_Ga against diffusivities of solutes in various carrier gases showed that k_Ga varies as the 0.5 power of the diffusivity. This conclusion is also used in this study when convert k_Ga values measured in SO_2/NaOH system to the targeted CO_2/NaOH system.

Mehta and Sharma also studied the gas flow rate effect and the submergence effect on gas film mass transfer coefficient. It is found that k_Ga varies as 0.75 power of the gas flow rate and 0.33 power of the submergence. The correlation is:

$$k_G a = C * D_G^{0.5} u_G^{0.75} S^{0.33} \qquad (2\text{-}25)$$

Where

C is the experimental constant;

S is the submergence height, (m).

It is recognized this is not a gas continuous packed column, however, it does show the effect of gas diffusivity on the gas film mass transfer coefficients.

2.2.2.3 Billet and Schultes

Billet and Schultes (1993) developed gas film mass transfer coefficient model based on surface renewal theory. The theoretical time interval required for the renewal of the contact area was defined by Equation (2-26):

$$\tau_G = (\varepsilon - h_L) l_\tau \frac{1}{u_G} \qquad (2\text{-}26)$$

Where

ε is the void fraction

h_L is the liquid fractional hold-up

u_G is the gas superficial velocity

l_τ is the length of flow path by Equation (2-27)

$$l_\pi = d_h = 4\frac{\varepsilon}{a_P} \tag{2-27}$$

The theoretical proposed correlations for k_G and k_L:

$$k_G = \frac{2}{\sqrt{\pi}}\sqrt{D_G \frac{u_G}{(\varepsilon - h_L)l_\pi}} \tag{2-28}$$

$$k_L = \frac{2}{\sqrt{\pi}}\sqrt{D_L \frac{u_L}{h_L l_\pi}} \tag{2-29}$$

2.2.2.4 Delft model

The Delft model developed by Olujic (1999) was mainly based on distillation systems. The gas film mass transfer coefficient can be represented as the combination of laminar flow and turbulent flow contributions:

$$k_G = \sqrt{k_{G,lam}^2 + k_{G,turb}^2} \tag{2-30}$$

with

$$k_{G,lam} = \frac{Sh_{G,lam} D_G}{d_{hG}} \tag{2-31a}$$

$$k_{G,turb} = \frac{Sh_{G,turb} D_G}{d_{hG}} \tag{2-31b}$$

The Sherwood number for laminar and turbulent flow can be expressed by:

$$Sh_{G,lam} = 0.664 Sc_G^{1/3}\sqrt{\mathrm{Re}_{Grv}\frac{d_{hG}}{l_{G,pe}}} \tag{2-32}$$

$$Sh_{G,turb} = \frac{\mathrm{Re}_{Grv}\, Sc_G \frac{\zeta_{GL}\varphi}{8}}{1+12.7\sqrt{\frac{\zeta_{GL}\varphi}{8}}(Sc_G^{2/3}-1)}[1+(\frac{d_{hG}}{l_{G,pe}})^{2/3}] \qquad (2\text{-}33)$$

Where:

($d_{hG}/l_{G,pe}$) is the ratio of hydraulic diameter and the length of gas flow channel within a packing element.

Re_{Grv} represents the gas phase Reynolds number based on relative velocity:

$$\mathrm{Re}_{Grv} = \frac{\rho_G(u_{Ge}+u_{Le})d_{hG}}{\mu_G} \qquad (2\text{-}34)$$

ξ_{GL} is the friction factor between liquid and gas:

$$\xi_{GL} = \{-2\log[\frac{(\delta/d_{hG})}{3.7} - \frac{5.02}{\mathrm{Re}_{Grv}}\log(\frac{(\delta/d_{hG})}{3.7}+\frac{14.5}{\mathrm{Re}_{Grv}})]\}^{-2} \qquad (2\text{-}35)$$

2.2.2.5 Rocha-Bravo-Fair model

Rocha et al (1993, 1996) also developed models for gas film mass transfer coefficient based on the distillation and absorption data measured by the Separations Research Program (SRP). The correlation was given by Equation (2-13) and has been explained in Section 2.1.2.3.

2.3 Liquid Film Mass Transfer Coefficient Measurements and Models

2.3.1 Methods of measuring liquid film mass transfer coefficient

Sharma and Danckwerts (Sharma,1970) explored the chemical methods of measuring liquid side mass transfer coefficient. For a first order reaction (2-36), under certain conditions the reaction is fast enough to keep the concentration of A in the bulk of the B phase equal to zero, while it is not fast enough for any appreciable amount of A to react in the diffusion film at the surface of the B phase.

$$A + zB \rightarrow p\,r\,o\,d\,u \qquad (2\text{-}36)$$

Under these conditions, the rate of transfer is that for physical mass transfer:

$$R = k_L C_A^* \qquad (2\text{-}37)$$

The condition to be satisfied if $[A]_B$ is to be zero is:

$$k_L a << V_B k_2 [B]^0 \qquad (2\text{-}38)$$

Where

$[A]_B$ is the bulk concentration of A in the B phase, (gmol/L);

C_A^* is the concentration of A at surface, (gmol/L);

$[B]^0$ is the concentration of B in the bulk phase, (gmol/L);

V_B is the volume of B phase per unit volume of the system, (m^3/m^3).

The condition to be satisfied if no A is to react in the diffusion film is:

$$D_{AB} k_2 [B]^0 / k_L^2 << 1 \qquad (2\text{-}39)$$

Where D_{AB} is the diffusivity of A in the B phase.

Sharma and Danckwerts also suggest possible experimental test systems to validate this theory. The gas-liquid system could be the absorption of CO_2 into a carbonate-bicarbonate buffer solution. The reaction is second order. Another system could be oxygen absorbed from air into dilute acid solutions of CuCl, which is oxidized to $CuCl^{2-}$. Oxygen may be also absorbed from air into sodium sulphite solution, using $CoSO_4$ or $CuSO_4$ as a catalyst. The reaction appears to be second order in O_2 and zero order in SO_3^{2-} under usual conditions. In all the above cases it is necessary to ensure that conditions (2-38) and (2-39) apply.

Although the chemical method of measuring the liquid film mass transfer coefficient is valid and has some advantages, it is more suitable for small scale experiments. For larger scale device, it is hard to keep conditions (2-38) and (2-39) valid at all the time.

Onda (1959) investigated the physical absorption of gas by water in a tower packed with Raschig ring. The liquid film mass transfer coefficient was separated by dividing the capacity coefficient by the wetted surface area. Fundamental equations to calculated k_L using dimensionless numbers were discussed from the standpoints of two-film theory and penetration theory. The purity of the gas used (CO_2 or H_2) was more than 99%. Tap water was introduced from the head tank into the tower through the thermostat. The liquid film mass transfer coefficient can be computed from:

$$k_L a = \{L/(\rho Z)\}\{\ln(C_S - C_1)/(C_S - C_2)\} \qquad (2\text{-}40)$$

Where

L is the mass flow rate of liquid, (kg/m^2*hr);

ρ is the density of liquid, (kg/m^3);

Z is the height of packing, (m);

C_1, C_2, and C_S are the concentration of liquid at the entrance, at the exit of the tower, and at the saturation, respectively, (kg/m^3).

To derive k_L from k_La, Onda assumed that the effective area a_e equals the wetted area a_w and used a formula developed by Fujita (1954).

Akita (1973) measured the volumetric liquid phase mass transfer coefficient k_La in gas bubble columns with various systems using the physical method. The systems used for k_La were water-oxygen, glycerol solution-oxygen, glycol solution-oxygen, methanol-oxygen and 0.15 M Na_2SO_3 solution-air. The column was operated continuously with respect to the gas flow. Values of the volumetric coefficient for liquid phase mass transfer k_La with respect to the unit volume of aerated liquid were obtained from experiments of oxygen absorption into various liquids. Oxygen from a cylinder was supplied to the gas chamber at the column bottom through a surge tank. Before an absorption experiment, oxygen was stripped from the liquid in the column by sparging nitrogen for 5-10 min at a superficial gas velocity of about 100 meters per hour. The concentration of dissolved oxygen in the liquid sample was analyzed chemically by the Winkler method. Since the gas phase resistance for mass transfer was negligible, the values of k_La for the batch experiments on the physical absorption of oxygen were obtained by the following relationship:

$$k_L a = \frac{1-\varepsilon_G}{t} \ln \frac{C^* - C_i}{C^* - C_f} \tag{2-41}$$

Where

t is the absorption time, (s);

C^* is the dissolved oxygen concentration at saturation, (gmol/L);

C_i, C_f is the initial and final concentrations of dissolved oxygen in liquid, respectively, (gmol/L).

In the experiment, C^* was determined by sparing pure oxygen through the liquid in the column for a sufficient length of time, in case published data were not available.

Linek (1984) measured the liquid side volumetric mass transfer coefficient k_La for Pall rings of nominal sizes 15, 25, 35 and 50 mm made of polypropylene and polyvinylidenflouride. The k_La values were obtained by physical desorption of oxygen from water into pure nitrogen stream. The column was packed to the height of one m. The set-up permitted the measurement of either the absorption of atmospheric oxygen into oxygen-free water or the desorption of oxygen dissolved in water into a pure nitrogen stream. The majority of their experiments were performed in the counter-current desorption mode. Nitrogen was led into the column at constant superficial velocity of 0.0253 m/s. At 20 C liquid superficial velocities from 2.02×10^{-3} up to 0.0252 m/s were used. A polar graphic oxygen probe was used to monitor the

oxygen concentration in the outlet gas and in the inlet and outlet liquid streams. The k_La values were calculated from the steady state oxygen concentrations in the column inlet, C_{LA1}, and outlet, C_{LA2}, liquid streams using the relationships for stripping efficiency analysis.

$$k_L a = \frac{v_L}{H} \ln(c_{LA1} / c_{LA2}) \tag{2-42}$$

For absorption experiments the equation was

$$k_L a = \frac{v_L}{H} \ln[(c_{LA}^{+} - c_{LA1}) / (c_{LA}^{+} - c_{LA2})] \tag{2-43}$$

Here C_{LA+} was the oxygen concentration in air-saturated water under the given experimental conditions. In deriving these two equations it was assumed (i) that the oxygen concentration in the gas phase was constant along the column and equaled its concentration in the incoming gas stream and (ii) that the liquid phase conformed to plug flow. The first assumption was met safely inasmuch as the oxygen concentration changes in the gas phase never exceeded 0.2 vol% in the experiments, due to low oxygen solubility in water. Such negligible concentration changes also were a guarantee of negligible influence of axial dispersion in the gas phase. The liquid phase axial dispersion had some effect on the k_La data and this should be taken into consideration. However, reliable data on liquid phase axial mixing is scarce and not available for this case. The results of this article fitted well with the data by Billet and Mackowiak (Billet, 1980) for 25mm Pall rings, Sahay and Sharma (Sahay, 1973) for 25.4 mm Pall rings.

Physical methods are preferred towards chemical methods for measuring liquid phase mass transfer coefficient, because it is difficult to satisfy conditions (2-38) and (2-39) simultaneously at all the time, especially for lager equipment being used in SRP. Desorption of oxygen from water by nitrogen is eliminated because the column height for our system is 3 times the column height used by Linek. The expected outlet oxygen concentration is lower than the range of any oxygen detector. While absorption of oxygen with water from nitrogen is possible, the ability of absorbing oxygen is limited so the inlet oxygen concentration has to be high enough so the outlet oxygen concentration in water accurately detectable.

Another physical method is the stripping of organic chemicals from water. Air striping of VOCs (volatile organic compounds) from water is a standard method and widely applied in industry (JPI, 1996; Kunesh, 1996; El-Behlil, 2012). Among the organic compounds, toluene is chosen for its relatively large Henry's constant and low toxicity. The toluene stripping from air method will be used for measurements of liquid film mass transfer coefficient. Low concentrations of toluene in the ppm level can be accurately measured using a concentration step and a FID gas chromatograph.

2.3.2 Previous Liquid Film Mass Transfer Coefficient Models

2.3.2.1 Onda et al

Onda and co-authors (1968) developed liquid film mass transfer coefficient models based on literature and experimental data of gas absorption into water and desorption from water. The packings investigated were mostly random packings: Raschig Rings, Berl Saddles, Pall Rings, Spheres, and Rods. Their correlation is given in Equation (2-44):

$$k_L(\rho_L/\mu_L g)^{1/3} = 0.0051(L/a_w\mu_L)^{2/3}(\mu_L/\rho_L D_L)^{-1/2}\times(a_P D_P)^{0.4} \qquad (2\text{-}44)$$

Where

a_w is the wetted area (effective area) given by Equation (2-5);

D_P is the packing nominal size, (m).

Onda also studied the gas absorption of pure CO_2 into methanol and carbon tetrachloride. The columns used were 6 and 12 cm I.D. and packed with 10-25 mm Raschig Rings, Berl saddles, spheres and rods for 20-30 cm height. The results were used to verify the k_L model by (2-44) and the agreement was satisfactory. The overall error of Equation (2-44) was within $\pm$20% for gas absorption and desorption into water as well as organic solvents.

2.3.2.2 Linek et al

Linek et al (2001) proposed an empirical model for predicting k_L based on their experimental results. The experiments were performed in a 0.29 m I.D. column with a packed height of 1.04 m. The random packings included RMSR 25, 40, and 50. The results were represented by

$$k_L = \frac{d_1}{b_1} B^{d_2 - b_2 + b_3 \log B} \qquad (2\text{-}45)$$

Where

B is the liquid load, (m/h);

b_1, b_2, b_3 and d_1 are experimental parameters differ between packings.

2.3.2.3 Mangers and Ponter

Mangers and Ponter (1980) investigated the effects of diffusivity and viscosity on the liquid film mass transfer coefficient. The system was absorption of carbon dioxide into pure water and aqueous glycerol mixtures at 25 C covering a viscosity range of

0.9 to 26 cP. The apparatus was a 10 cm I.D. glass column packed with 1 cm glass Raschig Rings. Thier correlation is:

$$\frac{k_L a}{D} = 3.90 \times 10^{-3} (\frac{L}{\mu})^{\alpha} (\frac{\mu}{\rho D})^{0.50} (\frac{\rho^2 g d^3}{\mu^2})^{0.27} (\frac{\rho \sigma^3}{\mu^4 g})^{0.33} \times (\frac{1}{M.W.R.})^{1.67} \qquad (2\text{-}46)$$

Where

L is the liquid flow rate, ($MT^{-1}L^{-2}$);

D is the diffusion coefficient, (L^2T^{-1});

μ is the viscosity, ($ML^{-1}T^{-1}$);

α is the slope for water system and for glycerol-water mixtures, can be calculated by:

$$\alpha = 0.49[(1 - \cos\theta)^{0.6} (\frac{\rho \sigma^3}{\mu^4 g})^{0.2}]^{0.108} \qquad (2\text{-}47)$$

M.W.R. refers to the minimum wetting rate, can be calculated by:

$$M.W.R. = 1.12[(1 - \cos\theta)^{0.6} (\frac{\rho \sigma^3}{\mu^4 g})^{0.2}] \qquad (2\text{-}48)$$

The relations between the liquid film mass transfer coefficient and diffusivity as well as viscosity from Mangers and Ponter's work will be adopted in this paper when converting k_L measured in the toluene/water system to the CO_2/piperazine system.

2.3.2.4 Brunazzi and Paglianti

Brunazzi and Paglianti (1997) studied the mixing in the junctions between packing elements. A parameter, H, representing the flow distance was defined. In the case of complete mixing, H is a function of the channel dimension, whereas in the case of partial mixing, H needs to be computed as the distance covered by the liquid phase flowing into the column. The author proposed a correlation to calculate H:

$$H = \frac{Z}{\sin\alpha} \qquad (2\text{-}49)$$

Where

Z is the packing height, (m);

α is the slope of the steepest descent line with respect to the horizontal axis, (deg).

Finally, a k_L correlation including the influence of mixing in the junctions was proposed:

$$Sh_L = A \frac{Gz^B}{Ka^C} \qquad (2\text{-}50)$$

Where

$$Sh_L = \frac{k_L d}{D_L} \tag{2-51}$$

$$Ka = \frac{\sigma^3 \rho_L}{\mu_L^4 g} \tag{2-52}$$

$$Gz = \mathrm{Re}_L \, Sc_L \, \frac{\delta}{H} \tag{2-53}$$

2.3.2.5 Delft model

The Delft model proposed by Olujic (1999) has been discussed in the area model section (2.1.2.5) and the k_G model section (2.2.2.4) before. As for the k_L model, the Delft model used the same expression as proposed by Bravo et al. (1992). However, instead of the corrugation side, s, the Delft model used the hydraulic diameter of the triangular flow channel as the characteristic length of liquid flow. The hydraulic diameter was defined by:

$$d_{hG} = \frac{\frac{(bh - 2\delta s)^2}{bh}}{[(\frac{bh - 2\delta s}{2h})^2 + (\frac{bh - 2\delta s}{b})^2]^{0.5} + \frac{bh - 2\delta s}{2h}} \tag{2-54}$$

Where

b is the corrugation base length, (m);

h is the corrugation height, (m);

s is the corrugation side length, (m);

δ is the liquid film thickness, (m).

The k_L correlation can then be calculated:

$$k_L = 2\sqrt{\frac{D_L u_{Le}}{\pi 0.9 d_{hG}}} \tag{2-55}$$

2.4 Conclusions

2.4.1 Methods of measuring effective area, gas and liquid film mass transfer coefficient

After reviewing various methods of measuring contact area a_e, the Danckwerts's method (1970), absorption of CO_2 from air into 0.1 gmol/L NaOH, is adopted for measuring a_e. The Sharma (1966) and Moucha (2005) method of absorbing SO_2 from air into 0.1 gmol/L NaOH is the most suitable method for determining the gas film mass transfer coefficient. Desorption of toluene from saturated water by air is used for determining the liquid film mass transfer coefficient.

2.4.2 Models of predicting effective area, gas and liquid film mass transfer coefficient

A large number of previous correlations for a_e, k_G and k_L have been discussed in this chapter. Table 2.1-2.3 summarizes the effective area models and mass transfer coefficient models. A major weakness of these models is the validation of a_e and k_G, k_L at the same time. Either a theoretical assumption of area or proposed theoretical film coefficient models were used to separate the "k" and "a" values. Thus, mechanistic mass transfer models developed from consistent measurements of a_e, k_L and k_G are needed which is the objective of this work.

Table 2.1. Summary of models for effective area

Author	Correlations
Onda (1968)	$\frac{a_e}{a_P} = 1 - \exp[-1.45(\frac{\sigma_C}{\sigma_L})^{0.75} \mathrm{Re}_L^{0.1} Fr_L^{-0.05} We_L^{0.2}]$
Billet and Schultes (1993)	$\frac{a_e}{a_P} = 1.5(a_P d_h)^{-0.5} \mathrm{Re}_L^{-0.2} We_L^{0.75} Fr_L^{-0.45}$
Rocha-Bravo-Fair (1996)	$\frac{a_e}{a_P} = F_{SE} \frac{29.12 u_L^{0.4} \nu_L^{0.2} S^{0.359}}{(1-0.93\cos\gamma)(\sin\alpha)^{0.3} \varepsilon^{0.6}} (\frac{\rho_L}{\sigma g})^{0.15}$
Tsai (2010)	$\frac{a_e}{a_P} = 1.34[(\frac{\rho_L}{\sigma}) g^{1/3} (\frac{Q}{L_P})^{4/3}]^{0.116}$
Olujic (1999)	$\frac{a_e}{a_P} = \frac{1-\Omega}{1 + A/u_{Ls}^B}$

Table 2.2. Summary of models for gas film mass transfer coefficient

Author	Correlations
Onda (1968)	$Sh_G = 5.23\,\mathrm{Re}_G^{0.7}\ Sc_G^{1/3}(a_P + D_P)^{-2.0},\ D_P > 15\ mm$ $Sh_G = 2.00\,\mathrm{Re}_G^{0.7}\ Sc_G^{1/3}(a_P + D_P)^{-2.0},\ D_P \le 15\ mm$
Mehta and Sharma (1966)	$k_G a = C * D_G^{0.5} u_G^{0.75} S^{0.33}$
Billet and Schultes (1993)	$k_G = \frac{2}{\sqrt{\pi}} \sqrt{D_G \frac{u_G}{(\varepsilon - h_L) l_\pi}}$
Olujic (1999)	$k_G = \sqrt{(\frac{Sh_{G,lam} D_G}{d_{hG}})^2 + (\frac{Sh_{G,turb} D_G}{d_{hG}})^2}$ $Sh_{G,lam} = 0.664 Sc_G^{1/3} \sqrt{\mathrm{Re}_{Grv} \frac{d_{hG}}{l_{G,pe}}}$ $Sh_{G,turb} = \frac{\mathrm{Re}_{Grv}\ Sc_G \frac{\zeta_{GL}\varphi}{8}}{1 + 12.7\sqrt{\frac{\zeta_{GL}\varphi}{8}}(Sc_G^{2/3} - 1)} [1 + (\frac{d_{hG}}{l_{G,pe}})^{2/3}]$
Rocha-Bravo-Fair (1996)	$\frac{k_G S}{D_G} = 0.054[\frac{\rho_G S(u_{Ge} + u_{Le})}{\mu_G}]^{0.8} (\frac{\mu_G}{D_G \rho_G})^{0.33}$

Table 2.3. Summary of models for liquid film mass transfer coefficient

Author	Correlations
Onda (1968)	$k_L(\rho_L / \mu_L g)^{1/3} = 0.0051(L / a_w \mu_L)^{2/3} (\mu_L / \rho_L D_L)^{-1/2} \times (a_P D_P)^{0.4}$
Linek (2001)	$k_L = \frac{d_1}{b_1} B^{d_2 - b_2 + b_3 \log B}$
Mangers and Ponter (1980)	$\frac{k_L a}{D} = 3.90 \times 10^{-3} (\frac{L}{\mu})^{\alpha} (\frac{\mu}{\rho D})^{0.50} (\frac{\rho^2 g d^3}{\mu^2})^{0.27} (\frac{\rho \sigma^3}{\mu^4 g})^{0.33} \times (\frac{1}{M.W.R.})^{1.67}$

Brunazzi (1997)	$Sh_L = A\frac{Gz^B}{Ka^C}, \quad Ka = \frac{\sigma^3 \rho_L}{\mu_L^4 g}, \quad Gz = \mathrm{Re}_L \, Sc_L \frac{\delta}{H}$
Olujic (1999)	$k_L = 2\sqrt{\frac{D_L u_{Le}}{\pi 0.9 d_{hG}}}$
Billet and Schultes (1993)	$k_L = \frac{2}{\sqrt{\pi}}\sqrt{D_L \frac{u_L}{h_L l_\pi}}$
Rocha-Bravo-Fair (1996)	$k_L = 2\sqrt{\frac{D_L C_E u_{Le}}{\pi S}}$

Chapter 3: Experimental Methods

3.1 Packed Column

3.1.1 Equipment Description

The equipment used in this work is the same as used by previous researchers. Wilson (2004) used the equipment to measure the effective area of several random and structured packings. Tsai (2010) continued the study of mass transfer area, and investigated the surface tension and viscosity effect on effective area. A pilot-scale PVC column with an inner diameter of 0.428 m (16.8 in) and a total column height of 7.62 m (25 ft) capable of a maximum packed height of 3.05 m (10 ft) was utilized to measure the effective area, gas and liquid film mass transfer coefficients, andpacking hydraulic properties. A packed bed of 3.05 m (10 ft) was used to measure the pressure drop, liquid hold-up and effective area. Different from previous researchers, reduced packing heights were used for liquid and gas film mass transfer coefficient measurements. A packed bed of 1.83 m (6 ft) was used for the k_L measurement to avoid the peak tailing problem for the outlet toluene concentration measurement. The packed bed was further reduced to approximately 0.51 m (20 in) for the k_G measurement to get a reliable outlet SO_2 concentration. Steel reinforced gloves are required to prevent being cut when handling sheet metal structured packings.

The column was located in the outdoor area. The DeltaV® control system provided by Emerson Process Management was utilized to operate the whole system and collect data. Ambient air fed from a 30 kW (40 hp) blower entered below the packed bed and flowed upward through the packing. The air flow rate was monitored by an annubar flow meter (Dietrich Standard, model #DCR15), which was basically an averaging pitot tube. The gas pressure drop was measured by two Rosemount differential pressure transmitters. One was employed to monitor the static pressure and was calibrated for 1020 kPa (150 psi); the other was directly associated with the annubar and was calibrated for 6215 Pa (25 in H_2O). The air flow meter and pressure transmitters were connected to the DeltaV® system.

The liquid was pumped from a 1.3 m^3 (350 gallon) storage tank through a centrifugal pump with a capacity of 0.57 m^3/min (150 gpm) in a closed loop. Part of the liquid flowed through the recycle loop controlled by valves for enhanced mixing. The rest of the liquid was pumped to the top of the column and distributed by a pressurized fractal distributor containing 108 drip points/m^2. The liquid flow rate was measured by a MicroMotion coriolis meter. Both the gas and liquid flow rate were controlled by changing the speed of the blower and the pump through the DeltaV® system.

Some auxiliary facilities were also used in this system. A bag filter located in the recycle loop was used to remove any possible solids in the liquid. A Trutna tray collector was located in the column segment above the distributor to prevent liquid from reaching the column exhaust by knocking it out and allowing it to drain back

into the storage tank. A level transmitter was installed on the column sump to measure the liquid level. A height of approximately 1.8 to 2.1 m (6 to 7 ft) between the bottom of the packing and the sump was allowed during normal operation. Thermocouples were used to measure the gas temperature at the inlet and the outlet of the column. The MicroMotion meter was used to measure the liquid temperature. A vacuum sample pump (Air Dimensions Inc., Micro Dia-Vac® pump) was used for the sampling of the gas to the CO_2 and SO_2 analyzers inside the control room. Heated sample lines were used to prevent water condensation along the sample line for SO_2 measurements. A cooling system was also utilized to cool down the column during summer time for SO_2 runs. These facilities will be described in detail in the k_G measurements.

3.1.2 Pack/unpack the column

The column was taken apart during packing change-outs. When packing the column, all the sample lines, column differential pressure transmitters, and thermocouples were disconnected from the column body. The column head was pulled up by the steel chain pulley system located at the very top. The new packing elements were carefully lowered one by one from the opened column top, and pushed down to the bottom with a circular (diameter ~ 35 cm) plunger. The packing element height varied from 0.2 to 0.25 m (8 to 10 inches), depending on packing type. The height of the gap between the packing and the distributor was measured before and after packing the column. The total packed height was then calculated. When unpacking the column, the bolts and nuts that fixed the column bottom flange were removed. The column can be lifted by the steel chain. The old packing was pushed out and removed from the bottom one by one.

A pressurized fractal distributor with 432 drip points/m^2 (40 points/ft^2) was utilized for liquid distribution in every experiment. This density and the pressurized nature are believed to be sufficient to avoid maldistribution and other undesirable effects, based on past distributor studies conducted by the Separation Research Program (SRP) at the University of Texas at Austin. The height of the distributor was adjusted according to the packed height to ensure the distributor-to-packing distance was never greater than 7.6 cm (3 inches). The CO_2 and SO_2 analyzer sampling system are described in detail in Appendix A.

The experiment setup is shown in Figure 3.1.

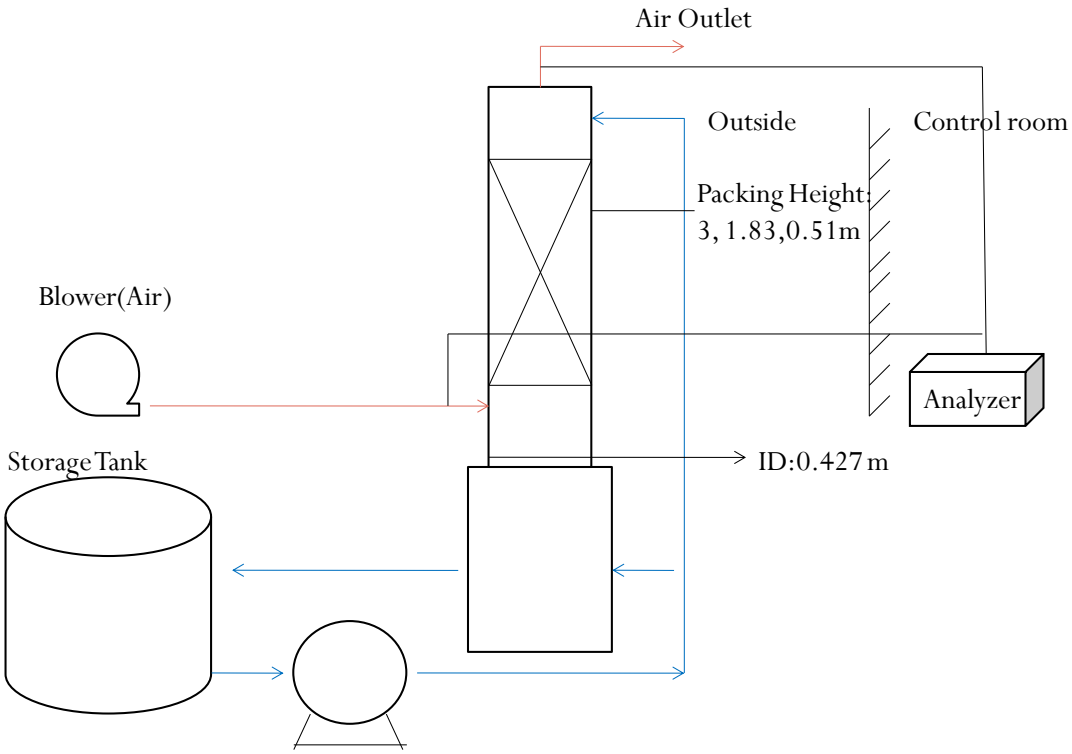

Figure 3.1. Process Flow Diagram for the 0.427 m Diameter (i.d.) Packed Column.

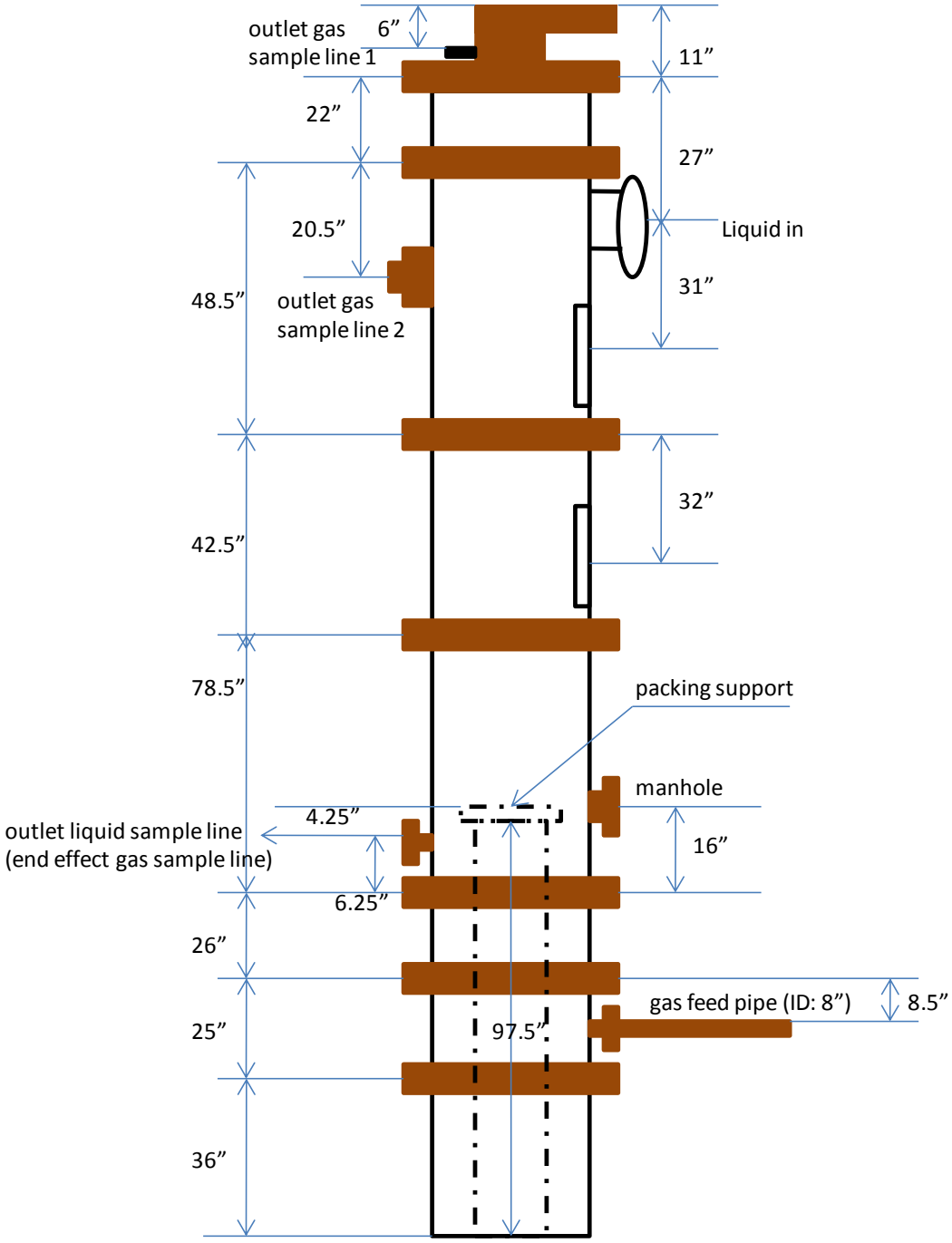

Figure 3.2. Drawing of the 0.427 m Diameter (i.d.) Packed Column.

3.1.3 Hydraulic experiments

Before mass transfer measurements for each packing, hydraulic experiments including pressure drop and liquid hold-up measurements were performed. Since high liquid and gas flow rates (e.g. flooding conditions) would be operated for hydraulic runs, the air/water system (no caustic) was chosen to avoid contamination of the gas sampling system. The physical properties of 0.1 gmol/L NaOH, which is the system used for

mass transfer measurements, is similar to the water system so there is not significant deviation. The packed height for hydraulic measurements was 3.3 m (10 ft).

Dry pressure drop was measured before wetting the packing. In dry pressure drop measurements, only the blower was turned on while the liquid pump was shut off. The liquid outlet valve was closed for the dry pressure drop runs. The gas flow rate was increased from 0.39 m/s (120 ACFM) to 4.25 m/s (1300 ACFM) with increments of 0.32 m/s (100 ACFM). The pressure drop data was recorded by the differential pressure transmitters (Rosemount) after the gas and liquid flow rates were stable. Pressure drop less than 750 Pa (3 in H_2O) was recorded by the low range transmitter while pressure drop higher than 750 Pa was recorded by the high range transmitter. All data were recorded in the Excel data sheets.

After the dry pressure drop measurement, the liquid pump was turned on to wet the packing before the wet pressure drop measurement. A typical wetting process usually took 10 minutes at pump rate of 60% VSD. For the wet pressure drop measurement, the gas flow rate was set constant while the liquid flow rate was increased from 5 gpm/ft^2 to 30 gpm/ft^2 for the first three points (gas flow rate from 120 ACFM to 250 ACFM). The purpose was to avoid any possible crosses between curves since the differences between data points were subtle at low gas flow rates. Then the liquid flow rate was set constant and the gas flow rate was increased by increment of 100 ACFM until flooding conditions were reached, generally indicated by a pressure drop of 1630 Pa/m (2 in H_2O/ft) or higher. The pressure drop for each nonloading condition was recorded when stable gas and liquid flow rates were reached (usually 4-5 minutes). The time to reach steady state can be longer (5-10 min) when operating in the near flooding regions.

The fractional liquid hold-up was measured separately from the pressure drop measurement. In the hold-up measurement, the column sump was initially filled by pumping water from the storage tank until sump level reached 30 inches. Then the loop to the tank was shut and liquid only circulated between the column and the sump in the measurement. The height of the liquid level was recorded by the level transmitter installed in the sump, and the data was sent to the computer control system. The liquid hold-up was calculated by the sump geometry and the difference between the current and baseline liquid levels (Equation 3-1). The equation was built in the computer system and liquid hold-up was calculated automatically.

$$h_L = \frac{d_{sump}^2 * (Current\ level - Calculated\ baseline\ level) + V_{F10} - V_{pip}}{d_c^2 Z} \qquad (3\text{-}1)$$

Where

d_{sump} and d_c are the diameters of the sump and column, (m);

V_{F10} is the estimated liquid hold-up volume in the F10 distributor, (m^3);

V_{pipe} is the liquid hold-up volume in the connecting pipes, (m^3);

Z is the column height, (m).

The evaporation of the liquid was also considered during the liquid hold-up measurement. An evaporation calculation equation based on the temperature and the relative humidity was built in the computer system to account for this loss. The baseline level was determined every four data points to ensure the accuracy of the calculation.

3.1.4 Mass Transfer Area experiments

As discussed in Section 2.1.1, the system used to measure the mass transfer area was the absorption of atmospheric CO_2 by 0.1 gmol/L NaOH solution. The reaction between CO_2 and NaOH is a pseudo first-order reaction, and the system is chemical reaction controlled. Thus, the liquid film mass transfer coefficient with chemical reactions can be calculated by Equation (3-2). The effective area and mass transfer coefficient can be separated, and the area can be calculated by Equation (3-3).

$$k_g^{'} = \frac{\sqrt{k_{OH^-}[OH^-]D_{CO2,L}}}{H_{CO2}} \tag{3-2}$$

$$a_e = \frac{u_G \ln(\frac{y_{CO_2 in}}{y_{CO_2 out}})}{ZK_G RT} \approx \frac{u_G \ln(\frac{y_{CO_2 in}}{y_{CO_2 out}})}{Zk_G^{'} RT} \tag{3-3}$$

Where

k_{OH-} is the second order reaction constant, (m^3/kmol*s);

$[OH^-]$ is the concentration of free hydroxyl ion in the liquid phase, (gmol/L);

$D_{CO2,L}$ is the diffusivity of CO_2 in the liquid phase, (m^2/s);

H_{CO2} is the Henry's constant of CO_2, (m^3*bar/kmol);

y_{CO2in} and y_{CO2out} are the concentration of CO_2 in the gas phase at inlet and outlet, (ppmv);

Z is the packed bed height, (m).

In a typical mass transfer area measurement, the storage tank was initially filled with 0.75 m^3 (200 gallons) of water. NaOH solid pellets with measured weight of 3.63 kg (8.0 lbs) were added to the tank. The solid pellets and the liquid were mixed by pumping liquid through the recycle loop to create 0.1 gmol/L NaOH solution. Chemical resistant lab gloves are required when handling a strong base. Lab safety goggles were used for eye protection during the experiments. The mixing time was set to 45 minutes to 1 hour to get a complete mixing and stable NaOH concentration. During mixing, the routes to the filter as well as to the column were closed to prevent solid pellets to be stuck in the filter and the packing. The pump rate was set at 40% VSD in the mixing process. After mixing, the NaOH concentration was measured by acid titration. The NaOH concentration can be seen as stable until three samples gave the same value. Then the value was recorded as the initial NaOH concentration value.

The measurement started with gas flow rate of 180 ACFM (superficial gas velocity ~ 0.59 m/s). The blower was set to maintain a constant gas flow while the liquid pump was set to increase the liquid flow rate from 2.5 gpm/ft^2 to 30 gpm/ft^2 (6.1 to 73.2 m^3/m^2*h). The gas phase sample of the inlet and outlet was pumped by two gas sample pumps (Air Dimensions Inc., Micro Dia-Vac® pump) to the CO_2 analyzer (Horiba VIA-510). The CO_2 analyzer was calibrated by zero (N_2) and span gases (450 ppmv CO_2/N_2) before each experiment. The mass transfer area was calculated based on the CO_2 removal from the air. Each condition was given at least 10 minutes to reach steady state, indicated by relatively constant readings of the various process parameters (CO_2 concentration, flow rate, temperature, etc.). Pressure drop was not allowed to exceed 815 Pa/m (1 in H_2O/ft) to avoid contamination of gas sample line and CO_2 analyzer by caustic solution. After all data points were taken for one gas flow rate, the NaOH solution would be neutralized, drained, and replaced by fresh NaOH solution. The purpose was to ensure the NaOH concentration to be around 0.1 gmol/L. There was an online calculator built into the DeltaV® system to calculate the current NaOH concentration based on initial NaOH concentration and total CO_2 consumption. Then the gas flow rate was changed to higher values (300 and 450 ACFM), and the procedure was repeated. After the three major curves (180, 300, 450 ACFM curve), two additional data points, gas flow rate at 600 ACFM and 750 ACFM with liquid flow rate of 15 gpm/ft^2, were measured to give effective area data for the k_G measurement.

3.1.5 Liquid Film Mass Transfer Coefficient

As discussed in Section 2.3.1, the system used to measure the liquid film mass transfer coefficient was the stripping of toluene from water into air. Air stripping toluene from water is a liquid phase control system because of its very high Henry's constant. The overall mass transfer can be assumed as equal to the liquid phase mass transfer coefficient. Once the inlet and outlet toluene concentration in water have been measured, the following equation can be used to calculate k_La:

$$k_L a = \frac{u_L}{Z} \ln(c_{LA1} / c_{LA2}) \qquad (3\text{-}4)$$

Where:

u_L is the liquid superficial velocity, m/s;

Z is the packing height, m;

$c_{LA1}/_{LA2}$ is the inlet and outlet toluene concentration in water, ppm;

The liquid film mass transfer coefficient, k_L, can be determined directly from the measured k_La and the effective area (a_e) obtained under the same liquid and gas rates:

$$k_L = \frac{k_L a}{a_e} \qquad (3\text{-}5)$$

In a typical k_L measurement, the packed height was reduced from 3.05 m (10 feet) to 1.83 m (6 feet) to obtain a reliable outlet toluene concentration and to avoid the peak

tailing problem in the GC as well. Initially, 600 ml of toluene was added to 200 gallons (757 liters) of water in the storage tank to make saturated toluene water solution. The mixing time was set to 20 minutes to get a complete mixing. During mixing, the routes to the column were closed to prevent toluene loss. The pump rate was set at 50% VSD in the mixing process. As the experiment was running, toluene was injected continuously using a feed pump (metering pump) to make up toluene loss during the experiment. The toluene concentration in the feed was maintained well below the saturation concentration by adjusting the toluene feed pump rate according to the toluene loss rate at different liquid flow rates.

Similar to effective area measurements, three gas flow rates (180, 300, 450 ACFM or superficial velocities of 1.96, 3.25, 4.87 ft/s) and seven liquid flow rates (from 2.5 to 30 gpm/ft^2 or 6.1 to 73.2 m^3/m^2*h) were studied for each packing k_La test. For each curve, the gas flow rate was fixed and the liquid flow rate was varied from 2.5 to 30 gpm/ft^2. Each condition was given at least 10 minutes to reach steady state.

When the system reached steady state, an inlet and an outlet toluene sample in water were taken at the inlet and outlet k_L sample point with two 40 ml test tubes. A Hewlett Packard 5890A Gas Chromatograph was used for the analysis. The range of the Gas Chromatograph is 0-1,000 ppm and can accurately measure both the inlet and outlet toluene concentration as an extraction technique was used to enhance the toluene concentration in the sample to the detectable level. However, as mentioned before, peak tailing was found when the concentration dropped below 5 ppm. Thus, the packed bed was reduced from 10 feet to 6 feet to avoid this problem.

Details regarding GC analysis will be described in Section 3.2.2.

The entire analysis time for one sample took 15 minutes, while one data point (inlet sample and outlet sample together) would take approximately 30 minutes. Because of the high volatility of toluene, samples need to be analyzed in a short period of time. One suggested procedure was to take three data points at a time, and then wait until all samples get analyzed before take new data points. A sample refrigerator was used to preserve samples.

3.1.6 Gas Film Mass Transfer Coefficients experiments

The gas film mass transfer coefficient was measured by absorption of SO_2 mixed with air with 0.1 gmol/L NaOH solution. The inlet SO_2 gas was made by mixing 2% SO_2 from the cylinder with air. The gas cylinder is located outside within the main SRP containment dike. Since SO_2 is a toxic gas, a gas mask with a respirator is required when changing SO_2 cylinders.

A gas flow meter with adjustable value was used to control the flow rate of the SO_2 coming out of the cylinder. The objective was to control the inlet SO_2 concentration to be around 90 ppm. Because of the high efficiency of SO_2 removal with NaOH, the packed height was reduced from 10 feet to 30-40 inches to obtain a reliable and measureable outlet SO_2 concentration. In this case, the mass transfer from the top section above the packing and the bottom section below the packing became

comparable with the mass transfer from the packing section. In the k_G measurement, the mass transfer from these two ends (NTU_{end}) was measured and deducted from the overall mass transfer (NTU_{total}). Details regarding end effect measurement will be further discussed in Section 3.3.2.
The reaction between SO_2 and NaOH is an instantaneous reaction making the liquid phase mass transfer resistance negligible. Thus, the overall mass transfer coefficient (K_{OG}) can be assumed to be equivalent to the gas film mass transfer coefficient (k_G). The gas film mass transfer coefficient can be calculated by:

$$k_G = \frac{u_G \ln(\frac{y_{SO2in}}{y_{SO2out}})}{ZRTa_e} \quad (3\text{-}6)$$

Where:
u_G is the gas superficial velocity, m/s;
y_{SO2in}, y_{SO2out} is the inlet and outlet SO_2 concentration, ppmv;
a_e is the effective mass transfer area, m^2/m^3.

Two trace level SO_2 analyzers (Thermo Scientific Model 43i) were used to measure the inlet and outlet SO_2 concentrations. The inlet SO_2 analyzer was set to the range of 0-100 ppm while the outlet SO_2 analyzer was set to the range of 0-2000 ppb. Calibration was performed every three months to ensure the accuracy of the analyzer. The major concern of SO_2 sampling system was the water condensation problem, especially for the outlet sample line. Endeavors had been made to solve this problem. Details regarding SO_2 sampling trouble shooting will be discussed in Section 3.3.1.

In the gas film mass transfer coefficient measurements, a wider range of gas flow rates were studied (1.96, 3.25, 4.87, 6.50, 8.12 ft/s, equivalent to 180, 300, 450, 600, 750 ACFM) since k_G was primarily a function of gas flow rates rather than liquid flow rates. The liquid flow rate was fixed at 80.2 m^3/m^2*h (10 gpm/ft^2) while gas flow rate changed. Two additional data points were taken at liquid flow rates of 5 gpm/ft^2 and 15 gpm/ft^2 and gas flow rate of 300 ACFM. For each condition the steady state inlet and outlet SO_2 concentration were recorded. Steady state was reached by the sign of stable inlet and outlet SO_2 concentration readings. With the inlet and outlet concentration, k_G can be calculated.

3.2 Analytical Methods and Equipment

3.2.1 Acid Base Titration

Acid base titration was used to calculate the NaOH concentration in the liquid phase for effective area measurement. Standard solution of 0.1 gmol/L hydrochloric acid (HCl) was used as the titrant. Chemical resistant lab gloves are required when handling bases and strong acids such as NaOH and HCl. Phenolphthalein was used as

the indicator. The reaction is:

$$HCl\ (aq) + NaOH\ (aq) \rightarrow H_2O\ (l) + N\,a\,C \qquad (3\text{-}7)$$

After complete mixing, samples of caustic solution from the sump of the column were taken to be analyzed. A Single-Channel Pipette (VWR VE 10000) designed to handle 5 ml liquid with locking system was used to transfer 10 ml of NaOH solution from the sample tube to the titration beaker. A magnetic stirring device with a rotating magnetic field (IKA CERAMAG) and a stir bar was used to maintain perfect mixing during the titration process. A burette with an electronic bottle top (Brinkmann Buret 50) which can record the volume consumed was used. The standard procedures of the titration process are listed in the appendix.

The concentration of NaOH solution can be calculated by:

$$C_{NaOH} = \frac{The\ volume\ of\ \ HCl\ used\ (ml) \times 0.1\ gmol/L}{10\ ml} \qquad (3\text{-}8)$$

The aqueous NaOH concentration can be seen as stable until three samples gave the same value. Then the concentration was recorded as the initial NaOH concentration.

3.2.2 Gas Chromatograph (GC) Analysis

The Gas Chromatograph (Hewlett Packard 6890) analysis was used to measure the toluene concentration in the liquid phase in the liquid film mass transfer coefficient (k_L) measurement. The sample taken from the column was toluene in water, and water was not allowed to run in the GC. Thus, toluene was extracted from the water sample to organic phase (heptane) before the GC analysis. Two auto-pipettes (VWR VE 10000) were used for the extraction, which can precisely take a certain volume of sample. One was set at 4 ml, and the other was set at 10 ml. 4 ml of heptane was used to extract toluene from 20 ml of sample.

For the GC analysis, an internal standard method was used. A stable chemical, 4BFB (1-Bromo-4-fluorobenzene, a non-volatile hydrocarbon chemical), was chosen as the internal standard. One drop of 4BFB (approximately 0.001g) was added to a 20 ml sample.

Before the experiment, the response factor for the toluene/4BFB system was calculated with standard solution.

$$\frac{x_{TOL}}{x_{4BFB}} = \frac{R_{TOL}A_{TOL}}{R_{4BFB}A_{4BFB}} \qquad (3\text{-}9)$$

Where

X is the concentration, (ppmw);

A is the peak area;

R_{TOL} is the response factor for toluene;

R_{4BFB} is the response factor for 4BFB.

Because 4BFB was chosen as the standard, so $R_{4BFB} = 1$.

For this calculation, standard solution of toluene and 4BFB was used, so x_{TOL} and

x_{4BFB} was known.
Then the response factor for toluene can be calculated:

$$R_{TOL} = \frac{x_{TOL}}{x_{4BFB}} * \frac{A_{4BFB}}{A_{TOL}} \quad (3\text{-}10)$$

The standard procedures of the GC analysis process are listed in the appendix.
In the internal standard method, the mass of the internal standard (4BFB) was weighed with a precision up to 0.0001g. So the 4BFB concentration in the extract can be calculated:

$$x_{4BFB} = \frac{m_{4BFB}}{m_{extract} + m_{4BFB}} \quad (3\text{-}11)$$

From GC result, the peak area for toluene and 4BFB (A_{tol} and A_{4BFB}) were recorded. Then the toluene concentration in heptane can be calculated:

$$x_{tol\ in\ hep} = \frac{R_{tol} * A_{tol} * x_{4BFB}}{A_{4BFB}} \quad (3\text{-}12)$$

Finally the toluene concentration in aqueous sample can be calculated:

$$x_{tol\ in\ water} = \frac{x_{tol\ in\ hep} * \rho_{hep} * V_{hep}}{\rho_{water} * V_{water}} \quad (3\text{-}13)$$

Where V_{hep} is 4 ml, and V_{water} is 20 ml.

3.2.3 SO_2 Analyzer and calibration

Two trace level SO_2 analyzers (Thermo Scientific 43i) were used in the gas film mass transfer coefficient (k_G) measurement. One was set to the range of 0-100 ppm for the inlet SO_2 concentration measurement while the other one was set to the range of 0-2000 ppb for the outlet SO_2 concentration. Zero air gas and standard 90 ppm SO_2 in N_2 span gas were used to calibrate the inlet SO_2 analyzer. Calibration were performed several rounds until both zero and span gas concentrations read correctly. For the outlet SO_2 analyzer, 1600 ppb SO_2 was used as the span gas. A Dynamic Gas Calibrator (Thermo Scientific Model 146i) was used to make 1600 ppb SO_2 span gas since that range of SO_2 span gas was not available on the market. Both analyzers were connected to the Delta V system so the SO_2 concentration can be recorded online.

3.3 Experimental Concerns

3.3.1 SO_2 Sampling Trouble-shooting

At the beginning stages of this work, the measured SO_2 outlet concentration was below 10 ppb independent of packing height. Also, when the gas flow rate or the liquid flow rate changed, the outlet SO_2 reading did not change dramatically. Water condensation was found along the sample line wall, which caused the inaccurate

measurement of the outlet SO_2 measurement. Efforts have been made troubleshooting the SO_2 sampling system:

1. Packing height was reduced from 10 feet to approximately 30 inches to increase outlet SO_2 concentration to a measurable level. The packing height was not reduced further because of concerns with maldistribution and end effects.
2. Heat tracing wires were added to the outlet sample line to prevent water condensation along the sample line walls.
3. A cooling system was installed to the water recirculation loop. Liquid and the overall column temperature were controlled between 60 and 65 ℉ to eliminate the air conditioning effect when gas sample transferred from outdoor to indoor analyzer.
4. A Micro-GASSTM Gas Analysis Sampling System from PERMA PURE LLC was installed at the end of the outlet sample line upstream from the analyzer. The sample conditioner used the exhaust gas from the analyzer to dry the sample gas. The sample inlet portion of the dryer was also heated to accelerate the drying process.

Figure 3.3 shows the flow schematic figure of the column with SO_2 sampling trouble-shooting devices. The sample lines are stainless steel tubes with an OD of 1/4". The outlet sample lines are heated by electric heating wires wound around. The length of sample lines with and without heating wires is marked in Figure 3.3. Details of heated sample line are shown by photos in the Appendix A.

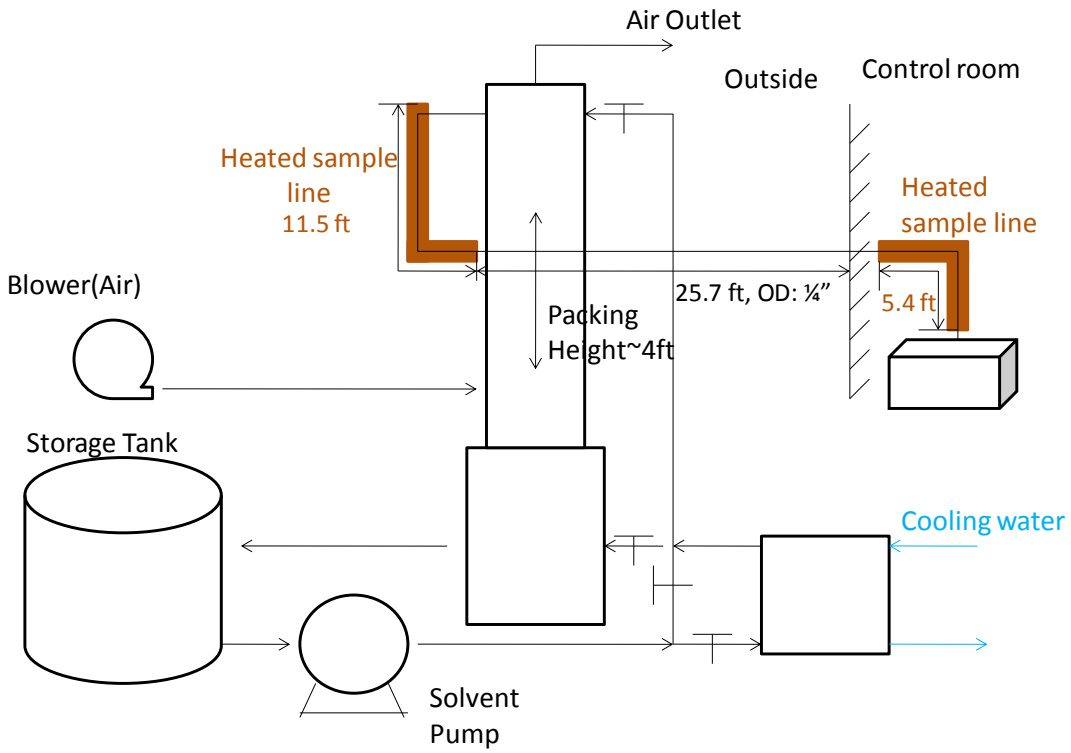

Figure 3.3. Flow schematic figure with SO_2 sampling trouble-shooting devices.

3.3.2 End effect measurements for SO_2 system

Because of the high efficiency of the SO_2/NaOH system, a short bed of packing was used to obtain a measureable outlet SO_2 concentration. Thus, there was a 7-foot gap between the outlet sample point and the packing section. It should be noted that the liquid distributor was lowered to a few inches above the packing. For the area and k_L measurement, the gap was 3-4 inches and negligible. The gap refers to the open space between the top of the packing and the outlet sample points, which may cause top end effect for k_G measurement since it is much bigger. However, the upper end effect for k_G measurement was not negligible. To measure the upper end effect, a sample line was attached to the distributor; the sample point was right above the packing. Figure 3.4 showed the upper end effect measurement. Data were taken from the outlet sample line and upper end effect sample line to obtain the number of transfer units (NTU) from the top. The NTU for the upper end effect was calculated to be approximately 0.5.

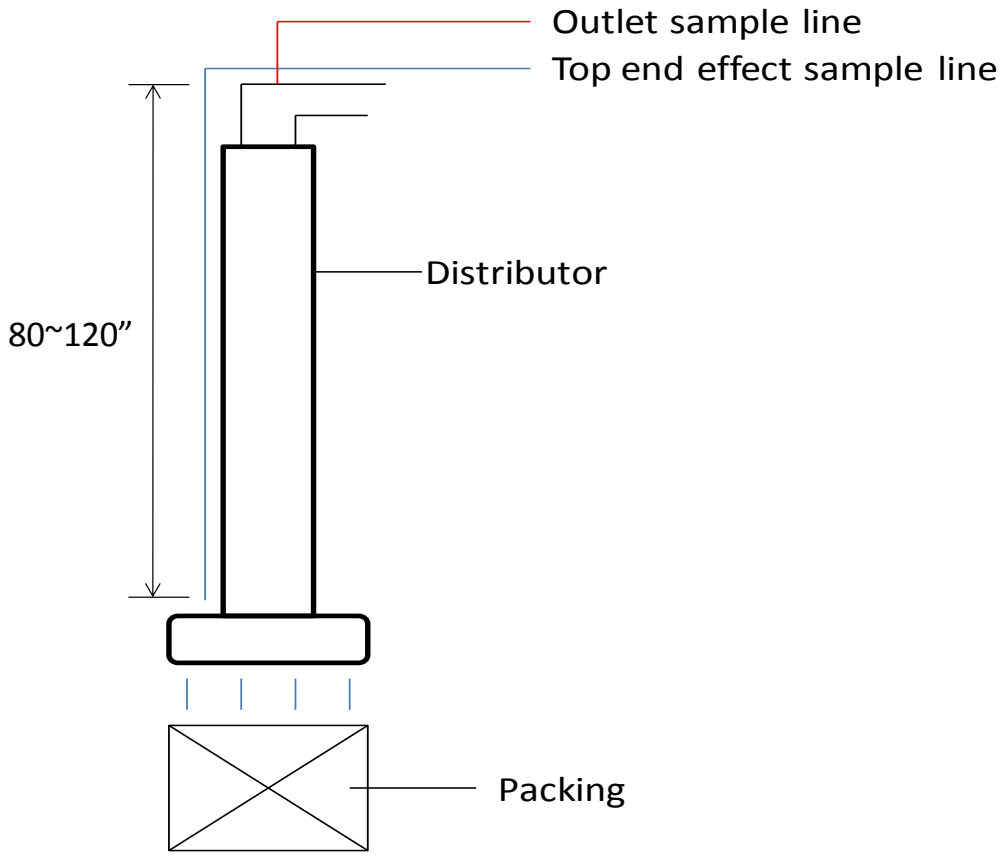

Figure 3.4. Upper End Effect Measurement

There was approximately 8 feet spacing between the bottom of the packing and the sump liquid at the bottom of the column. Thus liquid films flowing down from the bottom of the packing to the sump liquid could result in additional mass transfer. Since only 3 feet of packing was used, the lower end effect was not negligible relative to the total k_G measurement. The lower end effect was measured by sampling the inlet air and sampling just below the packing (Figure 3.5). The measured number of mass transfer units in the bottom section, NTU_{lower}, was at 1.1–1.3. The NTU_{lower} varied

somewhat with gas and liquid flow rate and was measured for each condition.

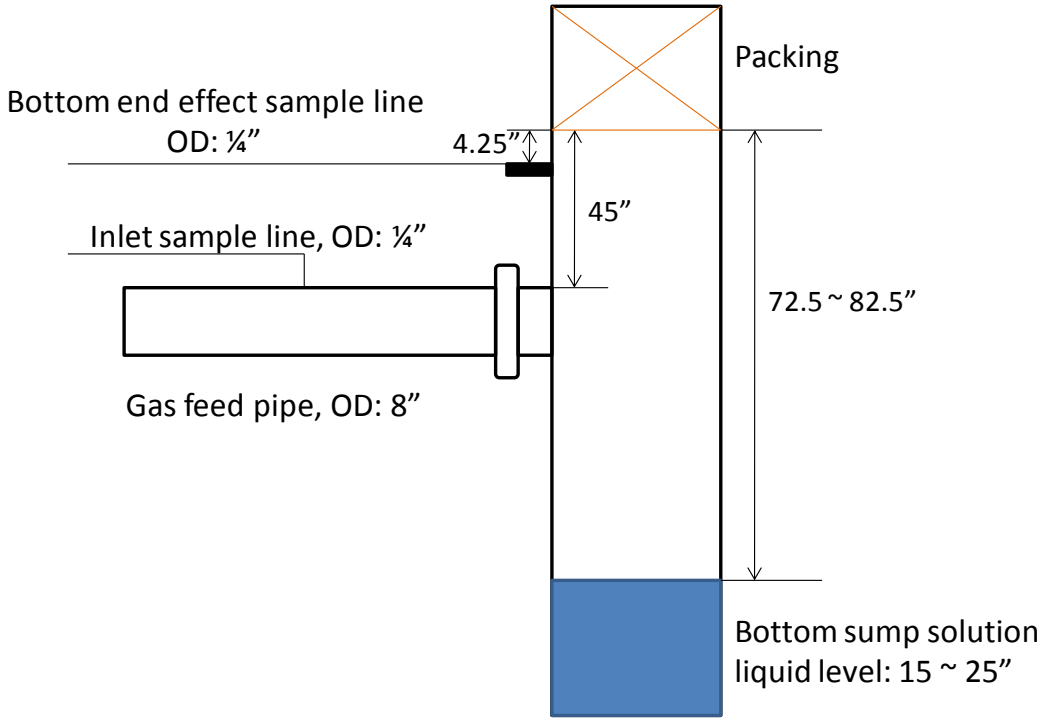

Figure 3.5. Lower End Effect Measurement

3.4 Experiment Safety

3.4.1 Safety with packed column

One of the major safety concerns regarding working is getting cut by metal packing. Steel reinforced gloves are required to prevent getting hurt when handling with metal packing. A hard hat should always be worn when working outside. A Fall Protection Harness is required when working at the top section of the pilot scale packed column.

3.4.2 Safety with chemicals

For the gas film mass transfer coefficient measurement, sulfur dioxide is used as the solute gas. It is a toxic gas with a pungent, irritating smell. Inhaling sulfur dioxide is associated with increased respiratory symptoms and disease, difficulty in breathing, and premature death. In 2008, the American Conference of Governmental Industrial Hygienists reduced the short-term exposure limit to 5 parts per million (ppm). For safety, the inlet SO_2 concentration is controlled to be less than 100 ppm. Before SO_2 runs, the leakage of the piping of the system was carefully checked to ensure no SO_2 is leaking. A gas mask was worn when changing the SO_2 cylinder. In the absorption process, the NaOH solution is in excess so no SO_2 or only ppb levels of SO_2 is exiting the system.

For the effective area measurement, base (0.1 gmol/L NaOH solution) is used. Acid (0.1 gmol/L HCl) is used in the titration process. Chemical resistant lab gloves were used when handling the base and acid. Lab safety goggles were used for eye

protection during the experiments. After the experiments, the remaining caustic solution was neutralized to pH 6-9 before disposal. Strong acid with high volatility (30 wt% HCl) was used in neutralization. A gas mask with respirator and rubber gloves were worn when dumping 30 wt% HCl to the tank.

For the liquid film mass transfer coefficient measurement, flammable chemicals such as toluene, heptanes, and 4BFB are used. Chemical resistant lab gloves were worn each time when dealing with these chemicals. After the experiments waste liquid was pumped to storage drums and disposed by an EHS (Environmental Health and Safety) assistant.

Chapter 4: Packed Column Results

4.1 Hydraulic

4.1.1 General overview

The packing hydraulic characteristics (pressure drop and liquid hold-up) were determined prior to the mass transfer measurements. The air/water system was used in the hydraulic tests. The gas flow factor (F_G) was chosen as the independent variable since it is theoretically meaningful (Bernoulli equation) and allows for the incorporation of temperature effects (via gas density).

The pressure drop results for Sulzer Mellapak^{TM} 250Y (MP250Y), a standard structured packing with surface area of 250 m^2/m^3, are shown in Figure 4.1. The dry pressure drop increases with gas F-factor to the power of 1.6-1.9. Theoretically, the power should be around 2 based on Bernoulli equation. However, the friction loss reduces the power slightly. Pressure drop increases by 30-40% when irrigated with 5 gpm/ft^2 (12 m^3/m^2*h) liquid flow (compared with dry pressure drop), and increases slightly (5%-10%) as liquid flow rate keeps increasing. In the pre-loading region, irrigated pressure drop increases steadily with gas flow rate to the power of 1.6-2.0, which is similar to the dry pressure drop curve. In the loading region, pressure drop increases dramatically with gas flow rate until flood. The power of pressure drop on F-factor increases from 2.0 to 10.0 in the loading region.

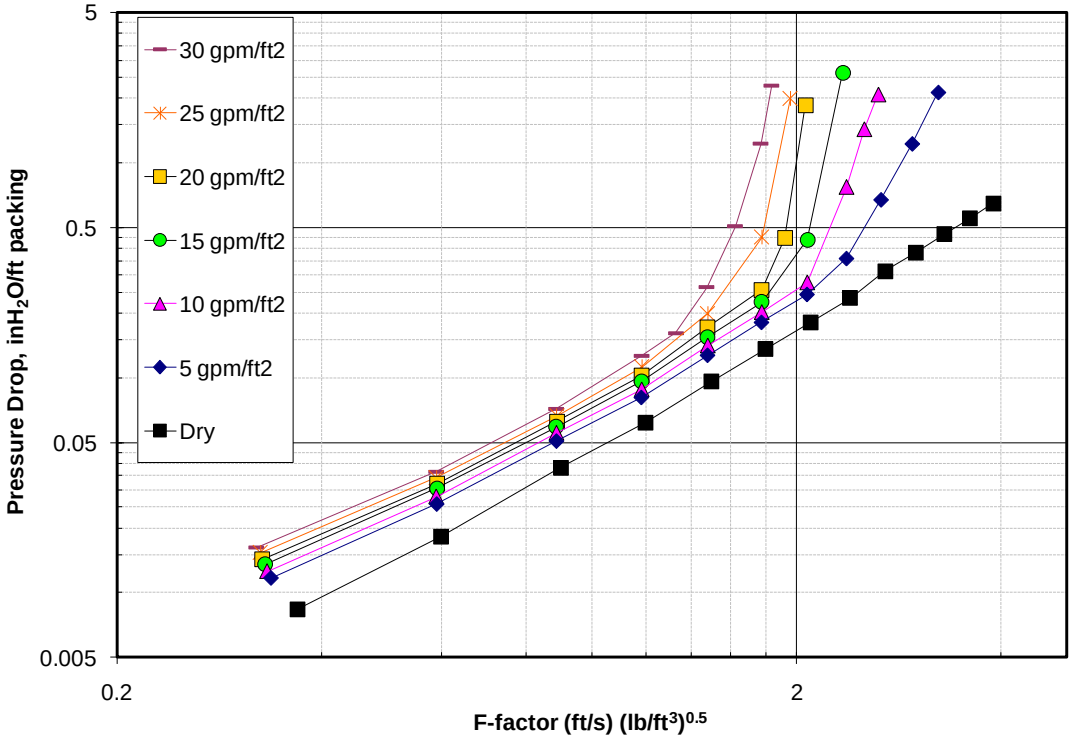

Figure 4.1. Pressure drop results for MP250Y

The fractional liquid hold-up characteristics for Mellapak 250Y are shown in Figure 4.2. Fractional liquid hold-up is the ratio of liquid volume in the packing to the packing void volume. In the pre-loading region, liquid hold-up increases slightly with gas flow rate because the gas and liquid have limited interaction in this region. In the loading region, liquid hold-up increase slightly with gas flow rate until the loading where it increases sharply. The interaction between gas and liquid is quite intensive in the loading region. For a fixed gas rate, the liquid hold-up increases with liquid flow rate. In the pre-loading region, the liquid hold-up for this packing is between 3%-13%, which is within the expected magnitude (1%-15%).

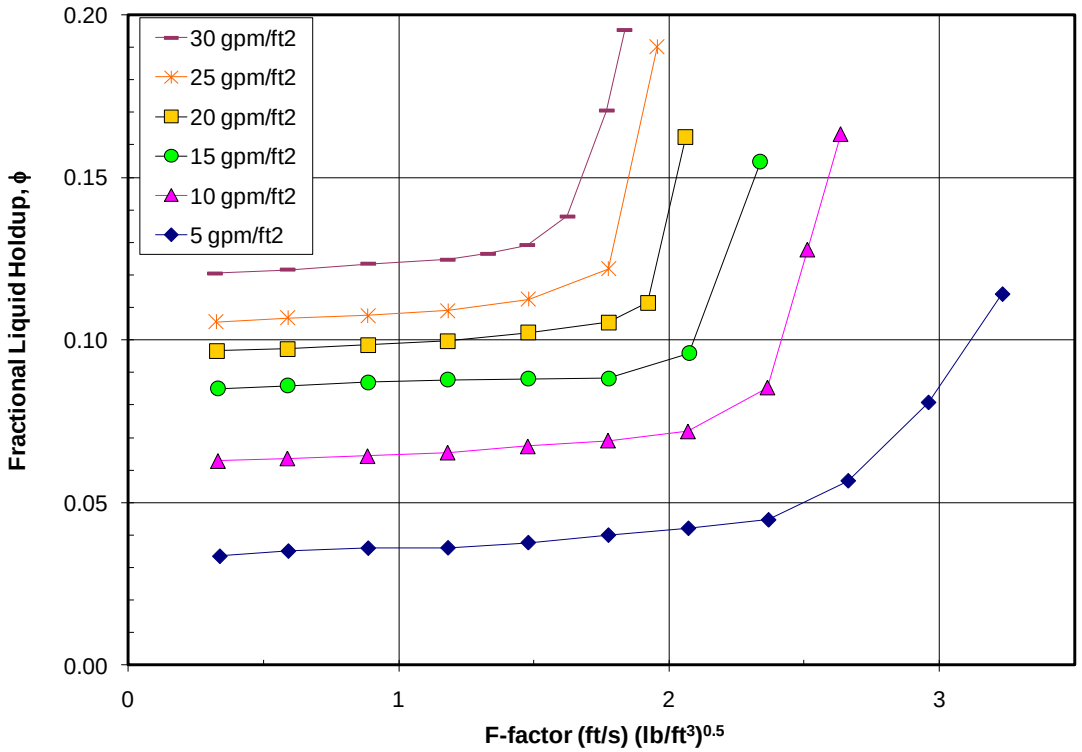

Figure 4.2. Liquid hold-up results for MP250Y

4.1.2 Effect of Packing Surface Area

The dry pressure drop data for four packings with specific area ranging from 125 to 500 m^2/m^3 (Mellapak 125Y, 250Y and GT-PAK™ 350Y, 500Y) are compared in Figure 4.3. Dry pressure drop can be correlated as a function of F-factor (F_G):

$$(DP/Z)_{dry} = C * F_G^n \qquad (4\text{-}1)$$

For each packing, the exponent n varies in a small range (1.75 to 1.88) while the constant C varies with packing specific area (a_P). The dry pressure drop can be expressed by a normalized correlation:

$$\frac{(DP/Z)_{dry}}{a_P} = 0.12 * F_G^{1.81} \qquad (4\text{-}2)$$

Equation (4-2) compares well with the correlation by Tsai (2010) shown in Equation (4-3):

$$\frac{(DP/Z)_{dry}}{a_P} = 0.125 * F_G^{1.84} \qquad (4\text{-}3)$$

There is a very small difference in the constant and the exponent which is expected considering experimental error and the difference of the database.

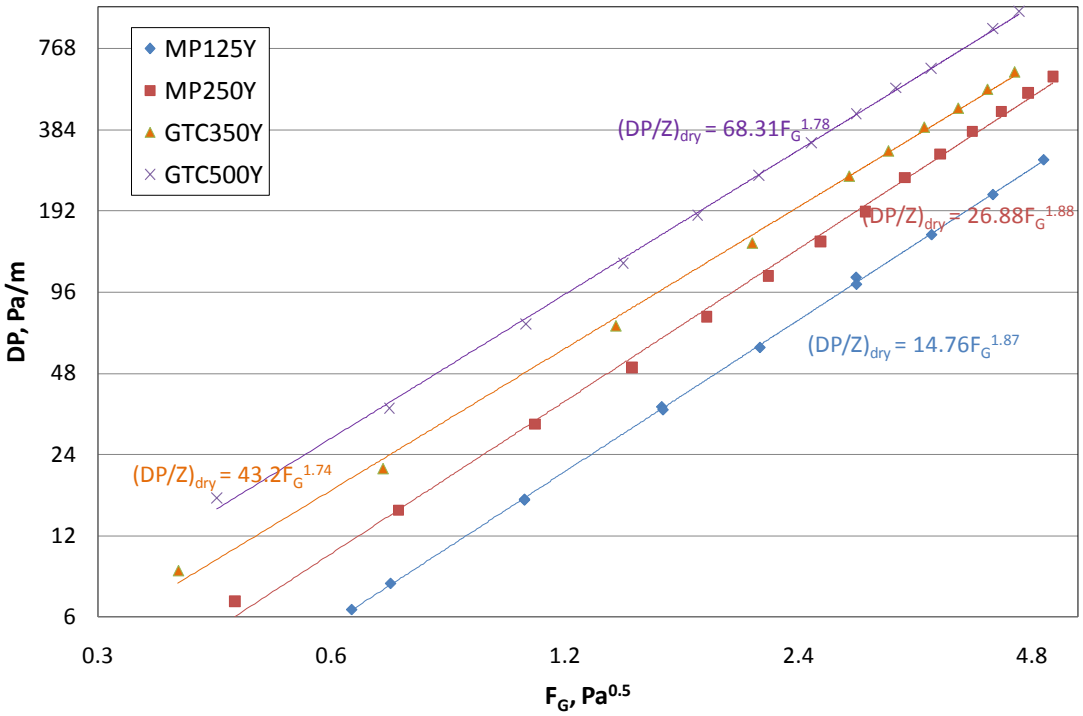

Figure 4.3. Dry pressure drop comparison

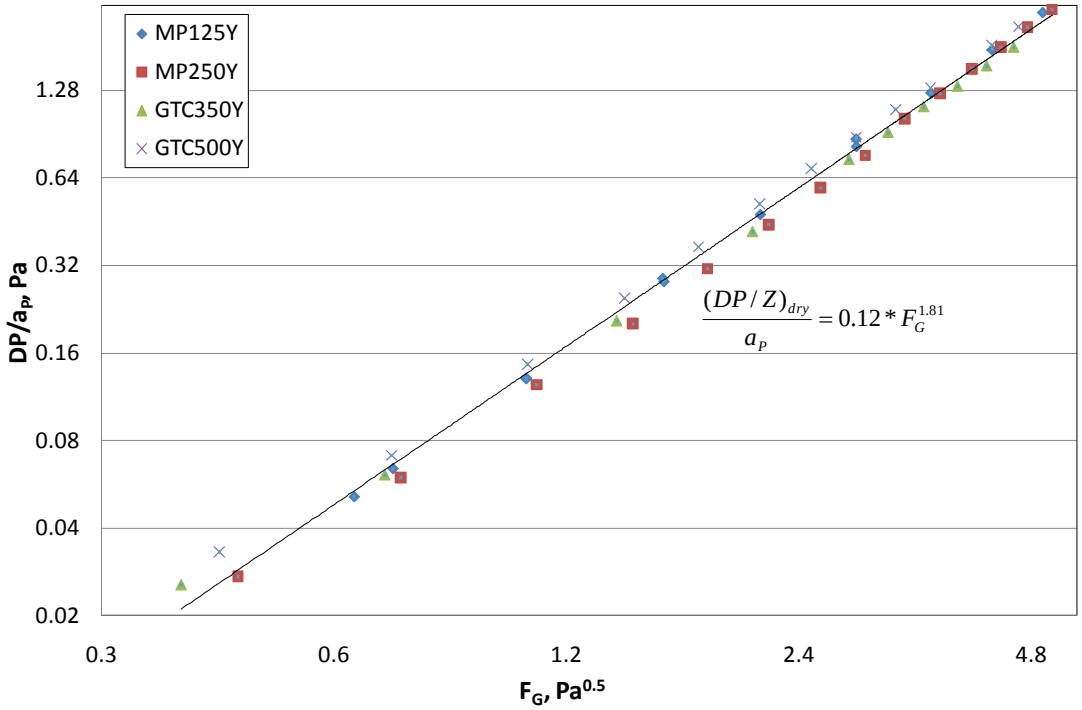

Figure 4.4. Normalized dry pressure drop

Irrigated pressure drop data (liquid flow rate at 24.4 m^3/m^2*h or 10 gpm/ft^2) are shown in Figure 4.5. The data are normalized by dividing pressure drop of packing MP250Y at the same condition. For each packing, normalized pressure drop is quite stable till flood. The capacity difference between the packings is shown, with MP500Y exhibiting a much earlier onset to flooding (F_G ~ 1.7 $Pa^{0.5}$) compared to MP125Y (F_G ~ 3.9 $Pa^{0.5}$). In the preloading region, the normalized pressure drop increases with packing specific area (MP125Y ~ 0.68, MP250Y ~ 1.45, GT-PAK™ 350Y~ 2.08, GT-PAK™ 500Y ~ 4.31), but the ratio is not constant. For high surface area packing, the value is higher than expected since resistance for gas and liquid flow is much higher.

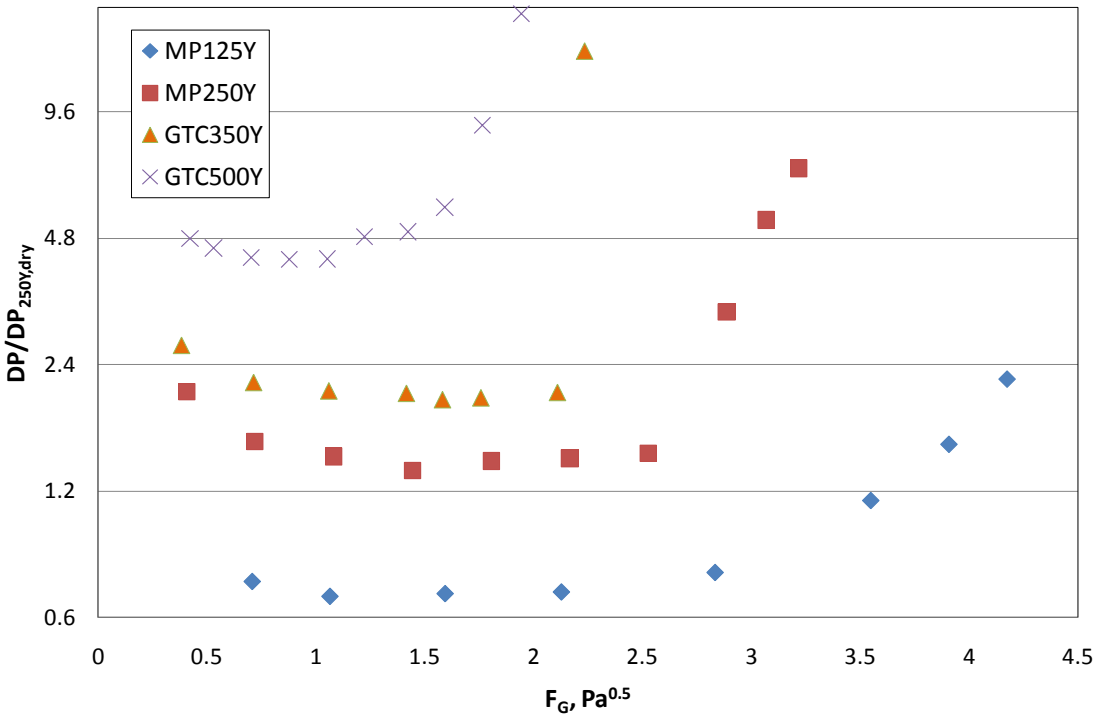

Figure 4.5. Normalized irrigated pressure drop at liquid load of 24.4 m^3/m^2*h

A comparison of liquid hold-up of these four packings is shown in Figure 4.6. The capacity difference between packings is also evident in this plot (MP125Y the largest capacity and GT-PAK™ 500Y the smallest capacity). Liquid hold-up increases with packing specific area but the relative value decreases (MP125Y ~ 3%, MP250Y ~ 6%, GT-PAK™ 350Y ~ 8%, GT-PAK™ 500Y ~ 9%). This can be explained for two reasons. One, the larger surface area packing is packed more intensively with higher resistance for liquid flowing down than smaller surface area packing which is why liquid hold-up increases with packing surface area. Two, the larger surface area packing has less void space for liquid to fill which is why the increasing ratio decreases.

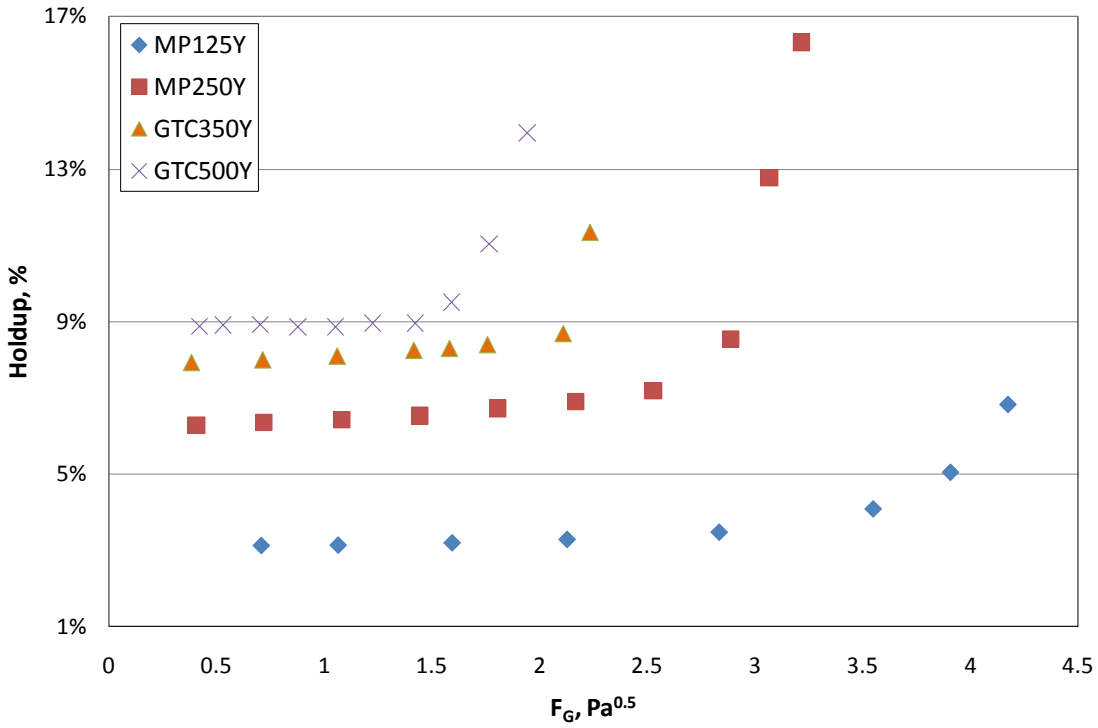

Figure 4.6. Liquid hold-up comparison at liquid load of 24.4 m^3/m^2*h

4.1.3 Effect of Packing Corrugation Angle

Besides the packing specific area, another factor that will influence the hydraulic performance of the packing is the corrugation angle. Figure 4.7 shows the normalized dry pressure drop of two pairs of packing: MP250Y/X and GT-PAK™ 350Y/Z. An increase in the corrugation angle will result in a significant reduction in pressure drop. A 51% pressure drop reduction is observed for the MP250X relative to MP250Y and 64% from GT-PAK™ 350Y to 350Z. The ratio is also maintained in the irrigated conditions (24.4 m^3/m^2*h or 10 gpm/ft^2) as shown in Figure 4.8 where pressure drop is reduced by 60% from MP250Y to MP250X and 68% from GT-PAK™ 350Y to 350Z. A larger increase in corrugation angle also causes a larger reduction in fractional liquid hold-up, though the difference is not as significant. Liquid hold-up comparisons of MP250Y/X and GT-PAK™ 350Y/Z are shown in Figure 4.9. Similar with pressure drop, liquid hold-up decreases as packing corrugation angle increases.

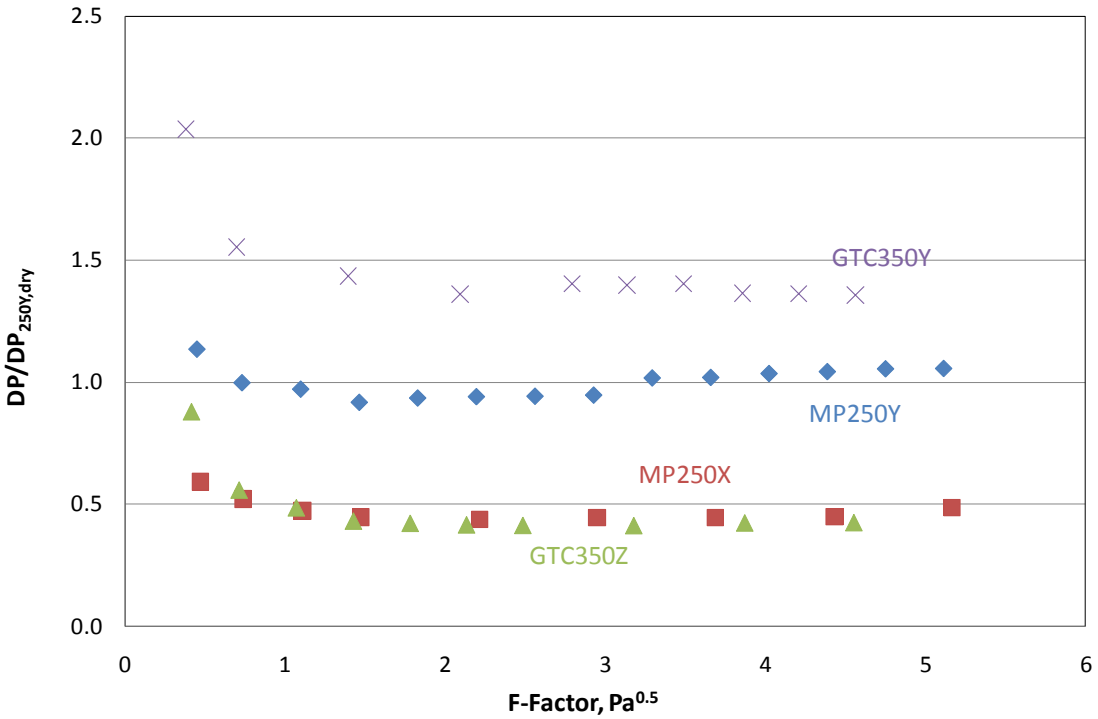

Figure 4.7. Normalized dry pressure drop of MP250Y/X, GT-PAK™ 350Y/Z

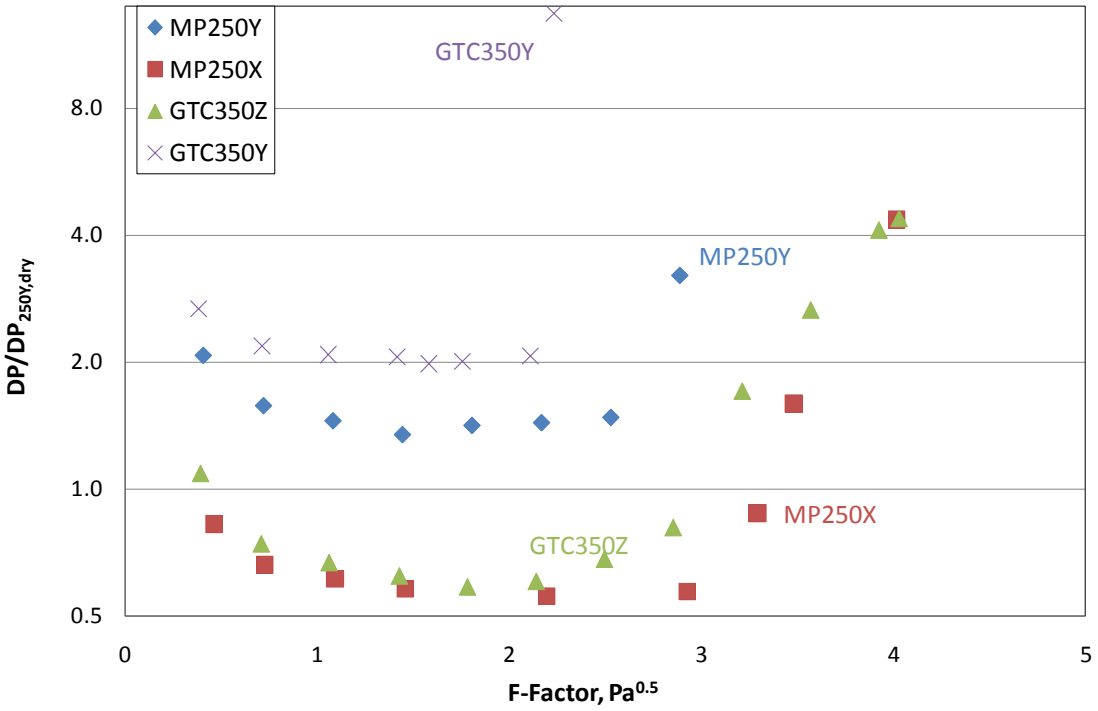

Figure 4.8. Normalized irrigated pressure drop of MP250Y/X, GT-PAK™ 350Y/Z at a liquid load of 24.4 m^3/m^2*h (10 gpm/ft^2)

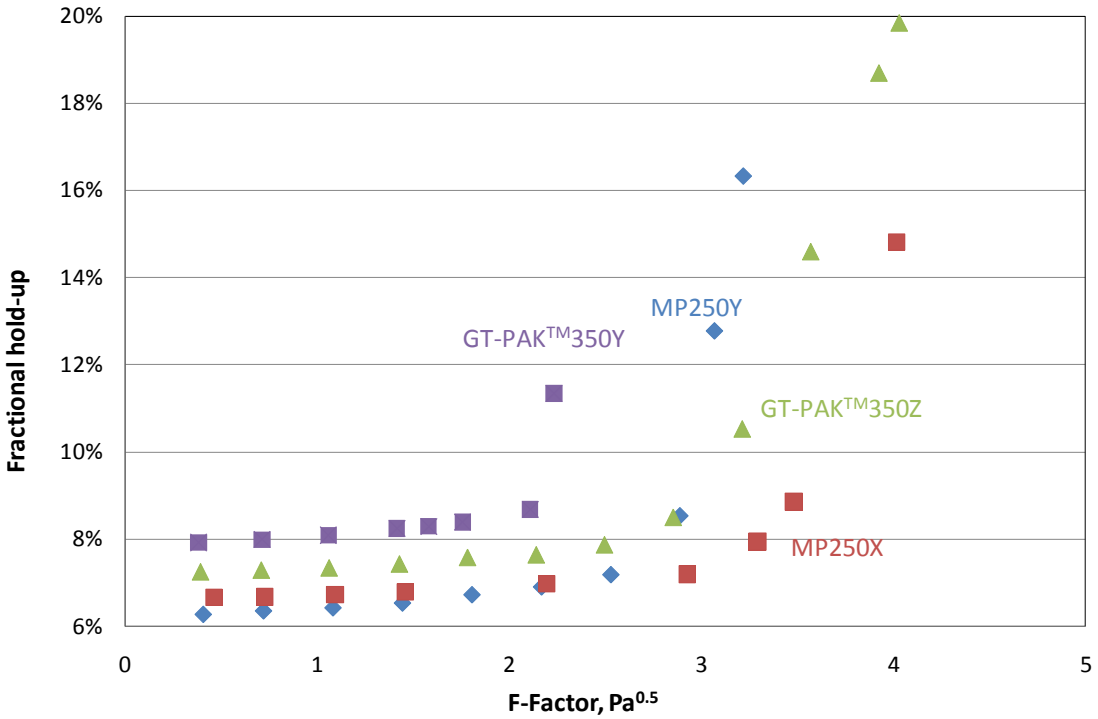

Figure 4.9. Liquid hold-up of MP250Y/X, GT-PAK™ 350Y/Z at a liquid load of 24.4 m^3/m^2*h (10 gpm/ft^2)

4.1.4 Effect of Packing Nominal Size (Random packing)

Several random packings were also studied in this work. For random packings, nominal size is the equivalent packing diameter that can describe the packing piece Larger nominal size packings have a higher void fraction and thus smaller specific area per volume. Figure 4.10 illustrates nominal size influence on dry pressure drop. Three packings with different nominal sizes are compared. The characteristics are listed in Table 4.1. Similar with larger surface area structured packings, the lower void fraction and larger resistance for liquid and gas flow, promote a higher pressure drop. Normalized pressure drop increases as a ratio of packing specific area (RSR#0.7 ~ 1.2, RSR#0.5 ~ 3.0, RSR#0.3 ~ 4.1). Irrigated pressure drop follows this trend (Figure 4.11) but the ratio is higher. The fractional liquid hold-up characteristics are compared in Figure 4.12. Liquid hold-up decreases as nominal size increases (packing specific area decreases). Packing capacity increases as nominal size increases. However, the difference between RSR#0.3 and #0.5 is not quite significant.

Table 4.1. Characteristics of Raschig Super Rings

	Nominal size	Void fraction	Specific area, a_P
	mm	%	m^2/m^3
RSR#0.3	15	96	315
RSR#0.5	20	97	250
RSR#0.7	25	98	180

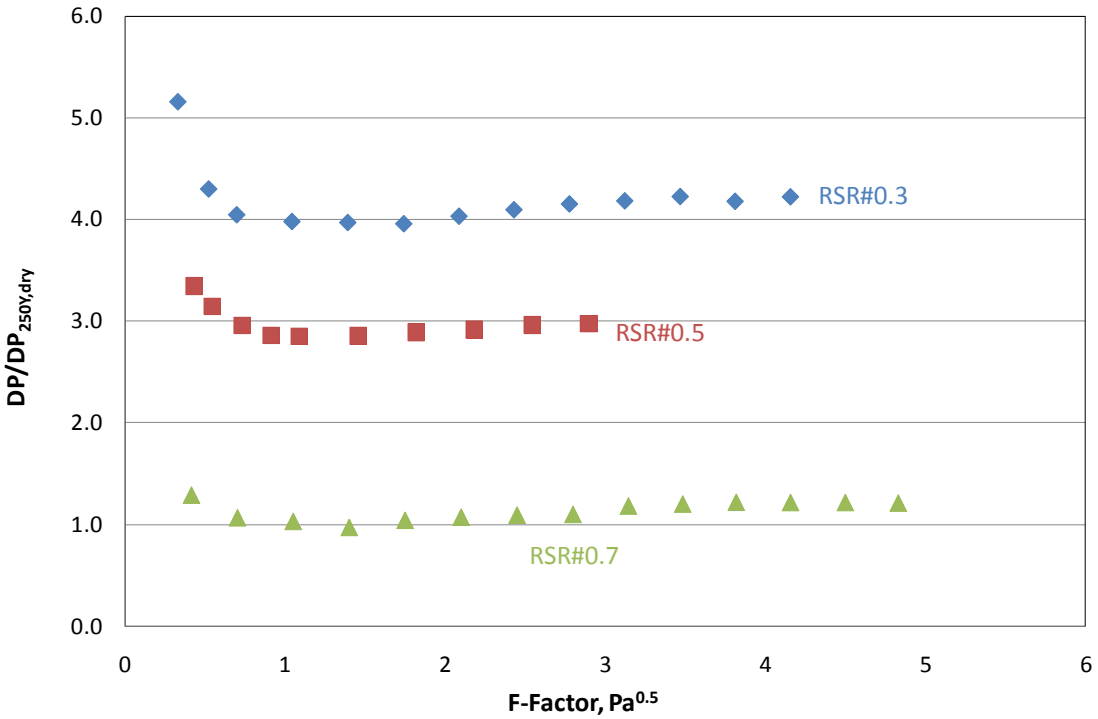

Figure 4.10. Normalized dry pressure drop of RSR#0.3, #0.5, #0.7

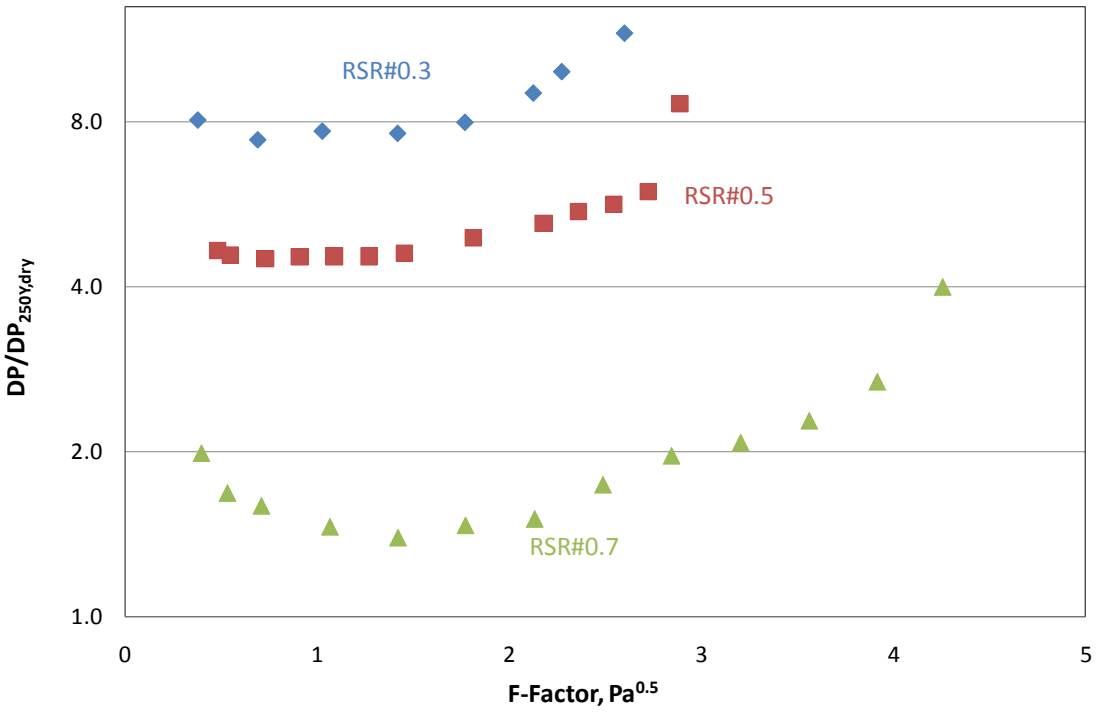

Figure 4.11. Normalized irrigated pressure drop of RSR#0.3, #0.5, #0.7 at liquid load of 24.4 m^3/m^2*h (10 gpm/ft^2)

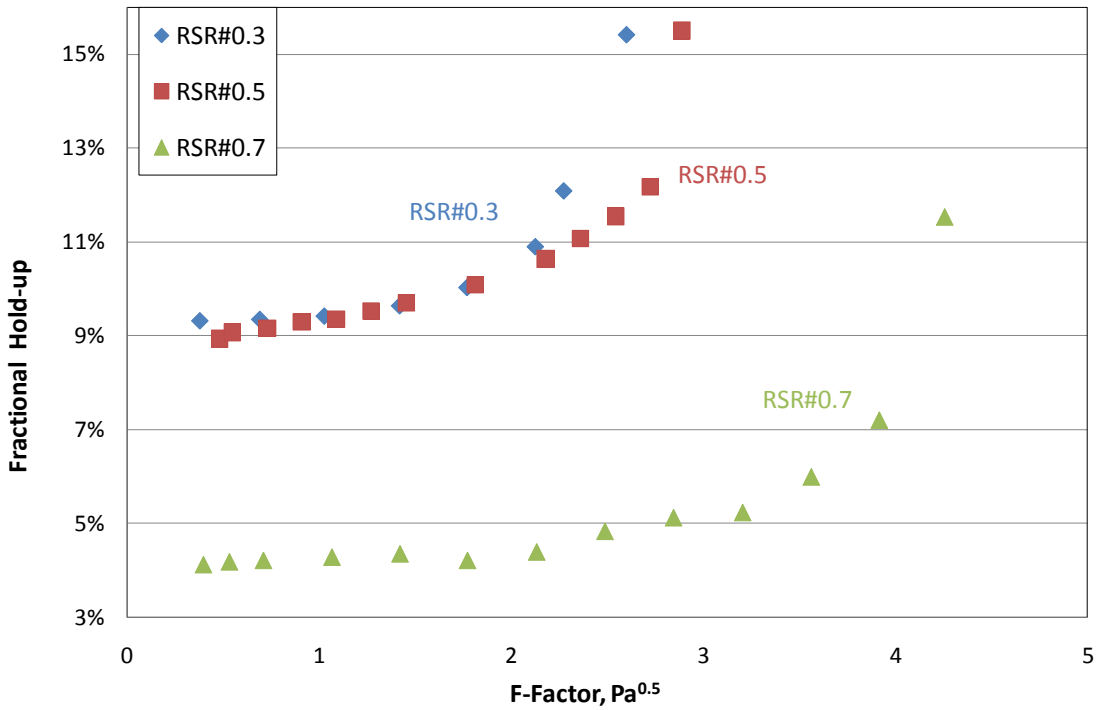

Figure 4.12. Fractional liquid hold-up of RSR#0.3, #0.5, #0.7

4.2 Mass Transfer Area

4.2.1 Effect of Gas and Liquid velocities

The first mass transfer property explored is the effective packing mass transfer area (effective area). Figure 4.13 shows the effective area measured at different gas and liquid velocities for MP250Y. The effective area increases with liquid velocity to 0.15 power for all gas velocities. The effective area increases by about 9% when gas velocity increases from 0.59 m/s to 1.48 m/s, and increases by 2-3% as gas velocity keeps increasing until flood. All other packings show similar results, where the effective area is a function of liquid velocity and a slight function of gas velocity.

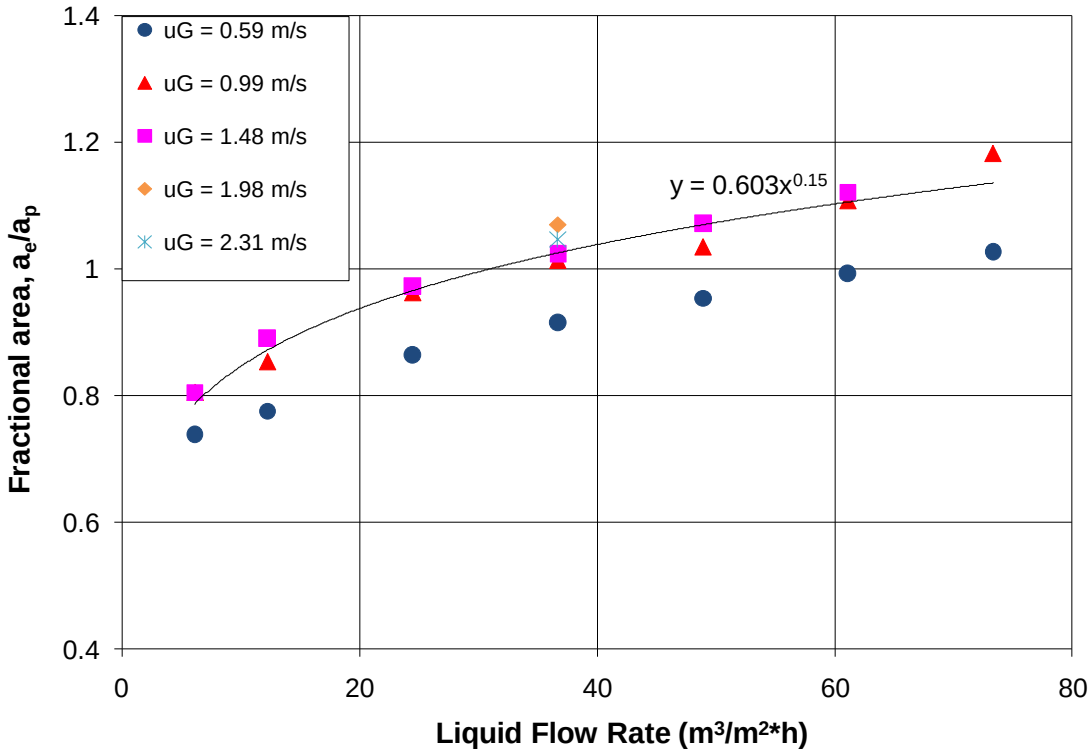

Figure 4.13. Fractional effective area of MP250Y

4.2.2 Effect of Packing Surface Area

The effective area of four structured packings with identical corrugation angles (45 degree) and surface area ranging from 125 to 500 m^2/m^3 are compared in Figure 4.14. The gas velocity is 0.99 m/s (300 ACFM) for all packings. Every packing shows an increase in effective area with increasing liquid load which confirms the conclusion in the previous section. At the same liquid load, the effective area increases with packing surface area. However, the effective area increases at a smaller ratio than the packing surface area increases. The effective area of 250Y is 43% greater than 125Y, which is less than the 50% difference between the surface areas. The effective area of 500Y is 14% greater than 350Y which is less than the 30% surface area difference. The phenomenon of lower specific surface area packing providing higher fractional effective area is illustrated in Figure 4.15. Rivulets, ripples, and droplets formation between the sheets, those mass-transfer-enhancing film instabilities (Henriques de Brito, 1994), are easily formed in coarser packings with high void fraction. End effects and wall effects could also have a relative higher impact on coarser packings. Finer packings such as 350Y and 500Y could be more subject to maldistribution and insufficient wetting, causing a relative lower fractional effective area.

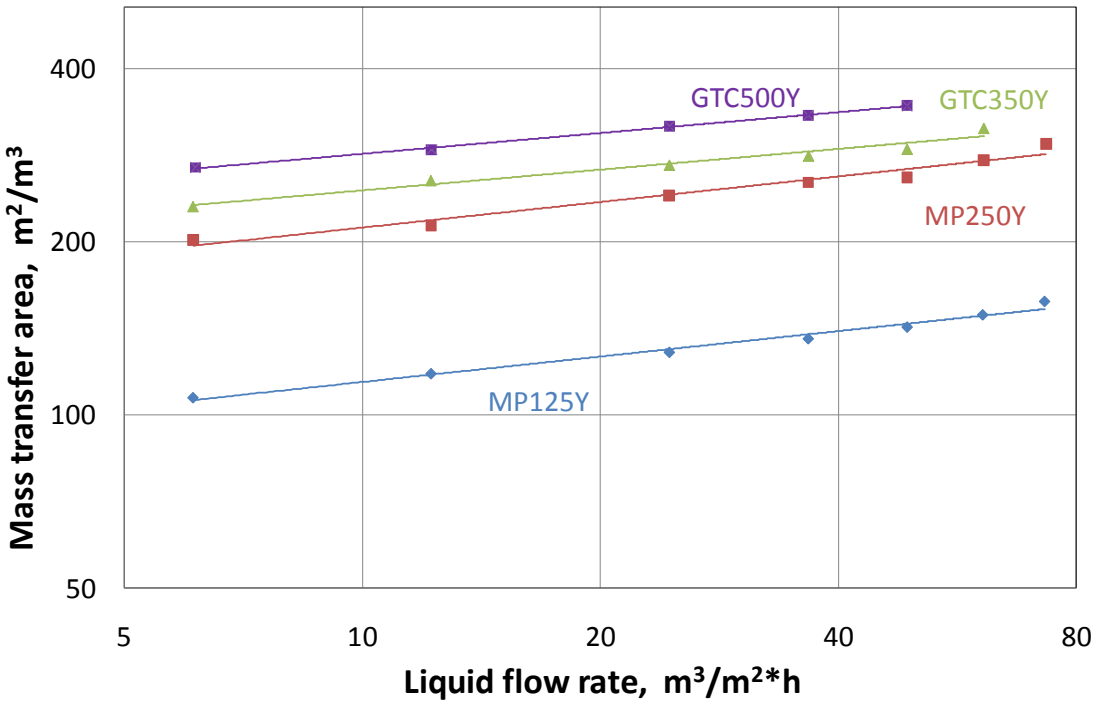

Figure 4.14. Mass transfer area comparison between 125Y, 250Y, 350Y, 500Y

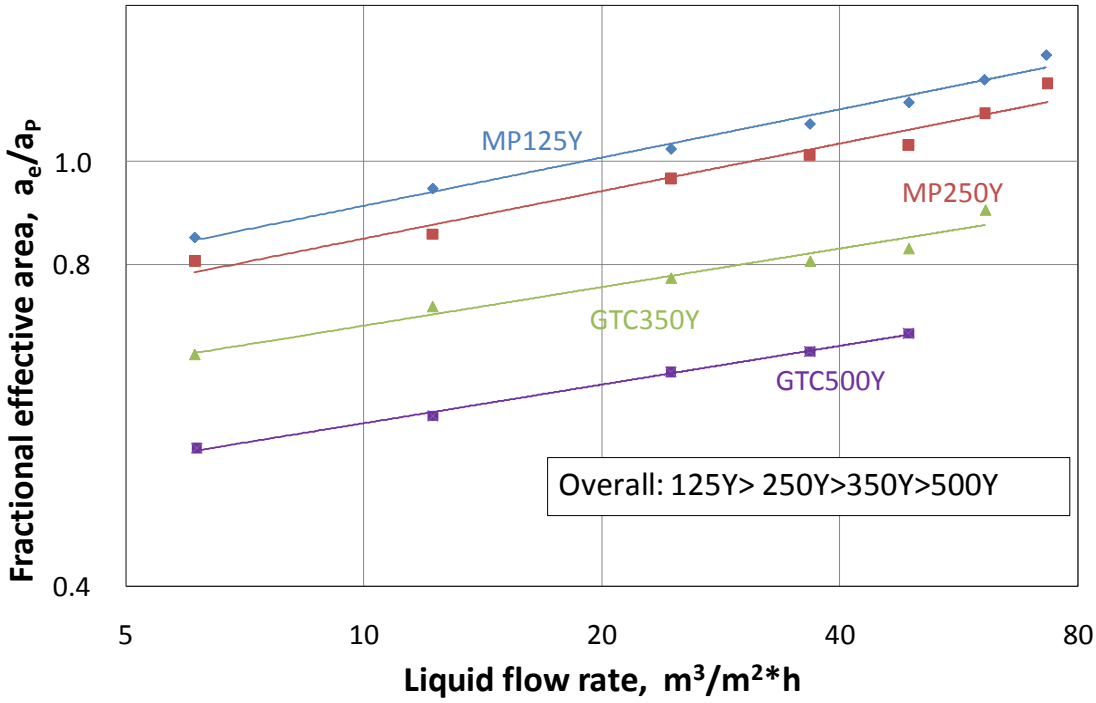

Figure 4.15. Fractional effective area comparison between 125Y, 250Y, 350Y, 500Y

4.2.3 Effect of Packing Corrugation Angle

The effective areas of MP250Y and 250X are compared in Figure 4.16. MP250X has an equivalent specific surface area and geometric structure except for its higher corrugation angle (60 degree) relative with MP250Y (45 degree). The solid dots are experimental data measured at all three gas velocities (0.6 m/s, 0.99 m/s, 1.48 m/s) and the solid lines are trend lines of experimental data. The measured effective area of MP250Y is 6% higher than MP250X. However, this difference is insufficient to distinguish from the experimental error. These two packings are assumed to have the same effective area.

A similar conclusion is also found in the comparison between GT-PAK™ 350Y/Z (Figure 4.17). These two packings have an equivalent surface area and geometric structure except for the corrugation angle. GT-PAK™ 350Y has a 45 degree corrugation angle while 350Z has a 70 degree angle. The difference of measured effective area between these two packings is 7%, which is still within the 10% experimental noise range.

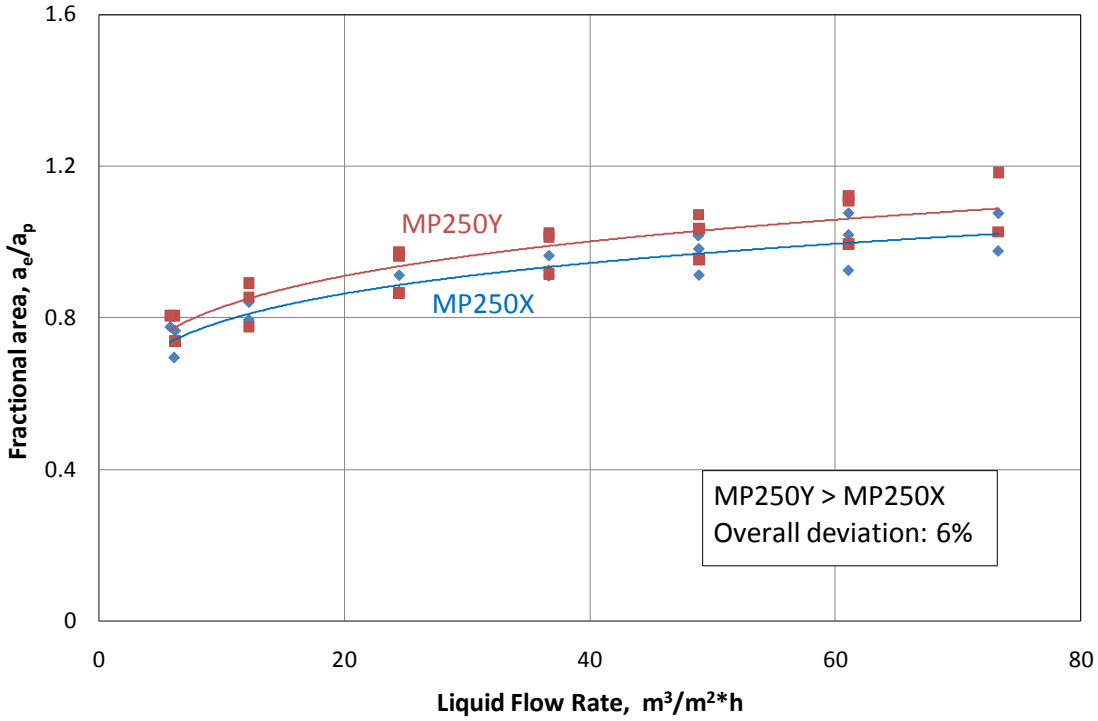

Figure 4.16. Fractional effective area comparison between MP250Y/X

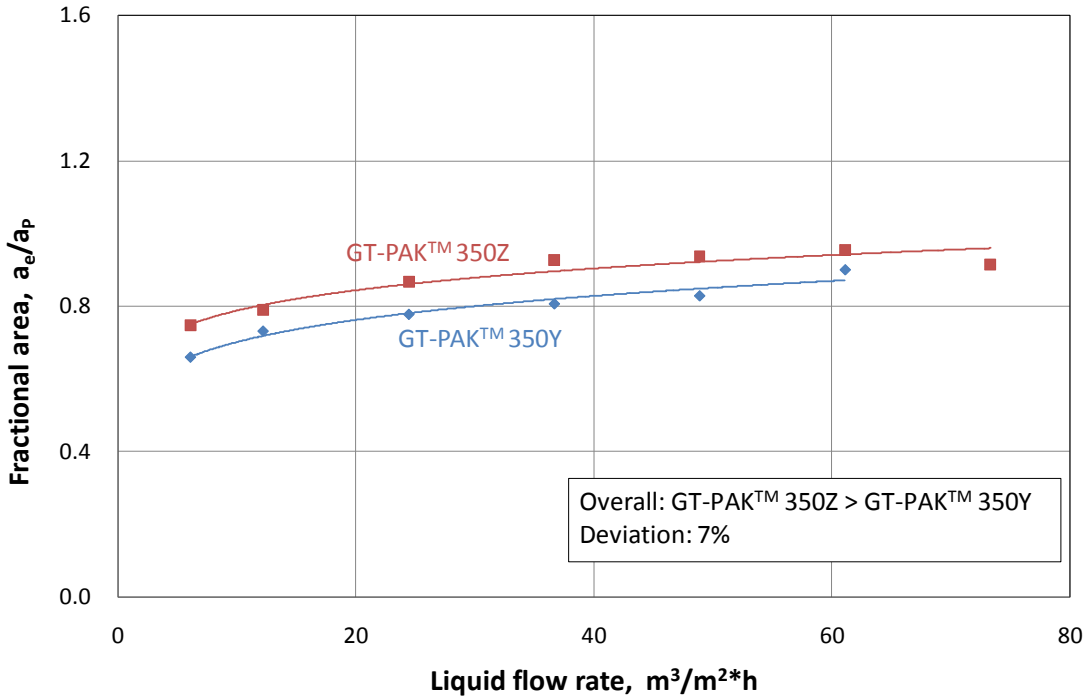

Figure 4.17. Fractional effective area comparison between GT-PAK™ 350Y/Z

The conclusion that the corrugation angle has little impact on the effective area was also confirmed by a previous University of Texas researcher (Tsai, 2010). It is believed that effective area is determined by the wettability of the packing surface. Thus, the effective area would be influenced by: (1) the surface tension which determines the contact angle of liquid and packing surface; and (2) the liquid phase Reynolds number which determines the liquid flow pattern. Other factors such as gas velocity, liquid viscosity, and packing corrugation angle would not have a significant impact on effective area. The effective area model is composed by these influencing factors and would be further discussed in Chapter 5.

4.2.4 Effect of Packing Packing Nominal Size (Random packing)

The effective areas of three Raschig Super Rings (RSR#0.3, 0.5, 0.7) with different nominal sizes are compared in Figure 4.18. The effective area increases as packing nominal size decreases (packing surface area increases). Similar with structured packing, the effective area of Raschig Super Rings increases at a smaller ratio than the surface area increases. The effective area of RSR#0.3 is 11% greater than RSR#0.5, which is less than the 19% difference between the surface areas. The effective area of RSR#0.5 is 6% higher than RSR#0.7, which is less than the 28% surface area difference. Considering fractional effective area, the large nominal size packing (RSR#0.7) has larger fractional area than small nominal size packing (RSR#0.5, 0.3) as shown in in Figure 4.19. Mass-transfer-enhancing film instabilities such as rivulets, ripples, and droplets which form easily between the sheets in large nominal size packing contribute to the mass transfer area.

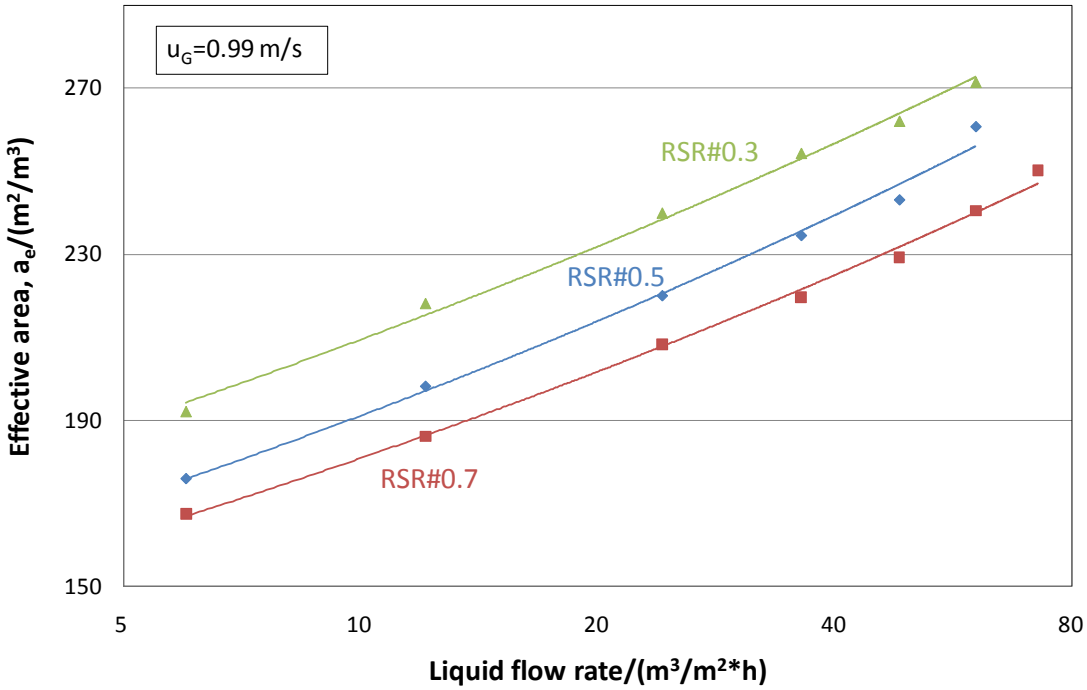

Figure 4.18. Effective area comparison between RSR#0.3, 0.5, 0.7

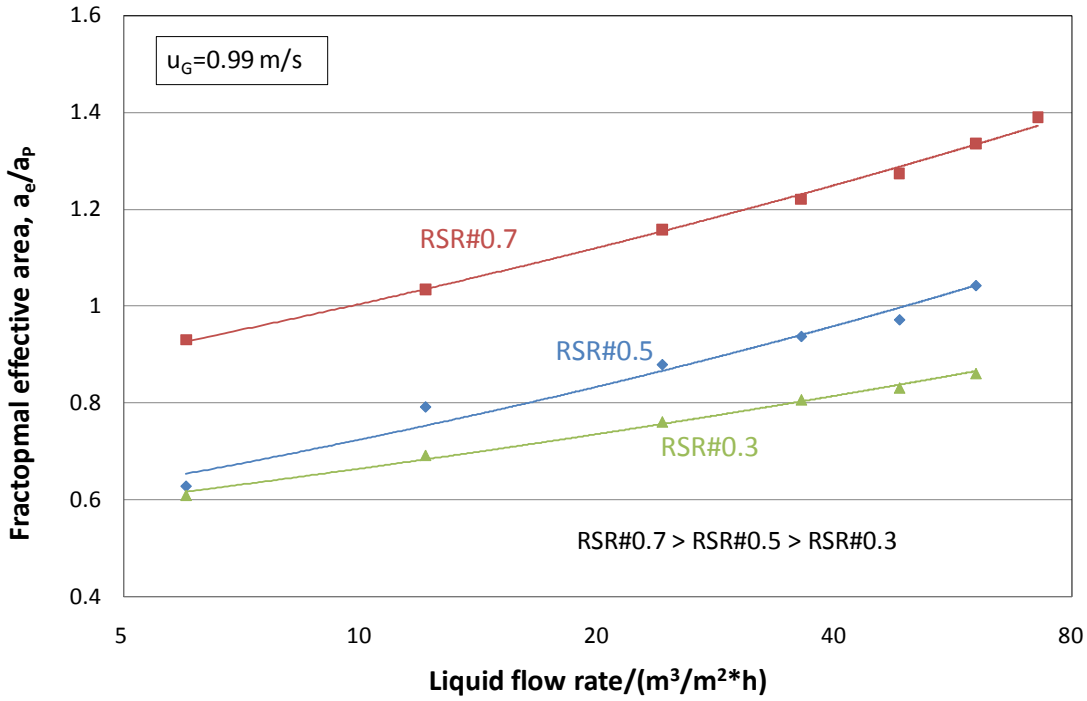

Figure 4.19. Fractional effective area comparison between RSR#0.3, 0.5, 0.7

4.2.5 Effective area summary

The effective area results are summarized in Figure 4.20 at moderate liquid and gas flow rate (0.99 m/s for gas velocity and 24.4 m/h for liquid velocity). In this work,

three types of packings were measured: Structured packing (blue points), hybrid packing (green points), and random packing (red points). For all packings, the fractional effective area decreases with packing surface area (decreasing ratio distinct between packing types). For structured packings, the fractional effective area barely changes with packing corrugation angle. The solid line in Figure 4.20 shows the area model developed in this work, which will be discussed in Chapter 5.

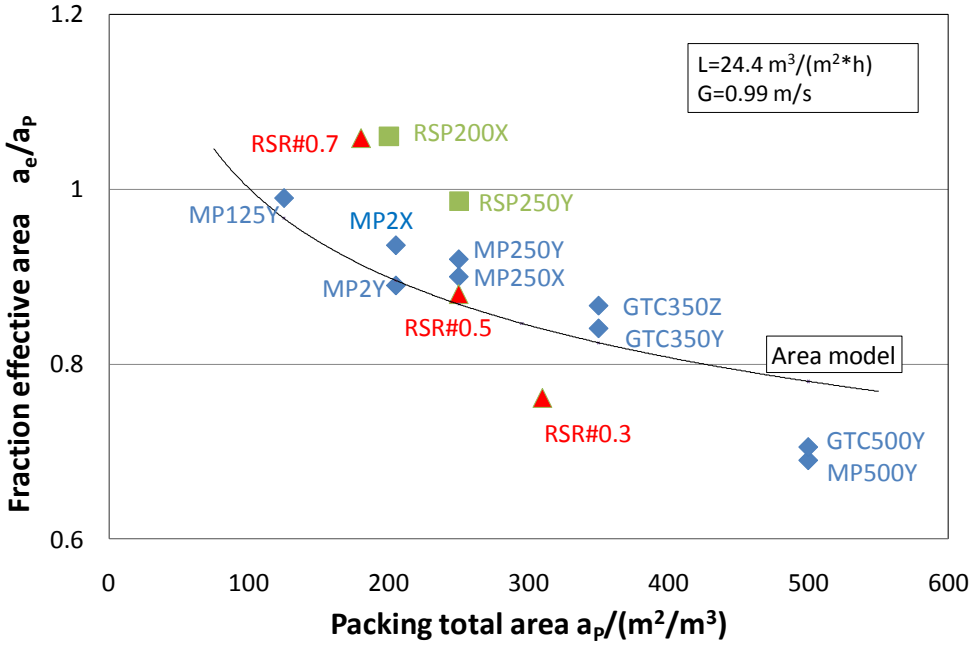

Figure 4.20. Fractional effective area summary

4.3 Liquid and Gas Film mass transfer coefficients (k_L and k_G)

4.3.1 Effect of Gas and Liquid velocities

Figure 4.21 shows the liquid film mass transfer coefficient measured at different gas and liquid velocities for GT-PAK™ 350Y. The liquid film mass transfer coefficient (k_L) increases with liquid velocity to 0.71 power. The effective area increases about 2% when gas velocity increases from 0.59 m/s to 0.99 m/s, and increases by 3% from 0.99 m/s to 1.48 m/s. All other packings show similar results, which is that liquid film mass transfer coefficient is a function of liquid velocity and essentially independent of gas velocity.

Figure 4.22 shows the gas film mass transfer coefficient for MP250Y. The gas film mass transfer coefficient (k_G) increases with gas velocity to 0.61 power while it barely changes with liquid velocity. For safety, environmental and cost concerns, only a few data points were repeated at different liquid velocities to minimize unnecessary SO_2 scrubbing experiments.

Results show that k_L is only a function of liquid velocity and k_G is only a function of gas velocity. It is because k_L relates to the mass transfer in the bulk liquid phase, and it should not be influenced by the gas flow. As for k_G, it should only be influenced by the turbulence in the bulk phase of gas, and not be influenced by the liquid flow.

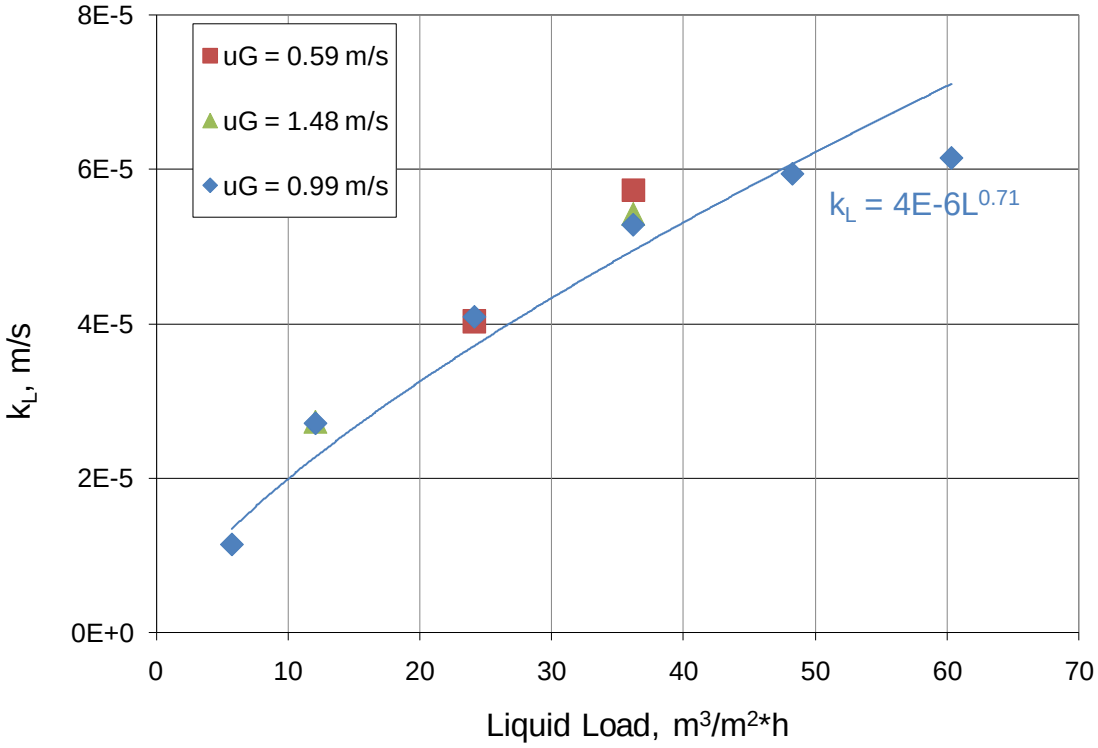

Figure 4.21. Liquid film mass transfer coefficient of GT-PAK™ 350Y

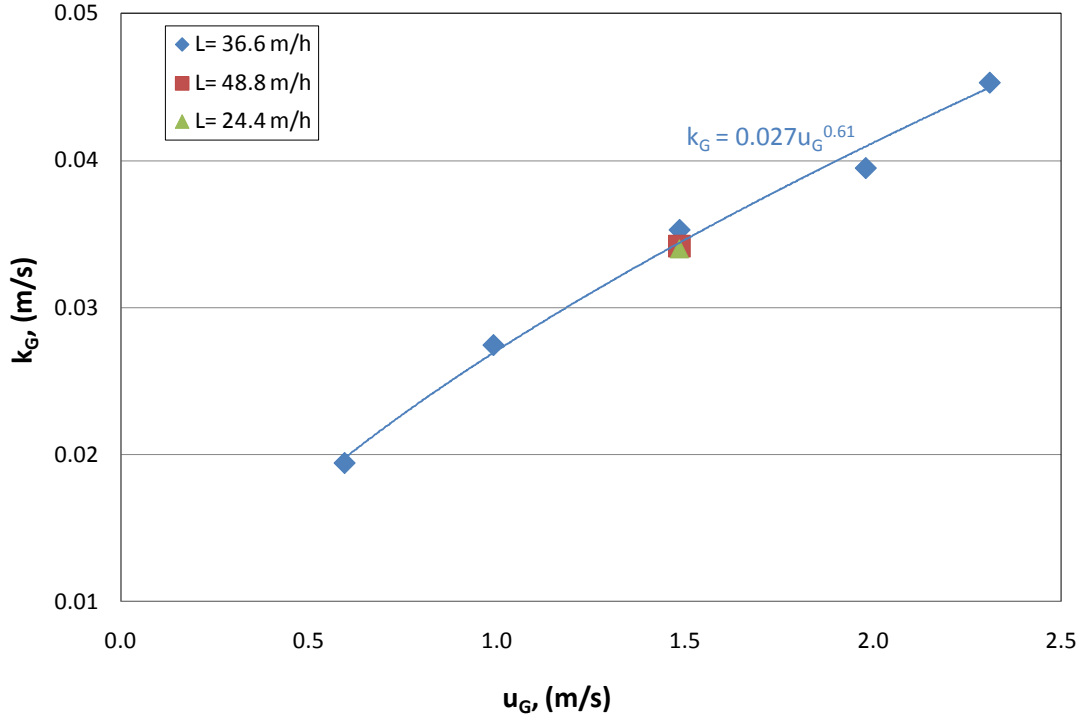

Figure 4.22. Gas film mass transfer coefficient of MP250Y

4.3.2 Effect of Packing Surface Area

Liquid film mass transfer coefficients of packings with same corrugation angle (45 degree) but different surface area (250, 350, 500 m^2/m^3) are compared in Figure 4.23. For all packings, the k_L value increases with liquid velocity which is consistent with the conclusion in Section 4.3.1. At the same gas and liquid flow rate, the k_L value increases as surface area increases. In general, the k_L value of 500Y is 33% higher than 350Y, and the k_L value of 350Y is 21% higher than 250Y. These differences are higher than the anticipated experimental error of 10%.

A similar conclusion is found when comparing the gas film mass transfer coefficient of packings with different surface areas (Figure 4.24). At similar gas and liquid flow rates, the k_G value of 500Y is 23% higher than 350Y, and the k_G value of 350Y is 22% higher than 250Y. The difference between 250Y and 125Y is negligible (only 3%) since there could be extra bubbles, ripples creating mass transfer in the low specific area packing like 125Y.

In general, both k_L and k_G increase with surface area. This tendency is also true for random packings (Section 4.3.5). To understand this phenomenon, the packing geometry is studied and a new concept is proposed in Section 4.3.4.

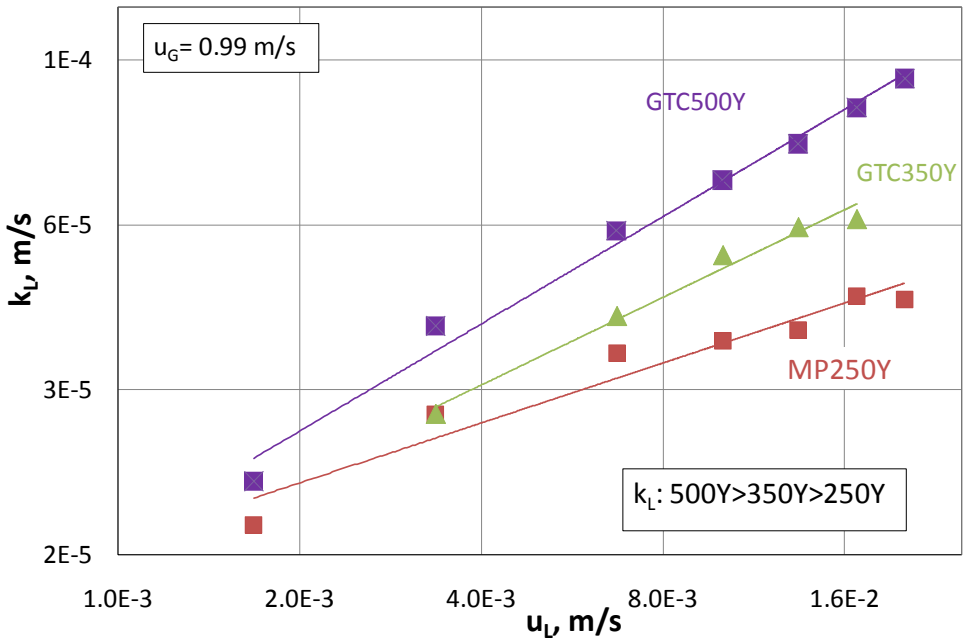

Figure 4.23. k_L comparison between 250Y, 350Y, 500Y

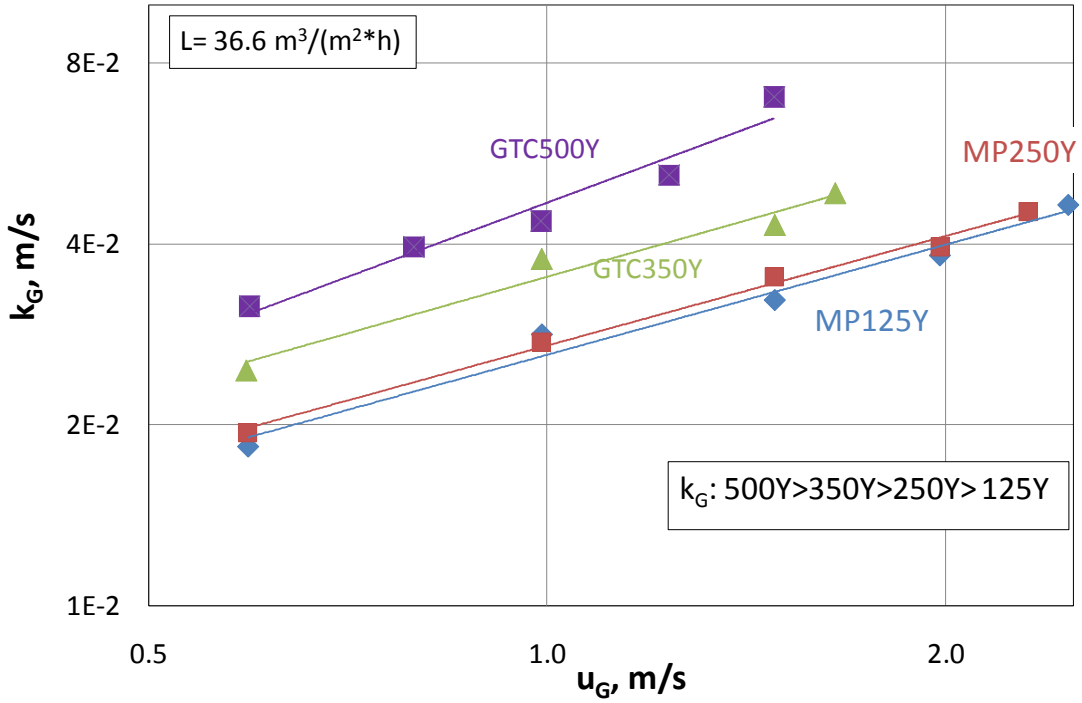

Figure 4.24. k_G comparison between 125Y, 250Y, 350Y, 500Y

4.3.3 Effect of Packing Corrugation Angle

The liquid film and gas film mass transfer coefficients (k_L and k_G) for two packings with the same surface area but different corrugation angles (GT-PAK™ 350Y and 350Z) are compared in Figure 4.25 and Figure 4.26. At the same liquid and gas flow rate, both k_L and k_G increase as corrugation angle decreases from 70 degree to 45 degree (350Z to 350Y). The mass transfer coefficient difference between these two packings is between 25% to 35%, which is not negligible. This result is consistent with previous work. Olujic and Fair (2000) reported that Montz B1-250Y (45 degree) had a 20% lower HETP than Montz B1-250X (60 degree). Rocha et al. (1996) also predicted the 45 degree packing to have a 15 to 20% greater gas and liquid film mass transfer coefficients than the 60 degree packing based on distillation data measured by the Separations Research Program at The University of Texas. Considering the previous result where the effective mass transfer area is independent of corrugation angle, it can be interpreted that the increase in the HETP from 60 degree packing to 45 degree packing is entirely attributable to a higher mass transfer coefficient.

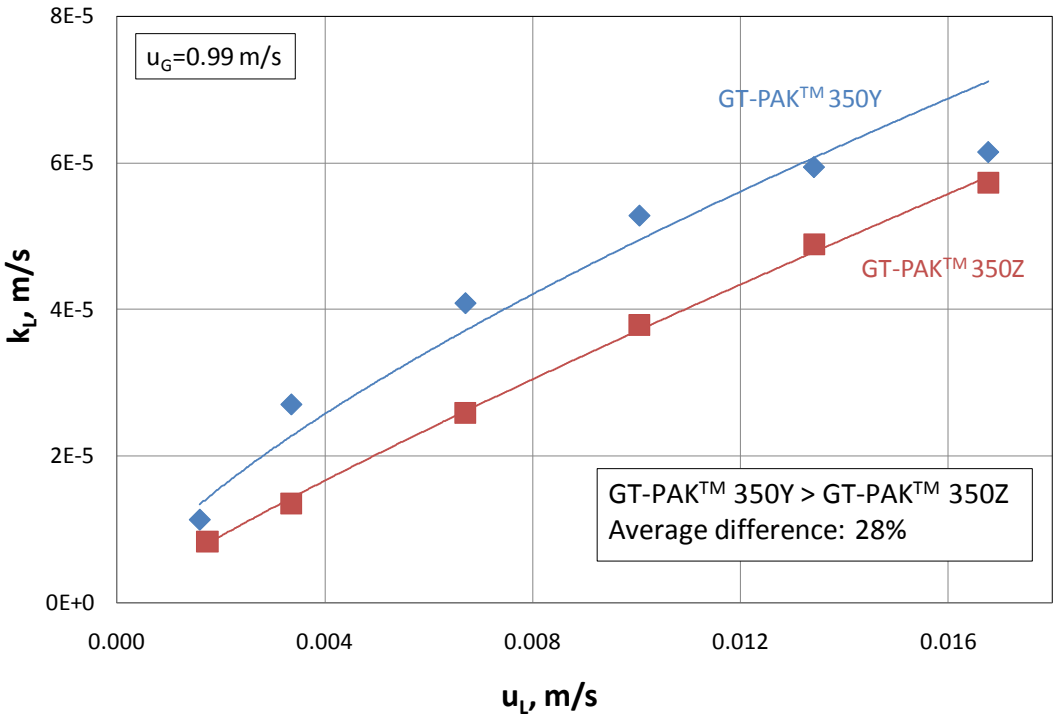

Figure 4.25. k_L comparison between GT-PAK™ 350Y and 350Z

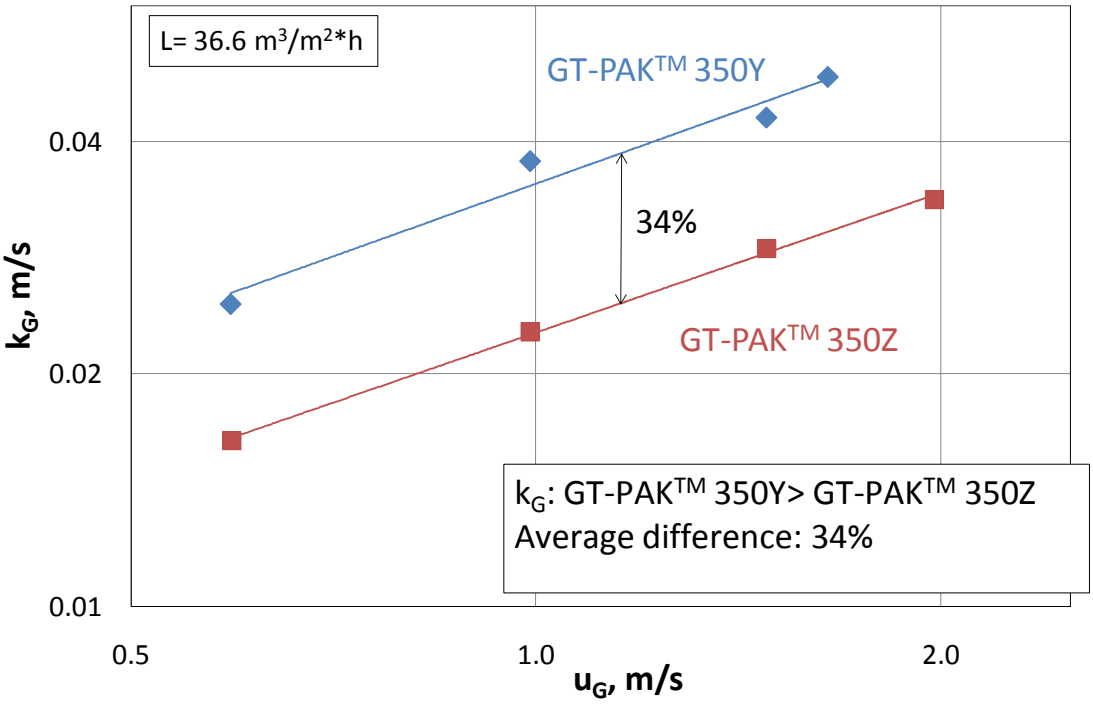

Figure 4.26. k_G comparison between GT-PAK™ 350Y and 350Z

4.4 Conclusions

In this chapter, the effects of operating conditions and packing geometries on hydraulic properties and mass transfer performance were explored. The pressure drop increases steadily with gas flow rate (F-factor) to the power of 1.6-1.9. The pressure drop increases by 30% from dry condition to a liquid load of 5 gpm/ft^2 (12 m^3/m^2*h), and increases slightly with increasing liquid flow rate. The liquid hold-up increases slightly with gas flow rate in the pre-loading region, and increases sharply with gas flow rate in the loading region until flood. Liquid hold-up increases with liquid flow rate at the constant gas flow rate. Both pressure drop and liquid hold-up increase with packing surface area and decrease with packing corrugation angle.

The effective mass transfer area increases with liquid velocity to the 0.15 power and is essentially independent of gas velocity. The fractional effective area decreases as packing surface area increases because of the inefficient wetting in the higher specific surface area packings. Rivulets, ripples, and droplets also provide additional mass transfer area in lower specific surface area packings. The effective mass transfer area is not a function of packing corrugation angle.

The liquid film mass transfer coefficient (k_L) is a function of liquid velocity and independent of gas velocity. Oppositely, the gas film mass transfer coefficient (k_G) is a function of gas velocity and independent of liquid velocity. The k_L increases with liquid velocity (u_L) to the power of 0.5-0.77 for all packings in this work. The k_G increases with liquid velocity (u_G) to the power of 0.43-0.76 for all packings in this work. Summaries of k_L and k_G are given in Figure 4.27 and 4.28.

Packing geometries have similar effects on k_L and k_G. Both k_L and k_G increases as packing surface area increases and decreases as corrugation angle increases. In the next chapter, studies on packing geometries are conducted to understand this phenomenon.

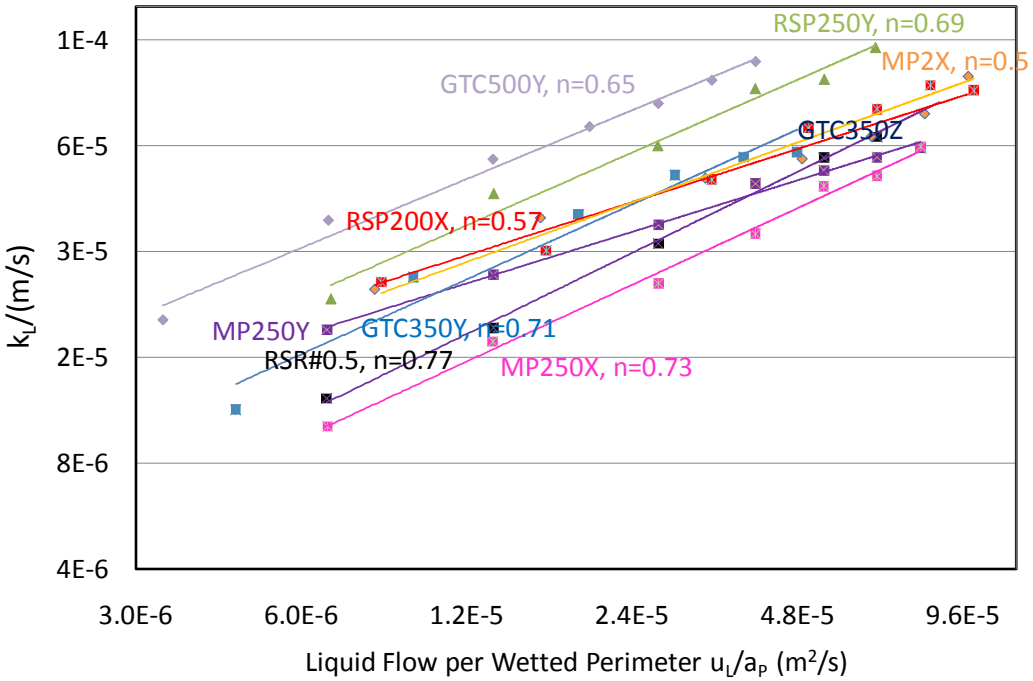

Figure 4.27. Liquid film mass transfer coefficient (k_L) summary

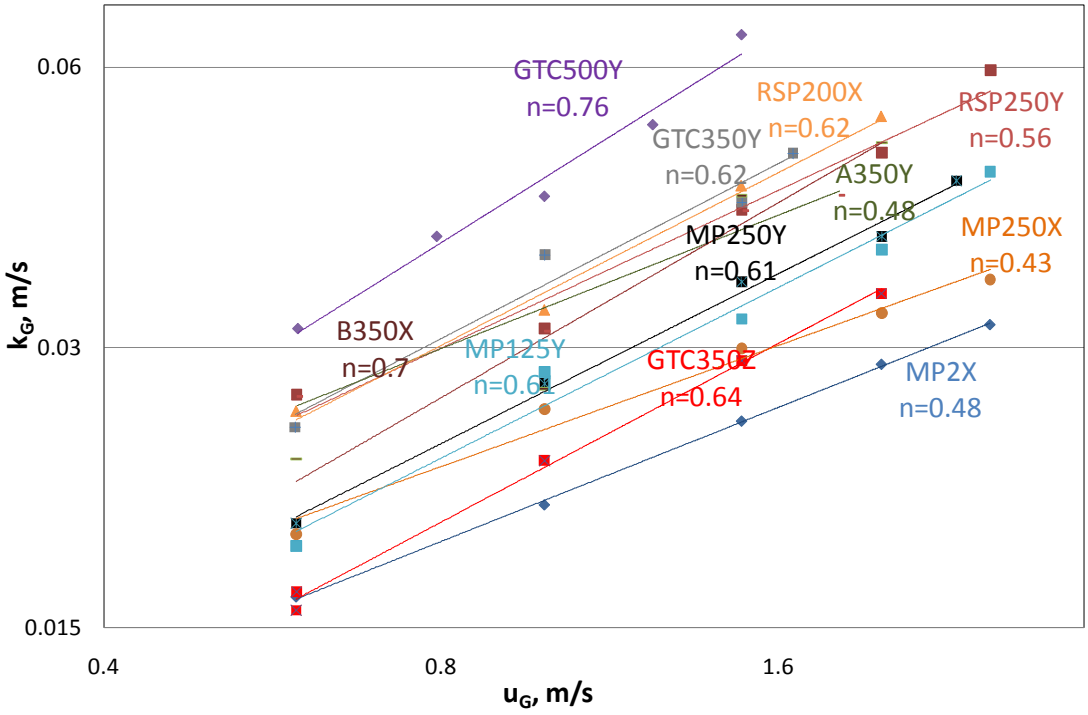

Figure 4.28. Gas film mass transfer coefficient (k_G) summary

Chapter 5: Mass Transfer Models

5.1 Area model

The effective mass transfer area model was developed based on the experimental data measured in this work. Table 5.1 lists the packings in the database along with their physical dimensions. The structured packings in the database were all stainless steel and manufactured by Sulzer ChemTech, GTC Technology, and Raschig. Every packing surface except those of Raschig SuperPak was perforated. The packing surface areas varied from 125 to 500 m^2/m^3 while the corrugation angles varied from 45 to 70 degrees. The channel dimensions (channel base B and crimp height h) in Table 5.1 are based on actual measurements. The channel dimensions and corrugation angle were used in the Mixing Points Density (M) calculation, which will be discussed in 5.2. Three random packings in the Raschig Super Ring family were also included in the database (Table 5.2).

Table 5.1 Structured packing information

Packing name	Surface area (m^2/m3)	Corrugation angle (deg)	Channel base, B (m)	Crimp height, h (m)
MP 125Y	125	45	0.0635	0.0254
RSP 200X	200	60	0.03175	0.004763
MP 2X	205	60	0.03175	0.014288
MP 250Y	250	45	0.03016	0.0111
MP 250X	250	60	0.0254	0.0111
RSP 250Y	250	60	0.03175	0.004763
GT-PAK™ 350Y	350	45	0.0167	0.00754
GT-PAK™ 350Z	350	70	0.0175	0.00794
A 350Y	350	45	0.0254	0.007938
B 350X	350	60	0.0175	0.009
GT-PAK™ 500Y	500	45	0.0143	0.00635

Table 5.2. Random packing information

	Nominal size	Void fraction	Surface area
	mm	%	m^2/m^3
RSR#0.3	15	96	315
RSR#0.5	20	97	250
RSR#0.7	25	98	180

The effective mass transfer area model was developed based on Tsai's area model

(2010). Tsai used dimensionless numbers to correlate the packing mass transfer area database. According to Tsai's experiments as well as effective area measurements conducted in this work, the effective area is assumed to be only a function of liquid flow rate, liquid density and surface tension, and considered to be independent of gas flow rate and liquid phase viscosity. This assumption is supported by the majority of experimental data, although at some conditions we do find the effective area slightly changes with gas flow rate. The effective mass transfer area model developed by Tsai is given in (5-1).

$$\frac{a_e}{a_P} = 1.34[(We_L)(Fr_L)^{-1/3}]^{0.116} \tag{5-1}$$

Where,
We_L is the liquid phase Weber number, $\rho_L u_L^2 \delta_L/\sigma$;
Fr_L is the liquid phase Froude number, $u_L^2/g\delta_L$.

In the Tsai model, the liquid film thickness (δ_L) was used as the characteristic length. To calculate the liquid film thickness, the classic Nusselt film thickness assumption (Bird et al., 2002) was used:

$$\delta_{Nusslet} = \sqrt{\frac{3u_{film}\mu_L}{\rho_L g \sin\theta}} = \sqrt[3]{\frac{3\mu_L}{\rho_L g \sin\theta}\left(\frac{Q}{L_P}\right)} \tag{5-2}$$

Thus, the dimensionless number group can be expressed by:

$$(We_L)(Fr_L)^{-1/3} = \left(\frac{\rho_L}{\sigma}\right) g^{1/3} \left(\frac{Q}{L_P}\right)^{4/3} \tag{5-3}$$

Where,
Q is the volumetric liquid flow rate, (m^3/s);
L_P is the wetted perimeter, m.
For structured packings, the wetted perimeter can be calculated from channel dimensions:

$$L_P = A * \frac{4S}{Bh} \tag{5-4}$$

Where,
A is the column cross section area, (m^2);
S is the packing channel side, (m);
B is the packing channel base, (m);
h is the packing crimp height, (m).

However, with a larger scope including random packings and hybrid packings such as Raschig Super-Pak family, the original form of the Tsai model is not applicable. In those situations where channel dimensions are not known or hardly defined, using liquid superficial velocity over packing total area (u_L/a_P) instead of (Q/L_P) is a good alternative. The mass transfer area model in this work is developed based on Tsai model, utilizes u_L/a_P as the liquid flow rate per wetted perimeter. The experimental

coefficient is changed from 1.34 to 1.41 which provides a better fit of the larger database.

$$\frac{a_e}{a_P} = 1.41[(\frac{\rho_L}{\sigma})g^{1/3}(\frac{u_L}{a_P})^{4/3}]^{0.116} \qquad (5\text{-}5)$$

Figure 5.1a shows the comparison of the experimental data and the modified Tsai model. Figure 5.1b shows the fractional mass transfer area plotted over the dimensionless number group $(We_L)(Fr_L)^{-1/3}$. The database includes 14 packings measured in this work and contains a large scope of packing type (structured, random, and hybrid). The model shows a good fit with most data except for GT-PAK^{TM} 500Y, which shows a lower effective area than predicted. The average deviation of this area model is 10.5%, which is quite acceptable considering the broad scope of the packing type.

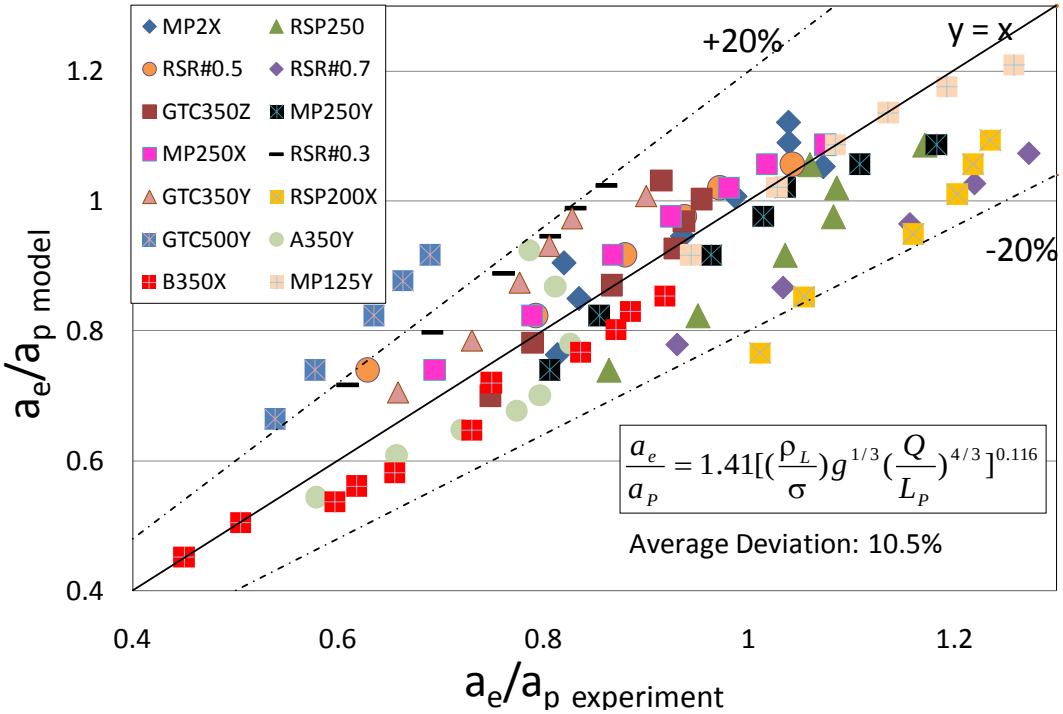

Figure 5.1a. Comparison of experimental data and modified Tsai model

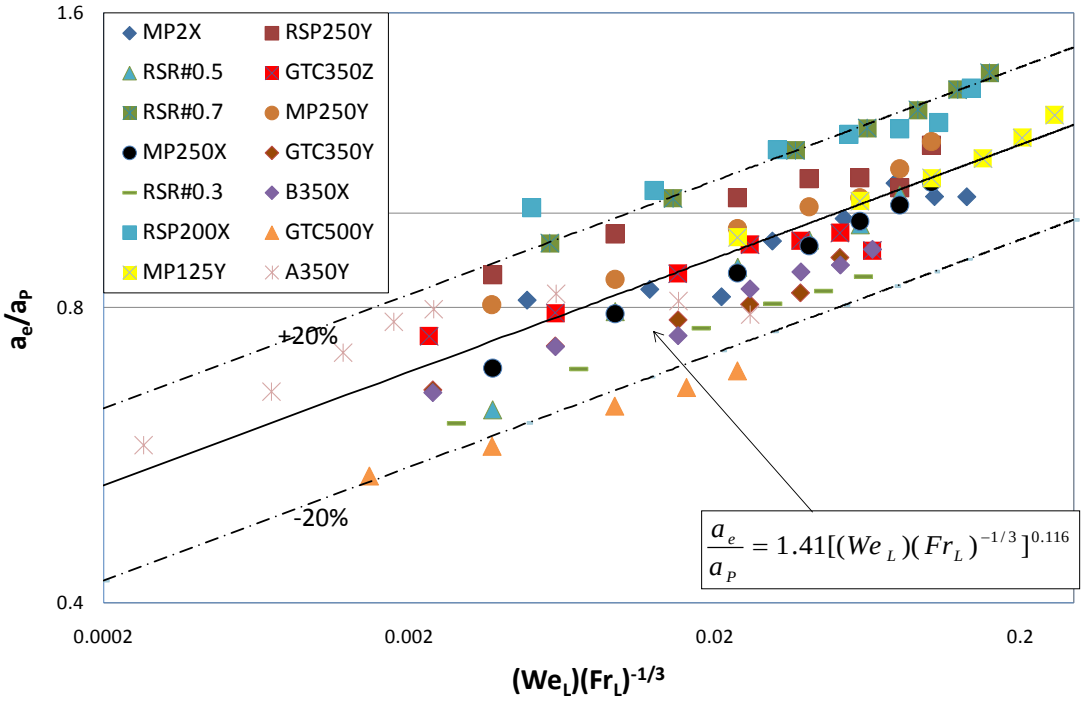

Figure 5.1b. Fractional mass transfer area shown in dimensionless group

5.2 Comparison with literature area models

Previous mass transfer models have been thoroughly discussed in Chapter 2. The mass transfer area model developed in this work is compared with previous mass transfer area models. The experimental data are also displayed for reference. The correlations are reproduced from Chapter 2.

Onda et al. (1968):

$$\frac{a_e}{a_P} = 1 - \exp[-1.45(\frac{\sigma_C}{\sigma_L})^{0.75} \mathrm{Re}_L^{0.1} Fr_L^{-0.05} We_L^{0.2}] \qquad (2\text{-}4)$$

Billet and Schultes (1993):

$$\frac{a_e}{a_P} = 1.5(a_P d_h)^{-0.5}(\frac{u_L d_h}{\nu_L})^{-0.2}(\frac{u_L^2 \rho_L d_h}{\sigma})^{0.75}(\frac{u_L^2}{g d_h})^{-0.45} \qquad (2\text{-}5a)$$

Bravo-Rocha-Fair (1985):

$$\frac{a_e}{a_P} = 0.498(\frac{\sigma^{0.5}}{Z^{0.4}})(Ca_L \mathrm{Re}_G)^{0.392} \qquad (2\text{-}11)$$

Rocha-Bravo-Fair (1996):

$$\frac{a_e}{a_P} = F_{SE}\frac{29.12u_L^{0.4}\nu_L^{0.2}S^{0.359}}{(1-0.93\cos\gamma)(\sin\alpha)^{0.3}\varepsilon^{0.6}}\left(\frac{\rho_L}{\sigma g}\right)^{0.15} \quad (2\text{-}14)$$

Delft (1999):

$$\frac{a_e}{a_P} = \frac{1-\Omega}{1+A/u_{Ls}^B} \quad (2\text{-}19)$$

Besides the above literature area models, the area model used in Aspen Plus® developed by Hanley and Chen (2011) was compared:

$$\frac{a_m}{a_d} = 0.539\,\mathrm{Re}_V^{0.145}\mathrm{Re}_L^{-0.153}We_L^{0.2}Fr_L^{-0.2}\left(\frac{\rho_V}{\rho_L}\right)^{-0.033}\left(\frac{\mu_V}{\mu_L}\right)^{0.090}\left(\frac{\cos(\theta)}{\cos(\pi/4)}\right)^{4.078} \quad (5\text{-}6)$$

A preliminary mass transfer area model based directly on Linek (2011) measurements for Mellapak packing was chosen to compare with the model developed in this work:

$$\frac{a_e}{a_P} = 1.343u_L^{0.104} \quad (5\text{-}7)$$

Figures 5.2 and 5.3 show the comparison between the area model developed in this work and the literature models. The differences between the model developed in this work and literature models are quite distinct. The differences are small for some recent literature models: 11% for Delft (1999), 13% for Linek (2011), 36% for Hanley (2011). The differences become large for models based on hydrocarbon systems or based mostly on random packing: 45% for Bravo (1992), 73% for Rocha (1996), 37% for Onda (1968), and 59% for Billet (1993).

The closest model was developed by Linek since it was based on a similar system (absorption of 1% CO_2 in air with 1 gmol/NaOH solution). The deviation is due to the larger gas phase resistance. It should be noted that the Delft model does not predict the effect of liquid superficial velocity on mass transfer area well with an exponent of 0.011, which is lower than the exponent predicted by all other models.

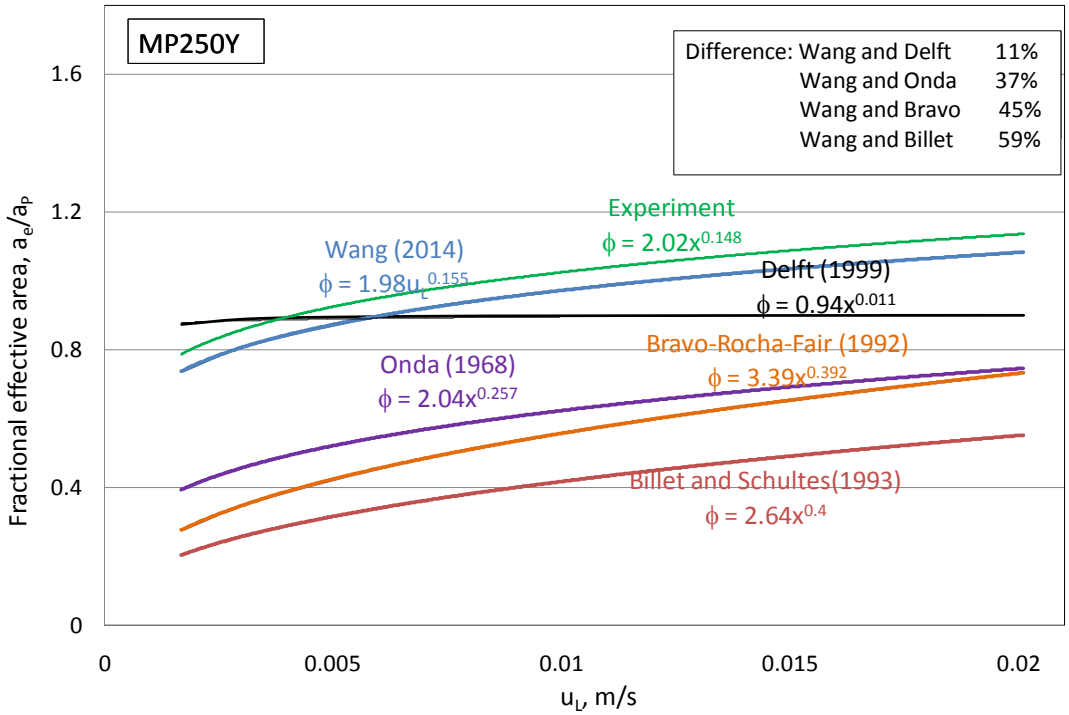

Figure 5.2. Comparison of literature area model (I) and model in this work

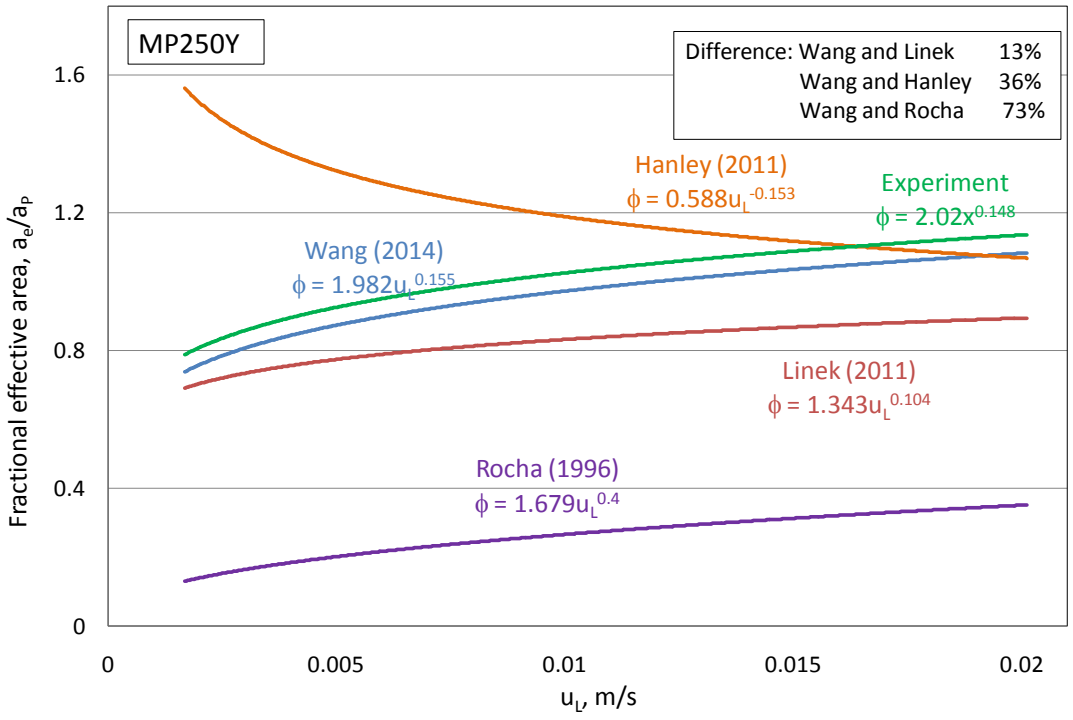

Figure 5.3. Comparison of literature area models (II) and the model of this work

5.3 Liquid film mass transfer coefficient

5.3.1 Mixing Point Density

In the previous chapter (Chapter 4), the effects of operating conditions and packing geometry on liquid and gas film mass transfer coefficients were explored. The liquid film mass transfer coefficient increases with packing surface area, and decreases with packing corrugation angle. In the model development, a new concept, Mixing Point Density (M), was introduced to account for the packing geometry effect on k_L and k_G.

Figure 5.4 shows the liquid flow mechanism inside structured packing (side view). Structured packing is composed of corrugated metal sheets. Liquid flows along these corrugated sheets. At the joint points of metal sheets (marked by circles in Figure 5.4), flows mix with each other, change directions, and create turbulence. Thus, these mixing points are believed to be the key points for mass transfer in structured packing. In packing with a lower corrugation angle or larger surface area, there will be more mixing points than packing with a higher corrugation angle at the same packed height, which means liquid and gas flows mix with each other more often, change directions more frequently, and create more turbulence. Therefore, the effect of surface area and corrugation angle on k_L and k_G can be quantified.

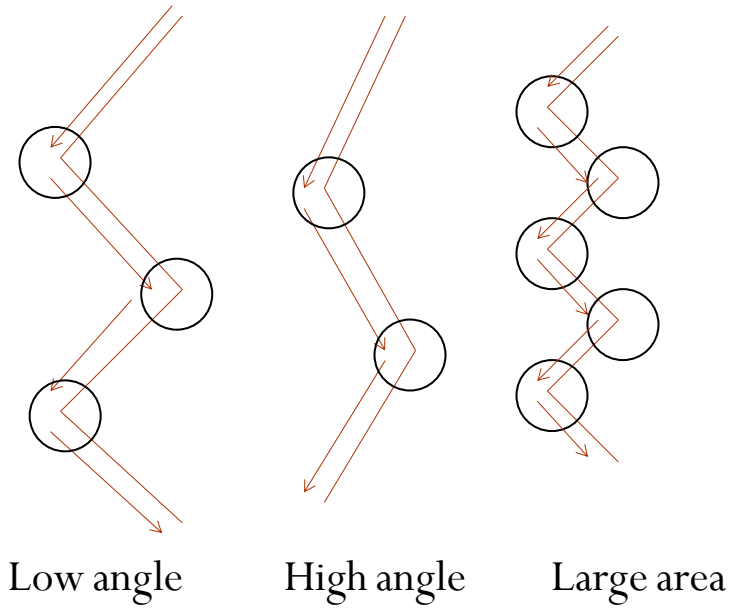

Figure 5.4. Liquid flow along corrugated metal sheets

To quantify the number of mixing points inside structured packing, their geometric structures were evaluated. Figure 5.5 shows the lateral view of a structured packing with a corrugation angle θ. From the lateral view, the corrugated metal sheets can be seen as bunches of parallel lines with a tilt angle θ to the horizontal line. In the structured packing, each corrugated metal sheet contacts with the one next to it. In the lateral view, it is expressed by the parallel lines crossing with another set of

parallel lines in a reversed angle (π-θ). The crossed corrugated metal sheets form hundreds of square pyramids, which are the triangles in the lateral view. The mixing points are the vertices of the triangles, which are marked in black circles in the lateral view. The bottom of the triangle is the channel base B, and the height of the triangle is (B/2)*tanθ.

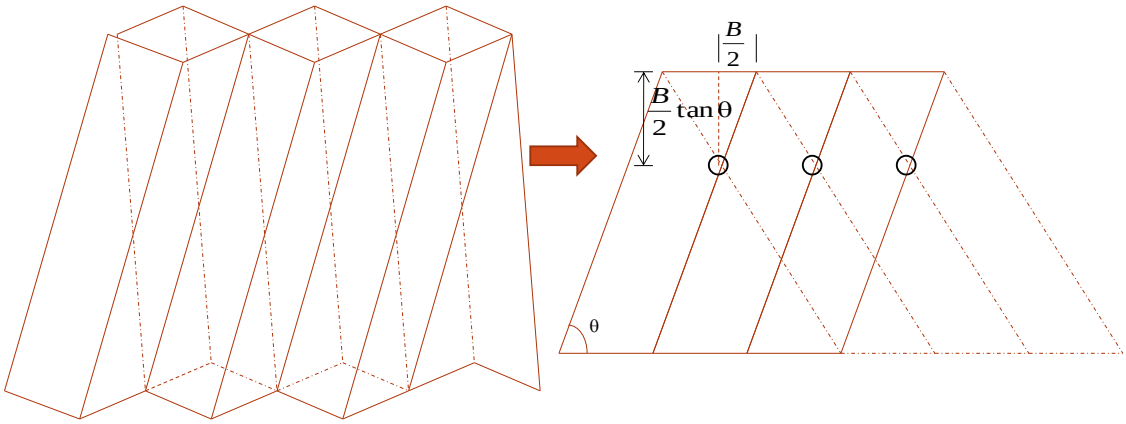

Figure 5.5. Lateral View of a Structured Packing with a Corrugation Angle θ

Structured packing is composed of those square pyramids formed by the crossed metal sheets. The pyramids can be better seen from the top view of the packing (Figure 5.6). The height of the square pyramid is (B/2)*tanθ, the bottom area of the pyramid is B*h. The volume of each square pyramid can be calculated:

$$V_{pyramid} = \frac{1}{3} * h * S_{bottom} = \frac{1}{6} B * h * B \tan\theta \qquad (5\text{-}8)$$

Where,
B is the packing channel base, (m);
h is the packing crimp height, (m);
θ is the packing corrugation angle.

Thus, the total amount of square pyramids per m^3 volume is:

$$N_{pyramid} = \frac{V_{total}}{V_{pyramid}} = \frac{6}{B * h * B \tan\theta} \qquad (5\text{-}9)$$

Each pyramid has five mixing points; however, each pyramid is also sharing mixing points with other four adjacent pyramids. Thus, the number of mixing points per pyramid is 5/5. Finally, the total number of mixing points per m^3 which is the Mixing Point Density can be calculated:

$$M = N_{pyramid} * mixing\ points\ per\ pyramid = \frac{6}{B * h * B \tan\theta} \qquad (5\text{-}10)$$

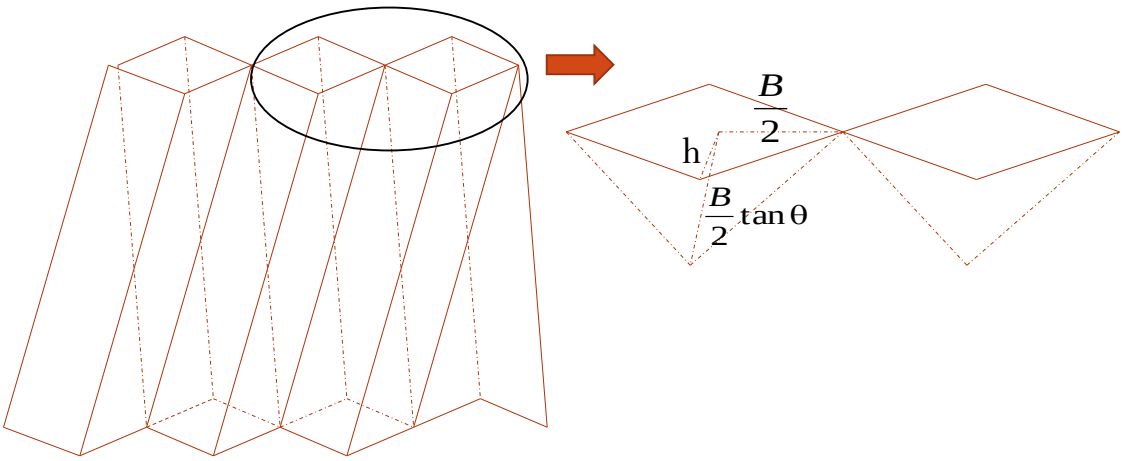

Figure 5.6. Top view of a Structured Packing with a Corrugation Angle θ

5.3.2 Preliminary k_L and k_G models

In previous work, the effects of liquid or gas superficial velocity ($u_{L/G}$), the packing surface area (a_P), and the mixing point density (M) on k_L and k_G were explored. The preliminary k_L and k_G correlations include these three factors ($u_{L/G}$, a_P, M):

$$k_{L/G} = f(u_{L/G}, M, a_P) \tag{5-11}$$

Taking a natural logarithm of both sides, Equation (5-11) can be written as:

$$\ln(k_{L/G}) = C + m\ln(u_{L/G}) + n\ln(M) + k\ln(a_P) \tag{5-12}$$

Through data regression, the experimental constant C and the exponents for each factor can be calculated. Finally, the preliminary k_L and k_G models for structured packings are developed:

$$k_L = 3.08E-3 * u_L^{0.72} M^{0.42} a_P^{-1.15} \tag{5-13}$$

$$k_G = 9.6E-3 * u_G^{0.54} M^{0.29} a_P^{-0.5} \tag{5-14}$$

The comparison between experimental data and values predicted by preliminary k_L and k_G models are shown in Figure 5.7 and Figure 5.8. The deviation between experimental data and model value is 22% for k_L while the deviation between experimental data and model value is 13% for k_G.

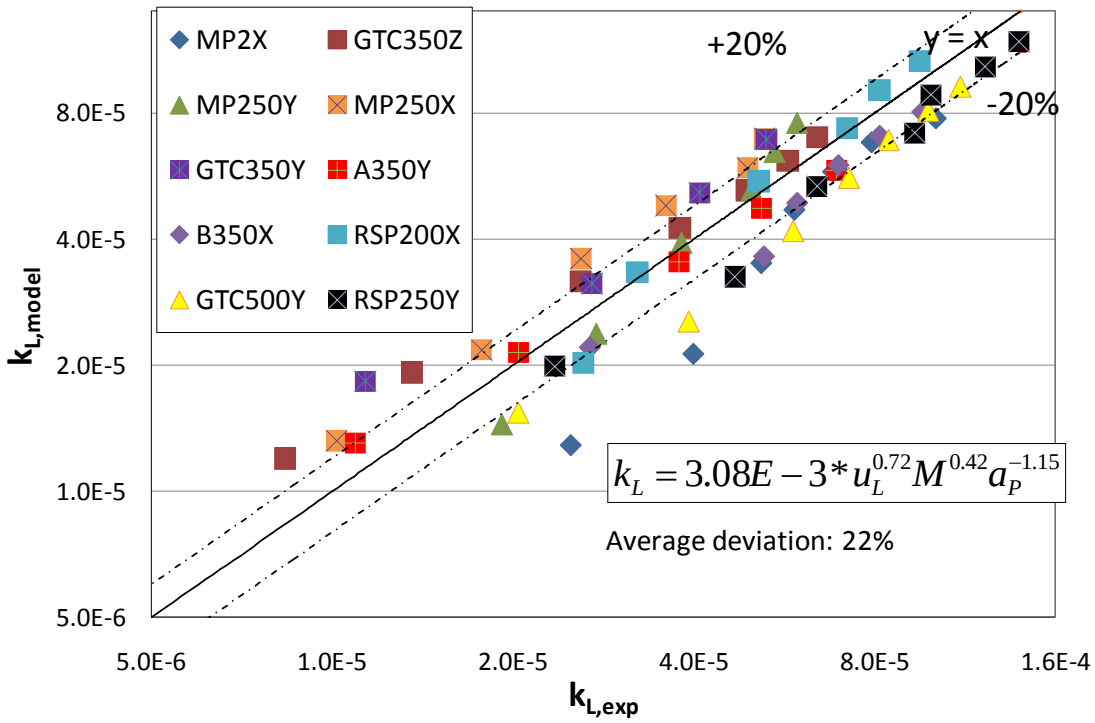

Figure 5.7. Comparison between experimental k_L and k_L predicted by preliminary model

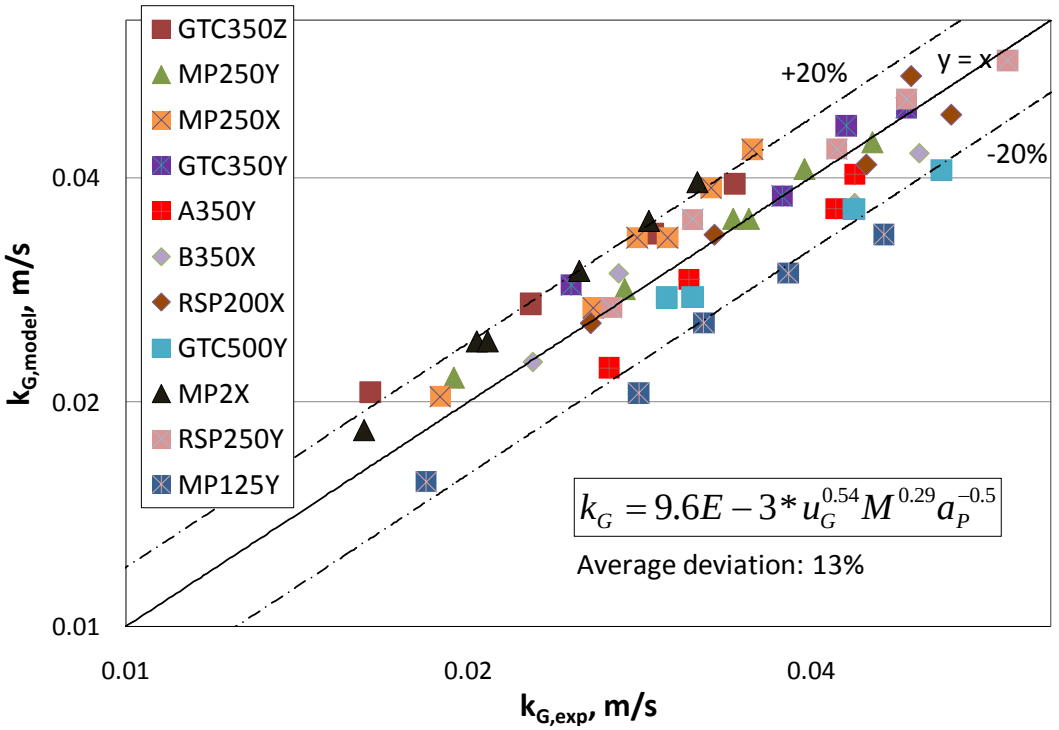

Figure 5.8. Comparison between experimental k_G and k_G predicted by preliminary model

5.3.3 Dimensionless k_L and k_G models

Fundamental models utilize the dimensionless form of velocity (Reynolds number, Re), the dimensionless form of liquid or gas phase physical properties (Schmidt number, Sc), and the dimensionless form of packing geometries (Mixing number, Mi) as the variables. The dimensionless form of k_L or k_G (Sherwood number, Sh) is used as the dependent variable. Thus, the model can be written as:

$$Sh_{L/G} = C * \mathrm{Re}_{L/G}^{m} \, Sc_{L/G}^{n} Mi^{p} \tag{5-15}$$

Other researchers' conclusions are used for the effect of Schmidt number on Sherwood number since the Schmidt number influence is not yet explored in this work. For the gas phase, Mehta's conclusion (1966) is used in this model, which is that Sh_G depends on Sc_G to the power of 0.5. For the liquid phase, Mangers' conclusion (1980) is used with a dependence of Sh_L on Sc_L to the power of 0.5.

The dimensionless k_L and k_G models for structured packings are:

$$Sh_L = 1.79 * \mathrm{Re}_L^{0.74} \, Mi^{0.42} Sc_L^{0.5}, \; k_L = Sh_L a_P D_L \tag{5-16}$$

$$Sh_G = 0.83 * \mathrm{Re}_G^{0.58} \, Mi^{0.3} Sc_G^{0.5}, \; k_G = Sh_G a_P D_G \tag{5-17}$$

Where,

Mixing number Mi is the number of mixing points in a certain volume and can be calculated by:

$$Mi = M * l_{eq}^3 = \frac{M}{a_P^3} = \frac{6}{a_P^3 * B * h * B \tan\theta} \tag{5-18}$$

The characteristic dimension here is the equivalent radius (r_{eq}) of the characteristic diamond formed by channel base B, channel side S, and crimp height h in regular structured packing, which is also the bottom area of pyramid mentioned in Figure 5.6.

$$l_{eq} = r_{eq} = \frac{Bh}{4S} = \frac{1}{a_P} \tag{5-19}$$

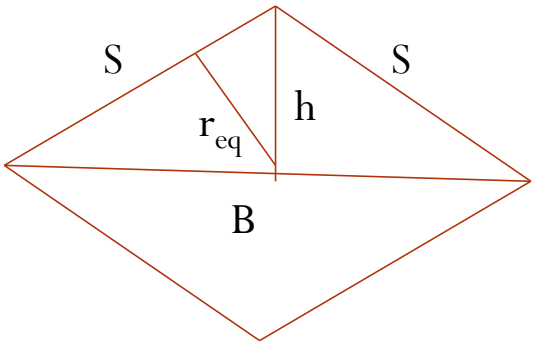

Figure 5.9. Characteristic diamond formed by B, S, h in regular structured packing

Sh, Re, and Sc are defined as:

$$Sh = \frac{k * l_{eq}}{D} = \frac{k}{D * a_P} \tag{5-20}$$

$$\mathrm{Re} = \frac{\rho u l_{eq}}{\mu} = \frac{\rho u}{\mu a_P} \tag{5-21}$$

$$Sc = \frac{\upsilon}{D} = \frac{\mu}{\rho D} \tag{5-22}$$

Figure 5.10a shows the liquid phase Sherwood number (Sh_L) plotted over the dimensionless number group $(Re_L)(Mi)^{0.42/0.74}(Sc_L)^{0.5/0.74}$. Figure 5.11a shows the gas phase Sherwood number (Sh_G) plotted over the dimensionless number group $(Re_G)(Mi)^{0.42/0.74}(Sc_G)^{0.5/0.74}$. The dimensionless correlations for k_L and k_G can then be determined. The comparisons between experimental data and values predicted by dimensionless k_L and k_G models are shown in Figures 5.10b and 5.11b. The deviation between experimental data and model value is 22% for k_L while the deviation between experimental data and model value is 12% for k_G.

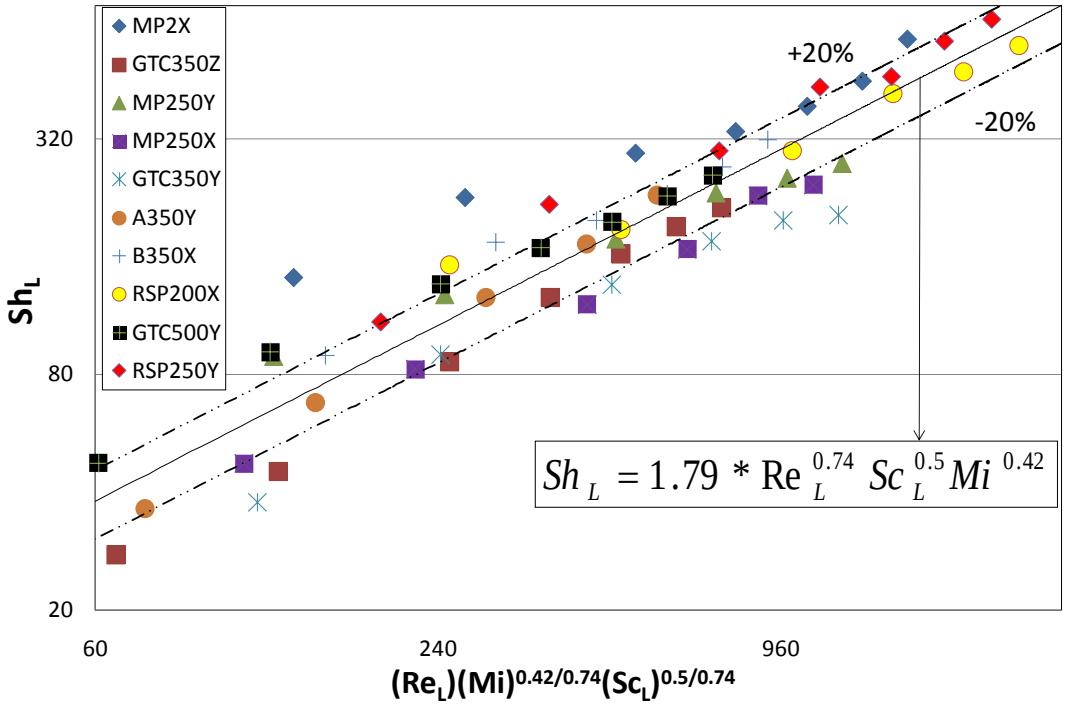

Figure 5.10a. Sh_L over dimensionless group $(Re_L)(Mi)^{0.42/0.74}(Sc_L)^{0.5/0.74}$

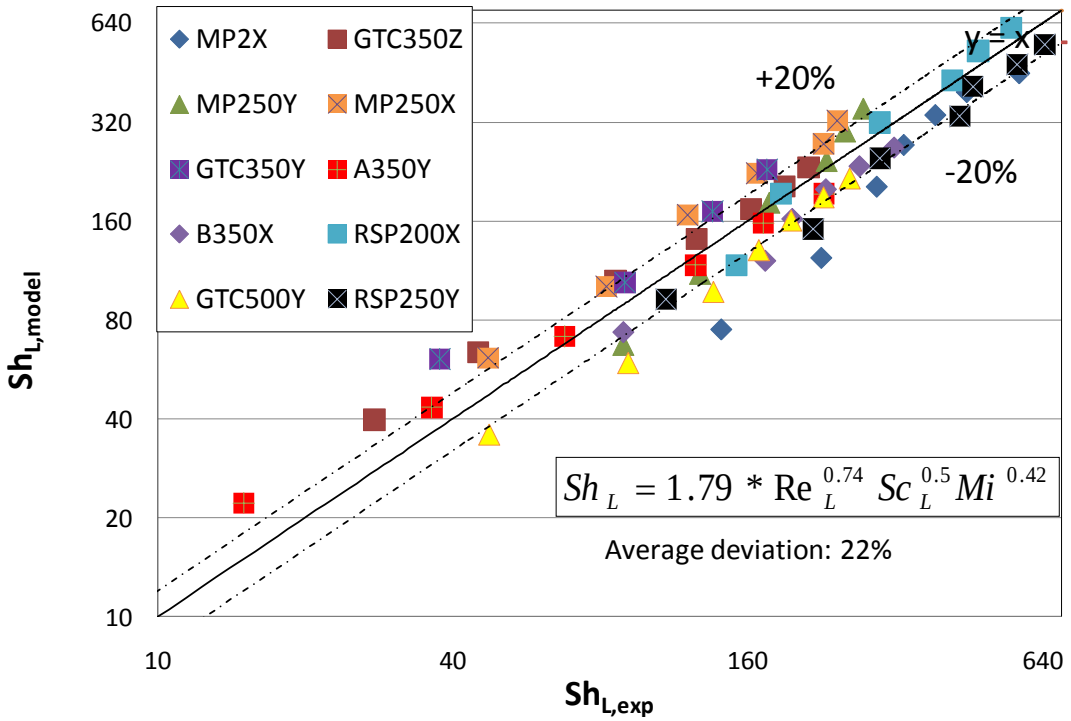

Figure 5.10b. Comparison between experimental Sh_L and Sh_L predicted by dimensionless model

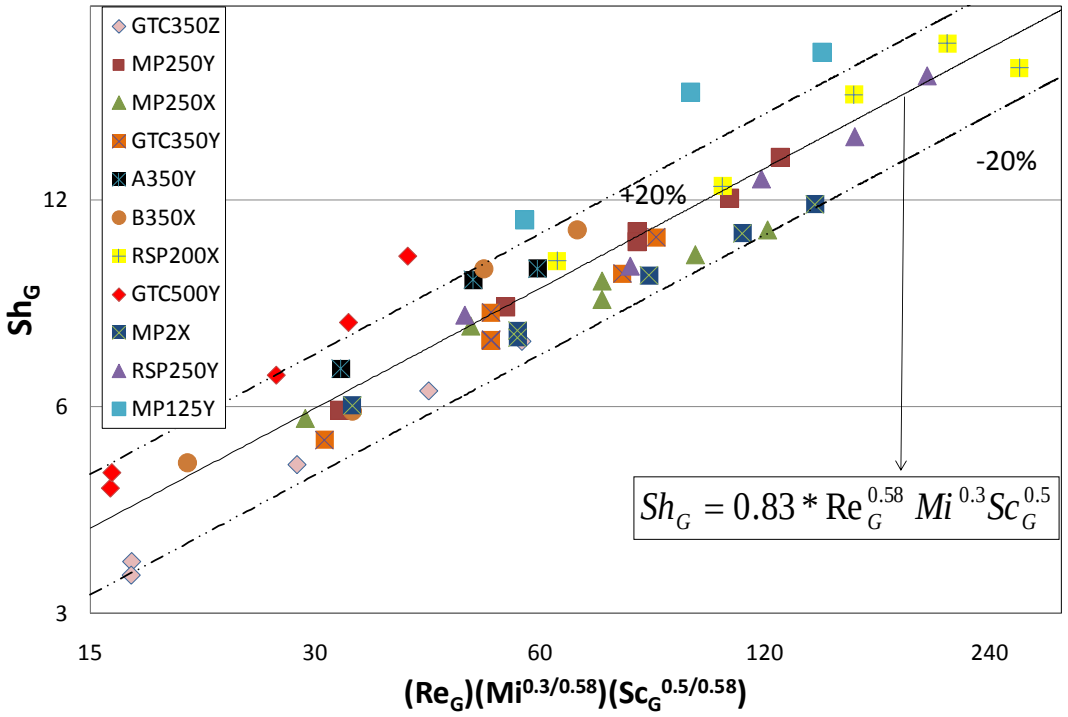

Figure 5.11a. Sh_G over dimensionless group $(Re_G)(Mi)^{0.3/0.58}(Sc_G)^{0.5/0.58}$

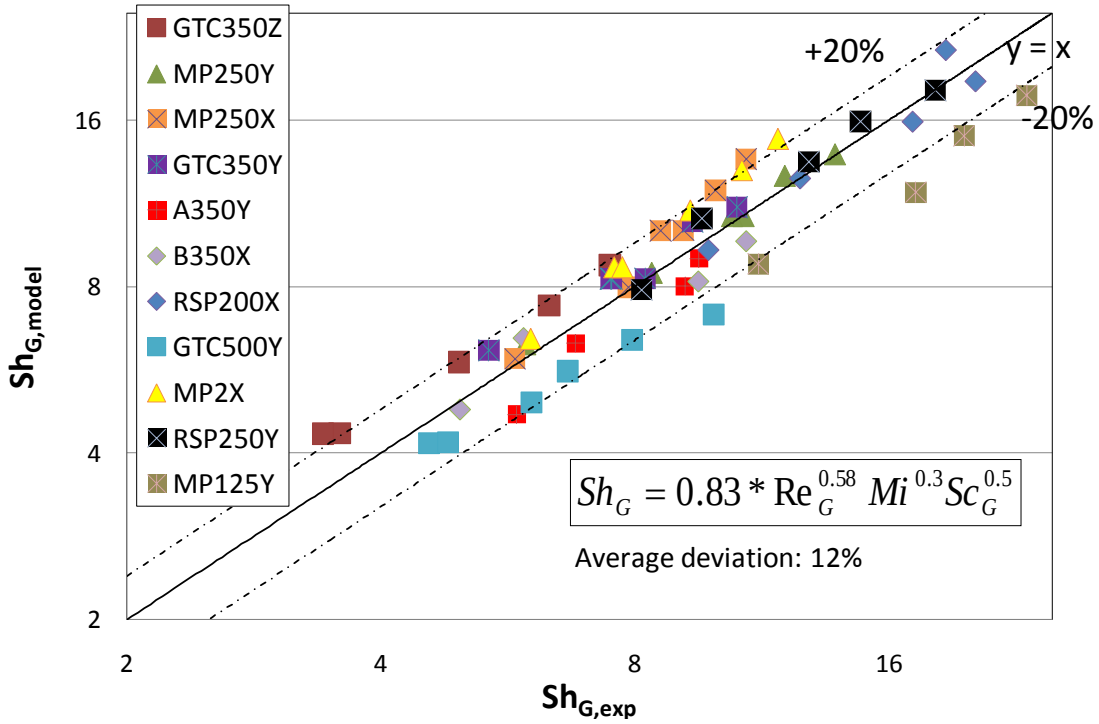

Figure 5.11b. Comparison between experimental Sh_G and Sh_G predicted by dimensionless model

5.4 Comparison with literature k_L and k_G models

Similar with the area model comparison, the liquid film and gas film mass transfer coefficient models developed in this work are compared with literature k_L and k_G models. The correlations are reproduced from Chapter 2.

Billet and Schultes (1993):

$$k_G = \frac{2}{\sqrt{\pi}}\sqrt{D_G \frac{u_G}{(\varepsilon - h_L) l_\pi}} \tag{2-27}$$

$$k_L = \frac{2}{\sqrt{\pi}}\sqrt{D_L \frac{u_L}{h_L l_\pi}} \tag{2-28}$$

Bravo-Rocha-Fair (1985):

$$\frac{k_G d_{eq}}{D_G} = 0.0328\left[\frac{d_{eq}\rho_G (u_{G,eff} + u_{L,eff})}{\mu_G}\right]^{0.77}\left(\frac{\mu_G}{\rho_G D_G}\right)^{0.33} \tag{2-9}$$

$$k_L = 2\sqrt{\frac{D_L u_{L,eff}}{\pi S}} \tag{2-10}$$

Rocha-Bravo-Fair (1996):

$$\frac{k_G S}{D_G} = 0.054\left[\frac{\rho_G S (u_{Ge} + u_{Le})}{\mu_G}\right]^{0.8}\left(\frac{\mu_G}{D_G \rho_G}\right)^{0.33} \tag{2-12}$$

$$k_L = 2\sqrt{\frac{D_L C_E u_{Le}}{\pi S}} \tag{2-13}$$

Delft (1999):

$$k_G = \sqrt{k_{G,lam}^2 + k_{G,turb}^2} \tag{2-29}$$

$$Sh_{G,lam} = 0.664 Sc_G^{1/3}\sqrt{\mathrm{Re}_{Grv}\frac{d_{hG}}{l_{G,pe}}} \tag{2-31}$$

$$Sh_{G,turb} = \frac{\mathrm{Re}_{Grv} Sc_G \frac{\zeta_{GL}\varphi}{8}}{1 + 12.7\sqrt{\frac{\zeta_{GL}\varphi}{8}}(Sc_G^{2/3} - 1)}\left[1 + \left(\frac{d_{hG}}{l_{G,pe}}\right)^{2/3}\right] \tag{2-32}$$

$$k_L = 2\sqrt{\frac{D_L u_{Le}}{\pi 0.9 d_{hG}}} \tag{2-54}$$

$$d_{hG} = \frac{\frac{(bh-2\delta s)^2}{bh}}{[(\frac{bh-2\delta s}{2h})^2 + (\frac{bh-2\delta s}{b})^2]^{0.5} + \frac{bh-2\delta s}{2h}} \tag{2-55}$$

$$\delta = (\frac{3\mu_L u_{LS}}{\rho_L g a \sin\alpha})^{1/3} \tag{2-56}$$

Besides the above literature k_G and k_L models, the k_G and k_L models used in Aspen Plus® developed by Hanley and Chen (2011) were also compared:

$$k_x = 0.33\,\mathrm{Re}_L^1\, Sc_L^{1/3}(\frac{c_L D_L}{d_e}) \tag{5-23}$$

$$k_y = 0.0084\,\mathrm{Re}_V\, Sc_V^{1/3}(\frac{c_V D_V}{d_e})(\frac{\cos(\theta)}{\cos(\pi/4)})^{-7.15} \tag{5-24}$$

The preliminary k_La model based directly on Linek (2011) measurements was compared with model developed in this work (k_Ga correlation was not developed):

$$k_L a = 0.562 * u_L^{0.668} \tag{5-25}$$

The analytical k_L equation (Pigford, 1941) used in the Wetted Wall Column (WWC) calculation (Dugas, 2009) was compared with the model developed in this work:

$$k_L^o = (\frac{3^{1/3}2^{1/2}}{\pi^{1/2}})(\frac{Q^{1/3}h^{1/2}W^{2/3}}{A})(\frac{g\rho}{\mu})^{1/6} D_{CO2}^{1/2} \tag{5-26}$$

Where
Q is the liquid flow rate, (m^3/s);
h is the height of the column cell, (m);
W is the column cell cross section perimeter, (m);
A is the column cell cross section area, (m^2).

When used Equation (5-26) to calculate k_L for packing, each packing cell was assumed as a wetted wall column. The following assumptions were made:

$$h = \frac{B}{2}\sin\theta \tag{5-26a}$$

$$W = 4S \tag{5-26b}$$

Figures 5.12-5.15 shows the comparison between literature k_La and k_Ga models with models developed in this work. Since most literature models were developed from measured k_La and k_Ga values with a theoretical assumption of area, the most reasonable comparison is with the respective ka.

In the k_La comparison, most literature models use the assumption of penetration theory (Higbie, 1935) with different expressions of equivalent liquid velocity (u) and characteristic length (L). The difference between the model developed in this work (absorption systems) and models from distillation systems (Bravo, Delft, Rocha) is from 30% to 40%. The difference becomes smaller (20% to 30%) when comparing with the model developed from absorption data (Linek) or models developed from distillation and absorption systems (Billet and Schultes, Hanley and Chen). The difference between k_La values predicted by different models is smaller than the difference would be expected. It is suggested to use the k_L model and the a_e model developed by the same author as a combination. (Use k_La models instead of k_L or a_e models separately since the errors from k_L model and from a_e model cancel out).

Another finding is that the liquid rate dependence of k_L models developed from penetration theory (Bravo; Rocha; Billet and Schultes; Delft; WWC) is smaller than k_L models developed based on experimental data (Linek; Hanley and Chen; Wang). Penetration theory assumes a 0.5 power of the liquid rate dependence of k_L ($k_L \sim u_L^{0.5}$). However, when applying penetration theory, most authors used the effective liquid velocity (u_{LE}) instead of u_L. Equation (5-27a) shows the effective liquid velocity form used by Bravo, Rocha, Billet and Schultes; and (5-27b) shows the effective liquid velocity form used by Delft.

$$u_{LE} = C * \frac{u_L}{h_L} \qquad (5\text{-}27a)$$

$$u_{LE} = C * \frac{u_L}{\delta_L} \qquad (5\text{-}27b)$$

The effective liquid velocity u_{LE} has the liquid hold-up term (h_L) or liquid film thickness term (δ_L) at the bottom, and either h_L or δ_L is a function of liquid velocity u_L. Thus, the actual liquid rate dependence of these models using effective liquid velocity is between 0.2 to 0.35, which is smaller than the power predicted by penetration theory.

From the experiments conducted in this work or the experiments conducted by other authors (Linek, 2005; Laso, 1997), the average liquid rate dependence of k_L is between 0.5 to 0.7, which means the previous k_L models using the effective liquid velocity (u_{LE}) under-predict the liquid rate dependence.

In the k_Ga comparison, the model developed in this work is higher than literature models by 40 to 80%. One possible reason could be that all literature models have been developed from distillation systems where equilibrium is critical to establishing the driving force in distillation systems. The driving force will depend on the liquid concentration. Imperfections in gas/liquid distribution, gas bypass, and other related

phenomena will reduce the apparent gas film coefficient and modify the apparent effect of gas rate. For the system used in this work which is absorption of SO_2 with NaOH, equilibrium is not relevant because there is excess hydroxide. Another possible reason could be the additional mass transfer caused by wall effects and end effects since this work used a short packed bed (20 to 40 inches), although careful end effect measurements have been conducted in this work to minimize this effect.

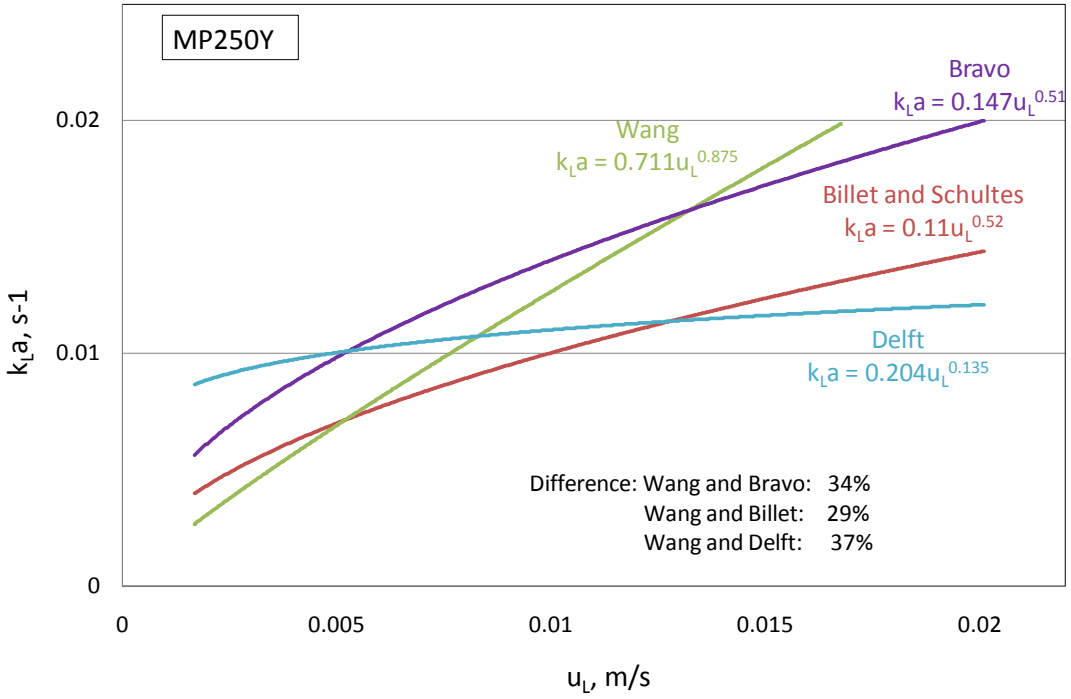

Figure 5.12. Comparison with literature k_La models consistent with the k_La model developed in this work (I)

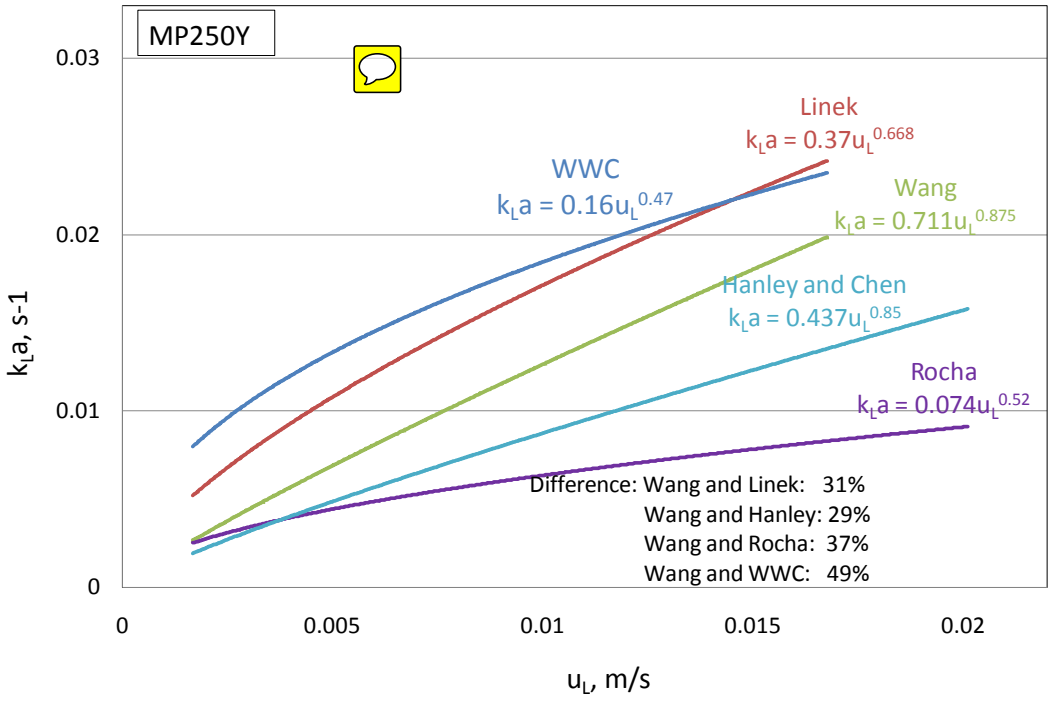

Figure 5.13. Comparison between literature k_La models inconsistent with the k_La model developed in this work (II)

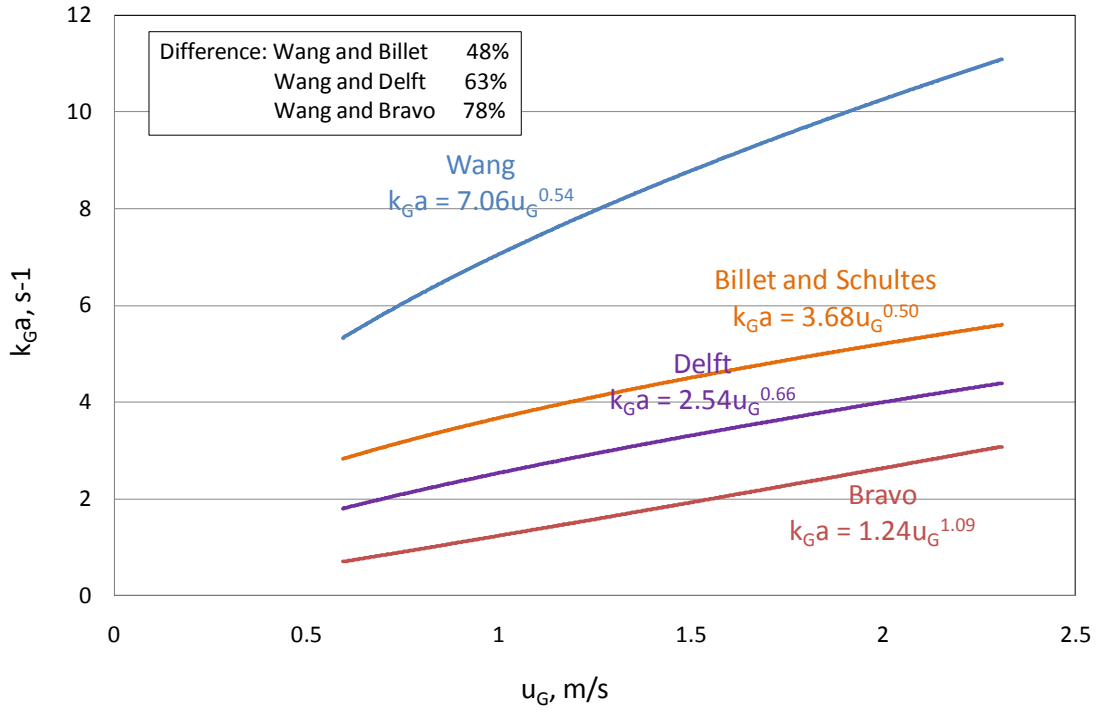

Figure 5.14. Comparison between literature k_Ga models and k_Ga model developed in this work (I)

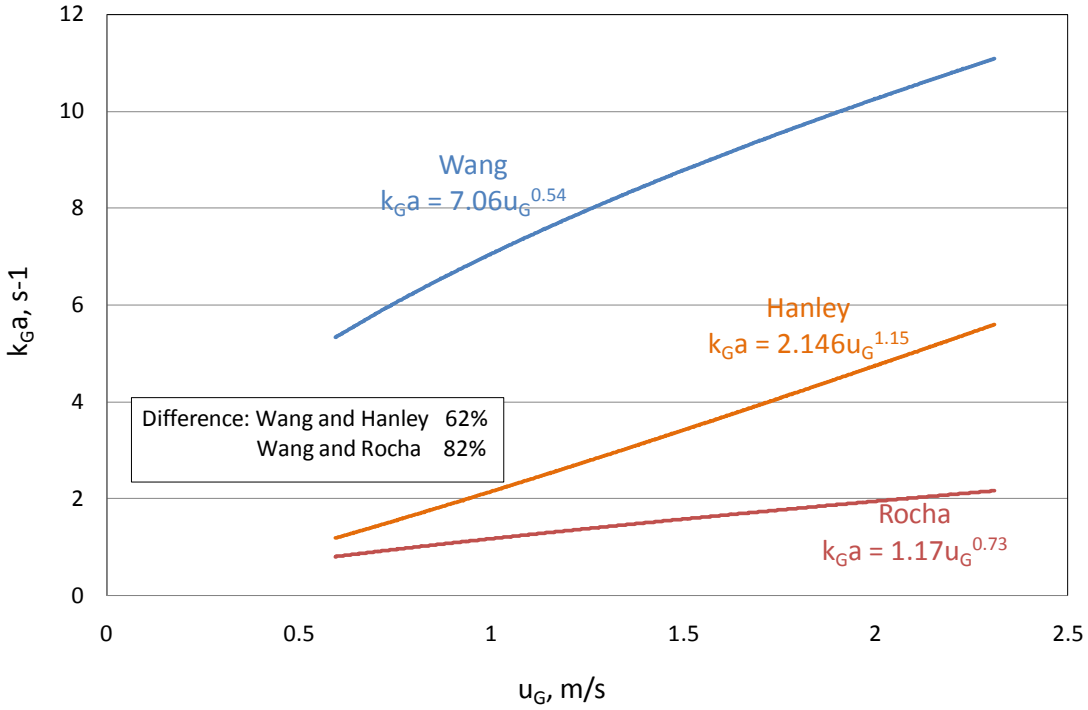

Figure 5.15. Comparison between literature k_Ga models and k_Ga model developed in this work (II)

5.5 k_L and k_G models for random packings

Another interest in this work is to extend the applied range of the k_L and k_G models to include random packings. In this work, three metal random packings from the Raschig Super Ring family (RSR#0.3, RSR#0.5, and RSR#0.7) were considered. The k_L and k_G correlations with mixing point density (Equation 5-13 and 5-14) are considered as mass transfer models for random packings. However, the mixing point density M needs to be defined and calculated from random packings when applying these models.

5.5.1 Calculated Mixing Point Density (M_{kL} and M_{kG}) for random packing

For structured packing, the mixing point density is defined as the number of contacting points between corrugated metal sheets per m^3. Mixing points divide structured packing into hundreds of small pyramids. The volume of each pyramid can be calculated by channel base B, crimp height h, and corrugation angle θ. Then the mixing point density can be calculated (Equation 5-10). For random packing whose structure is not as regular as structured packing, so it is difficult to apply the same calculation. The calculated mixing point density (M_{kL} or M_{kG}) is used for random packings.

The calculated mixing point density (M_{kL}) means the value of M in the k_L model that can give the lowest deviation from experimental data. M_{kL} is back calculated from experimental data and Equation (5-13). Microsoft® Excel Solver program is used in the calculation. M_{kG} is calculated in the same way. The concept of M_{kL} and M_{kG} comes from the concept of packing factor F_P, which is a characteristic constant used in packing pressure drop calculation and can be calculated from experimental data.

Table 5.3 lists the calculated M_{kL} and M_{kG} values for the random packings studied in this work. According to Table 5.3, the calculated mixing point density for k_L and k_G are close except for RSR#0.3, whose M_{kG} value is 1.8 times of M_{kL} value.

Table 5.3. Calculated Mixing Point Density for Random Packings

RSR#0.3		RSR#0.5		RSR#0.7	
M_{kL}	M_{kG}	M_{kL}	M_{kG}	M_{kL}	M_{kG}
2.44E6	4.33E6	0.47E6	0.56E6	0.73E6	0.39E6

5.5.2 Global mass transfer coefficient models for structured and random packings

Since the mixing point density for random packing can be calculated, Equations (5-13) and (5-14) can be used as global mass transfer coefficient models. For random packings, the M_{kL} and M_{kG} values back calculated from experimental data are used in the model. Figure 5.16 and 5.17 show the comparison between values predicted by global mass transfer k_L and k_G models and experimental data. For random packings, k_L and k_G correlations have good prediction. For k_L model, the average deviation is 3.8% for RSR#0.3, 2.9% for RSR#0.5, and 11.5% for RSR#0.7. For k_G model, the average deviation is 4.2% for RSR#0.3, 10% for RSR#0.5, and 3.4% for RSR#0.7.

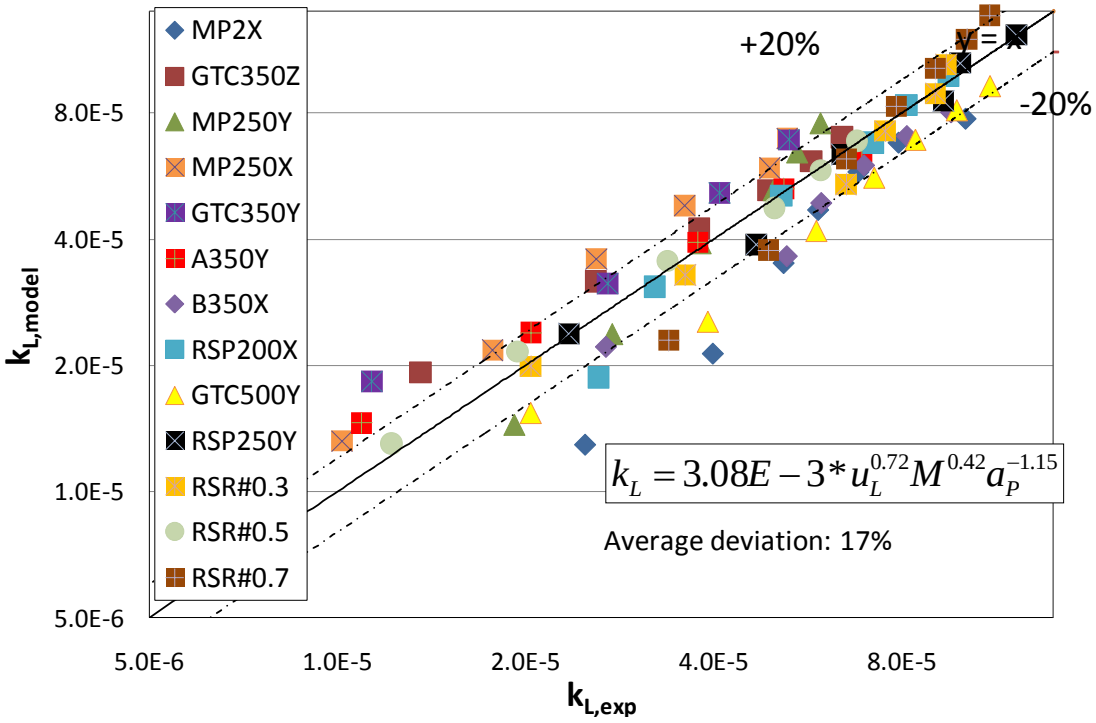

Figure 5.16. Comparison between global k_L model and experimental data

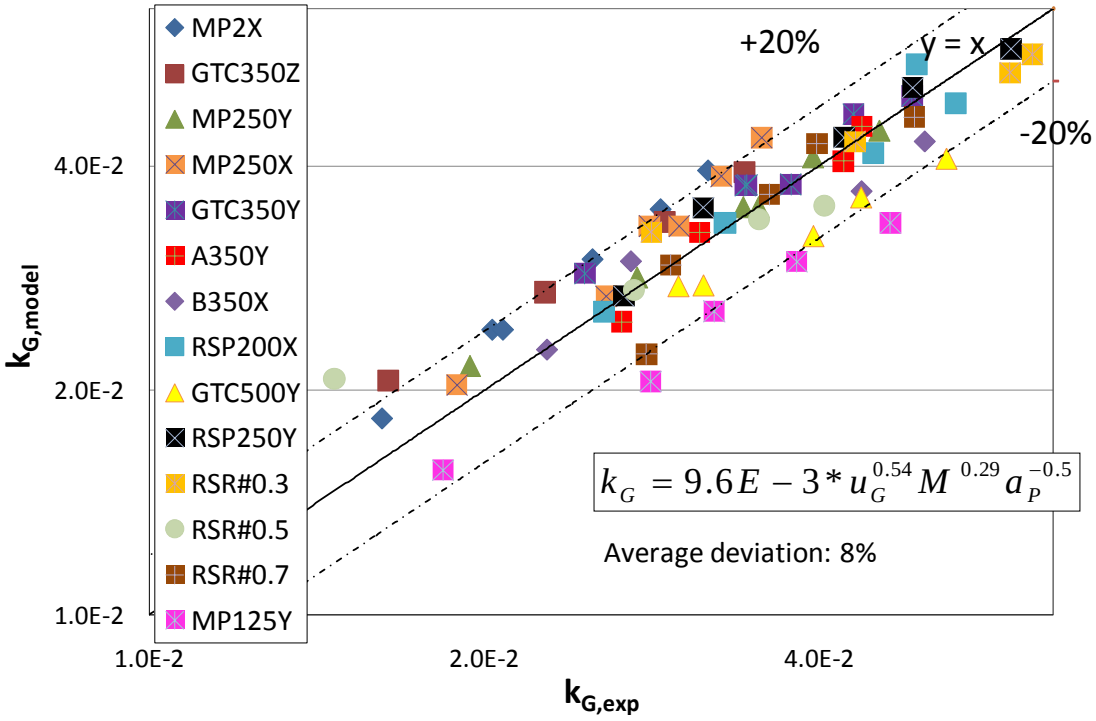

Figure 5.17. Comparison between global k_G model and experimental data

5.6 Mixing Point Density calculated from packing surface area (a_P) and corrugation angle (θ)

The mixing point density calculated by Equation (5-10) needs the specific structured packing geometry information: channel base B and crimp height h. However, this kind of information is not always available. To solve this problem, another way to calculate mixing point density using packing surface area (a_P) and corrugation angle (θ) instead of channel base and crimp height is explored. This method builds the relationship between B, S, h and a_P, θ. Then, B, S, h can be expressed by a_P and θ. Finally, Equation (5-10) can be expressed by a_P and θ.

For a given structured packing, the distance between channels is unique. Figure 5.18 shows the channel distance L. Like channel base B and crimp height h, the channel distance L is also a structured packing geometric characteristic. Figure 5.19 shows the lateral view of a structured packing channel. For regular structured packing, the two side surfaces of the packing channel are mutually perpendicular. In other words, the angle α between the two side planes equals to 90 degree. Thus, the cross section of the packing channel is an isosceles right triangle. The two right-angle sides are channel distance L. The hypotenuse equals to $\sqrt{2}$L, shown by dash line in Figure 5.18 and 5.19.

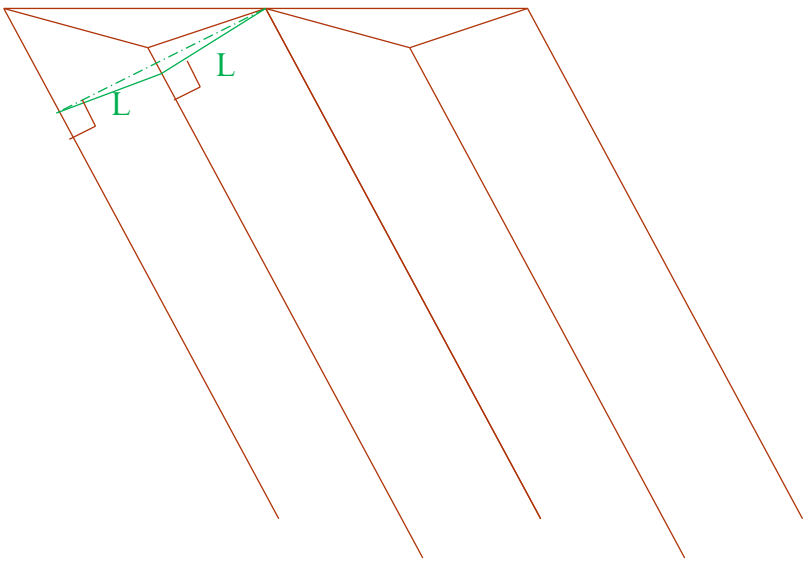

Figure 5.18. Structured packing with a channel distance L

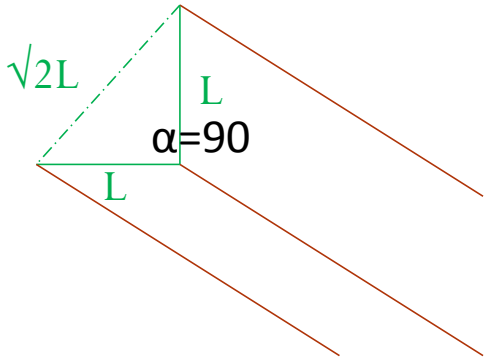

Figure 5.19. Lateral view of structured packing channel

The top surface of the packing channel is the triangle formed by channel base B and channel side S (details shown in Figure 9). The channel base B, hypotenuse of channel cross section √2L, and the ridge of packing channel D form a right angle triangle in the longitudinal section (Figure 5.20). In the right angle triangle, the angle between the packing channel base B and packing channel ridge D is the packing corrugation angle θ. Thus, channel base B can be expressed by L:

$$B = \frac{\sqrt{2}L}{\sin\theta} \tag{5-26}$$

The other right-angle side (channel ridge D) can be expressed by L:

$$D = \frac{\sqrt{2}L}{\tan\theta} \tag{5-27}$$

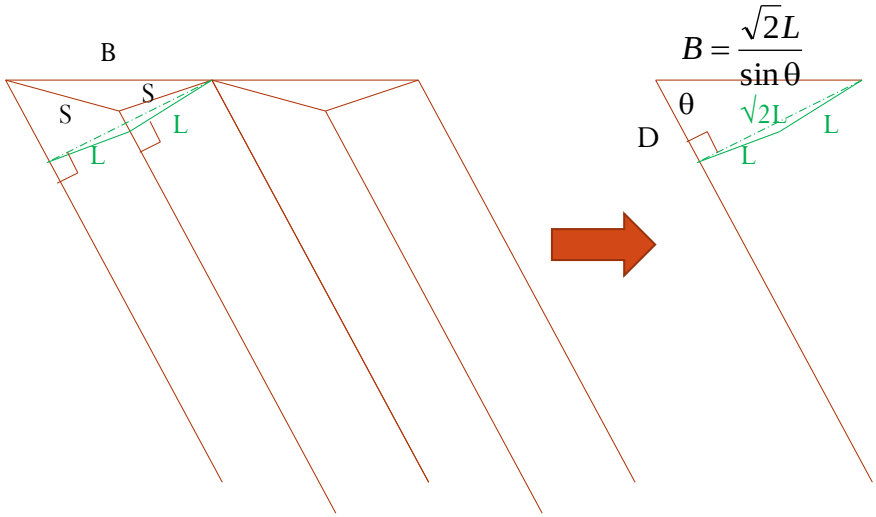

Figure 5.20. Longitudinal section of structured packing channel (I)

Figure 5.21 shows the relation between channel side S and channel ridge D. S is the hypotenuse in the right-angle triangle formed by S, L, and D/2. S can be expressed by L and D:

$$S^2 = (D/2)^2 + L^2 \tag{5-28}$$

Combine (5-27) and (5-28), channel side S can be expressed by L:

$$S = \frac{\sqrt{2\tan^2\theta + 1}}{\sqrt{2}\tan\theta} L \tag{5-29}$$

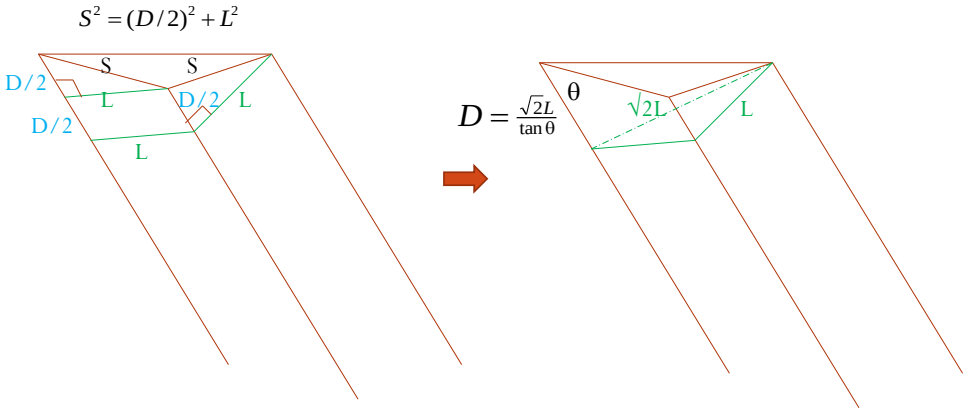

Figure 5.21. Longitudinal section of structured packing channel (II)

Since B and S are expressed by L, the crimp height h can then be expressed by L:

$$h = \sqrt{S^2 - (\frac{B}{2})^2} = \sqrt{\frac{(2\tan^2\theta + 1)L^2}{2\tan^2\theta} - \frac{L^2}{2\sin^2\theta}} = \frac{L}{\sqrt{2}} \tag{5-30}$$

In structured packings, geometric characteristics B, S, h have the relation with packing surface area a_P:

$$\frac{Bh}{4S} = \frac{1}{a_P} \tag{5-31}$$

Combine equations (5-26), (5-29), (5-30), (5-31), the channel distance L can then be calculated by a_P and θ:

$$L = \frac{2\sqrt{2}\sqrt{\sin^2\theta + 1}}{a_P} \tag{5-32}$$

Since B and h can be expressed by L, and L can be expressed by a_P and θ, finally the mixing point density can be calculated from packing surface area a_P and corrugation angle θ:

$$M' = \frac{6}{BhB * \tan\theta} = \frac{3 * a_P^3 \sin\theta\cos\theta}{16(\sin^2\theta + 1)^{3/2}} \tag{5-33}$$

The mixing point density calculated in this way is an alternative to calculating it from B and h, especially in the cases when B and h values are not available. Table 5.4 shows the mixing point density (M′) calculated from a_P and θ compared with the mixing point density (M) calculated directly from B and h. The deviation between M′ and M is most likely due to bended packing channels (the packing channel angle α differs from 90 degree) in packing transportation and installation. Generally, the

deviation is acceptable for most packings (around 20%), except for A350Y whose surface area is believed to be less than 350 m^2/m^3.

Table 5.4. Comparison between mixing point density M calculated from B, h and M′ calculated from a_P, θ

	MP2X	GT-PAK^{TM}350Z	GT-PAK^{TM}350Y	MP250Y	MP250X
M	0.27E6	0.90E6	2.87E7	0.59E6	0.48E6
M′	0.30E6	0.99E6	2.19E7	0.79E6	0.55E6
Deviation	13%	11%	-23%	-34%	13%
M	A350Y	B350X	GT-PAK^{TM}500Y	RSP250Y	
M′	1.17E6	1.26E6	4.63E6	1.25E6	
Deviation	2.19E6	1.50E6	6.38E6	0.80E6	
	87%	20%	38%	-36%	

Figure 5.22 and 5.23 show the comparison between experimental data and k_L, k_G models using mixing point density calculated from a_P and θ. The k_L and k_G models using alternative mixing point density (M′ calculated from a_P and θ with the assumption of standard structured packing geometry) is not as accurate as the models using original mixing point density, but still predicts experimental data. It provides an alternative when packing characteristic lengths are not available.

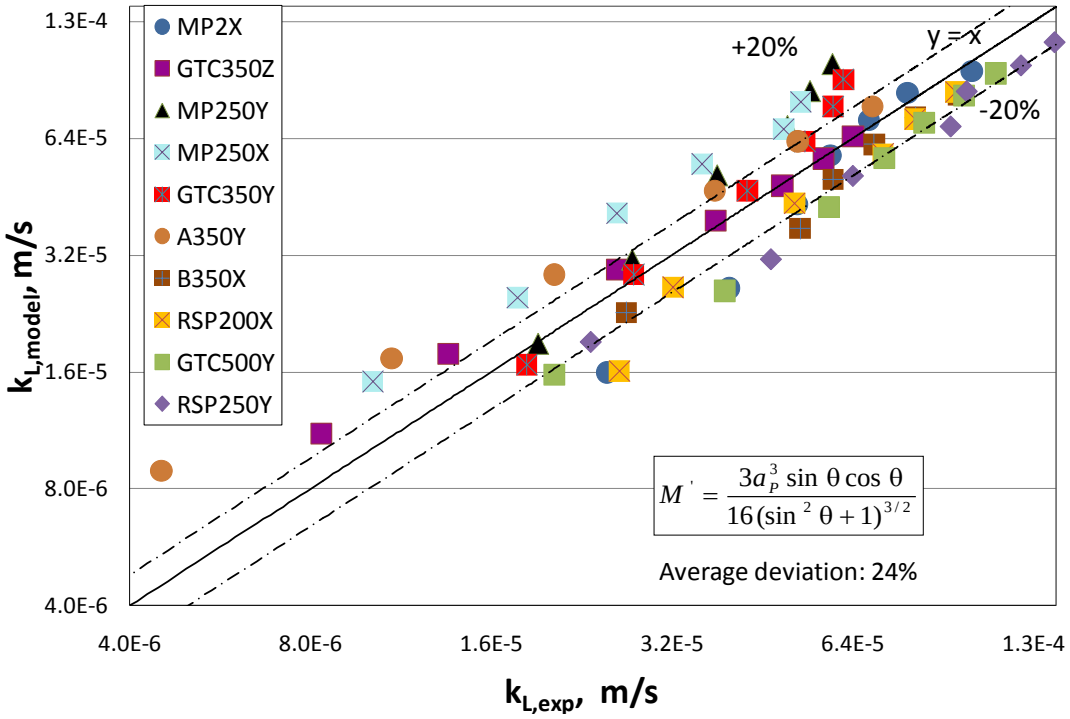

Figure 5.22. Comparison between experimental data and k_L models using mixing point density calculated from a_P and θ

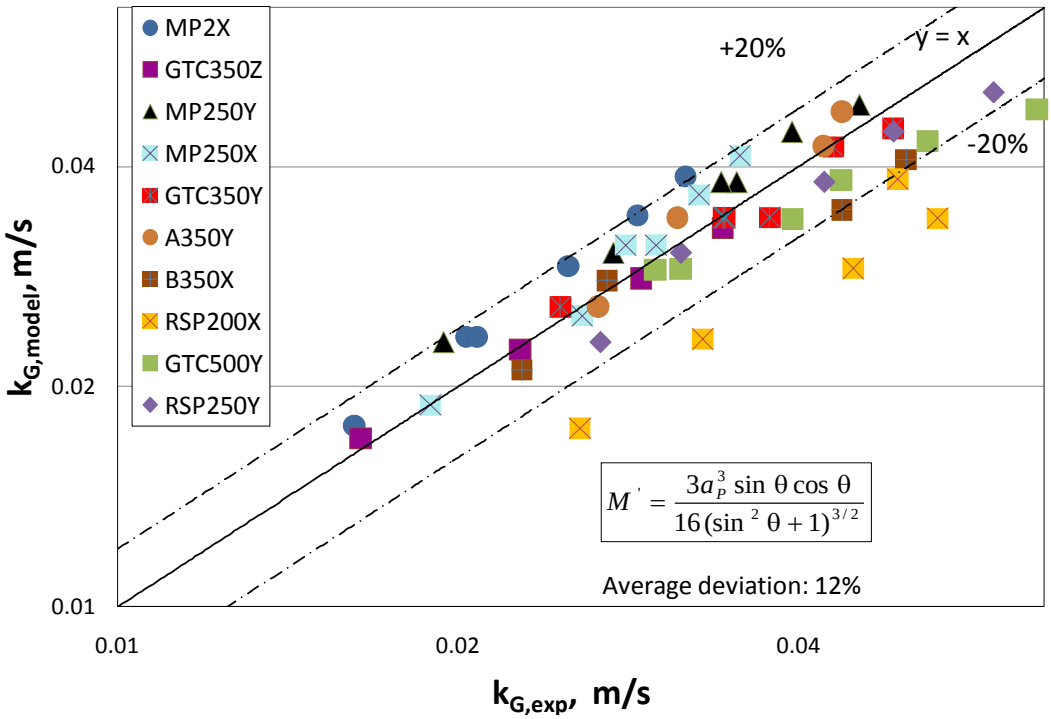

Figure 5.23. Comparison between experimental data and k_G models using mixing point density calculated from a_P and θ

5.7 Conclusions

In this chapter, three mass transfer models are developed. The database includes eleven structured packings with surface area ranging from 125 m^2/m^3 to 500 m^2/m^3 and corrugation angle from 45 degree to 70 degree, and three random packings from Raschig Super Ring family. The experimental systems use the absorption/desorption from aqueous solvents with liquid physical properties close to those of pure water.

The three dimensionless mass transfer correlations developed in this work are:

$$\frac{a_e}{a_P} = 1.41[(\frac{\rho_L}{\sigma})g^{1/3}(\frac{u_L}{a_P})^{4/3}]^{0.116}$$

$$Sh_L = 1.79 * \mathrm{Re}_L^{0.74} Mi^{0.42} Sc_L^{0.5},\ k_L = Sh_L a_P D_L$$

$$Sh_G = 0.83 * \mathrm{Re}_G^{0.58} Mi^{0.3} Sc_G^{0.5},\ k_G = Sh_G a_P D_G$$

$$M_i = \frac{M}{a_P^3}$$

Where,

a_e is the effective mass transfer area, (m^2/m^3);

a_P is the total surface area, (m^2/m^3);

ρ_L is the liquid density, (kg/m^3);

σ is the liquid phase surface tension, (N/m);

g is the gravity constant, (9.8 m/s^2);

u_L is the superficial liquid velocity, (m/s);

k_L is the liquid film mass transfer coefficient, (m/s);

k_G is the gas film mass transfer coefficient, (m/s);

u_G is the superficial gas velocity, (m/s).

M is the mixing point density calculated from B and h by Equation (5-10), (pts/m^3);

An alternative estimate of the mixing point density (M') from packing surface area (a_P) and corrugation angle (θ) is given by Equation (5-33) if direct measurement of B and h is not available.

The simple k_L and k_G models are given by:

$$k_L = 3.08E-3 * u_L^{0.72} M^{0.42} a_P^{-1.15}$$

$$k_G = 9.6E-3 * u_G^{0.54} M^{0.29} a_P^{-0.5}$$

The effective area model uses the basic form of the Tsai model (2010). Liquid superficial velocity over packing total area (u_L/a_P) is used as the liquid flow rate per wetted perimeter instead of (Q/L_P). Thus the applied range of this area model is extended to include hybrid packings and random packings. The experimental coefficient is changed from 1.34 to 1.41 which provides a better fit of the larger database. The wetted area varies with liquid rate to the 0.155 power and is independent of the corrugation angle and the mixing point density (Mi).

Mass transfer models developed in this work are compared with literature models. The models have good consistency with models developed from aqueous absorption systems. There are significant differences between models developed in this work and models developed from hydrocarbon systems (distillation systems). The

measurements of $k_G a$ with SO_2/NaOH give larger values of $k_G a$ than correlations of measurements in distillation systems. Gas and liquid back-mixing and maldistribution may play a critical role in commercial distillation separations that is not observed with the NaOH/SO_2 system.

Chapter 6: Absorber Economic Analysis

6.1 Case study and methodology

The objective of this chapter is to conduct an economic analysis on the absorber and explore the effect of operating condition and selected packing type on the total cost of the absorber. The stripper is assumed to be designed at optimum conditions. The three mass transfer correlations (a_e, k_G, k_L) developed in this work are used to calculate the installed capital cost (CAPEX) of the absorber. The measured pressure drop data for different packings are used to calculate the energy cost (Energy) of the absorber. Finally, the annualized CAPEX and Energy are combined together to obtain the total annualized cost (Total). From this study, the optimum fraction flood is found to be 50% to 80% for amine scrubbing CO_2 absorber, which is lower than normal distillation design. Details regarding optimum fraction flood for absorber will be discussed further in Section 6.6.

In this study, the base case is a 250 MW coal-fired power plant with 90% CO_2 removal from flue gas containing 12 mol % CO_2. The solvent used is 8 m (8 mol/kg water) piperazine (PZ) because it has high reaction rate, high capacity, low volatility, and low degradation rate. According to the stripper optimization (Lin, 2014), the total equivalent work of the regeneration process reaches a minimum at lean loading of 0.26-0.30 mol CO_2/mol alkali. Considering the solubility of the solvent, the lean and rich loadings are set at 0.3 and 0.4 mol CO_2/mol alkali in this analysis. The absorber operating temperature was controlled around 40 C.

6.2 Solvent physical and kinetic properties

The kinetic properties of the solvent at the lean and rich loading were obtained from Dugas (2009). At lean loading condition (0.305 mol CO_2/mol alkali), the liquid film mass transfer coefficient with chemical reactions ($k_{g,P}$') is 1.98E-6 mol/(s*Pa*m^2) with the driving force in pressure drop difference. At rich loading condition (0.404 mol CO_2/mol alkali), the $k_{g,P}$' is 3.53E-7 mol/(s*Pa*m^2). The mass transfer coefficients (k_G, k_L) used in this work are in units of m/s, with the driving force in concentration difference. Equation (6-1) is used to transformed the $k_{g,P}$' value to $k_{g,C}$' value in consistent unit of k_G and k_L. After transformation, the $k_{g,C}$' for 8 m PZ at lean and rich loading are 5.27E-3 m/s and 9.32E-4 m/s. The logarithmic mean value of $k_{g,C}$' at lean and rich loading is used in this work.

$$k'_{g,C} = k'_{g,P} * RT \tag{6-1}$$

The physical properties of 8 m PZ were obtained from Freeman (2011). Equation 6-2 from Xu (2011) is used to calculate the partial pressure of CO_2 in 8 m PZ at this lean and rich loading.

$$\ln P_{CO2}(Pa) = a + b\frac{1}{T} + c\alpha + d\alpha^2 + e\frac{\alpha}{T} + f\frac{\alpha^2}{T} \quad (6\text{-}2)$$

Where
T is the temperature (K);
α is the CO_2 loading in the solvent (mol CO_2/mol alkali);
a, b, c, d, e, and f are adjustable parameters with values shown in Table 6.1.

Table 6.1. Adjustable parameters used in CO_2 partial pressure calculation

a	b	c	d	e	f
35.3	-11054	0	-18.9	4958	10163

Finally, the slope of the equilibrium curve (m) can be calculated (6-3, 6-4, 6-5).

$$m = \frac{\Delta C_{CO2,G}}{\Delta C_{CO2,L}} \quad (6\text{-}3)$$

$$C_{CO2,G} = \frac{P^*_{CO2}}{RT} \quad (6\text{-}4)$$

$$C_{CO2,L} = \frac{n_{CO2,L}}{V_{total}} \quad (6\text{-}5)$$

Where
$\Delta C_{CO2,G}$ is the difference of CO_2 concentration in the gas phase, (mol/m^3);
$\Delta C_{CO2,L}$ is the difference of CO_2 concentration in the liquid phase, (mol/m^3);
P_{CO2}^* is the partial pressure of CO_2 in the gas phase, (Pa);
$n_{CO2,L}$ is the number of moles of CO_2 in the liquid phase, (mol);
V_{total} is the total volume of the liquid phase, (m^3).

The value of m is 7.37E-4 at lean loading and 8.57E-3 at rich loading. The average of these two values was used in this work to calculate the overall mass transfer coefficient K_{OG} (Equation 6-10). The kinetic and physical properties of the solvent are summarized in Table 6.2.

Table 6.2. Kinetic and physical properties of 8 m PZ at 40 ℃

	$k_{g,C}'$	Density	P_{CO2}^*	m
	m/s	kg/m^3	Pa	
Lean	5.27E-3	1121	795	7.37E-4

Rich	9.32E-4	1150	7891	8.57E-3
Average	2.50E-3	1136		3.19E-3

6.3 Purchased Equipment Cost

6.3.1 Packing cost

The absorber used stainless steel structured packing. The packing purchase costs were estimated based on the quotes from a packing vendor. Since most of the metal structured packings have similar geometry, a general cost equation can represent them. Equation (6-6) is a representation of the packing cost as a function of specific area, a_P.

$$Packing\ cost\ per\ surface\ area\ (\$/m^2) = 7.31 + 203.05/a_P \qquad (6\text{-}6)$$

Where

a_P is the surface area per volume, (m^2/m^3).

The packing purchase cost can be calculated by Equation (6-7).

$$Packing\ \ purchased\ \cos t\ (\$) = \mathrm{Re}\,quired\ \ surface\ area * (7.31 + \frac{203.05}{a_P}) \qquad (6\text{-}7)$$

The required packing surface area equals the packed volume (Z*A) multiplied by the total surface area per volume (a_P). The packed height can be calculated by (6-8).

$$Z = HTU * NTU = \frac{u_G}{K_{OG} a_e} * \ln(\frac{C_{CO2,in}}{C_{CO2,out}}) \qquad (6\text{-}8)$$

The required packing surface area can be calculated by (6-9):

$$Z * A * a_P = \frac{u_G * NTU * A * a_P}{K_{OG} a_e} \qquad (6\text{-}9)$$

Where

A is the column cross section area, (m^2);

NTU is the number of transfer units required to obtain 90% removal. NTU can be calculated by:

$$NTU = 1.2 * \ln \frac{CO_{2,in} - CO^*_{2,in}}{CO_{2,out} - CO^*_{2,out}} \qquad (6\text{-}10)$$

Since the equilibrium concentration of CO_2 is negligible compared to the CO_2 concentration in the gas phase, Equation (6-10) can be simplified as:

$$NTU = 1.2 * \ln \frac{CO_{2,in}}{CO_{2,out}} = 2.76 \qquad (6\text{-}10a)$$

The overall mass transfer coefficient K_{OG} is given by Equation (6-11).

$$\frac{1}{K_{OG}} = \frac{1}{k_G} + \frac{H_{CO2}}{\sqrt{k_2[Am]D_{CO2}}} + \frac{1}{k_L}\left(\frac{\Delta C_{CO2,G}}{\Delta C_{CO2,L}}\right) \qquad (6\text{-}11)$$

The effective area (a_e), liquid film mass transfer coefficient (k_L), and gas film mass transfer coefficient (k_G) have been measured and correlations have been developed. The packed height and the required packing area were calculated based on these mass transfer correlations.

$$\frac{a_e}{a_P} = C*\left[\left(\frac{\rho_L}{\sigma}\right)g^{1/3}\left(\frac{Q}{A}*\frac{1}{a_P}\right)^{4/3}\right]^{0.116} \qquad (6\text{-}12)$$

$$k_L = 3.08E-3*u_L^{0.72}M^{0.42}a_P^{-1.15} \qquad (6\text{-}13)$$

$$k_G = 9.6E-3*u_G^{0.54}M^{0.29}a_P^{-0.5} \qquad (6\text{-}14)$$

Where
k_L, k_G are the liquid film and gas film mass transfer coefficients, (m/s);
u_L, u_G are the liquid and gas phase superficial velocities, (m/s);
M is the mixing point density, (points/m^3);
a_P is the packing surface area, (m^2/m^3);
C is the experimental constant used in the effective area correlation, specific for each packing. The values of C for each packing is given in Table 6.7.

6.3.2 Column Shell Cost

The purchase cost for the absorber column is divided into three parts: shell, internals, and auxiliary. The cost for column shell was estimated on the basis of weight. In this study, the majority of the column shell was specified as carbon steel with a shell thickness of 3/8 inches. A stainless steel (304SS) layer 1/4 inches was clad on the inner side of the column to minimize corrosion. The shell thickness was set based on a previous design assumption (Tsai, 2010). The carbon steel and stainless steel shell costs were calculated by Equations (6-15) and (6-16) from Peters and Timmerhaus (1991). The shell weight was calculated according to Equation (6-17). The costs were converted to current dollars (2014) by applying the inflation index (Bureau of Labor Statistics, 2014). For reference, the index values in 1990 and 2014 are listed as 130.7 and 237.3, so the costs from Peters and Timmerhaus were converted to current prices by dividing a factor 0.55 (130.7/237.3 = 0.55).

$$Carbon\ steel\ \cos t(\$) = 276.1*(Shell\ weight)^{0.6016} \qquad (6\text{-}15)$$

$$Stainless\ steel\ \cos t(\$) = 575*(Shell\ weight)^{0.609} \qquad (6\text{-}16)$$

$$Shell\ weight = Steel\ density * V_T * S * d \qquad (6\text{-}17)$$

Where

Z_T is the total height of the column, (m);
S is the column side length, (m);
d is the shell thickness, (m).

The column was assumed to be square, and the column side length was calculated based on the column cross section area. The total height of the column was the sum of the packed height, the water wash height, the sump height, and the auxiliary heights (inlet and outlet ducts, distributor, miscellaneous heights). Table 6.3 lists the heights for different column sections.

Table 6.3. Heights for different column sections

Sections	Value	Unit
Packing	$\frac{u_G}{K_{OG}a_e} * \ln \frac{C_{CO2,in}}{C_{CO2,out}}$	
Water wash	$\frac{u_G}{k_G a_e} * 4$	
Sump	$u_L * t_{hold-up}$	
Inlet/Outlet duct	4.57	m
Distributor	1.83	m
Miscellaneous	1.83	m

6.3.3 Auxiliaries Cost

The costs for auxiliaries (cladding, distributor, connections, ladders, platforms and handrails, etc) were also calculated. Equations to calculate capitals costs are shown in Table 6.4.

Table 6.4. Equipment purchase costs equations

Items	Equations
Column shell cost	Stainless steel = 575*[Shell weight (lb)]$^{0.609}$
	Carbon steel = 276.1*[Shell weight (lb)]$^{0.6016}$
Packing cost	($/m^3) = 7.31 a_P+203.05
Distributor	15355*[Column diameter (m)]$^{0.1764}$
Distributor support (beams)	5/6*Distributor purchased cost
Chimney tray collector	15350*[Column diameter (m)]$^{0.1281}$
Packing support grid	12019*[Column diameter (m)]$^{0.1792}$
Plat forms/handrails	985.33*[Column diameter (m)]+759.33
Connections/manholes	870*[Column height (m)]
Ladders	111.55*[(Column height (m)]

6.3.4 Annualized capital costs

The equipment costs were converted to an annualized basis ($/yr) based on Equation (6-18). The costs were then converted to $/tonne CO_2 removed by Equation (6-19). In this work, the amount of CO_2 removed is 2.06E+06 tonnes/year. The installation factor (α) scales the purchased equipment cost to the total investment and was set to be 5 based on several analysis methods and reports (Frailie, 2013). The annualizing factor (β) was set to be 20% based on a cash flow analysis including the rate of return, taxes, maintenance, and depreciation (assuming a 5-year MACRS depreciation schedule, a 10-year project life, a 2-year construction period). The percentages used for parameters such as rate of return (ROI) are listed in Table 6.5.

Table 6.5. Parameters used in cash flow analysis

Parameter	Percentage (%)
ROI	10%
Income tax	3.5%
Maintenance	2%
Depreciation	4.5%

$$Annualized\ CAPEX = Equipment\ cost * \alpha * \beta \quad (6\text{-}18)$$

$$Costs\ per\ tonne\ CO_2\ removed = \frac{Annualized\ Costs}{tonne\ of\ CO_2\ removed\ per\ year} \quad (6\text{-}19)$$

6.4 Energy Cost

The blower and pump costs were calculated to arrive at the energy cost. The blower work cost was calculated using Equation (6-20). The electricity price was specified as $61.4/MWh according to data from US Energy Information Administration (EIA, 2013). The blower work rate was calculated by Equation (6-21).

$$C_{Blower} = N_{Blower} * (\$ / MWh) * t \quad (6\text{-}20)$$

$$N_{Blower} = \frac{\Delta P_T G}{10^6 \eta} \quad (6\text{-}21)$$

Where
G is the gas flow rate, (m^3/s);
ΔP_T is the total pressure drop, (Pa);
η is the blower efficiency (75% used in this analysis).

Table 6.6 gives the estimated pressure drop for each absorber section. The ΔP/Z for each packing is calculated from the GPDC correlations:

$$CP = \frac{3.8617(\frac{\Delta P}{Z})^{0.6609}}{[1+6.3763(\frac{\Delta P}{Z})^{(0.6609/0.7206)} * F_{LV}^{0.2898}]^{0.7206}}[1-\exp(-0.9093 * F_{LV}^{(-0.6819)})] \quad (6\text{-}22)$$

$$CP = C_S F_P^{0.5} \nu_L^{0.05} \quad (6\text{-}23)$$

$$C_S = u_G(\frac{\rho_G}{\rho_L - \rho_G})^{0.5} \quad (6\text{-}24)$$

$$F_{LV} = (\frac{L_m}{G_m}) * (\frac{\rho_G}{\rho_L})^{0.5} \quad (6\text{-}25)$$

Where
ν_L is the kinetic viscosity of liquid phase, (cSt);
u_G is the superficial gas velocity, (m/s);
ρ_G and ρ_L are the gas and liquid density, (kg/m^3);
L_m and G_m are the mass flow rate of liquid and gas flows, (kg/s);
F_P is the packing factor, (m^{-1}).

The packing factor (F_P) could be obtained either from the packing vendor or from back calculation based on the measurements. In this work, the packing factor is back calculated from the pressure drop measurements using the above equations (6-22) to (6-25). The calculated packing factor (F_P) is then used in pressure drop calculation for the absorber. The calculated packing factor (F_P) is listed in Table 6.7.

Table 6.6. Pressure drop for each section

Section	ΔP	Unit
SO_2 polisher	1245.4	Pa
Direct contact cooler	1245.4	Pa
Absorber	$Z_{Pack} * (\frac{\Delta P}{Z})$	
Water wash	$Z_{WW} * (\frac{\Delta P}{Z})$	

Table 6.7. Packing factor and experimental constant for each packing used in this work

	F_P (ft^{-1})	C (used in Equation 6-12)
MP250Y	20.1	1.49
MP250X	7.9	1.36
RSP250Y	16.8	1.56
GT-PAK™ 350Z	12.1	1.39
MP125Y	10.1	1.42
GT-PAK™ 350Y	32.4	1.27
GT-PAK™ 500Y	38.6	1.10

RSP200X	14.4	1.70
MP2X	6.8	1.38

The pump work cost was calculated from similar assumptions as blower work calculation. The pump work was calculated by Equation (6-26).

$$N_P = N_e / \eta = Q_L \rho g H_{T,L} / \eta \quad (6\text{-}26)$$

Where
Q_L is the liquid flow rate, (m^3/s);
$H_{T,L}$ is the liquid total head, (m).

The blower equipment cost and pump equipment cost were also calculated based on the collaborative report between Rochelle and Trimeric Corporation (Rochelle, 2005). The gas flow scale factor (S_G) was set at 0.6; the pressure drop scale factor (S_P) was set at 0.5; and the liquid flow scale factor (S_L) was set at 0.33.

$$C_{\text{blower}} = \left(C_{\text{Trimeric, blower}}\right)\left(\frac{G}{G_{\text{Trimeric}}}\right)^{S_G}\left(\frac{\Delta P}{\Delta P_{\text{Trimeric}}}\right)^{S_P} \quad (6\text{-}27)$$

$$C_{\text{pump}} = C_{\text{Trimeric,pump}}\left(\frac{L}{L_{\text{Trimeric}}}\right)^{S_L} \quad (6\text{-}28)$$

Where
$C_{\text{Trimeric,blower}}$ is \$510,000;
G_{Trimeric} is 620,000 kg/hr;
$\Delta P_{\text{Trimeric}}$ is 10.3 kPa;
$C_{\text{Trimeric,pump}}$ is \$68,000;
L_{Trimeric} is 732 liters/s.

6.5 Economic Analysis

6.5.1 Capital cost and energy cost analysis

The capital cost results for 250Y are given in Figure 6.1. The column height increases as gas superficial velocity increases while column side length will decrease. The mass transfer properties (a_e, k_G, k_L) will increase with gas velocity. The required packing volume (V_{pack}) decreases with increasing a_e and K_{OG} according to the calculation:

$$V_{pack} = A * Z_{pack} \quad (6\text{-}29)$$

The cross section area A (m^2) can be calculated by:

$$A = \frac{G}{u_G} \quad (6\text{-}30)$$

The packed height Z (m) can be calculated by:

$$Z = NTU * HTU = \frac{NTU * u_G}{K_{OG} a_e} \qquad (6\text{-}31)$$

Thus, the required packing volume:

$$V_{pack} = A * Z_{pack} = \frac{G * NTU}{K_{OG} a_e} \qquad (6\text{-}32)$$

Where
G is the total gas flow rate, (354 m^3/s);
NTU is the total number of transfer units, (2.76 transfer units).

The total gas flow rate G and total number of transfer units (NTU) are fixed. Thus, the required packing volume will decrease as effective area (a_e) and mass transfer coefficients (k_L and k_G) increase, which results in a reduced packing cost. The column cost will also decrease as gas velocity increases.

The energy cost results for 250Y are given in Figure 6.2. The pump cost increases with gas velocity mainly due to the increased column height. There are two factors influencing the blower cost: the packed height and the pressure drop per ft packing. The packed height increases linearly with gas velocity while the pressure drop per ft packing increases with gas velocity squared. Compared with the pump cost, the blower cost is much higher and dominates the operating cost.

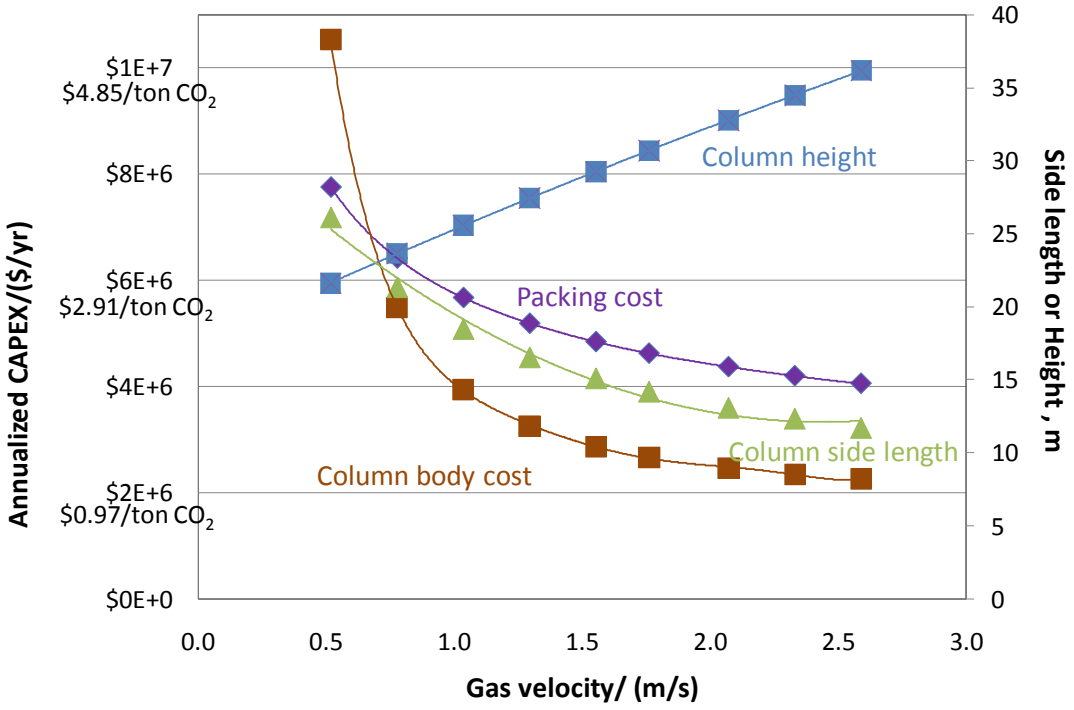

Figure 6.1. Capital cost results for 250Y

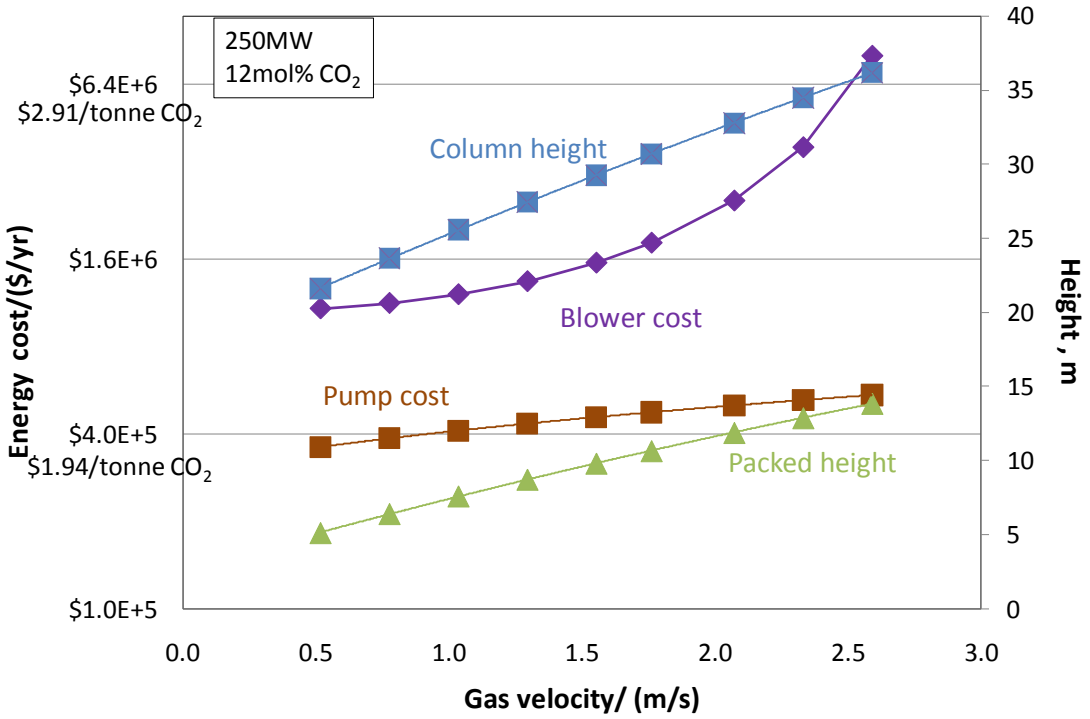

Figure 6.2. Energy cost for 250Y

6.5.2 Total cost analysis and discussion

Figure 6.3 shows the total cost results for 250Y. As in the previous discussion, the Energy increases with gas velocity squared. Meanwhile, the CAPEX decreases with gas velocity. At low gas velocity, the benefits from the reduced CAPEX compensate for the expenses from the increased Energy. Therefore, the total cost decreases in this CAPEX dominant region. As gas velocity increases, the slope of the Energy curve becomes larger and the slope of the CAPEX curve becomes smaller. The CAPEX benefits cannot make up for the Energy expenses, resulting in the ascending total cost curve in the Energy dominant region. The lowest total cost represents a tradeoff between CAPEX and Energy, and it is achieved at the intersection of the CAPEX and Energy regions. The optimum gas superficial velocity for this packing is 1.76 m/s (68% flood).

Table 6.8 summarizes the results at the minimum cost for 250Y and Figure 6.4 shows the composition of total cost at the optimum case. At the optimum case, the column total height is 30.7 m and the side length (diameter) is 14.2 m. Another interesting finding is that 68% of flood is the optimum condition for the absorber design, which is different from the normal distillation column design (usually 70–90% of flood). From the cost analysis, the packing cost accounts for 48.2% of the total cost and column cost accounts for 27.8%. The total CAPEX comprises 76% of the total cost and the Energy is 24%, primarily from the blower cost. The optimum total for this packing is \$4.64/tonne CO_2.

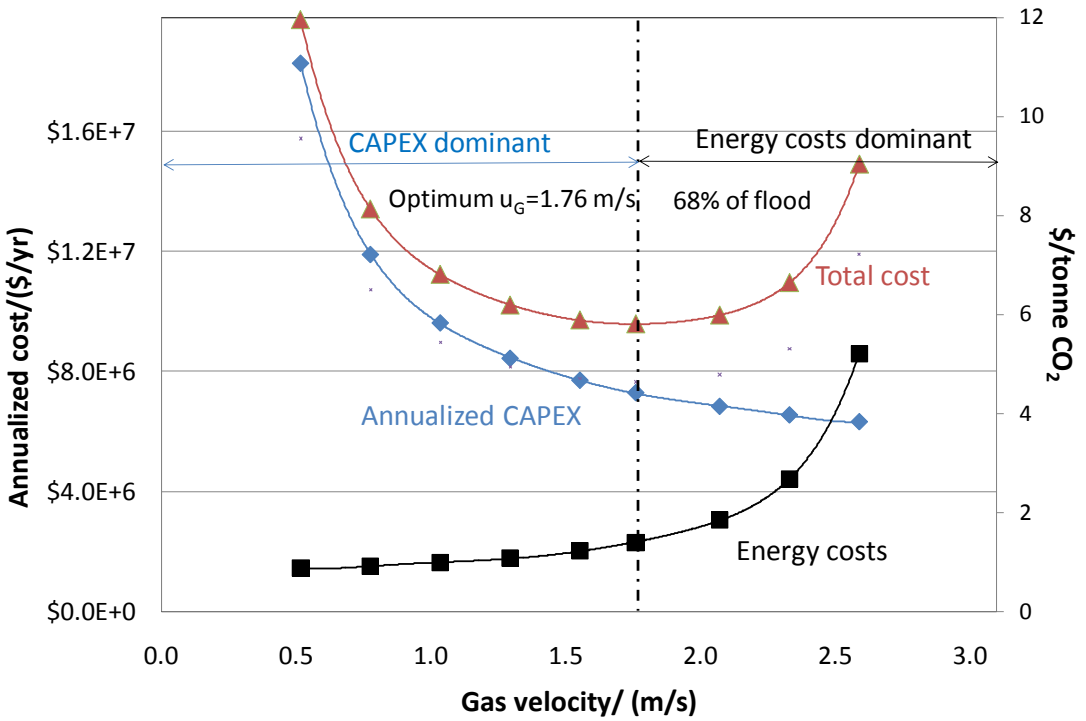

Figure 6.3. Total cost results for 250Y

Table 6.8. The optimum case results for 250Y

Item	Value	Unit
u_G	1.76	m/s
u_L	25.1	m/h
flood	68	%
Total column height	30.7	m
Column side length	14.2	m
Annualized CAPEX	7.28E+06	$/yr
CAPEX	3.53	$/tonne CO_2
Energy	2.30E+06	$/yr
	1.12	$/tonne CO_2
Total cost	9.58E+06	$/yr

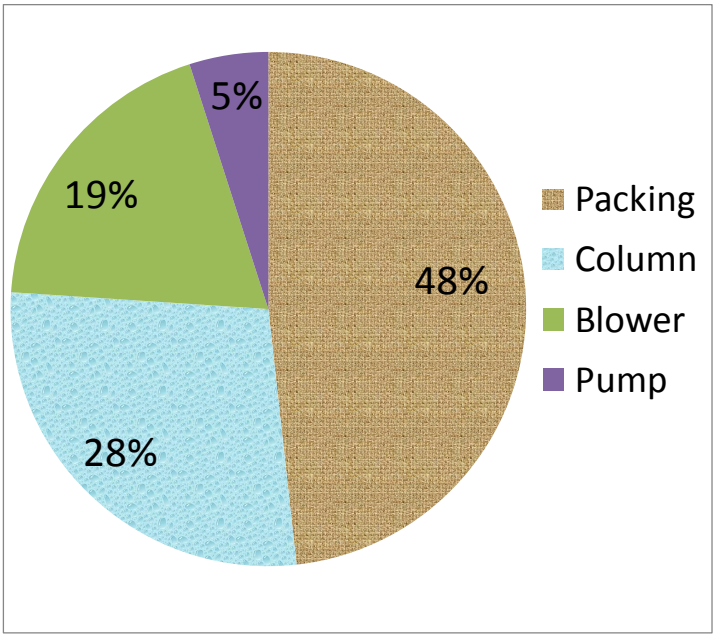

Figure 6.4. Total Cost distribution for the optimum case (250Y)

The economic analysis was also performed for all packings studied in this work. The packings show different optimum gas velocities. For high surface area packing (500Y), the optimum gas velocity becomes small because of the low capacity of the packing and the high pressure drop (Figure 6.5). For low surface area packing (200X) the optimum gas velocity becomes larger because of the low pressure drop (Figure 6.6).

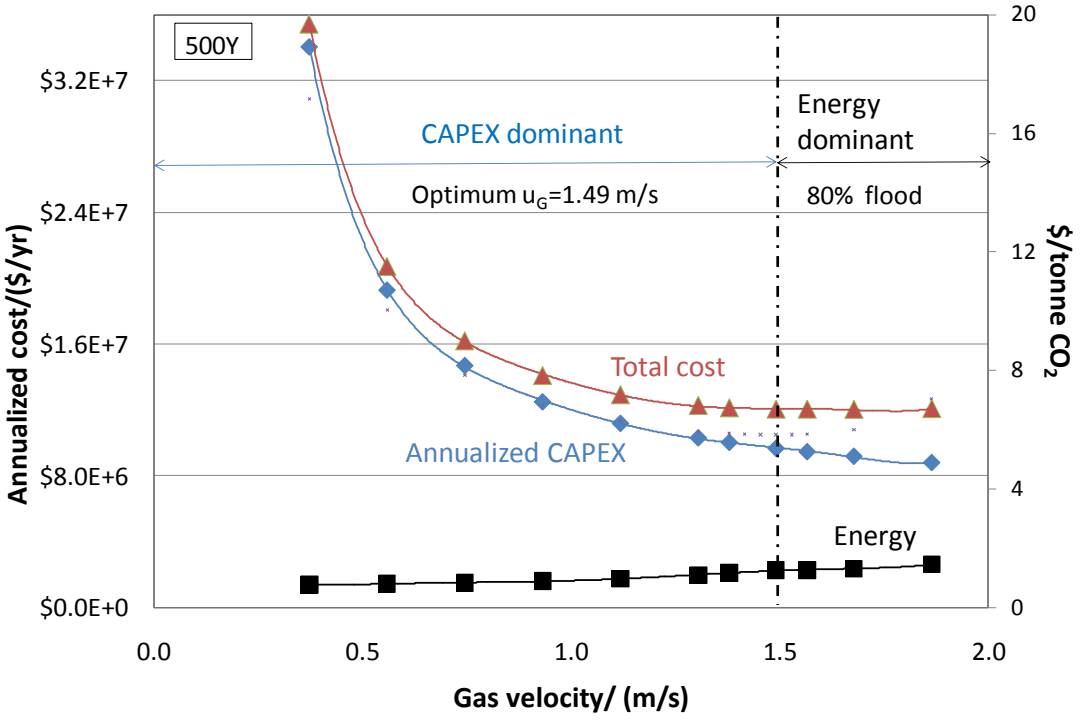

Figure 6.5. Total cost results for high surface area packing (500Y)

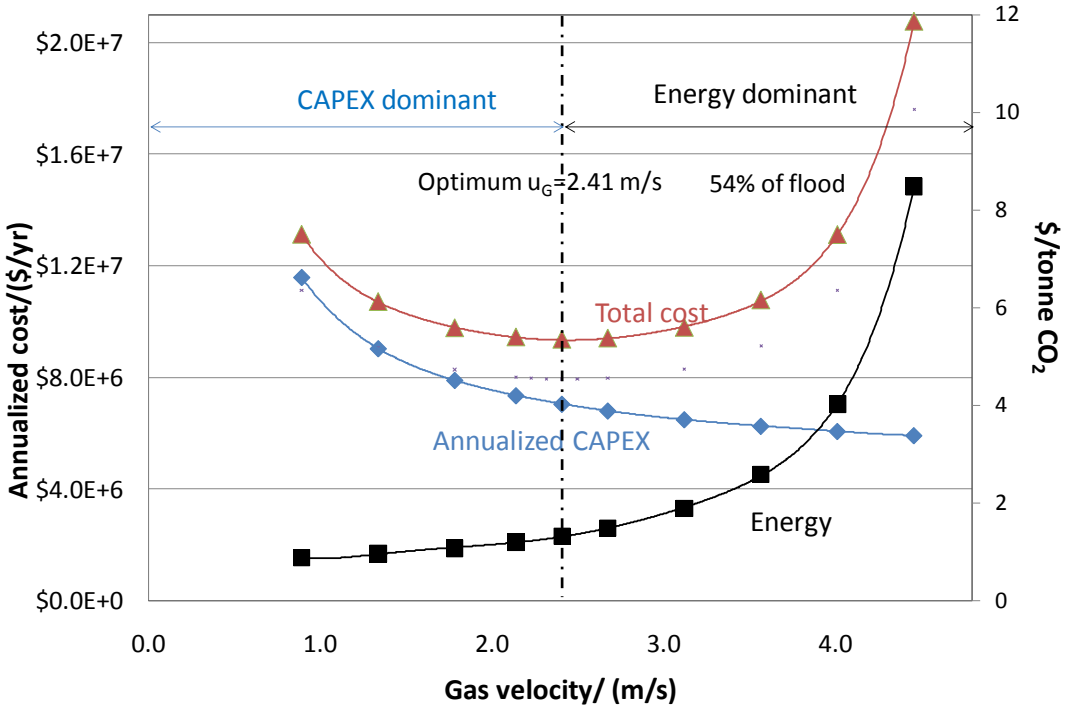

Figure 6.6. Total cost results for low surface area packing (200X)

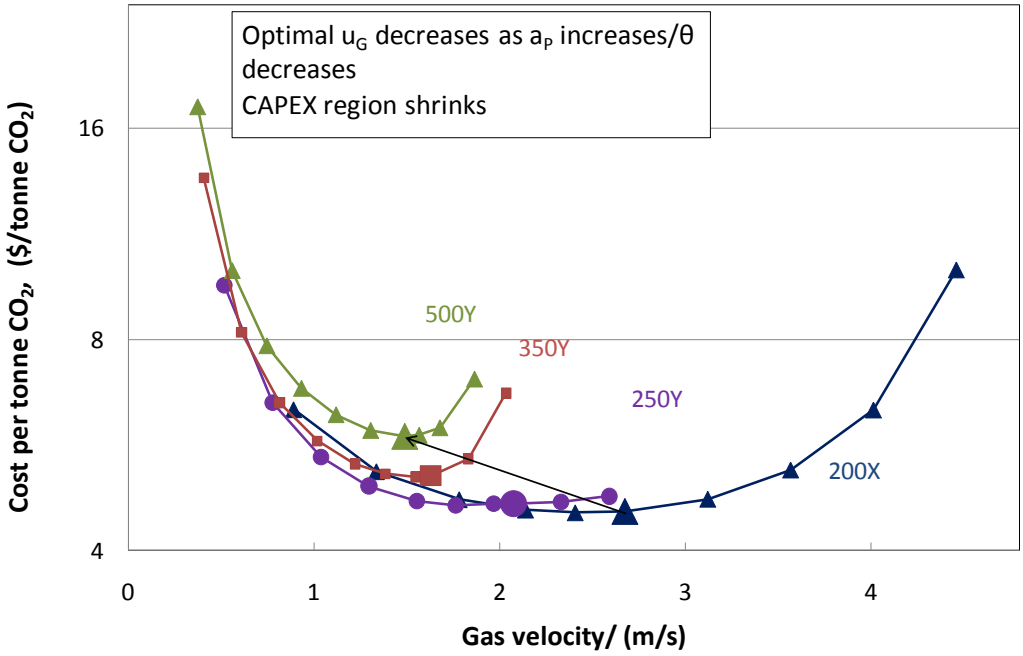

Figure 6.7. Total cost comparison between packings with different area

A comprehensive comparison of the total cost is given in Figure 6.7. As surface area increases from 200 to 500 m^2/m^3, the optimum gas velocity decreases from 2.41 to 1.49 m/s due to the decrease of packing capacity.

6.6 Optimum Percent of Flood

One of the major interests in this study is to determine the optimum operating percent of flood for the absorber. Figure 6.8 shows the total cost results at different fractional flood including all structured packings analyzed in this work. The shape of the total cost curve for each packing is quite similar. The bold solid points in each curve correspond to the optimal percent of flood for each packing. Although the optimal percent of flood changes from packing to packing, all the optimum points fall in the range of 50% to 80% of flood. The total cost curves are relatively flat in this region. Thus, the optimum operating region is between 50% to 80% flood for the absorber. Similar results were also found in Razi (2013) for a CO_2 absorber with MEA, where the optimum total cost was found to be at 74% of flooding velocity. Distinction among curves is also shown in Figure 8, but the difference does not appear to be especially high.

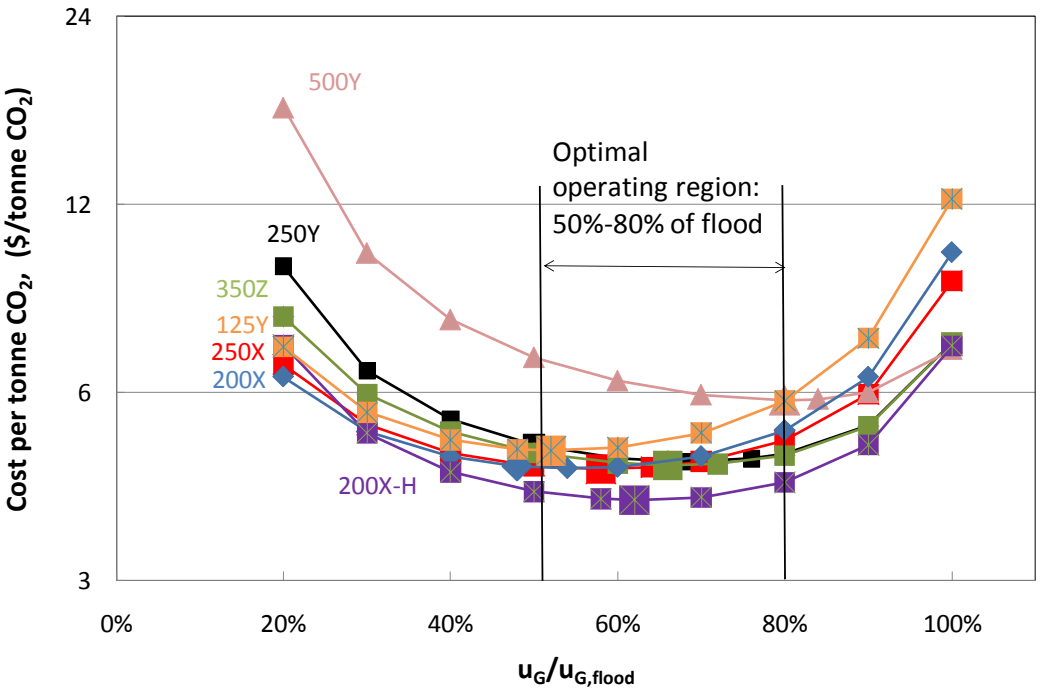

Figure 6.8. Total cost vs $u_G/u_{G,flood}$

Another interest of this study is to explore how the optimum percent flood ($u_{G,opt}/u_{G,flood}$) and the optimum total cost change with packing type (in Figure 6.9 and Figure 6.10). Results show that the optimum percent flood increases with packing surface area for both Y packings (45 degree corrugation angle) and X/Z packings (60 or 70 degree corrugation angle). The two hybrid packings (200X-H and 250Y-H) studied in this work show the same tendency and fall on the same curve with Y packings. For packings with the same surface area, Y packings and hybrid packings have higher optimum percent flood than X and Z packings.

The optimum total cost decreases with packing surface area initially and then increases. For packings with the same surface area, a higher corrugation angle packing has a lower pressure drop and similar effective area resulting in a lower total cost. Hybrid packings have lower optimum total costs than Y packings and X packings because of the higher effective area. In this work all the packing costs are calculated based on the same equation (Equation 6-6). However, there might be differences in the packing cost between different packing types or from different vendors which is not considered in this work. Thus, the optimum total costs are subject to change.

The economic analysis for all packings at the optimum gas velocity is summarized in Table 6.9. In conclusion, the optimum velocity ranges between 50% to 80% of flood for all packings, and increases as packing surface area increases. The optimum total cost ranges from \$8.34E+06 to \$1.2E+07 per year (\$4.04 to \$5.83 per tonne CO_2). The lowest total costs are obtained with packings with 200 and 250 m^2/m^3 surface area and 60 degree corrugation angle.

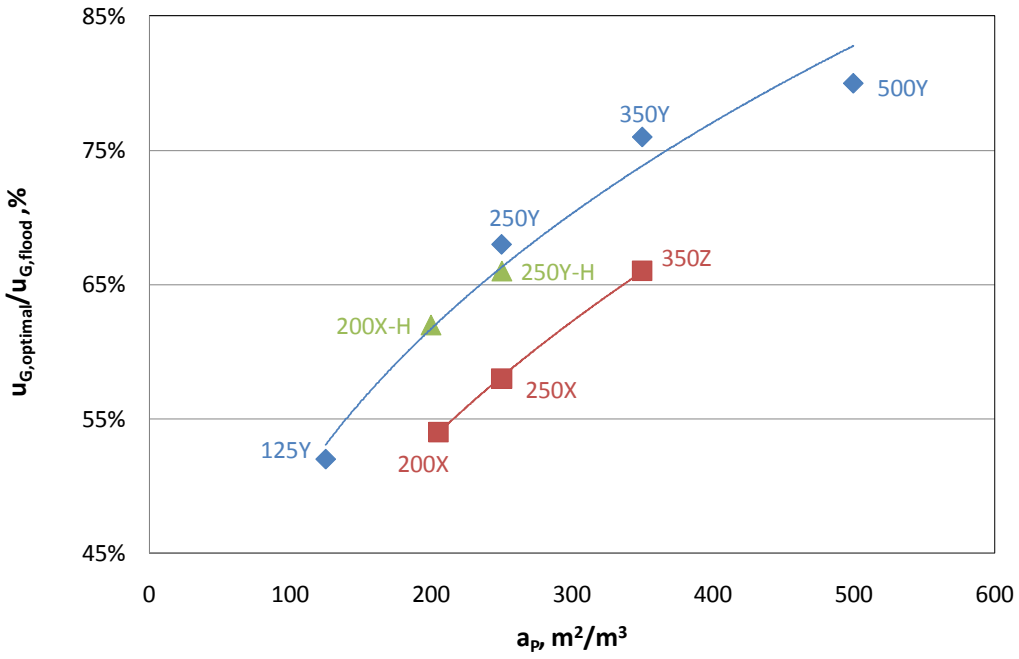

Figure 6.9. Optimum velocity/flooding velocity

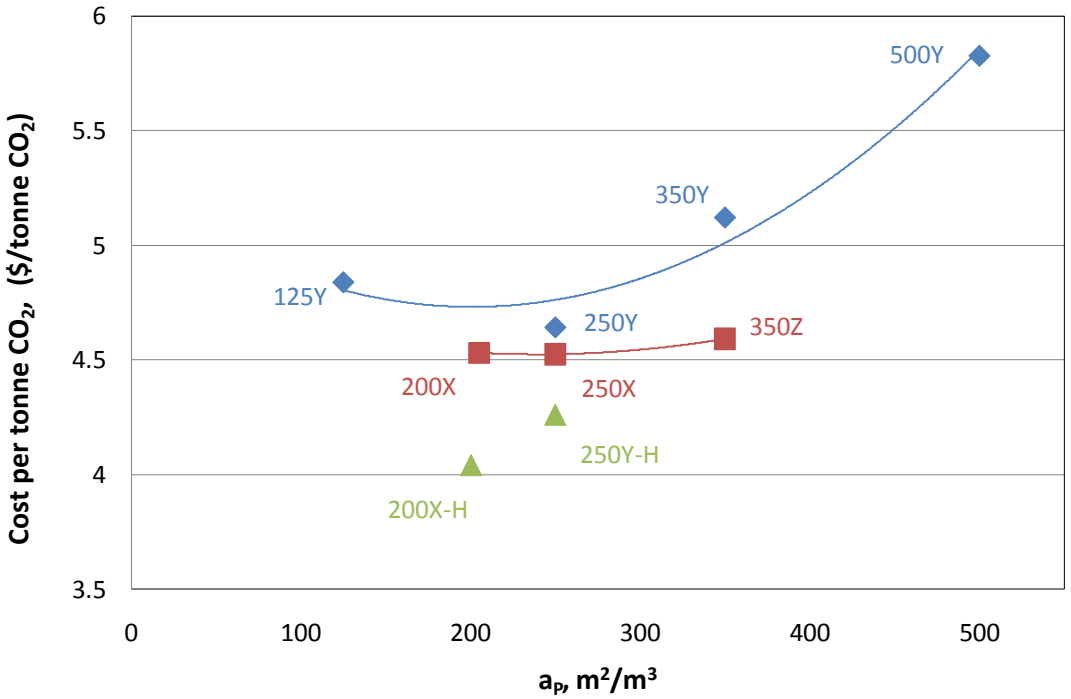

Figure 6.10. Optimum total cost changes with packing

Table 6.9. Economic analysis summary for a 250MWe coal-fired power plant

Packing	Optimum u_G	Flooding	Column height	Side length	Total cost	
	m/s	%	m	m	$/yr	$/tonne CO_2 removed
125Y	1.90	52	43.5	13.7	1.00E+6	4.84
200X	2.41	54	39.5	12.1	9.36E+6	4.53
200X-H	1.89	62	30.9	13.9	8.34E+6	4.04
250Y	1.76	68	31.0	14.0	9.60E+6	4.64
250X	2.39	58	37.1	12.0	9.34E+6	4.52
250Y-H	1.87	66	30.8	13.4	8.80E+6	4.26
350Y	1.55	76	26.5	15.8	1.06E+7	5.12
350Z	2.20	66	32.3	12.3	9.48E+6	4.59
500Y	1.49	80	26.1	15.4	1.20E+7	5.83

6.7 Sensitivity analysis

The sensitivity of the total annual cost is affected by two factors. One is the conversion factor of purchased equipment cost to installed plant cost and to annualized cost (α*β), which will determine the annualized CAPEX. The other is the electricity price ($E), which will influence the Energy cost. In this study, a cost

sensitivity analysis with respect to these factors was performed for the 250 MW CO_2 capture plant. A range of 4–7 was considered for α, and a range of 10–30% for β. For the electricity price, a range of \$42.9/MWh to \$112/MWh was considered based on the electricity prices of different states in the US (EIA, 2013). The ranges of sensitivity analysis factors are listed in Table 6.10.

Table 6.10. Ranges of sensitivity analysis factors

Factors	Installed cost factor (α)	Annualized cost factor (β)	Electricity price (\$E)
Ranges	3	10%	\$42.9/MWh
	4	20%	\$61.4/MWh
	5	30%	\$112/MWh
	6		
	7		

The effect of annualizing factor (α*β) on optimum percent of flood ($u_{G,opt}/u_{G,flood}$) for packing 250Y is shown in Figure 6.11. The base case is at α = 5 and β = 20% (αβ = 1). At the lowest annualizing factor (αβ = 0.3), $u_{G,opt}/u_{G,flood}$ is the lowest. As annualizing factor increases, the CAPEX dominant region expands and thus pushes the optimum flood to higher values. At the greatest annualizing factor (αβ = 2.1), $u_{G,opt}/u_{G,flood}$ is the greatest (76% of flood). The influence of annualizing factor is strong at low values and diminishes as αβ increases.

The effect of electricity price (\$E) on $u_{G,opt}/u_{G,flood}$ for 250Y is shown in Figure 6.12. The base case is at \$E = \$61.4/MWh, which is the industrial electricity price in the state of Texas. The lowest case is at \$E = \$42.9/MWh, which is the price in the state of Washington. The highest case is at \$E = \$112/MWh, which is the price considering carbon capture costs (adding another \$50/MWh to the base case). Unlike annualizing factor, as electricity price increases, the Energy dominant region expands and pushes the optimum percent of flood to lower values.

The total sensitivity analysis considers the combination of these two factors, which is αβ/\$E, on $u_{G,opt}/u_{G,flood}$. Figure 6.13 shows the influence of αβ/\$E on three selected packings with different surface area and corrugation angle (250X, 250Y, 500Y). For all packings, the optimum percent of flood increases as αβ/\$E increases. At the same αβ/\$E, $u_{G,opt}/u_{G,flood}$ shows this order: 500Y > 250Y > 250X, which confirms the results derived from Figure 6.9.

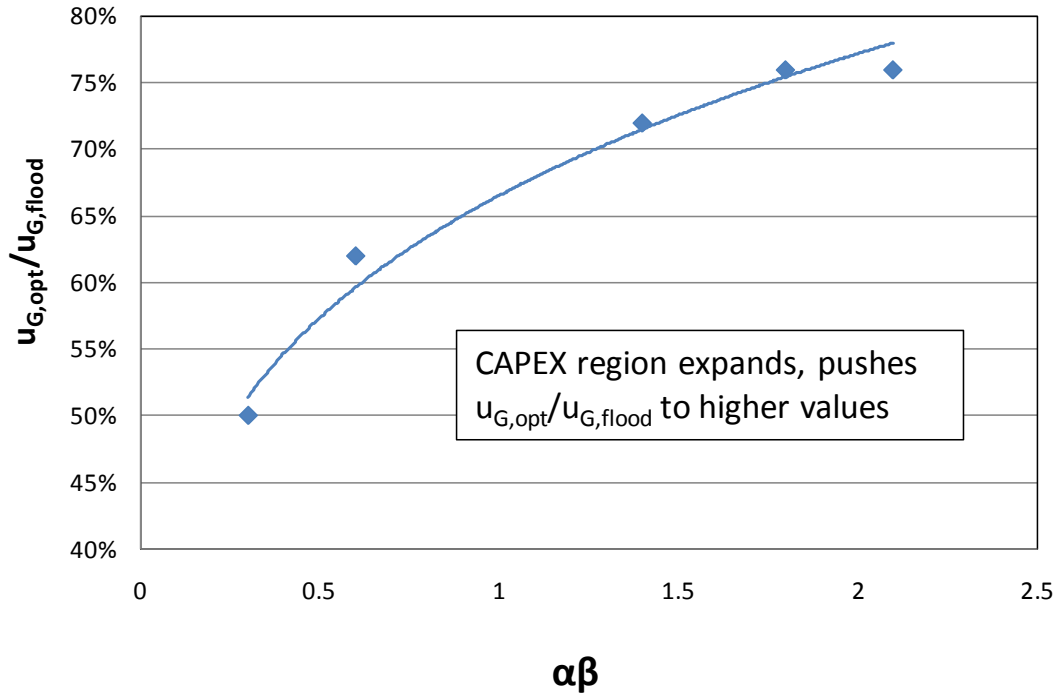

Figure 6.11. Effect of annualizing factor on $u_{G,opt}/u_{G,flood}$ (250Y)

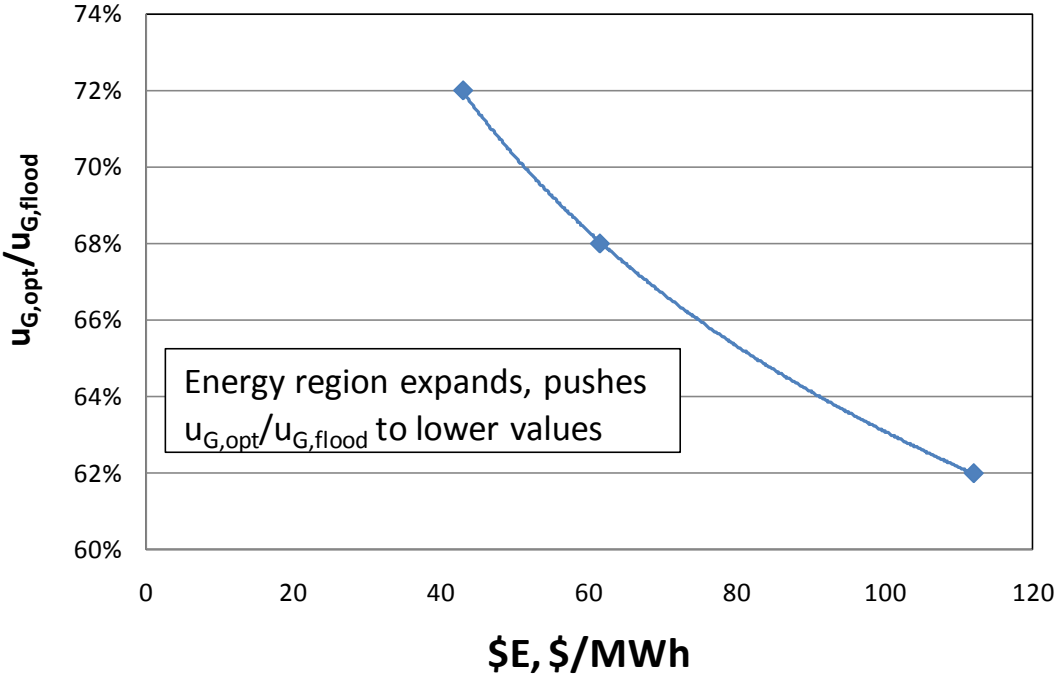

Figure 6.12. Effect of electricity price on $u_{G,opt}/u_{G,flood}$ (250Y)

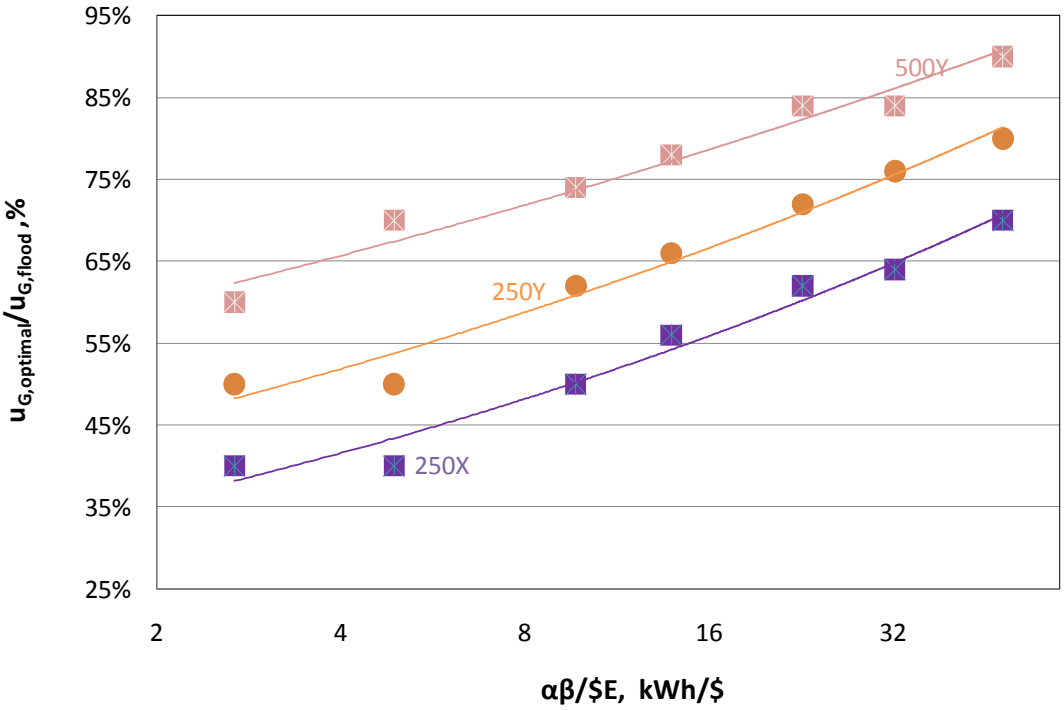

Figure 6.13. Effect of αβ/$E on $u_{G,opt}/u_{G,flood}$

6.8 Conclusions

In this chapter, an economic analysis of the absorber was conducted for a 250 MW coal-fired power plant. CAPEX decreases when u_G increases because the mass transfer properties (a_e, k_G, k_L) increase with gas velocity. Unlike CAPEX, the Energy curve rises with gas velocity exponentially. Total cost initially decreases with u_G and then increases.

As packing surface area increases from 200 to 500 m^2/m^3, the CAPEX region shrinks and the optimum gas velocity decreases from 2.41 to 1.49 m/s.

One of the most important findings in this work is that the optimum operating gas velocity for amine scrubbing CO_2 absorber (50% to 80% flood) is lower than normal distillation design which is usually between 70 to 90% flood (McCabe, 1993; Kister, 1992; Perry, 2008). For the amine scrubbing CO_2 absorption process, the mass transfer is determined by the effective mass transfer area (a_e), and a_e is not a strong function of velocity ($a_e \sim u_L^{0.16}$). However, for distillation columns, the mass transfer is usually determined by the volumetric overall mass transfer coefficient ($K_{OG}*a_e$), and $K_{OG}*a_e$ is a strong function of velocity ($K_{OG}*a_e \sim u_G^{0.7}$). Thus, operating at high gas and liquid velocities (70 to 90% of flood) will not get much benefit from the mass transfer, but at a high cost of operating cost.

The optimum percent flood increases with packing surface area and decreases with packing corrugation angle. Sensitivity analysis shows that increasing the ratio of the annualizing factor to the electricity price ($\alpha\beta$/\$E) will push the $u_{G,opt}/u_{G,flood}$ to higher values.

The optimum total cost decreases with packing surface area at first and then increases. The optimum total cost ranges from \$4.04 to \$5.83 per tonne CO_2 for all packings studied in this work. The lowest total costs are associated with packings with 200 and 250 m^2/m^3 surface area and 60 degree corrugation angle.

Chapter 7: Conclusions and Recommendations

7.1 Summary of work completed

In this work, the pressure drop (ΔP), liquid hold-up (h_L), effective mass transfer area (a_e), liquid film mass transfer coefficient (k_L), and gas film mass transfer coefficient (k_G) were measured for eleven structured packings and three random packings. Three experimental systems were used for mass transfer measurements: (1) absorption of ambient CO_2 with 0.1 gmol/L NaOH solution for a_e; (2) desorption of toluene in water with air for k_L; and (3) absorption of 100 ppm SO_2 in air with 0.1 gmol/L NaOH for k_G. All experiments were conducted consistently in the 0.428 m diameter PVC column under the same conditions so the k_L and k_G can be separated from the measured ka values.

The effects of liquid and gas superficial velocities (u_L and u_G), packing surface area (a_P), and corrugation angle (θ) on packing hydraulic and mass transfer performance were explored. Eleven structured packings with different surface area and corrugation angle and three random packings were measured. Based on experimental data, three global mass transfer models (effective area, k_G and k_L) were developed to predict the effect of the operating condition and packing geometry effects on mass transfer. A new concept using the mixing point density (M) was proposed to predict the effect of the packing geometry on k_L and k_G. The mixing point density can be calculated from the by packing characteristic lengths (channel base B and crimp height h). When the packing characteristic lengths were not available, a alternative method calculated the mixing point density from packing surface area a_P and corrugation angle θ.

An economic analysis for the absorber on a 250 MW coal-fired power plant was conducted. The capital costs and the energy costs were calculated and combined to get the total costs. The effects of operating conditions and packing geometries on total costs were explored. The optimal absorber design for amine scrubbing CO_2 capture was then suggested based on the analysis.

7.2 Conclusions

7.2.1 Mass transfer area

The effective mass transfer area is a function of liquid velocity, surface area, and is independent of gas velocity and corrugation angle. A correlation has been developed to predict the mass transfer area:

$$\frac{a_e}{a_P} = 1.41[(\frac{\rho_L}{\sigma})g^{1/3}(\frac{u_L}{a_P})^{4/3}]^{0.116} \quad (5\text{-}5)$$

7.2.2 Liquid and Gas film mass transfer coefficient

The dimensionless k_L and k_G models can then be developed based on the effects of liquid/gas velocity, mixing point density, packing surface area:

$$Sh_L = 1.79 * \mathrm{Re}_L^{0.74} Mi^{0.42} Sc_L^{0.5},\ k_L = Sh_L a_P D_L \quad (5\text{-}16)$$

$$Sh_G = 0.83 * \mathrm{Re}_G^{0.58} Mi^{0.3} Sc_G^{0.5},\ k_G = Sh_G a_P D_G \quad (5\text{-}17)$$

Where,

Mixing number Mi is the number of mixing points in a certain volume and can be calculated by:

$$Mi = M * l_{eq}^3 = \frac{M}{a_P^3} = \frac{6}{a_P^3 * B * h * B\tan\theta} \quad (5\text{-}18)$$

The new concept, Mixing Point Density (M), was introduced to account for the packing geometry effect on k_L and k_G. Mixing points are the joint points of packing corrugated sheets where liquid and gas flows mix with each other, change directions, and create turbulence. The mixing point density can be calculated by either packing characteristic length (5-10) or by surface area and corrugation angle (5-33):

$$M = \frac{6}{B * h * B\tan\theta} \quad (5\text{-}10)$$

$$M' = \frac{3 * a_P^3 \sin\theta\cos\theta}{16(\sin^2\theta + 1)^{3/2}} \quad (5\text{-}33)$$

The simple k_L and k_G correlations are:

$$k_L = 3.08E-3 * u_L^{0.72} M^{0.42} a_P^{-1.15} \quad (5\text{-}13)$$

$$k_G = 9.6E-3 * u_G^{0.54} M^{0.29} a_P^{-0.5} \quad (5\text{-}14)$$

The models developed in this work have been compared with literature models. A smaller difference between k_La values predicted by different models than the difference we would expected was found, suggesting use the k_L model and the a_e model developed by the same author as a combination. The average liquid rate dependence of k_L is between 0.5 to 0.7 from experiments, which means the previous k_L models using the effective liquid velocity (u_{LE}) under-predict the liquid rate dependence.

In the k_Ga comparison, the model developed in this work is higher than literature models by 40 to 80%. Most literature models are developed from distillation systems where equilibrium is critical to establishing the driving force. Imperfections in gas/liquid distribution, gas bypass, and other related phenomena will reduce the apparent gas film coefficient and modify the apparent effect of gas rate. For the system used in this work which is absorption of SO_2 with NaOH, equilibrium is not relevant because there is excess hydroxide.

7.2.3 Absorber economic analysis

An economic analysis of the absorber was conducted for a 250 MW coal-fired power plant. The total cost initially decreases with u_G and then increases. The optimum gas velocity $u_{G,opt}$ is between 50 to 80 % of flooding velocity for all packings, which is different from the normal distillation column design (usually 70 to 90% of flooding velocity). For the amine scrubbing CO_2 absorption process, the mass transfer is determined by the effective mass transfer area (a_e), and a_e is not a strong function of velocity ($a_e \sim u_L^{0.16}$). However, for distillation columns, the mass transfer is usually determined by the volumetric overall mass transfer coefficient ($K_{OG}*a_e$), and $K_{OG}*a_e$ is a strong function of velocity ($K_{OG}*a_e \sim u_G^{0.7}$). Thus, operating at high gas and liquid velocities (70 to 90% of flood) will not get much benefit from the mass transfer, but at a high cost of pressure drop.

The optimum total cost decreases with packing surface area at first and then increases. The optimum total cost ranges from \$4.04 to \$5.83 per tonne CO_2 for all packings studied in this work. The lowest total costs are associated with packing with 200 and 250 m^2/m^3 surface area and 60 degree corrugation angle.

7.2.4 Hydraulic

The dry pressure drop of conventional structured packing is given by:

$$\frac{(DP/Z)_{dry}}{a_P} = 0.12 * F_G^{1.81} \qquad (4\text{-}2)$$

Where the f-factor is given by:

$$F_G = u_G * \sqrt{\rho_G} \qquad (4\text{-}3)$$

The irrigated pressure drop increases with f-factor to a power from 1.8 to 2 in the pre-loading region. The irrigated pressure drop also increases with packing specific area. For high surface area packing, the value is higher than expected since resistance for gas and liquid flow is much higher. Both dry pressure drop and irrigated pressure drop decrease largely with increase of corrugation angle.

7.3 Recommendations for future work

In this work, a systematic investigation of operating condition (u_G, u_L) and packing geometries (a_P, θ) effects on packing mass transfer performance has been conducted. The study makes significant contributions not only to our database, but also the understanding of packings.

7.3.1 Liquid physical properties influence on mass transfer

A consistent study of liquid viscosity influence on liquid film mass transfer coefficient is highly needed. Liquid physical properties including viscosity (μ_L), diffusion coefficient (D_L), and surface tension (σ_L) are believed to influence k_L. Literature shows that the dependence of k_L on liquid viscosity varies from 0.53 to -0.103, which is a large disagreement. Most experiments on k_L use only an aqueous system which has insignificant variance in viscosity. For the few correlations in which liquid viscosity was varied over a wide range, either the column size is small, or only random packing was investigated. For amine scrubbing CO_2 capture, the μ_L of concentrated and CO_2-loaded amine solution can be 10-30 times more viscous than water.

The proposed research plan is to use the existing system (water/toluene system) by adding certain amount of glycerol to change the liquid viscosity (Song, 2014). Glycerol was chosen as the viscosity enhancer for its complete solubility in water and the Newtonian behavior of its aqueous solution. The proposed range of μ_L is 1-100 cP for water/toluene/glycerol system.

7.3.2 Packing material and texture influence on mass transfer

Further studies are needed for a systematic understanding of packing material and texture influence on mass transfer. Most packings measured in this work are made of stainless steel. Besides stainless steel, commercial packings are also made of other materials such as carbon steel, polypropylene, ceramic, etc. Different materials will influence the contact angle between packing surface and liquid phase. Thus, the mass transfer the effective area, k_L and k_G will also be influenced. Some exploratory work was done in this study by measuring the mass transfer area of 1 inch Plastic Pall Ring (PPR) made of polypropylene. The effective area of 1 inch PPR was 20 to 30% lower than the metal packings with the same surface area. Besides the material,

packing textures such as surface enhancement, perforation may also influence the mass transfer performance.

7.3.3 More emphasis on random packings

A systematic study on random packing shapes and geometries influences on mass transfer is needed. Unlike structured packings which usually have uniform geometry, random packings have quite different shapes and structures from each other. Random packings can be divided into different families, such as Pall Ring family, IMTP family, Raschig Super Ring family, etc. Studies can be focused on comparison between packings in the same family (like the work in this study), or focused on comparison between packings in different families.

7.3.4 More emphasis on extreme operating conditions

A Computational Fluid Dynamics (CFD) study on high corrugation angle packing operated at these conditions is recommended. In this study, the effective area for GT-PAK^{TM} 350Z (high corrugation angle packing) was found to start to decrease when operated at high liquid flow rate and low gas flow rate. This phenomenon was confirmed by area measurements for other high corrugation angle packings (RSP200X, B350X). It is believed that liquid flows will start to bridge at the packing surface. However, more data are needed to prove this phenomenon.

7.3.5 Absorber economics with inter-cooling

The economics study on intercooling cost is recommended. The study in this work was based on a simple absorber design without intercooling. However, intercooling should be considered in the real absorber design. In the advanced absorber design, in-and-out inter-cooling or pump-around inter-cooling are suggested. Intercooling system costs are composed by the cost from the pump, heat exchanger, and cooling water. It would be interesting to include the intercooling costs into absorber economics, and determine the optimal intercooling design and operating conditions.

7.3.6 Stripper economics

A rigorous stripper economics analysis is highly recommended. In the amine scrubbing CO_2 capture system, it is believed that most of the costs are from the stripper side, especially the energy costs from the reboiler and heat-exchanger. It is highly recommended to conduct a rigorous stripper economics analysis, and explore the effects of lean loading, packing selection, and operating velocity on stripper costs.

Appendix A: Detailed Gas/Liquid Sample system

This appendix contains detailed description for the CO_2, SO_2, and toluene/water sample system. Pictures of the sample points are included to show the layout and clearly label the experimental system.

A.1 CO_2 sample system

A.1.1 Photographs and Labels

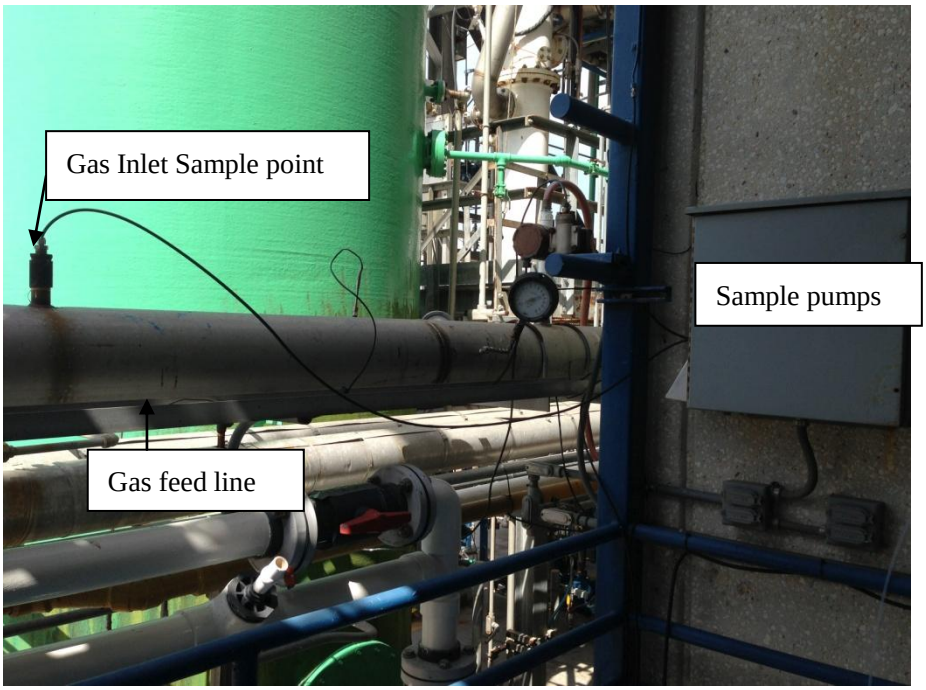

Figure A.1. CO_2 Inlet sample point

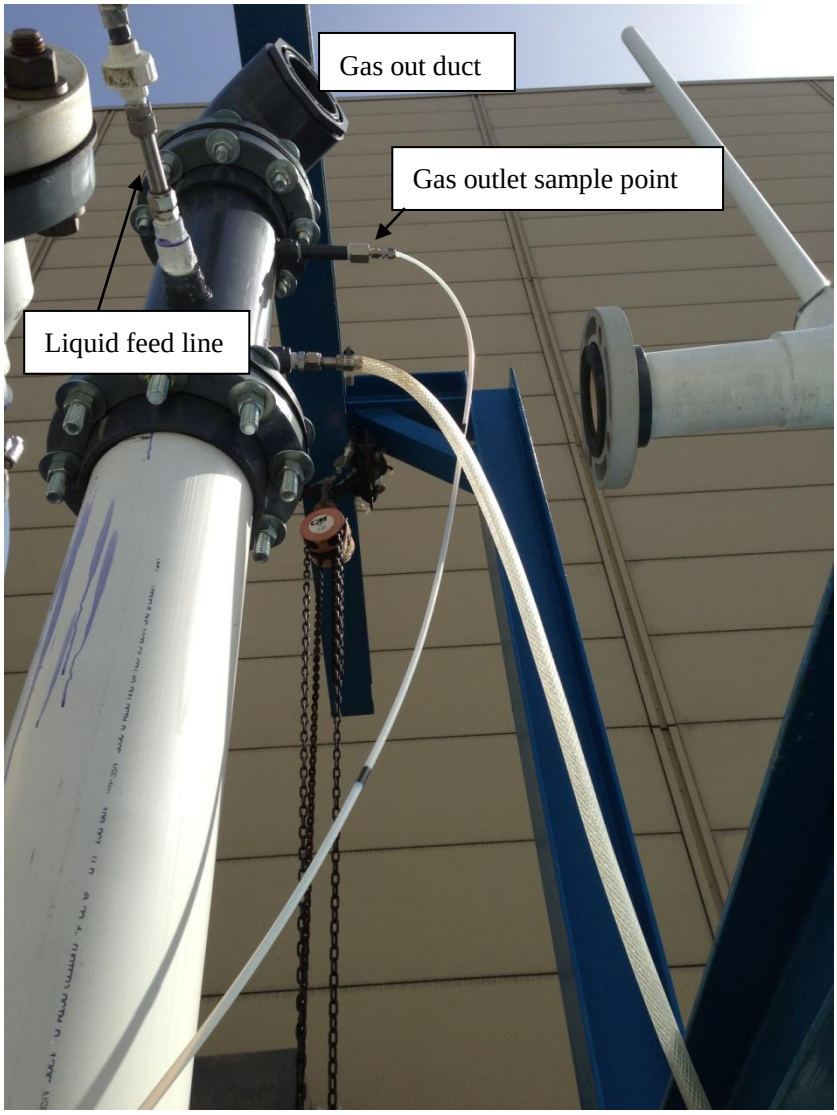

Figure A.2. CO_2 Outlet sample point

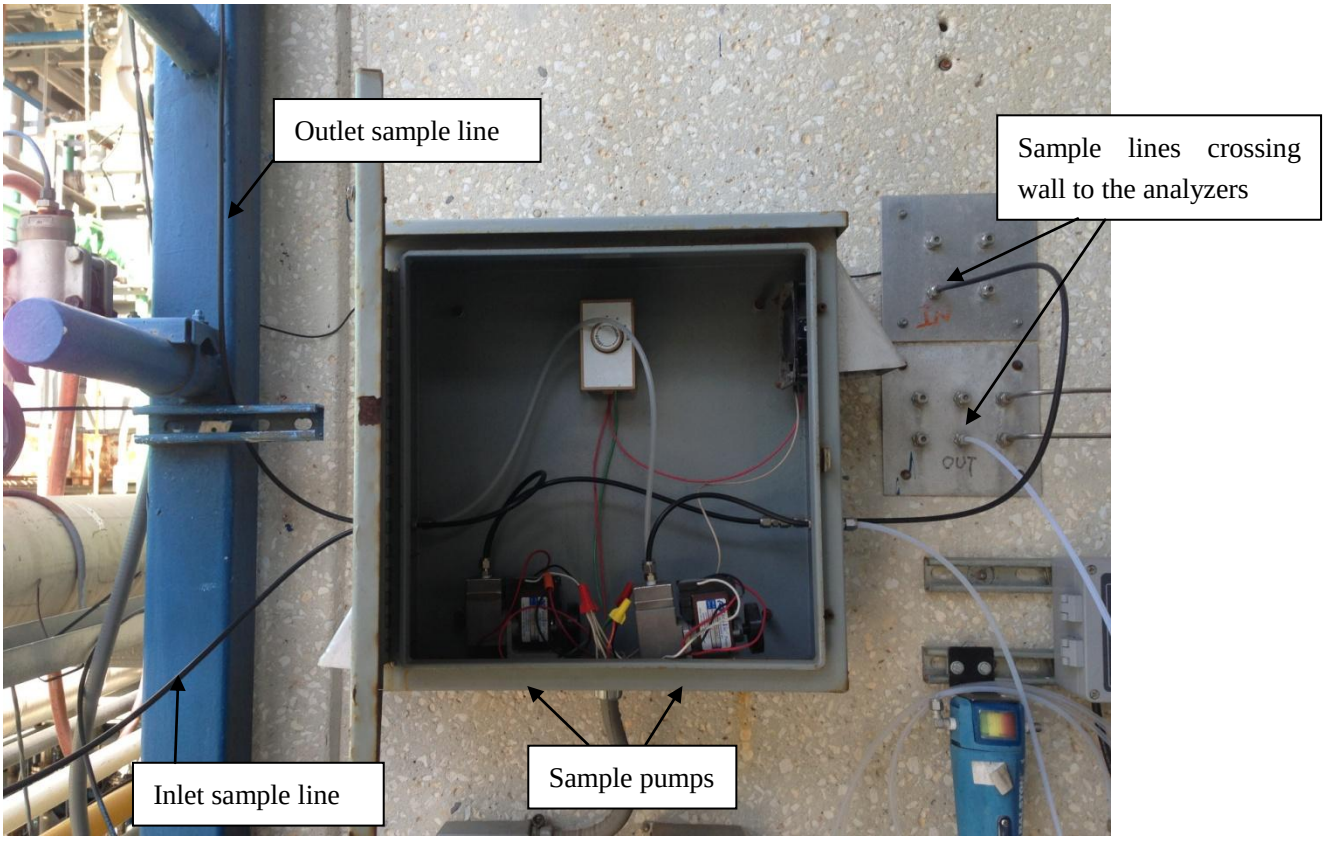

Figure A.3. Sample pump box

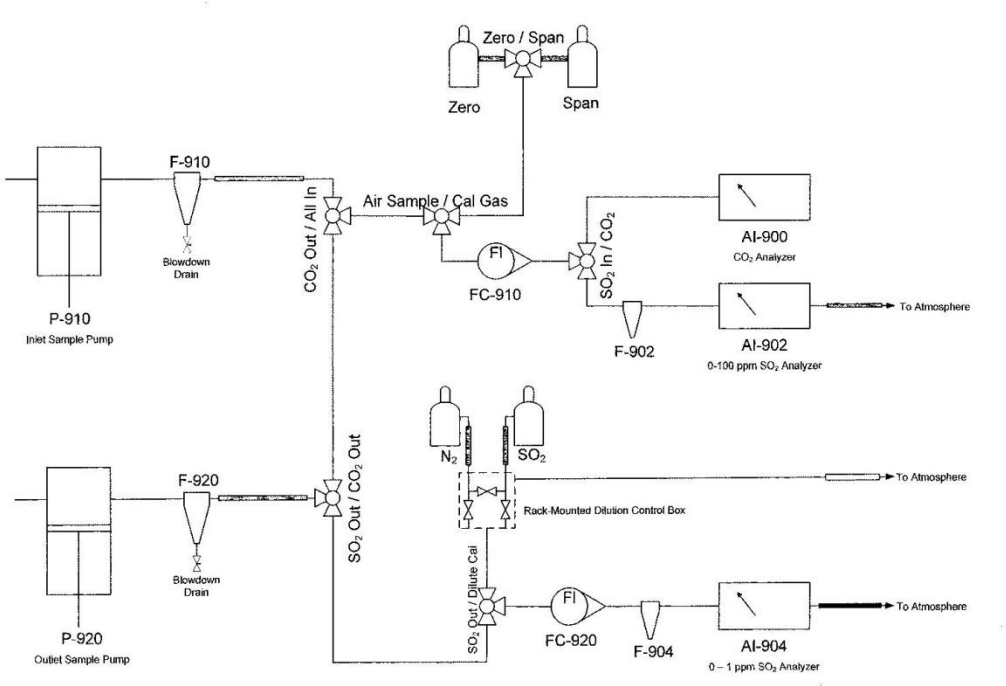

Figure A.4. Gas sample system routes

Gas samples were taken at the inlet and the outlet of the column (Figure A.1 and Figure A.2), and were transported to the inlet gas analyzers through two sample pumps (Figure A.3). For different measurements, the routes were changed by controlling three-way-valves marked in Figure A.4. For CO_2 inlet measurement, the inlet sample pump was connected with the CO_2 analyzer (Figure A.5). For CO_2 outlet measurement, the outlet sample pump was connected with the CO_2 analyzer (Figure A.6).

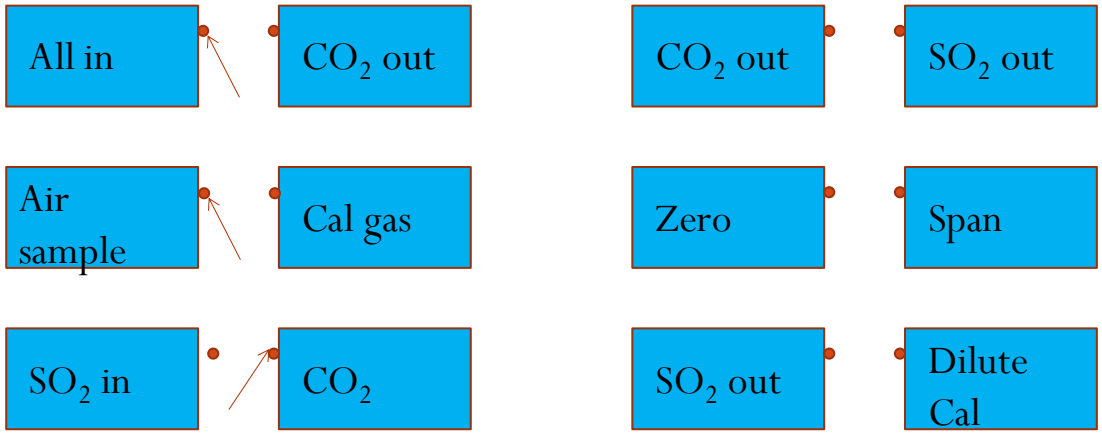

Figure A.5. CO_2 inlet measurement setting

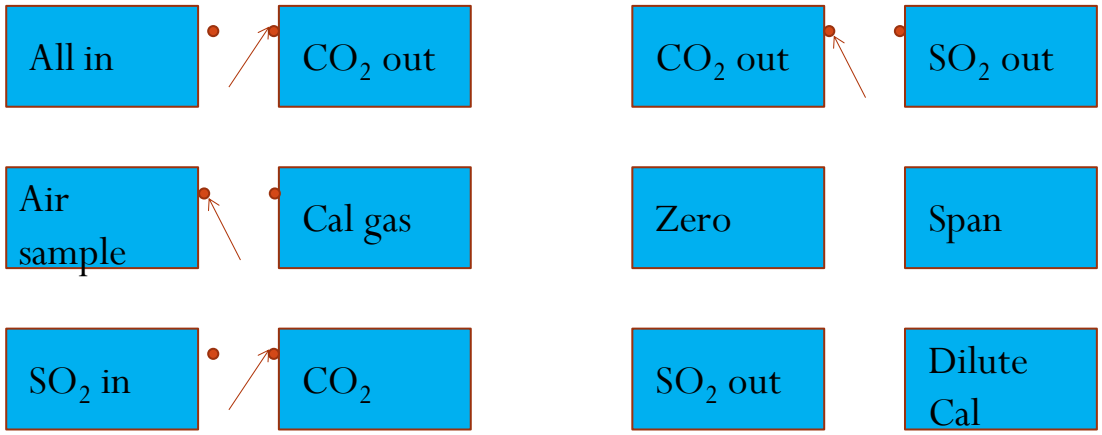

Figure A.6. CO_2 outlet measurement setting

A.2 SO_2 sample system

For SO2 measurement, the inlet and outlet sample points were the same with the CO2 measurement. Electric heating wires were twined along the outlet sample line to

prevent water condensation (Figure A.7 and Figure A.8).

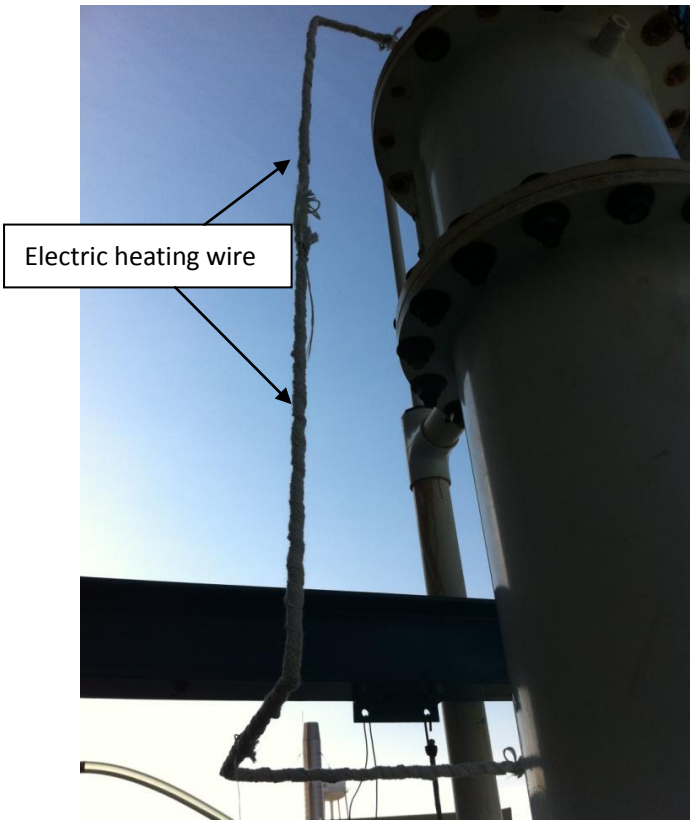

Figure A.7. Heated sample line (outside)

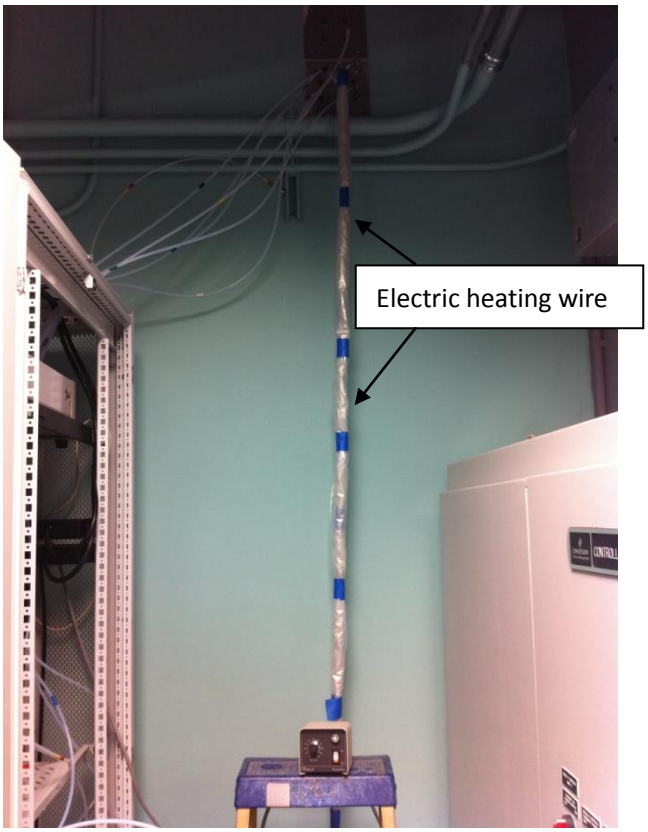

Figure A.8. Heated sample line (inside)

Figure A.9. Chilled water cooling system

Appendix B: Detailed standard procedures of analytics

B.1 SOP of titration process in effective area measurements

The standard procedures of the titration process are listed in the appendix.

1. Before beginning the experiment, obtain all necessary materials and clean all necessary items with distilled water.
2. Measure out a precise amount (10 ml) of analyte (NaOH solution); transfer the analyte into a beaker.
3. Add one to two drops of the color indicator (phenolphthalein) into the beaker.
4. Put the beaker on the magnetic stirring device, place the stir bar into the solution and turn on the stirring system.
5. Fill the burette with an excess amount of titrant. The titrant is the standard solution of 0.1 gmol/L hydrochloric acid (HCl).
6. Record the initial volume of the burette.
7. Turn on the stopcock (tap) of the burette, so that standard solution is added to the beaker. This should cause a color change. The endpoint is when the solution turns slightly pink.

8. Stop when you've reached endpoint.
9. Measure and record your final volume of the burette. Calculate the volume of standard solution used (x ml) by subtracting the initial volume measurement from the final volume measurement of the burette.
10. Calculate the concentration of the analyte. It can be calculated by:

$$C_{NaOH} = \frac{The\ volume\ of\ \ HCl\ used\ \ (ml) \times 0.1\ gmol/L}{10\ ml} \qquad (3\text{-}8)$$

B.2 SOP of toluene concentration measurements in GC

The standard procedures of the GC analysis process are listed in the appendix.

1. Two auto-pipettes (VWR VE 10000) are used for the extraction, which can preciously take certain volume of sample. One is set at 4 ml, and the other is set at 10 ml.
2. Take 20 ml aqueous sample (use the 10 ml auto-pipettes twice), and use 4 ml heptane to extract toluene from water phase to organic phase.
3. Shake vial to mix heptane and water sample well.
4. Pipette off 2 ml of heptanes extract to small vials. Weigh the mass of extract.
5. Add known amount of 4BFB (1-Bromo-4-fluorobenzen, a non-volatile hydrocarbon chemical) into the extract (~0.01g). Weigh the mass of 4BFB added. So the 4BFB concentration in the extract can be calculated:

$$x_{4BFB} = \frac{m_{4BFB}}{m_{extract} + m_{4BFB}} \qquad (3\text{-}11)$$

6. Shoot heptane samples into the GC.
7. From GC result, read the peak area for toluene and 4BFB
8. The toluene concentration in heptane can be calculated:

$$x_{tol\ in\ hep} = \frac{R_{tol} * A_{tol} * x_{4BFB}}{A_{4BFB}} \qquad (3\text{-}12)$$

9. Finally the toluene concentration in aqueous sample can be calculated:

$$x_{tol\ in\ water} = \frac{x_{tol\ in\ hep} * \rho_{hep} * V_{hep}}{\rho_{water} * V_{water}} \qquad (3\text{-}13)$$

Where V_{hep} is 4 ml, and V_{water} is 20 ml.

Appendix C: Detailed packing hydraulic data

This appendix lists all the hydraulic data (pressure drop and liquid hold-up) for packings measured in this work. The hydraulic data are measured in air/water system and under atmosphere condition.

Table C.1. Detailed packing hydraulic data.

L (m^3/m^2*h)	F_G ($Pa^{0.5}$)	$T_{air,in}$ (℃)	$T_{liq,in}$ (℃)	$T_{air,out}$ (℃)	ΔP/Z (Pa/m)	h_L	Re_L
MP2X	SRP0915		Height	2.85 m			
0.00	0.49	21.17	21.00	16.71	3.63	0.00	0.00
0.00	0.72	21.01	20.99	16.70	6.62	0.00	0.00
0.00	1.08	20.63	21.03	16.07	12.84	0.00	0.00
0.00	1.45	19.91	21.09	15.44	21.68	0.00	0.00
0.00	1.81	20.00	21.14	15.08	32.68	0.00	0.00
0.00	2.17	20.28	21.22	15.25	45.76	0.00	0.00
0.00	2.54	21.24	21.34	15.24	61.15	0.00	0.00
0.00	2.90	22.49	21.37	15.31	79.16	0.00	0.00
0.00	3.26	23.65	21.39	15.31	97.78	0.00	0.00
0.00	3.62	25.85	21.41	15.55	119.28	0.00	0.00
0.00	3.98	28.80	21.44	16.62	143.85	0.00	0.00
0.00	4.33	32.54	21.46	17.28	169.74	0.00	0.00
0.00	4.69	34.91	21.50	18.64	196.22	0.00	0.00
11.97	0.54	21.20	21.34	15.82	4.72	0.03	16.15
12.21	0.65	19.44	21.33	15.72	6.09	0.03	16.48
12.17	1.09	18.55	21.28	15.72	14.90	0.03	16.42
12.23	1.45	18.01	21.17	15.61	24.70	0.03	16.51
12.19	1.63	17.68	21.02	15.47	30.56	0.03	16.45
12.24	1.81	17.57	20.78	15.29	37.39	0.03	16.52
12.19	2.18	17.89	20.59	15.09	52.57	0.03	16.46
12.18	2.54	18.74	20.37	14.89	70.79	0.03	16.44
12.27	2.90	19.76	20.26	14.71	92.06	0.03	16.56
12.24	3.27	21.25	20.27	14.60	116.13	0.03	16.52
12.20	3.62	23.11	20.32	14.50	145.58	0.03	16.47
12.21	3.99	26.05	20.62	14.68	197.75	0.04	16.48
12.24	4.35	28.80	21.00	14.68	287.85	0.04	16.52
12.14	4.71	32.15	21.71	15.12	549.13	0.05	16.38
24.53	0.54	18.75	20.73	15.00	5.46	0.05	33.11
24.43	0.72	17.23	20.66	14.95	8.48	0.05	32.98
24.51	1.09	16.29	20.59	14.82	16.60	0.06	33.08
24.48	1.45	15.50	20.49	14.78	27.35	0.06	33.04
24.50	1.82	15.26	20.34	14.61	41.24	0.05	33.07

L (m^3/m^2*h)	F_G ($Pa^{0.5}$)	$T_{air,in}$ (℃)	$T_{liq,in}$ (℃)	$T_{air,out}$ (℃)	ΔP/Z (Pa/m)	h_L	Re_L
24.43	2.18	15.55	20.25	14.42	58.17	0.06	32.97
24.45	2.54	16.41	20.15	14.35	78.15	0.06	33.00
24.38	2.91	17.65	20.16	14.25	102.20	0.06	32.91
24.44	3.26	18.88	20.19	14.25	127.86	0.06	32.99
24.54	3.63	20.71	20.30	14.35	192.34	0.06	33.12
24.49	3.99	23.28	20.54	14.35	370.88	0.07	33.06
24.39	4.35	27.71	21.05	14.44	1006.02	0.09	32.92
24.42	4.53	31.21	22.07	14.89	1201.44	0.10	32.95
36.62	0.54	12.50	20.61	14.77	6.10	0.07	49.42
36.67	0.72	12.38	20.40	14.58	9.30	0.07	49.49
36.67	1.09	12.40	20.19	14.42	17.72	0.07	49.49
36.64	1.45	12.51	20.00	14.25	29.07	0.07	49.44
36.70	1.81	12.68	19.74	13.99	43.64	0.07	49.53
36.64	2.18	13.06	19.48	13.75	61.46	0.07	49.45
36.70	2.54	14.10	19.16	13.53	83.81	0.07	49.53
36.73	2.91	14.76	19.05	13.24	110.90	0.07	49.57
36.73	3.27	15.96	18.88	13.05	144.35	0.07	49.57
36.60	3.64	17.40	18.91	12.89	338.16	0.08	49.40
36.74	4.00	20.29	19.11	12.84	1167.92	0.11	49.58
36.50	4.17	22.87	19.50	13.06	1561.61	0.12	49.26
48.91	0.54	12.29	21.87	16.05	7.40	0.08	66.01
48.89	0.73	12.43	21.62	15.92	11.05	0.08	65.98
48.88	0.91	12.60	21.35	15.69	15.34	0.08	65.97
48.90	1.08	12.76	21.02	15.43	20.42	0.08	66.00
48.88	1.27	13.10	20.70	15.00	26.62	0.08	65.97
48.88	1.45	13.45	20.33	14.83	33.55	0.08	65.97
48.89	1.63	13.68	20.15	14.55	41.35	0.08	65.98
48.89	1.81	14.10	19.97	14.20	50.37	0.08	65.98
48.89	2.00	14.58	19.88	14.10	60.04	0.08	65.98
48.90	2.18	15.16	19.80	14.01	70.93	0.08	65.99
48.91	2.54	16.20	19.81	13.99	96.64	0.09	66.00
48.88	2.90	17.74	19.89	13.99	129.77	0.08	65.97
48.89	3.27	19.60	20.09	14.06	256.00	0.09	65.98
49.00	3.61	23.23	20.50	14.19	1188.61	0.20	66.12
48.89	2.19	14.71	17.00	12.01	86.36	0.09	65.99
61.10	0.50	24.31	22.39	16.91	8.56	0.09	82.47
61.11	0.72	23.50	22.48	16.88	13.35	0.09	82.48
61.11	0.91	22.91	22.48	17.13	17.49	0.09	82.47
61.15	1.08	22.36	22.45	17.03	22.76	0.09	82.53
61.12	1.26	21.01	22.31	16.90	29.20	0.09	82.48
61.11	1.45	20.20	22.13	16.70	36.70	0.09	82.48
61.11	1.81	19.93	21.93	16.53	55.07	0.09	82.48

L (m^3/m^2*h)	F_G ($Pa^{0.5}$)	$T_{air,in}$ (℃)	$T_{liq,in}$ (℃)	$T_{air,out}$ (℃)	ΔP/Z (Pa/m)	h_L	Re_L
61.11	2.17	20.04	21.66	16.11	79.61	0.09	82.48
61.12	2.53	20.53	21.41	16.07	111.49	0.09	82.49
61.12	2.90	21.48	21.26	15.77	157.61	0.10	82.49
61.13	3.25	23.39	21.15	15.46	700.71	0.11	82.50
61.35	3.43	26.69	21.28	15.30	1727.78	0.21	82.80
73.30	0.49	25.37	22.86	17.28	10.55	0.10	98.92
73.34	0.72	22.85	23.08	17.54	15.66	0.10	98.98
73.33	0.90	21.82	23.09	17.57	20.70	0.10	98.96
73.36	1.08	21.20	23.05	17.58	26.69	0.10	99.01
73.34	1.26	20.81	22.96	17.49	34.09	0.10	98.98
73.38	1.44	20.51	22.79	17.28	42.62	0.10	99.03
73.31	1.80	20.87	22.56	17.01	67.03	0.11	98.94
73.32	2.16	21.71	22.36	16.88	98.96	0.11	98.96
73.38	2.53	22.60	22.25	16.69	147.94	0.11	99.03
73.30	2.89	23.80	22.09	16.34	345.71	0.12	98.93
73.35	3.06	25.56	22.07	16.33	878.41	0.12	98.99
73.53	3.20	27.87	22.17	16.33	1666.41	0.14	99.24

RSP250Y	SRP1002		Height	3.04 m			
0.00	0.48	11.15	15.88	14.33	10.71	0.00	0.00
0.00	0.54	11.09	15.85	13.47	12.81	0.00	0.00
0.00	0.72	11.05	15.84	12.23	19.56	0.00	0.00
0.00	0.91	10.95	15.81	11.89	27.79	0.00	0.00
0.00	1.10	10.77	15.79	11.69	37.56	0.00	0.00
0.00	1.47	10.83	15.76	11.41	61.02	0.00	0.00
0.00	1.82	11.01	15.73	11.21	89.62	0.00	0.00
0.00	2.19	11.85	15.68	11.44	124.50	0.00	0.00
0.00	2.55	12.48	15.62	11.59	164.20	0.00	0.00
0.00	2.91	13.97	15.55	12.62	209.24	0.00	0.00
0.00	3.27	15.31	15.49	13.19	258.02	0.00	0.00
0.00	3.62	16.94	15.45	14.72	311.82	0.00	0.00
0.00	3.98	19.65	15.36	16.61	371.13	0.00	0.00
0.00	4.33	21.52	15.35	17.65	435.17	0.00	0.00
12.23	0.55	2.91	17.17	10.72	15.78	0.05	13.53
12.26	0.73	3.37	15.29	9.72	24.67	0.05	13.57
12.23	0.91	4.11	13.97	8.46	35.31	0.05	13.53
12.24	1.10	1.43	15.67	10.19	47.18	0.05	13.55
12.26	1.46	2.09	15.01	9.79	77.45	0.05	13.56
12.22	1.83	2.66	14.55	9.57	116.06	0.05	13.53
12.22	2.20	4.23	13.55	8.71	163.83	0.05	13.52
12.28	2.56	5.26	13.06	8.19	220.30	0.05	13.59
12.23	2.94	6.81	12.55	7.68	288.30	0.05	13.53

L (m^3/m^2*h)	F_G ($Pa^{0.5}$)	$T_{air,in}$ (℃)	$T_{liq,in}$ (℃)	$T_{air,out}$ (℃)	ΔP/Z (Pa/m)	h_L	Re_L
12.23	3.31	8.70	12.03	7.21	376.93	0.05	13.53
12.22	3.68	12.03	11.45	6.36	486.77	0.06	13.52
12.23	4.05	15.97	10.94	5.72	629.38	0.06	13.53
12.21	4.24	17.53	10.90	5.31	762.75	0.06	13.51
12.21	4.42	18.84	11.12	5.44	869.70	0.07	13.52
12.19	4.61	20.33	11.31	5.58	1029.95	0.07	13.49
12.23	4.69	21.59	11.42	5.73	1140.51	0.08	13.53
12.24	4.79	22.76	11.75	5.93	1207.82	0.10	13.55
24.49	0.55	2.96	16.59	11.05	17.88	0.07	27.10
24.41	0.73	3.40	15.05	9.63	27.74	0.07	27.01
24.44	0.92	4.16	13.77	8.57	39.37	0.07	27.05
24.47	1.11	10.15	10.89	5.69	53.79	0.07	27.08
24.49	1.47	7.93	10.83	5.57	88.30	0.07	27.10
24.46	1.84	6.67	10.74	5.49	132.63	0.07	27.07
24.45	2.21	6.25	10.59	5.40	189.08	0.07	27.05
24.43	2.58	6.77	10.40	5.21	256.88	0.08	27.04
24.43	2.95	8.11	10.20	5.03	344.25	0.08	27.04
24.39	3.32	10.13	10.05	4.97	469.14	0.08	26.99
24.43	3.69	12.50	9.94	4.65	629.63	0.09	27.04
24.41	4.06	16.79	10.02	4.70	925.46	0.11	27.01
24.46	4.23	20.14	10.43	4.73	1625.74	0.18	27.07
36.68	0.55	3.00	16.05	10.56	19.80	0.09	40.59
36.67	0.73	3.47	14.67	9.19	30.99	0.09	40.59
36.66	0.92	4.22	13.46	8.12	43.99	0.09	40.57
36.65	1.10	13.17	12.67	7.88	60.53	0.09	40.56
36.67	1.47	12.56	12.74	7.96	99.23	0.09	40.59
36.68	1.84	12.24	12.78	7.98	150.71	0.10	40.59
36.68	2.21	12.46	12.77	7.91	218.67	0.10	40.59
36.68	2.57	13.00	12.73	7.87	303.45	0.10	40.60
36.68	2.93	13.98	12.70	7.86	443.60	0.11	40.59
36.68	3.30	15.48	12.67	7.80	645.14	0.11	40.59
36.68	3.48	20.18	13.19	7.97	903.28	0.14	40.59
36.63	3.67	20.34	12.77	7.65	1473.99	0.15	40.54
36.66	3.70	21.86	12.94	7.75	1628.07	0.17	40.57
48.90	0.54	3.03	15.85	10.36	21.88	0.10	54.11
46.76	0.73	3.53	14.51	9.03	33.64	0.11	51.75
48.85	0.92	4.35	13.36	8.01	49.93	0.11	54.06
48.88	1.10	16.52	13.39	8.47	68.96	0.11	54.09
48.90	1.47	14.81	13.44	8.51	114.40	0.11	54.12
48.90	1.83	13.71	13.48	8.65	176.47	0.11	54.12
48.90	2.20	12.91	13.47	8.54	257.70	0.12	54.12
48.90	2.57	13.14	13.39	8.47	396.06	0.12	54.12

L (m^3/m^2*h)	F_G ($Pa^{0.5}$)	$T_{air,in}$ (℃)	$T_{liq,in}$ (℃)	$T_{air,out}$ (℃)	ΔP/Z (Pa/m)	h_L	Re_L
48.90	2.93	14.04	13.29	8.38	613.56	0.13	54.11
48.90	3.12	16.33	13.18	8.21	930.09	0.15	54.12
48.89	3.21	17.61	13.17	8.16	1128.36	0.16	54.10
48.87	3.26	19.79	13.24	8.08	1633.14	0.18	54.09
61.06	0.53	3.01	15.69	10.17	23.86	0.11	67.58
61.11	0.73	3.72	14.32	8.77	39.14	0.11	67.63
61.11	0.92	4.36	13.30	7.97	56.10	0.12	67.63
61.11	1.10	15.06	13.44	8.55	78.20	0.12	67.63
61.08	1.46	12.83	13.51	8.56	133.63	0.12	67.59
61.12	1.83	11.08	13.42	8.46	219.49	0.12	67.64
61.13	2.20	10.71	13.30	8.32	355.35	0.13	67.65
61.12	2.57	11.77	13.15	8.09	599.06	0.14	67.64
61.13	2.75	14.58	12.94	8.01	993.18	0.17	67.65
61.09	2.85	16.72	12.82	7.57	1630.91	0.19	67.61
73.31	0.52	3.18	15.61	10.02	25.65	0.12	81.13
73.39	0.73	3.83	14.22	8.68	43.04	0.12	81.21
73.38	0.92	4.37	13.30	7.96	61.91	0.12	81.21
73.35	1.10	13.62	12.96	7.83	86.79	0.12	81.17
73.36	1.47	11.84	12.99	7.85	164.49	0.13	81.18
73.29	1.84	10.55	12.99	7.85	299.25	0.14	81.11
73.36	2.20	10.77	12.94	7.83	561.49	0.15	81.18
73.34	2.39	12.39	12.78	7.64	1023.32	0.21	81.17
73.36	2.46	14.37	12.71	7.43	1671.41	0.00	81.18

GTC350Z	SRP1101		Height	2.79 m			
0.00	0.42	24.49	25.54	23.26	4.55	0.00	0.17
0.00	0.71	24.97	25.79	24.10	7.97	0.00	0.00
0.00	1.07	25.17	25.88	24.40	14.86	0.00	0.00
0.00	1.43	25.34	25.99	24.88	22.63	0.00	0.00
0.00	1.78	25.48	26.08	25.40	33.59	0.00	0.00
0.00	2.13	25.77	26.25	26.30	46.41	0.00	0.00
0.00	2.48	25.96	26.41	27.31	61.46	0.00	0.00
0.00	3.18	27.99	28.01	30.71	97.27	0.00	0.00
0.00	3.87	26.74	26.78	33.03	144.56	0.00	0.00
0.00	4.55	26.96	26.97	36.00	196.57	0.00	0.00
12.22	0.39	33.56	29.63	29.14	4.90	0.05	9.66
12.27	0.71	33.69	30.42	29.42	9.89	0.05	9.70
12.25	1.06	33.77	30.11	29.10	18.05	0.05	9.68
12.23	1.42	34.33	29.04	28.22	27.98	0.05	9.67
12.24	1.77	34.61	28.77	28.17	41.84	0.05	9.68
12.22	2.13	34.23	28.39	27.92	58.50	0.05	9.66
12.24	2.49	24.83	26.55	25.13	78.24	0.05	9.68

L (m^3/m^2*h)	F_G ($Pa^{0.5}$)	$T_{air,in}$ (℃)	$T_{liq,in}$ (℃)	$T_{air,out}$ (℃)	ΔP/Z (Pa/m)	h_L	Re_L
12.22	2.85	24.98	25.97	24.68	116.58	0.06	9.66
12.20	3.21	25.05	25.64	24.35	154.62	0.06	9.64
12.23	3.57	25.12	25.34	23.98	294.24	0.06	9.66
12.21	3.75	25.27	25.23	23.85	393.46	0.07	9.65
12.23	3.93	25.56	25.29	23.87	503.46	0.08	9.67
12.24	4.10	25.82	25.39	24.01	654.79	0.10	9.67
12.23	4.28	25.73	25.32	23.64	822.77	0.11	9.66
24.45	0.39	33.06	29.60	29.09	5.05	0.07	19.33
24.48	0.71	33.96	30.28	29.59	10.43	0.07	19.35
24.45	1.06	34.13	29.66	28.97	20.11	0.07	19.33
24.45	1.43	26.14	25.71	24.34	32.60	0.07	19.33
24.45	1.78	28.15	26.01	24.86	46.56	0.08	19.33
24.46	2.14	26.36	25.62	24.35	67.64	0.08	19.33
24.46	2.50	28.03	26.06	24.79	101.85	0.08	19.33
24.45	2.85	26.44	25.42	24.23	155.63	0.08	19.33
24.45	3.21	26.55	25.22	23.97	409.52	0.11	19.33
24.45	3.57	26.90	25.25	23.89	777.00	0.15	19.33
24.47	3.92	27.60	25.45	24.03	1435.70	0.19	19.34
24.46	4.03	27.54	25.75	24.19	1608.58	0.20	19.34
36.65	0.38	33.55	29.67	28.99	5.48	0.10	28.97
36.67	0.71	33.96	30.14	29.33	11.61	0.10	28.99
36.69	1.06	34.19	29.40	28.66	22.32	0.10	29.00
36.68	1.43	28.48	25.91	24.77	34.66	0.10	28.99
36.67	1.78	28.80	25.88	24.73	52.21	0.10	28.99
36.68	2.14	28.91	25.83	24.66	73.20	0.10	29.00
36.67	2.50	29.79	25.70	24.56	130.95	0.11	28.99
36.67	2.85	29.23	25.73	24.59	268.23	0.12	28.99
36.68	3.21	29.68	25.79	24.58	943.47	0.16	28.99
36.70	3.55	29.91	25.86	24.60	1782.23	0.24	29.01
48.89	0.37	33.11	29.88	29.05	5.70	0.14	38.65
48.90	0.71	33.82	30.04	29.12	13.95	0.14	38.66
48.89	1.06	33.96	29.19	28.30	25.14	0.14	38.65
48.91	1.42	34.20	27.88	26.99	38.39	0.14	38.66
48.89	1.78	34.42	27.86	26.99	58.08	0.14	38.65
48.90	2.13	34.39	27.70	26.80	83.08	0.14	38.66
48.89	2.31	34.80	27.20	26.36	136.60	0.15	38.65
48.88	2.49	34.12	26.91	26.04	215.30	0.17	38.64
48.89	2.67	35.08	26.46	25.53	611.15	0.19	38.65
48.90	3.10	35.13	26.27	25.31	1603.71	0.24	38.66
61.14	0.38	33.67	30.06	29.14	6.87	0.17	48.33
61.13	0.71	33.86	30.00	29.04	16.17	0.18	48.32
61.14	1.06	34.22	29.09	28.17	30.12	0.18	48.33

L (m^3/m^2*h)	F_G ($Pa^{0.5}$)	$T_{air,in}$ (℃)	$T_{liq,in}$ (℃)	$T_{air,out}$ (℃)	ΔP/Z (Pa/m)	h_L	Re_L
61.12	1.42	35.58	26.45	25.48	42.30	0.18	48.32
61.12	1.78	35.54	26.55	25.59	67.00	0.18	48.31
61.12	2.14	35.26	26.58	25.63	130.28	0.19	48.32
61.12	2.49	35.15	26.51	25.55	625.45	0.22	48.31
61.12	2.85	35.21	26.50	25.50	1697.05	0.25	48.31
73.39	0.36	33.30	30.31	29.45	8.53	0.18	58.01
73.36	0.71	34.13	30.06	29.08	21.99	0.18	57.99
73.33	1.06	34.28	29.04	28.08	41.75	0.18	57.97
73.34	1.42	35.55	26.60	25.50	62.25	0.19	57.98
73.36	1.78	35.38	26.69	25.61	101.69	0.18	57.99
73.35	2.13	35.31	26.73	25.67	200.83	0.21	57.98
73.34	2.22	35.37	26.73	25.67	393.85	0.21	57.97
73.34	2.32	27.80	25.98	24.66	721.67	0.23	57.98
73.34	2.52	27.98	26.00	24.68	1141.35	0.26	57.98
73.46	2.66	28.06	26.01	24.68	1749.42	0.33	58.07

MP250Y	SRP1201		Height	2.92 m			
0.00	0.45	6.80	9.59	9.44	6.83	0.00	0.00
0.00	0.73	6.91	9.56	9.44	14.93	0.00	0.00
0.00	1.10	7.41	9.60	9.44	31.14	0.00	0.00
0.00	1.46	8.01	9.61	9.44	50.44	0.00	0.00
0.00	1.83	8.16	9.63	9.44	78.03	0.00	0.00
0.00	2.19	7.63	9.65	9.44	110.58	0.00	0.00
0.00	2.56	7.71	9.71	9.50	147.98	0.00	0.00
0.00	2.93	8.34	9.74	9.56	191.05	0.00	0.00
0.00	3.29	8.84	9.81	9.61	255.91	0.00	0.00
0.00	3.66	9.60	9.94	9.72	312.42	0.00	0.00
0.00	4.02	10.08	10.11	9.89	379.10	0.00	0.00
0.00	4.39	10.42	10.32	10.17	449.35	0.00	0.00
0.00	4.75	11.45	10.58	10.44	527.46	0.00	0.00
0.00	5.11	11.76	10.72	10.56	606.35	0.00	0.00
12.23	0.41	12.60	18.78	18.61	9.54	0.03	13.53
12.25	0.72	13.81	18.74	18.58	21.07	0.04	13.56
12.20	1.08	15.12	18.50	18.39	41.38	0.04	13.50
12.22	1.44	16.33	18.11	18.00	66.08	0.04	13.53
12.22	1.80	19.32	17.58	17.44	103.86	0.04	13.52
12.22	2.17	20.89	17.15	17.00	147.77	0.04	13.53
12.23	2.53	21.82	17.10	16.94	199.44	0.04	13.53
12.22	2.89	19.80	16.97	16.83	293.10	0.04	13.52
12.22	3.25	20.41	16.93	16.78	549.96	0.06	13.52
12.23	3.61	19.92	16.96	16.78	1002.18	0.08	13.54
12.21	3.95	20.44	17.07	16.89	1739.13	0.11	13.51

L (m^3/m^2*h)	F_G ($Pa^{0.5}$)	$T_{air,in}$ (℃)	$T_{liq,in}$ (℃)	$T_{air,out}$ (℃)	ΔP/Z (Pa/m)	h_L	Re_L
24.42	0.41	12.80	18.87	18.67	10.27	0.06	27.03
24.44	0.72	13.85	18.75	18.56	22.86	0.06	27.05
24.45	1.08	15.56	18.40	18.28	45.20	0.06	27.05
24.43	1.44	16.64	17.93	17.78	72.02	0.07	27.03
24.44	1.81	20.64	17.23	17.11	115.24	0.07	27.05
24.45	2.17	21.92	17.02	16.89	164.85	0.07	27.06
24.46	2.53	21.74	16.94	16.83	226.53	0.07	27.07
24.40	2.89	20.02	17.65	17.50	630.05	0.09	27.01
24.45	3.07	20.69	17.75	17.61	1169.33	0.13	27.05
24.44	3.22	20.33	17.82	17.67	1696.28	0.16	27.04
36.67	0.40	13.03	18.78	18.61	11.02	0.09	40.59
36.66	0.72	13.76	18.58	18.39	24.96	0.09	40.57
36.66	1.08	15.26	18.23	18.11	48.08	0.09	40.57
36.67	1.44	16.62	17.68	17.50	78.41	0.09	40.59
36.65	1.81	19.91	17.14	17.00	126.50	0.09	40.56
36.69	2.17	22.16	16.92	16.78	183.72	0.09	40.60
36.66	2.53	20.33	16.91	16.78	358.34	0.10	40.57
36.63	2.85	20.27	17.92	17.78	2147.35	0.15	40.54
48.87	0.40	13.27	18.76	18.56	11.65	0.10	54.08
48.89	0.72	14.21	18.50	18.33	26.14	0.10	54.11
48.89	1.08	15.36	18.16	18.00	50.93	0.10	54.11
48.87	1.44	17.15	17.56	17.44	83.49	0.10	54.08
48.89	1.81	19.58	17.08	16.94	140.45	0.10	54.11
48.89	2.17	22.38	16.93	16.78	209.31	0.11	54.10
48.89	2.34	20.32	18.21	18.06	362.66	0.11	54.10
48.89	2.52	19.88	18.30	18.17	1509.85	0.16	54.11
61.05	0.40	13.42	18.77	18.56	12.52	0.11	67.56
61.05	0.72	14.49	18.49	18.33	28.06	0.11	67.57
61.10	1.08	15.86	18.12	18.00	54.13	0.11	67.61
61.10	1.44	17.24	17.53	17.39	91.43	0.11	67.62
61.09	1.81	21.16	17.13	17.00	162.16	0.11	67.60
61.09	2.17	21.48	17.03	16.89	367.44	0.12	67.61
61.11	2.39	19.84	18.35	18.22	1630.39	0.19	67.62
73.22	0.39	13.76	18.85	18.67	13.18	0.12	81.03
73.32	0.72	14.59	18.56	18.39	29.88	0.12	81.15
73.27	1.08	15.75	18.18	17.94	58.60	0.12	81.09
73.35	1.44	18.81	17.64	17.50	103.17	0.12	81.18
73.29	1.62	20.31	18.52	18.33	131.94	0.13	81.11
73.33	1.80	19.87	18.68	18.56	215.22	0.13	81.15
73.35	1.98	19.99	18.70	18.50	411.92	0.14	81.17
73.30	2.16	19.89	18.70	18.50	999.47	0.17	81.12
73.28	2.24	19.62	18.67	18.50	1867.49	0.20	81.10

L (m^3/m^2*h)	F_G ($Pa^{0.5}$)	$T_{air,in}$ (℃)	$T_{liq,in}$ (℃)	$T_{air,out}$ (℃)	ΔP/Z (Pa/m)	h_L	Re_L
MP250X	SRP1104		Height	2.92 m			
0.00	0.47	3.38	5.34	5.00	3.90	0.00	0.00
0.00	0.74	3.66	5.28	5.00	7.91	0.00	0.00
0.00	1.11	3.16	5.26	5.00	15.38	0.00	0.00
0.00	1.48	2.36	5.17	5.00	24.89	0.00	0.00
0.00	2.21	2.87	5.14	5.00	52.37	0.00	0.00
0.00	2.95	2.66	5.12	5.00	90.92	0.00	0.00
0.00	3.69	3.73	5.14	5.00	137.95	0.00	0.00
0.00	4.43	3.94	4.86	4.44	196.53	0.00	0.00
0.00	5.16	3.89	4.91	4.44	283.75	0.00	0.00
12.23	0.47	5.13	15.11	14.28	4.85	0.04	13.54
12.22	0.73	5.40	13.17	12.94	9.31	0.04	13.53
12.22	1.09	5.58	12.12	12.11	17.50	0.04	13.52
12.22	1.46	5.28	10.96	10.94	28.32	0.04	13.53
12.18	2.20	5.28	9.40	9.39	60.28	0.04	13.48
12.25	2.93	5.12	9.17	9.17	106.11	0.04	13.56
12.24	3.30	5.08	8.92	8.89	135.06	0.04	13.54
12.20	3.66	5.05	8.65	8.61	274.48	0.05	13.51
12.22	3.85	4.97	8.48	8.33	393.86	0.06	13.53
12.24	4.03	4.98	8.40	8.39	584.19	0.07	13.55
12.22	4.22	4.66	8.50	8.50	777.40	0.08	13.52
12.26	4.40	4.64	8.79	8.78	949.79	0.09	13.57
12.23	4.76	4.69	9.23	9.22	1197.21	0.11	13.53
24.46	0.46	5.15	14.11	14.00	5.25	0.07	27.07
24.41	0.73	5.32	12.86	12.78	9.78	0.07	27.01
24.46	1.09	5.61	11.94	11.94	19.45	0.07	27.06
24.45	1.46	5.35	10.66	10.67	31.60	0.07	27.06
24.42	2.20	4.48	9.85	9.83	65.48	0.07	27.03
24.44	2.93	4.58	9.82	9.78	114.99	0.07	27.05
24.45	3.29	4.56	9.58	9.56	220.23	0.08	27.06
24.42	3.48	4.25	9.10	8.89	444.87	0.09	27.03
24.47	4.02	4.44	9.18	9.17	1589.85	0.15	27.08
36.68	0.46	5.13	13.77	13.72	5.73	0.08	40.59
36.68	0.73	5.26	12.60	12.61	11.70	0.08	40.60
36.67	1.09	5.48	11.62	11.61	21.79	0.08	40.58
36.69	1.46	5.24	10.34	10.33	34.94	0.08	40.61
36.72	2.20	4.30	8.90	8.89	73.14	0.08	40.63
36.65	2.57	4.14	8.78	8.78	98.92	0.09	40.56
36.67	2.93	4.10	8.61	8.61	131.87	0.09	40.58
36.64	3.12	3.88	8.40	8.33	279.27	0.10	40.54
36.67	3.30	3.84	8.24	8.22	630.17	0.13	40.58
36.66	3.48	3.86	8.15	8.11	1489.95	0.18	40.57

L (m^3/m^2*h)	F_G ($Pa^{0.5}$)	$T_{air,in}$ (℃)	$T_{liq,in}$ (℃)	$T_{air,out}$ (℃)	ΔP/Z (Pa/m)	h_L	Re_L
48.97	0.45	5.10	13.57	13.17	6.97	0.09	54.19
48.89	0.73	5.21	12.46	12.44	12.62	0.09	54.11
48.90	1.09	5.33	11.43	11.39	23.39	0.09	54.12
48.90	1.46	5.36	10.16	10.17	38.78	0.10	54.11
48.89	2.21	4.15	6.73	6.67	83.35	0.10	54.10
48.89	2.57	4.12	6.71	6.67	113.73	0.10	54.11
48.90	2.76	3.47	6.63	6.11	132.10	0.10	54.11
48.88	2.94	3.16	6.51	6.11	359.99	0.11	54.10
48.90	3.13	3.02	6.36	6.11	1469.06	0.16	54.12
61.14	0.45	5.39	13.39	13.17	7.73	0.11	67.67
61.11	0.73	5.35	12.34	12.33	13.95	0.11	67.63
61.16	1.09	5.39	11.26	11.22	27.12	0.11	67.68
61.12	1.46	5.42	10.06	10.06	43.96	0.11	67.64
61.12	2.21	3.73	6.42	6.11	99.01	0.11	67.64
61.11	2.39	3.65	6.45	6.11	115.73	0.11	67.63
61.12	2.58	3.68	6.42	6.11	136.53	0.11	67.64
61.08	2.76	2.94	6.32	6.11	544.03	0.13	67.59
61.09	2.90	3.26	6.29	6.11	1982.95	0.19	67.61
73.38	0.43	10.11	15.48	15.50	8.54	0.12	81.21
73.42	0.72	9.71	15.51	15.51	16.01	0.12	81.25
73.34	1.09	10.34	15.43	15.43	32.32	0.12	81.17
73.32	1.45	10.34	15.29	15.29	55.49	0.12	81.14
73.32	1.81	10.40	14.89	14.89	89.24	0.12	81.14
73.33	1.99	11.15	14.74	14.74	109.65	0.12	81.16
73.34	2.18	10.85	14.19	14.17	131.76	0.13	81.16
73.35	2.36	10.96	13.85	13.83	183.91	0.13	81.17
73.33	2.54	10.89	13.58	13.56	494.73	0.15	81.15
73.35	2.68	11.33	13.49	13.44	1903.81	0.19	81.17

GTC350Y	SRP1201		Height	2.79 m			
0.00	0.38	34.62	31.86	37.84	8.93	0.00	0.00
0.00	0.70	36.58	32.93	37.90	21.31	0.00	0.00
0.00	1.40	37.72	32.88	37.89	72.08	0.00	0.00
0.00	2.09	39.54	32.81	38.05	146.12	0.00	0.00
0.00	2.79	40.81	32.73	37.60	258.69	0.00	0.00
0.00	3.14	41.31	32.91	38.03	320.74	0.00	0.00
0.00	3.49	43.82	32.95	37.71	392.96	0.00	0.00
0.00	3.86	45.55	33.13	34.23	462.04	0.00	0.00
0.00	4.21	47.66	33.11	34.19	542.85	0.00	0.00
0.00	4.56	50.39	33.07	34.13	629.45	0.00	0.00
12.67	0.39	28.34	27.67	26.46	10.94	0.05	10.02
12.21	0.71	26.93	27.62	27.66	27.75	0.05	9.65

L (m^3/m^2*h)	F_G ($Pa^{0.5}$)	$T_{air,in}$ (℃)	$T_{liq,in}$ (℃)	$T_{air,out}$ (℃)	ΔP/Z (Pa/m)	h_L	Re_L
12.24	1.06	31.57	27.20	30.18	55.57	0.05	9.67
12.23	1.42	28.70	27.64	28.55	94.25	0.05	9.67
12.24	1.76	32.65	27.92	31.52	136.11	0.06	9.68
12.25	2.11	33.89	27.61	31.65	192.62	0.06	9.69
12.19	2.46	35.75	27.38	32.18	422.81	0.06	9.63
12.20	2.64	41.28	26.95	32.41	1629.18	0.10	9.65
24.46	0.38	27.37	27.47	26.42	11.86	0.08	19.34
24.45	0.71	27.13	27.43	28.05	31.15	0.08	19.33
24.44	1.06	30.92	27.06	30.15	62.37	0.08	19.32
24.47	1.42	28.97	27.44	29.09	106.03	0.08	19.35
24.48	1.58	35.41	27.01	33.20	125.99	0.08	19.35
24.44	1.76	35.46	26.80	33.17	155.23	0.08	19.32
24.47	2.11	35.77	26.88	33.13	225.09	0.09	19.34
24.42	2.23	38.26	26.88	33.03	1629.18	0.11	19.30
36.67	0.38	26.97	27.42	26.61	13.20	0.10	28.98
36.57	0.71	27.29	27.33	28.19	34.97	0.10	28.91
36.63	1.06	30.67	27.01	30.40	71.55	0.10	28.96
36.70	1.40	35.11	27.30	33.85	120.51	0.10	29.01
36.64	1.58	35.41	27.36	33.86	143.64	0.11	28.96
36.63	1.76	35.90	27.42	33.69	177.75	0.11	28.96
36.68	1.93	41.54	27.72	34.65	212.40	0.11	28.99
36.65	2.10	42.04	27.76	34.92	1830.28	0.14	28.97
48.89	0.36	26.76	27.43	26.82	14.49	0.12	38.64
48.87	0.71	27.43	27.29	28.33	41.49	0.12	38.63
48.88	1.06	30.57	27.11	30.45	86.42	0.12	38.64
48.91	1.23	37.45	28.05	34.90	117.03	0.12	38.67
48.89	1.40	37.33	28.15	35.24	151.70	0.12	38.65
48.86	1.58	37.50	28.24	35.35	184.72	0.12	38.62
48.87	1.77	42.43	28.32	36.00	1765.60	0.16	38.63
61.11	0.38	36.75	31.81	40.67	26.75	0.13	48.30
61.06	0.71	27.72	27.43	28.25	63.10	0.13	48.27
61.10	0.87	37.37	28.98	36.58	93.99	0.13	48.30
61.13	1.06	31.01	27.43	31.18	132.98	0.13	48.32
61.11	1.22	37.64	29.08	36.14	174.41	0.13	48.31
61.12	1.41	30.80	26.98	30.03	284.19	0.13	48.31
61.14	1.59	41.38	29.09	36.41	1676.34	0.17	48.33
73.33	0.38	37.09	31.44	40.94	59.63	0.14	57.96
73.35	0.43	37.32	30.77	40.98	67.69	0.14	57.98
73.33	0.53	38.43	29.63	37.00	85.99	0.14	57.96
73.31	0.71	27.89	27.60	28.53	124.49	0.14	57.95
73.32	0.87	37.83	29.96	37.52	166.37	0.14	57.96
73.30	1.06	31.63	27.89	31.55	259.31	0.15	57.94

L (m^3/m^2*h)	F_G ($Pa^{0.5}$)	$T_{air,in}$ (℃)	$T_{liq,in}$ (℃)	$T_{air,out}$ (℃)	ΔP/Z (Pa/m)	h_L	Re_L
73.32	1.22	38.33	30.12	37.68	353.81	0.15	57.96
73.28	1.40	33.53	27.14	29.91	1850.18	0.20	57.93

A350Y	SRP1304		Height	3.04 m			
0.00	0.44	13.01	12.75	10.85	11.94	0.00	0.00
0.00	0.73	12.92	12.79	11.02	29.72	0.00	0.00
0.00	1.09	12.88	12.85	10.87	63.39	0.00	0.00
0.02	1.46	12.88	12.88	11.13	107.09	0.00	0.01
0.00	1.82	12.89	12.96	11.23	159.99	0.00	0.00
0.00	2.19	12.93	13.04	11.06	232.97	0.00	0.00
0.00	2.55	13.04	13.14	11.65	306.57	0.00	0.00
0.04	2.92	13.17	13.25	11.77	391.35	0.00	0.03
0.00	3.28	13.34	13.52	11.84	487.83	0.00	0.00
0.00	3.64	13.52	13.88	12.28	586.96	0.00	0.00
0.00	4.01	13.69	14.21	11.93	698.02	0.00	0.00
0.00	4.37	13.90	14.49	12.25	819.50	0.00	0.00
0.00	4.73	14.10	14.80	12.57	953.41	0.00	0.00
0.00	5.09	14.36	15.20	12.54	1090.67	0.00	0.00
6.12	0.43	12.84	18.21	15.16	14.07	0.00	4.84
6.11	0.72	13.16	18.13	18.40	36.71	0.00	4.83
6.11	1.08	13.29	18.72	20.72	76.41	0.00	4.83
6.12	1.42	13.97	20.78	27.11	129.34	0.00	4.83
6.11	1.77	14.05	20.94	28.04	194.14	0.00	4.83
6.10	2.12	14.15	20.96	29.63	269.93	0.00	4.82
6.12	2.48	14.21	20.65	29.36	360.38	0.00	4.83
6.10	2.83	14.31	20.47	29.69	471.44	0.00	4.82
6.13	3.18	14.43	20.34	29.74	611.30	0.00	4.85
6.10	3.54	14.56	20.22	29.44	722.45	0.00	4.82
6.11	3.89	14.67	20.29	29.15	921.06	0.00	4.83
6.12	4.25	14.86	20.55	28.94	1174.92	0.00	4.83
6.11	4.64	15.12	20.79	28.67	1557.05	0.00	4.83
12.21	0.43	12.87	18.01	15.44	16.05	0.06	9.65
12.23	0.72	13.19	17.98	19.06	39.50	0.06	9.67
12.23	1.08	13.32	18.62	20.80	81.60	0.06	9.67
12.22	1.42	13.99	20.62	27.44	138.35	0.07	9.66
12.21	1.77	14.06	20.74	28.29	209.71	0.07	9.65
12.22	2.12	14.15	20.48	29.50	293.53	0.07	9.66
12.21	2.47	14.25	20.36	29.53	397.06	0.07	9.65
12.21	2.83	14.35	20.25	29.84	532.68	0.07	9.65
12.22	3.18	14.47	20.07	29.37	727.04	0.08	9.66
12.21	3.54	14.58	20.14	29.44	890.70	0.08	9.65
12.22	3.89	14.79	20.30	29.08	1268.99	0.09	9.66

L (m^3/m^2*h)	F_G ($Pa^{0.5}$)	$T_{air,in}$ (℃)	$T_{liq,in}$ (℃)	$T_{air,out}$ (℃)	ΔP/Z (Pa/m)	h_L	Re_L
12.18	4.21	14.92	20.54	28.94	1815.80	0.10	9.63
24.45	0.43	12.89	17.82	15.76	18.18	0.09	19.33
24.46	0.72	13.26	17.92	19.66	44.84	0.09	19.34
24.46	1.07	13.84	19.54	25.76	92.56	0.09	19.33
24.44	1.42	14.02	20.55	27.92	155.69	0.09	19.32
24.45	1.77	14.08	20.52	28.73	233.77	0.10	19.33
24.45	2.12	14.15	20.32	29.28	341.30	0.10	19.33
24.45	2.54	13.51	17.48	13.35	498.27	0.10	19.32
24.46	2.91	13.52	16.85	13.26	817.61	0.10	19.33
24.43	3.26	13.69	16.33	13.41	1683.94	0.13	19.31
36.64	0.43	12.91	17.77	15.94	20.87	0.11	28.97
36.66	0.72	13.29	18.00	20.05	50.52	0.11	28.98
36.68	1.07	13.86	19.74	26.13	104.67	0.11	28.99
36.66	1.42	14.04	20.66	28.26	175.73	0.11	28.98
36.67	1.77	14.08	20.58	29.13	270.34	0.12	28.99
36.68	2.12	14.17	20.34	29.43	467.59	0.12	28.99
36.65	2.36	13.52	15.75	13.80	771.68	0.12	28.97
36.65	2.54	13.59	15.34	13.94	1236.54	0.13	28.97
36.63	2.69	13.65	15.23	13.94	1664.51	0.16	28.95
48.88	0.43	12.97	17.81	16.44	24.38	0.13	38.64
48.90	0.72	13.32	18.24	20.58	58.62	0.13	38.65
48.87	1.07	13.89	20.01	26.55	119.06	0.13	38.63
48.95	1.45	13.48	15.90	16.13	214.97	0.13	38.69
48.91	1.63	13.63	15.81	16.90	421.80	0.13	38.67
48.90	1.81	13.59	15.84	16.18	667.05	0.13	38.65
48.88	1.99	13.70	15.76	16.68	1156.13	0.14	38.64
48.82	2.13	13.76	15.74	16.46	1687.71	0.18	38.59
60.46	0.43	13.02	18.08	17.06	37.88	0.14	47.79
61.08	0.72	13.29	18.64	20.50	83.59	0.14	48.29
61.13	0.90	13.55	16.80	18.27	143.06	0.14	48.32
61.12	1.08	13.50	16.04	16.86	179.86	0.15	48.32
61.11	1.26	13.53	16.30	17.62	410.68	0.15	48.31
61.13	1.44	13.53	16.14	17.21	666.46	0.15	48.32
61.13	1.63	13.69	16.41	17.98	1513.13	0.16	48.32
61.04	1.74	13.73	16.44	18.06	1938.71	0.19	48.25
73.34	0.43	13.38	17.99	18.34	66.47	0.15	57.97
73.35	0.58	13.37	18.35	18.29	113.67	0.15	57.98
73.33	0.72	13.37	18.54	18.26	154.23	0.15	57.97
73.33	0.90	13.39	18.71	18.28	348.27	0.16	57.97
73.34	1.08	13.40	18.74	18.50	570.88	0.16	57.97
73.35	1.26	13.49	18.58	17.88	1171.84	0.17	57.98
73.26	1.38	13.55	18.54	17.95	1987.77	0.19	57.91

L (m^3/m^2*h)	F_G ($Pa^{0.5}$)	$T_{air,in}$ (℃)	$T_{liq,in}$ (℃)	$T_{air,out}$ (℃)	ΔP/Z (Pa/m)	h_L	Re_L
B350X	SRP1303		Height	3.01 m			
0.00	0.46	13.01	16.80	17.59	6.96	0.00	0.00
0.00	0.72	13.01	16.84	17.58	13.07	0.00	0.00
0.00	1.08	13.02	16.89	17.62	25.87	0.00	0.00
0.00	1.44	13.05	16.93	17.71	42.44	0.00	0.00
0.00	1.80	13.09	16.96	17.68	62.32	0.00	0.00
0.00	2.16	13.16	17.02	17.71	85.55	0.00	0.00
0.00	2.52	13.25	17.06	17.82	112.41	0.00	0.00
0.00	2.88	13.37	17.11	17.89	143.53	0.00	0.00
0.00	3.24	13.48	17.14	18.00	178.57	0.00	0.00
0.00	3.60	13.60	17.20	18.06	211.07	0.00	0.00
0.00	3.97	13.76	17.25	18.03	252.45	0.00	0.00
0.00	4.33	13.92	17.28	18.04	295.59	0.00	0.00
0.00	4.69	14.06	17.31	18.13	342.31	0.00	0.00
0.00	5.05	14.28	17.37	18.10	392.46	0.00	0.00
0.00	5.41	14.44	17.39	18.03	444.62	0.00	0.00
6.12	0.45	13.48	19.52	19.02	8.23	0.00	4.84
6.10	0.71	13.75	22.34	25.12	16.71	0.00	4.82
6.12	1.42	13.78	22.44	27.14	51.37	0.00	4.84
6.11	2.13	13.89	20.81	27.82	105.94	0.00	4.83
6.10	2.93	12.86	17.17	9.39	184.94	0.00	4.82
6.10	3.23	13.68	16.76	20.29	440.89	0.00	4.82
6.10	3.59	13.80	16.67	20.36	573.07	0.00	4.82
6.12	4.02	13.46	13.87	10.52	791.77	0.00	4.84
6.11	4.38	13.77	13.32	10.93	1012.15	0.00	4.83
6.10	4.96	14.26	13.28	12.55	1571.63	0.00	4.82
12.26	0.45	13.36	19.66	19.50	8.54	0.05	9.69
12.23	0.71	13.73	22.16	25.91	17.50	0.05	9.67
12.23	1.42	13.80	21.91	27.42	54.68	0.05	9.67
12.22	2.13	13.90	20.42	27.71	111.85	0.05	9.66
12.23	2.54	13.46	14.24	14.50	198.72	0.05	9.67
12.22	2.90	13.51	13.99	15.12	404.22	0.06	9.66
12.23	3.25	13.47	13.98	16.24	699.87	0.08	9.66
12.22	3.62	13.67	14.59	15.66	1148.67	0.11	9.66
12.22	3.98	13.84	14.35	15.36	1618.96	0.13	9.66
24.44	0.45	13.33	19.70	19.99	9.18	0.07	19.32
24.45	0.71	13.69	22.03	26.38	18.11	0.07	19.32
24.46	1.42	13.83	21.10	27.73	59.30	0.07	19.34
24.45	1.81	13.20	13.90	15.48	91.50	0.07	19.33
24.44	2.13	13.91	19.34	27.53	122.99	0.07	19.32
24.45	2.54	13.34	14.04	14.62	313.33	0.08	19.33
24.45	2.88	13.55	13.65	18.40	999.82	0.12	19.33

L (m^3/m^2*h)	F_G ($Pa^{0.5}$)	$T_{air,in}$ (℃)	$T_{liq,in}$ (℃)	$T_{air,out}$ (℃)	ΔP/Z (Pa/m)	h_L	Re_L
24.44	3.24	13.68	13.64	18.43	1675.29	0.17	19.32
36.72	0.45	13.31	19.89	20.44	9.91	0.09	29.03
36.67	0.71	13.65	21.97	25.96	19.43	0.09	28.99
36.68	1.08	13.55	13.73	18.50	40.71	0.09	28.99
36.68	1.42	13.82	20.78	27.60	63.72	0.09	29.00
36.66	1.80	13.39	13.85	19.10	98.51	0.09	28.98
36.67	2.13	13.91	19.03	27.48	133.24	0.09	28.99
36.66	2.52	13.47	13.87	19.53	695.46	0.11	28.98
36.69	2.80	13.55	13.86	19.54	1551.41	0.19	29.00
48.93	0.45	13.36	20.08	20.84	11.09	0.10	38.68
48.85	0.71	13.66	21.97	26.02	20.93	0.10	38.61
48.89	1.08	13.48	15.42	20.09	42.02	0.10	38.65
48.89	1.42	13.82	20.62	27.57	68.24	0.10	38.65
48.90	1.62	13.50	15.65	20.09	86.93	0.10	38.65
48.89	1.79	13.52	15.74	20.69	105.68	0.10	38.65
48.89	1.97	13.50	15.76	20.82	126.64	0.10	38.65
48.90	2.13	13.90	18.78	27.12	148.68	0.10	38.65
48.89	2.33	13.70	15.66	21.78	764.34	0.10	38.65
48.90	2.45	13.73	15.64	21.79	1904.29	0.19	38.66
60.75	0.45	13.39	20.63	21.01	12.09	0.11	48.02
61.12	0.71	13.69	22.08	26.44	22.81	0.11	48.32
61.12	1.08	13.49	15.94	20.05	45.94	0.11	48.32
61.12	1.26	13.42	16.10	20.96	60.37	0.11	48.31
61.10	1.42	13.84	20.55	27.66	75.44	0.11	48.30
61.12	1.61	13.42	16.17	20.98	96.82	0.11	48.32
61.10	1.79	13.45	16.19	21.57	120.26	0.11	48.30
61.13	1.97	13.47	16.18	21.02	149.94	0.11	48.33
61.11	2.13	13.89	18.65	26.98	175.06	0.12	48.31
61.11	2.28	13.61	16.13	21.38	1814.47	0.19	48.31
73.35	0.45	13.74	21.98	24.43	13.25	0.12	57.98
73.31	0.71	13.72	22.30	26.54	24.50	0.12	57.95
73.34	0.90	13.47	16.35	20.39	36.37	0.12	57.97
73.33	1.08	13.41	16.58	19.98	50.62	0.12	57.97
73.35	1.26	13.38	16.76	20.84	67.03	0.12	57.98
73.34	1.42	13.83	20.67	27.80	83.11	0.12	57.97
73.33	1.62	13.38	16.83	19.93	112.93	0.12	57.97
73.33	1.80	13.39	16.85	20.15	169.52	0.12	57.97
73.34	1.97	13.45	16.83	20.77	250.01	0.12	57.97
71.88	2.10	13.51	16.81	20.41	1632.27	0.20	56.82

RSR#0.3	SRP1202		Height	2.84 m			
0.00	0.33	39.44	35.43	39.34	17.18	0.00	0.00

L (m^3/m^2*h)	F_G ($Pa^{0.5}$)	$T_{air,in}$ (℃)	$T_{liq,in}$ (℃)	$T_{air,out}$ (℃)	ΔP/Z (Pa/m)	h_L	Re_L
0.00	0.52	39.94	35.71	39.59	34.07	0.00	0.00
0.00	0.70	40.50	35.95	39.31	55.24	0.00	0.00
0.00	1.04	41.11	36.15	40.44	115.64	0.00	0.00
0.00	1.39	42.39	36.35	40.38	198.37	0.00	0.00
0.00	1.74	43.28	36.48	39.33	301.42	0.00	0.00
0.00	2.09	44.61	36.63	40.37	431.10	0.00	0.00
0.00	2.43	47.33	36.72	41.04	582.82	0.00	0.00
0.00	2.78	49.50	36.80	40.98	758.93	0.00	0.00
0.00	3.12	55.11	36.89	40.87	952.94	0.00	0.00
0.00	3.47	58.00	36.96	41.02	1172.49	0.00	0.00
0.00	3.81	59.61	37.00	41.63	1384.09	0.00	0.00
0.00	4.16	60.06	36.99	41.93	1646.24	0.00	0.00
12.23	0.38	41.50	30.43	41.79	30.64	0.06	10.74
12.24	0.69	41.39	31.91	42.47	85.98	0.06	10.75
12.24	1.03	42.00	31.31	47.55	185.89	0.06	10.75
12.23	1.42	37.22	27.79	27.94	324.91	0.07	10.74
12.23	1.77	13.98	26.45	27.74	499.15	0.07	10.74
12.22	2.13	14.06	26.01	27.79	730.85	0.08	10.73
12.20	2.48	14.21	25.50	27.86	1028.33	0.09	10.72
12.23	2.83	14.49	24.77	28.12	1446.17	0.12	10.74
12.19	3.03	15.28	26.79	39.55	1810.56	0.15	10.71
24.47	0.38	43.69	30.57	41.37	35.46	0.09	21.49
24.45	0.69	41.72	31.34	43.24	100.09	0.09	21.48
24.46	1.03	41.64	30.49	49.74	217.70	0.09	21.48
24.47	1.42	30.44	26.99	27.83	395.23	0.10	21.49
24.48	1.77	33.50	24.08	28.82	626.01	0.10	21.50
24.46	2.12	36.15	23.82	28.99	997.77	0.11	21.48
24.47	2.27	44.63	25.37	36.87	1238.24	0.12	21.49
24.46	2.60	15.02	26.59	38.73	1871.91	0.15	21.48
36.69	0.38	42.61	30.79	40.64	41.70	0.12	32.22
36.69	0.69	41.78	31.15	46.24	119.78	0.12	32.22
36.59	1.02	41.94	30.19	50.89	275.09	0.12	32.14
36.68	1.41	14.20	23.83	30.52	514.78	0.12	32.22
36.68	1.59	14.21	23.89	31.09	646.85	0.13	32.22
36.69	1.76	14.28	23.93	31.53	871.35	0.13	32.22
36.68	1.94	14.38	24.01	32.07	1170.27	0.14	32.22
36.68	2.09	15.00	26.14	38.40	1498.04	0.15	32.22
36.66	2.23	15.04	26.22	38.48	2084.69	0.19	32.20
48.89	0.38	42.44	31.03	40.44	50.98	0.14	42.94
48.94	0.68	41.78	31.08	49.17	147.42	0.14	42.98
48.92	1.03	42.11	29.93	49.87	370.18	0.14	42.97
48.89	1.23	14.37	24.50	33.33	495.01	0.15	42.94

L (m^3/m^2*h)	F_G ($Pa^{0.5}$)	$T_{air,in}$ (℃)	$T_{liq,in}$ (℃)	$T_{air,out}$ (℃)	ΔP/Z (Pa/m)	h_L	Re_L
48.89	1.40	14.37	24.65	33.87	713.49	0.15	42.94
48.89	1.58	14.42	24.78	34.24	939.48	0.15	42.94
48.87	1.75	14.51	24.91	34.70	1258.80	0.16	42.93
48.93	1.89	14.57	24.96	34.73	1789.82	0.20	42.98
61.17	0.38	42.11	31.30	41.12	60.65	0.15	53.72
61.11	0.68	14.73	31.10	50.27	186.30	0.15	53.67
61.10	0.87	15.00	27.55	39.54	290.53	0.16	53.67
61.15	1.05	14.93	27.94	38.33	434.26	0.16	53.71
61.12	1.22	14.92	28.27	40.08	689.31	0.16	53.68
61.21	1.39	14.97	28.51	40.75	977.18	0.17	53.77
61.13	1.56	15.13	28.87	41.62	1396.26	0.18	53.69
61.15	1.65	15.15	28.92	41.75	1756.98	0.22	53.71
73.45	0.38	41.44	31.78	41.05	71.20	0.17	64.51
73.31	0.52	15.03	30.05	41.10	126.15	0.17	64.39
73.49	0.69	41.94	31.31	48.25	248.94	0.17	64.55
73.34	0.87	15.07	29.59	41.58	371.43	0.17	64.41
73.33	1.04	14.98	30.46	40.16	642.34	0.18	64.40
73.34	1.21	14.98	30.63	41.39	941.27	0.19	64.42
73.30	1.37	15.06	30.70	40.65	1790.90	0.20	64.38
73.44	1.49	14.76	30.47	38.56	1702.45	0.24	64.51

GTC500Y	SRP1307		Height	3.06 m			
0.00	0.43	13.52	25.43	24.77	16.57	0.00	0.00
0.00	0.71	13.53	25.43	24.88	35.60	0.00	0.00
0.00	1.07	13.54	24.31	24.99	73.08	0.00	0.00
0.00	1.43	13.57	24.31	25.06	123.22	0.00	0.00
0.00	1.78	13.63	24.31	25.03	185.30	0.00	0.00
0.00	2.14	13.72	24.31	25.05	260.68	0.00	0.00
0.00	2.49	13.80	24.31	25.19	344.57	0.00	0.00
0.00	2.85	13.91	24.31	25.28	441.48	0.00	0.00
0.00	3.20	14.08	24.49	25.43	550.39	0.00	0.00
0.00	3.56	14.21	24.49	25.58	651.15	0.00	0.00
0.00	4.27	14.52	24.49	25.82	913.26	0.00	0.00
0.00	4.62	14.82	24.49	25.88	1059.36	0.00	0.00
12.23	0.42	14.13	26.94	33.13	22.37	0.07	6.77
12.22	0.53	13.96	25.23	29.90	32.36	0.07	6.76
12.23	0.70	14.19	27.72	32.86	52.71	0.07	6.77
12.26	0.88	14.18	28.25	33.61	78.72	0.07	6.78
12.23	1.05	14.18	28.52	34.50	110.56	0.07	6.77
12.26	1.40	14.29	26.71	35.07	190.38	0.07	6.78
12.22	1.75	14.37	26.72	35.64	359.14	0.07	6.76
12.22	2.10	14.50	26.66	36.02	721.37	0.09	6.76

L (m^3/m^2*h)	F_G ($Pa^{0.5}$)	$T_{air,in}$ (℃)	$T_{liq,in}$ (℃)	$T_{air,out}$ (℃)	ΔP/Z (Pa/m)	h_L	Re_L
12.17	2.45	14.73	26.61	36.54	1430.97	0.11	6.73
12.17	2.75	14.86	26.67	36.77	2326.23	0.14	6.73
24.44	0.42	14.19	26.95	33.13	25.48	0.09	13.52
24.47	0.53	13.92	25.32	30.19	37.13	0.09	13.54
24.46	0.70	14.22	27.68	32.93	59.89	0.09	13.54
24.48	0.88	14.16	28.12	33.67	90.17	0.09	13.55
24.47	1.05	14.20	28.39	34.51	126.94	0.09	13.54
24.46	1.22	14.31	27.67	36.10	190.20	0.09	13.54
24.44	1.42	13.71	25.72	26.10	259.24	0.09	13.53
24.46	1.59	13.88	25.42	29.19	366.10	0.10	13.53
24.45	1.77	13.96	25.13	30.16	697.96	0.11	13.53
24.44	1.94	14.18	25.13	29.67	1539.70	0.14	13.52
36.67	0.42	14.18	27.10	33.17	27.81	0.10	20.29
36.67	0.53	13.92	25.41	30.37	41.48	0.10	20.29
36.65	0.70	14.20	27.72	33.08	66.52	0.10	20.28
36.69	0.88	14.19	28.07	33.88	100.18	0.10	20.30
36.65	1.05	14.20	28.27	34.61	142.02	0.10	20.28
36.68	1.23	14.25	28.30	35.45	219.34	0.10	20.30
36.66	1.40	14.25	28.17	35.59	348.52	0.11	20.29
36.66	1.71	14.42	27.82	35.52	1579.33	0.16	20.28
48.92	0.42	14.14	27.19	33.14	30.59	0.12	27.07
48.91	0.53	13.95	25.49	30.50	45.33	0.12	27.06
48.96	0.70	14.20	27.79	33.35	73.06	0.12	27.09
48.89	0.88	14.21	28.11	34.16	110.63	0.12	27.05
48.92	1.06	13.71	25.05	29.68	179.49	0.12	27.07
48.91	1.25	13.61	25.97	25.01	273.77	0.12	27.06
48.91	1.42	13.87	25.41	28.39	744.09	0.15	27.06
48.87	1.57	14.33	27.61	36.12	1784.14	0.20	27.04
61.12	0.42	14.15	27.35	32.99	34.06	0.14	33.82
61.13	0.53	13.97	25.66	30.72	49.92	0.14	33.83
61.13	0.70	14.20	27.89	33.38	81.48	0.14	33.83
61.10	0.88	14.18	28.21	34.41	126.56	0.14	33.81
61.15	1.06	13.74	25.13	30.14	198.07	0.14	33.84
61.12	1.25	13.65	25.91	25.23	396.20	0.16	33.82
61.13	1.35	13.93	25.44	28.55	1727.75	0.20	33.83
73.33	0.42	14.15	27.57	32.75	39.33	0.15	40.57
73.34	0.53	13.97	25.88	31.02	57.49	0.15	40.58
73.35	0.70	14.17	28.13	33.56	95.71	0.15	40.59
73.29	0.88	14.18	28.43	34.54	179.26	0.16	40.56
73.29	1.05	13.93	26.25	32.86	329.17	0.16	40.55
73.40	1.22	13.73	25.96	25.36	1653.70	0.20	40.62

L (m^3/m^2*h)	F_G ($Pa^{0.5}$)	$T_{air,in}$ (℃)	$T_{liq,in}$ (℃)	$T_{air,out}$ (℃)	ΔP/Z (Pa/m)	h_L	Re_L
RSP200X	SRP1306		Height	3.05 m			
0.00	0.44	30.59	27.21	29.24	5.34	0.00	0.00
0.00	0.71	30.63	27.31	29.31	11.40	0.00	0.00
0.00	1.06	30.86	27.39	29.36	22.19	0.00	0.00
0.00	1.41	31.21	27.49	29.44	36.35	0.00	0.00
0.00	1.77	31.81	27.54	29.54	53.80	0.00	0.00
0.00	2.12	32.83	27.62	29.74	73.68	0.00	0.00
0.00	2.47	34.27	27.69	29.76	96.23	0.00	0.00
0.00	2.83	35.80	27.77	30.24	121.44	0.00	0.00
0.00	3.18	37.64	27.80	30.26	149.93	0.00	0.00
0.00	3.53	38.79	27.85	30.17	174.00	0.00	0.00
0.00	3.88	40.80	27.88	30.24	205.37	0.00	0.00
0.00	4.24	43.08	27.93	30.28	240.90	0.00	0.00
0.00	4.59	45.79	27.98	30.32	276.86	0.00	0.00
0.00	4.95	48.37	28.01	30.16	316.63	0.00	0.00
12.24	0.43	27.32	24.87	27.71	7.21	0.04	16.93
12.28	0.71	25.65	26.12	25.90	15.68	0.04	16.98
12.09	1.07	25.75	26.13	25.83	30.05	0.04	16.72
12.26	1.46	12.53	21.26	9.45	48.34	0.04	16.96
12.22	2.19	12.73	15.15	10.15	103.08	0.04	16.91
12.23	2.92	12.87	14.30	9.67	173.46	0.04	16.92
12.22	3.66	13.05	13.90	9.27	277.17	0.04	16.91
12.21	4.39	13.39	13.57	9.27	409.58	0.05	16.90
12.19	5.12	13.78	13.60	9.49	636.83	0.10	16.87
24.42	0.43	26.83	25.14	27.28	8.41	0.06	33.77
24.44	0.71	25.63	25.98	25.91	18.59	0.06	33.80
24.42	1.07	25.83	25.85	25.77	36.23	0.06	33.78
24.44	1.46	12.54	19.58	9.50	59.25	0.06	33.80
24.45	2.19	12.88	13.63	11.75	119.85	0.06	33.82
24.44	2.91	13.16	13.29	12.74	214.25	0.07	33.81
24.47	3.64	13.41	13.36	13.16	347.14	0.07	33.85
24.46	4.00	13.60	13.58	13.46	434.16	0.08	33.84
24.46	4.36	13.74	13.79	13.38	564.82	0.10	33.84
24.44	4.73	14.02	14.30	13.32	902.97	0.00	33.81
24.43	4.93	14.26	14.84	13.70	1277.73	0.00	33.79
36.67	0.42	26.54	25.24	26.82	9.92	0.07	50.73
36.50	0.71	25.59	26.00	25.87	22.09	0.07	50.49
36.64	1.07	25.86	25.70	25.70	43.76	0.07	50.69
36.68	1.46	12.56	18.46	9.46	74.16	0.07	50.74
36.67	2.18	13.30	15.47	14.03	155.29	0.08	50.73
36.66	2.90	13.30	15.19	14.11	298.90	0.08	50.71
36.67	3.26	13.39	15.03	14.34	424.07	0.09	50.73

L (m^3/m^2*h)	F_G ($Pa^{0.5}$)	$T_{air,in}$ (℃)	$T_{liq,in}$ (℃)	$T_{air,out}$ (℃)	ΔP/Z (Pa/m)	h_L	Re_L
36.65	3.63	13.57	14.92	14.05	665.30	0.10	50.70
36.67	3.99	13.89	15.05	14.71	1034.79	0.12	50.73
36.69	4.35	14.24	15.57	15.24	1522.87	0.00	50.76
48.86	0.43	26.19	25.54	26.41	11.85	0.08	67.58
48.89	0.71	25.52	26.07	25.85	26.07	0.08	67.64
48.91	1.07	25.85	25.61	25.75	52.21	0.08	67.66
48.90	1.46	12.58	17.67	9.46	92.80	0.08	67.64
48.89	1.81	13.60	15.97	15.35	139.71	0.09	67.64
48.90	2.17	13.42	15.95	15.38	204.75	0.09	67.64
48.90	2.54	13.39	15.86	15.47	297.11	0.09	67.65
48.88	2.89	13.46	15.73	15.78	428.78	0.10	67.62
48.90	3.26	13.59	15.66	15.95	706.91	0.11	67.64
48.87	3.62	13.99	15.82	16.04	1863.49	0.14	67.61
61.12	0.43	25.82	25.96	26.29	14.02	0.09	84.55
60.99	0.71	25.55	26.14	25.89	30.10	0.09	84.37
61.10	1.07	25.69	25.61	25.52	61.96	0.09	84.52
61.12	1.46	12.60	17.01	9.76	125.12	0.10	84.55
61.12	1.81	13.67	16.24	16.48	183.63	0.10	84.54
61.10	2.17	13.51	16.26	16.71	287.10	0.11	84.53
61.09	2.53	13.48	16.18	17.07	433.36	0.11	84.51
61.12	2.89	13.56	16.10	17.00	718.86	0.12	84.56
61.09	3.25	13.76	16.08	16.84	1932.53	0.16	84.51
73.33	0.43	25.67	26.12	26.01	16.53	0.11	101.45
73.33	0.71	25.52	26.10	25.78	35.48	0.11	101.44
73.33	1.07	25.49	25.58	25.17	78.03	0.11	101.43
73.34	1.46	12.63	16.28	9.78	169.04	0.11	101.46
73.32	1.81	13.41	16.25	16.49	266.06	0.12	101.43
73.33	1.99	13.35	16.23	16.42	331.56	0.12	101.44
73.31	2.17	13.33	16.17	16.27	423.55	0.13	101.42
73.32	2.53	13.54	16.03	16.75	1138.44	0.14	101.43
73.34	2.80	13.63	16.03	16.77	1822.37	0.17	101.46

RSR#0.7	SRP1102		Height	2.92 m			
0.00	0.42	33.31	31.24	32.03	6.69	0.00	0.00
0.00	0.70	33.57	31.29	33.14	14.83	0.00	0.00
0.00	1.05	33.40	31.36	34.93	30.46	0.00	0.00
0.00	1.40	33.34	31.42	35.61	49.22	0.00	0.00
0.00	1.75	33.05	31.53	35.91	80.06	0.00	0.00
0.00	2.10	33.60	31.68	35.76	116.00	0.00	0.00
0.00	2.45	32.88	31.80	36.11	157.64	0.00	0.00
0.00	2.80	33.31	31.88	36.22	203.77	0.00	0.00
0.00	3.14	33.57	31.95	37.02	272.60	0.00	0.00

L (m^3/m^2*h)	F_G ($Pa^{0.5}$)	$T_{air,in}$ (℃)	$T_{liq,in}$ (℃)	$T_{air,out}$ (℃)	ΔP/Z (Pa/m)	h_L	Re_L
0.00	3.48	34.28	32.06	39.05	335.71	0.00	0.00
0.00	3.82	34.25	32.18	41.05	404.50	0.00	0.00
0.00	4.16	34.25	32.29	42.55	473.43	0.00	0.00
0.00	4.50	33.79	32.37	42.82	549.07	0.00	0.00
0.00	4.83	34.30	32.49	44.97	624.61	0.00	0.00
12.22	0.41	25.11	26.81	25.60	8.91	0.02	18.78
12.22	0.53	26.31	27.65	26.28	13.01	0.02	18.78
12.29	0.71	27.19	27.79	26.45	20.81	0.02	18.90
12.22	1.07	28.22	27.93	26.73	40.76	0.02	18.78
12.22	1.42	29.88	27.95	26.69	66.80	0.02	18.78
12.24	1.77	32.95	28.73	28.13	103.22	0.02	18.81
12.22	2.13	34.23	27.15	26.40	151.47	0.02	18.79
12.24	2.49	35.01	27.49	26.38	210.04	0.03	18.81
12.21	2.84	25.47	27.78	26.15	333.90	0.03	18.76
12.22	3.20	26.30	26.84	25.33	413.28	0.03	18.78
12.20	3.56	27.14	26.34	24.79	524.75	0.03	18.75
12.22	3.92	27.26	26.35	24.96	679.41	0.03	18.78
12.23	4.19	27.56	26.36	25.01	824.54	0.04	18.80
12.23	4.63	27.68	26.48	25.35	1148.65	0.06	18.79
24.43	0.40	25.29	26.78	25.59	9.49	0.04	37.56
24.44	0.53	26.48	27.63	26.27	13.89	0.04	37.56
24.46	0.71	27.46	27.74	26.45	22.54	0.04	37.60
24.44	1.07	28.39	27.81	26.66	44.26	0.04	37.57
24.44	1.42	29.94	27.83	26.73	72.38	0.04	37.57
24.46	1.77	33.11	28.58	28.06	115.36	0.04	37.60
24.46	2.13	34.52	26.92	26.43	167.68	0.04	37.59
24.44	2.49	34.54	27.30	26.49	258.53	0.05	37.56
24.46	2.84	25.58	27.34	26.23	375.46	0.05	37.59
24.46	3.20	26.54	26.69	25.42	496.14	0.05	37.60
24.45	3.56	27.84	26.91	25.31	663.20	0.06	37.58
24.45	3.92	28.26	27.05	25.67	933.35	0.07	37.58
24.44	4.26	28.26	27.16	25.74	1625.98	0.12	37.57
36.67	0.40	25.55	26.74	25.52	10.04	0.05	56.37
36.67	0.53	26.63	27.58	26.23	15.44	0.06	56.36
36.68	0.71	27.55	27.68	26.40	24.54	0.06	56.37
36.66	1.07	28.69	27.70	26.49	48.20	0.06	56.35
36.67	1.42	30.88	27.77	26.62	78.30	0.06	56.36
36.68	1.77	33.30	28.48	27.58	126.16	0.06	56.38
36.68	2.13	34.46	26.99	26.13	187.63	0.06	56.38
36.69	2.49	33.98	27.16	26.26	298.62	0.06	56.39
36.70	2.84	34.69	26.92	26.13	446.09	0.07	56.41
36.67	3.20	26.41	26.62	25.33	617.14	0.08	56.36

L (m^3/m^2*h)	F_G ($Pa^{0.5}$)	$T_{air,in}$ (℃)	$T_{liq,in}$ (℃)	$T_{air,out}$ (℃)	ΔP/Z (Pa/m)	h_L	Re_L
36.67	3.56	28.21	27.36	26.05	898.84	0.09	56.36
36.75	3.87	28.30	27.38	26.04	1712.19	0.14	56.49
48.90	0.39	25.37	26.79	25.46	11.04	0.06	75.16
48.89	0.53	26.69	27.57	26.21	17.15	0.06	75.15
48.89	0.71	27.69	27.67	26.37	26.29	0.06	75.14
48.90	1.07	28.99	27.69	26.45	52.44	0.06	75.16
48.89	1.42	30.97	27.77	26.56	84.91	0.07	75.15
48.90	1.77	33.47	28.45	27.52	138.34	0.07	75.16
48.89	2.13	34.32	26.95	26.21	215.90	0.07	75.15
48.89	2.49	34.69	27.13	26.20	345.52	0.07	75.14
48.89	2.85	34.26	26.90	25.98	543.29	0.08	75.14
48.90	3.20	26.69	26.65	25.32	834.89	0.10	75.16
48.90	3.53	28.19	27.45	26.13	1752.96	0.18	75.17
61.14	0.38	25.71	26.97	25.56	12.37	0.07	93.98
61.11	0.53	26.67	27.60	26.23	18.80	0.07	93.92
61.12	0.71	27.85	27.74	26.38	28.61	0.07	93.95
61.10	1.07	29.16	27.78	26.55	56.56	0.07	93.92
61.13	1.42	29.93	27.79	26.58	92.07	0.07	93.96
61.14	1.77	33.45	28.46	27.48	153.19	0.08	93.97
61.12	2.13	35.00	27.05	26.15	257.99	0.08	93.94
61.16	2.49	34.36	27.12	26.23	407.44	0.09	94.01
61.12	2.85	34.87	26.96	26.00	683.97	0.11	93.95
61.02	3.18	26.87	26.76	25.41	1701.76	0.17	93.80
73.34	0.38	26.18	27.57	26.16	13.22	0.08	112.73
73.31	0.53	27.06	27.73	26.35	20.21	0.08	112.68
73.33	0.71	28.03	27.88	26.55	30.74	0.08	112.71
73.32	1.07	29.46	27.89	26.65	59.82	0.08	112.70
73.33	1.42	31.04	27.95	26.66	99.08	0.08	112.72
73.53	1.77	33.78	28.50	27.44	164.66	0.09	113.02
73.34	2.13	34.10	27.34	26.28	297.63	0.09	112.72
73.33	2.49	34.72	27.20	26.26	488.11	0.11	112.71
73.34	2.84	34.20	27.14	26.13	983.24	0.17	112.72
73.36	2.97	28.65	27.52	26.23	1658.70	0.00	112.77

Appendix D: Detailed packing mass transfer data

The packing mass transfer data (effective area, liquid film mass transfer coefficient, gas film mass transfer coefficient) are listed in this section. The effective area was measured at the packed height of around 3.3 m (10 ft). Reduced packed bed was used for k_L (6 ft) and k_G (20-40 inches) measurements.

Table D.1. Detailed packing effective area data.

L (m^3/m^2*h)	u_G (m/s)	T_{corr} (℃)	$k_{OH-}*10^{-3}$ (m^3/kmol*s)	$D_{CO2}*10^9$ (m^2/s)	$H_{CO2}*10^{-5}$ (m^3*Pa/kmol)	[OH-] kmol/m^3	CO_2In ppm	CO_2 out ppm	a_f
MP2X	SRP0915			Height	2.85 m				
73.4	1.48	24.4	8.23	2.03	30.2	0.11	385	245	1.12
61.2	1.48	24.0	8.03	2.00	29.9	0.11	386	249	1.11
48.9	1.48	23.6	7.84	1.97	29.5	0.11	386	254	1.07
36.7	1.48	23.3	7.69	1.95	29.3	0.11	391	264	1.01
24.5	1.48	23.0	7.56	1.93	29.0	0.11	387	266	0.98
18.3	1.48	22.8	7.46	1.91	28.9	0.10	386	278	0.87
12.2	1.48	22.6	7.38	1.90	28.7	0.10	386	280	0.86
6.0	1.48	22.5	7.32	1.89	28.6	0.10	387	288	0.80
6.1	1.00	22.3	7.22	1.87	28.4	0.10	395	250	0.85
12.2	0.99	21.8	7.04	1.83	28.1	0.10	386	245	0.87
18.3	0.99	21.9	7.09	1.84	28.2	0.09	386	247	0.85
24.5	0.99	21.7	7.00	1.82	28.0	0.09	387	235	0.98
36.7	0.99	21.6	6.92	1.81	27.9	0.09	386	229	1.04
48.9	0.99	21.4	6.86	1.79	27.8	0.09	397	227	1.13
61.1	0.99	21.3	6.82	1.78	27.7	0.09	387	226	1.09
73.4	0.99	21.2	6.78	1.77	27.6	0.09	386	228	1.09
73.4	0.59	21.0	6.68	1.75	27.4	0.08	390	174	1.04
61.1	0.59	20.9	6.64	1.75	27.3	0.08	400	179	1.04
48.9	0.59	20.7	6.57	1.73	27.2	0.08	388	174	1.05
36.6	0.59	20.5	6.47	1.72	27.0	0.08	391	185	0.99
24.4	0.59	20.2	6.37	1.70	26.8	0.08	393	187	1.00
18.4	0.60	19.9	6.26	1.69	26.6	0.08	393	194	0.97
12.2	0.59	19.7	6.16	1.67	26.4	0.08	407	208	0.91
6.1	0.59	19.4	6.08	1.66	26.2	0.08	402	220	0.83
24.4	1.98	19.2	5.98	1.64	26.0	0.07	408	331	0.95
24.5	2.47	19.2	5.98	1.64	26.0	0.07	415	352	0.95
49.0	1.98	18.8	5.78	1.69	25.6	0.09	394	284	1.34

L (m^3/m^2*h)	u_G (m/s)	T_{corr} (℃)	$k_{OH-}*10^{-3}$ (m^3/kmol*s)	$D_{CO2}*10^9$ (m^2/s)	$H_{CO2}*10^{-5}$ (m^3*Pa/kmol)	[OH-] kmol/m^3	CO_2In ppm	CO_2 out ppm	a_f
RSP250Y	SRP1002			Height	3.04 m				
24.4	0.59	16.9	5.09	1.66	24.2	0.11	401	114	1.01
73.3	0.59	17.1	5.14	1.67	24.3	0.11	401	124	0.95
61.1	0.59	17.0	5.13	1.67	24.3	0.11	401	121	0.97
36.6	0.59	16.7	5.03	1.66	24.1	0.11	401	113	1.04
48.6	0.59	17.0	5.11	1.67	24.3	0.11	401	118	1.00
6.1	0.60	17.0	5.14	1.67	24.4	0.11	401	147	0.81
12.2	0.60	17.0	5.14	1.67	24.4	0.11	401	124	0.96
12.3	0.99	12.0	3.69	1.44	20.9	0.12	411	211	0.95
48.9	0.99	11.3	3.52	1.41	20.4	0.12	411	195	1.09
6.1	0.99	12.4	3.81	1.46	21.2	0.12	411	223	0.86
36.6	0.99	11.4	3.54	1.42	20.4	0.12	411	195	1.08
24.4	0.99	11.4	3.56	1.42	20.5	0.12	411	201	1.04
61.1	0.99	11.3	3.51	1.41	20.4	0.12	411	200	1.06
73.3	0.99	11.4	3.54	1.42	20.4	0.12	411	185	1.17
6.1	1.48	17.2	5.20	1.68	24.5	0.11	401	253	0.94
36.7	1.48	11.5	3.56	1.42	20.5	0.12	411	247	1.13
61.1	1.48	16.8	5.03	1.66	24.1	0.11	401	221	1.25
24.4	1.48	17.0	5.12	1.67	24.3	0.11	401	233	1.10
12.1	1.49	16.7	5.02	1.66	24.1	0.11	401	246	1.02
48.9	1.49	11.5	3.56	1.43	20.5	0.11	411	244	1.16
48.9	1.98	17.0	5.11	1.68	24.3	0.10	401	259	1.22
24.4	1.98	16.9	5.06	1.67	24.1	0.10	401	269	1.12
24.4	0.59	16.9	5.09	1.66	24.2	0.11	401	114	1.01
73.3	0.59	17.1	5.14	1.67	24.3	0.11	401	124	0.95
61.1	0.59	17.0	5.13	1.67	24.3	0.11	401	121	0.97
36.6	0.59	16.7	5.03	1.66	24.1	0.11	401	113	1.04
48.6	0.59	17.0	5.11	1.67	24.3	0.11	401	118	1.00
6.1	0.60	17.0	5.14	1.67	24.4	0.11	401	147	0.81
12.2	0.60	17.0	5.14	1.67	24.4	0.11	401	124	0.96
12.3	0.99	12.0	3.69	1.44	20.9	0.12	411	211	0.95
48.9	0.99	11.3	3.52	1.41	20.4	0.12	411	195	1.09
6.1	0.99	12.4	3.81	1.46	21.2	0.12	411	223	0.86
36.6	0.99	11.4	3.54	1.42	20.4	0.12	411	195	1.08
24.4	0.99	11.4	3.56	1.42	20.5	0.12	411	201	1.04
61.1	0.99	11.3	3.51	1.41	20.4	0.12	411	200	1.06
73.3	0.99	11.4	3.54	1.42	20.4	0.12	411	185	1.17
6.1	1.48	17.2	5.20	1.68	24.5	0.11	401	253	0.94
36.7	1.48	11.5	3.56	1.42	20.5	0.12	411	247	1.13
61.1	1.48	16.8	5.03	1.66	24.1	0.11	401	221	1.25
24.4	1.48	17.0	5.12	1.67	24.3	0.11	401	233	1.10
12.1	1.49	16.7	5.02	1.66	24.1	0.11	401	246	1.02

L (m^3/m^2*h)	u_G (m/s)	T_{corr} (℃)	$k_{OH-}*10^{-3}$ (m^3/kmol*s)	$D_{CO2}*10^9$ (m^2/s)	$H_{CO2}*10^{-5}$ (m^3*Pa/kmol)	[OH-] kmol/m^3	CO_2In ppm	CO_2 out ppm	a_f
48.9	1.49	11.5	3.56	1.43	20.5	0.11	411	244	1.16
48.9	1.98	17.0	5.11	1.68	24.3	0.10	401	259	1.22
24.4	1.98	16.9	5.06	1.67	24.1	0.10	401	269	1.12

RSR#0.5	SRP1003			Height	2.79 m				
6.1	0.59	18.7	5.71	1.75	25.6	0.11	404	191	0.61
12.2	0.59	18.6	5.67	1.74	25.5	0.11	404	160	0.76
24.5	0.59	18.9	5.80	1.76	25.7	0.11	404	142	0.85
36.7	0.59	19.1	5.85	1.77	25.9	0.11	404	136	0.88
48.9	0.59	19.2	5.90	1.77	25.9	0.11	404	135	0.89
61.1	0.59	20.1	6.24	1.82	26.6	0.11	404	127	0.93
73.4	0.60	19.7	6.08	1.80	26.3	0.11	404	120	0.99
6.1	0.99	23.2	7.61	1.97	29.1	0.11	400	239	0.63
12.2	0.99	22.6	7.34	1.94	28.7	0.11	400	212	0.79
24.4	0.99	22.3	7.19	1.92	28.4	0.11	400	198	0.88
36.6	0.99	22.0	7.05	1.91	28.2	0.11	400	190	0.94
48.9	0.99	21.6	6.88	1.89	27.8	0.11	400	186	0.97
61.1	0.99	21.3	6.76	1.88	27.6	0.11	400	177	1.04
6.1	1.48	17.0	5.13	1.67	24.3	0.11	406	296	0.67
12.2	1.48	16.6	4.97	1.65	24.0	0.11	406	274	0.84
24.5	1.48	16.1	4.81	1.63	23.6	0.11	406	260	0.96
36.7	1.49	16.1	4.81	1.63	23.6	0.11	406	249	1.06
24.5	1.65	16.0	4.80	1.63	23.6	0.10	406	268	1.01

GTC350Z	SRP1101			Height	2.79 m				
6.3	0.60	27.5	9.87	2.21	32.7	0.10	399	116	0.80
12.2	0.59	27.5	9.87	2.21	32.7	0.10	399	111	0.84
24.4	0.59	27.5	9.85	2.21	32.7	0.10	399	99	0.94
36.7	0.59	27.4	9.82	2.21	32.6	0.10	399	88	1.05
48.9	0.59	27.6	9.92	2.22	32.8	0.10	399	82	1.12
61.1	0.59	27.9	10.07	2.23	33.0	0.10	399	99	0.95
73.3	0.59	26.9	9.52	2.17	32.2	0.10	404	108	0.88
6.0	0.99	26.6	9.37	2.15	32.0	0.11	398	170	0.85
12.2	0.99	26.5	9.34	2.15	31.9	0.11	398	163	0.90
24.4	0.99	26.4	9.24	2.14	31.8	0.11	398	151	1.01
36.7	0.99	27.1	9.59	2.19	32.3	0.09	404	133	1.23
48.9	0.99	26.3	9.17	2.14	31.7	0.10	398	142	1.10
61.1	0.99	27.1	9.62	2.19	32.3	0.10	404	142	1.15
73.3	0.99	27.0	9.57	2.18	32.3	0.10	404	146	1.07
61.1	0.59	26.7	9.36	2.17	32.0	0.10	398	106	0.92
73.3	0.59	26.7	9.41	2.17	32.0	0.10	398	116	0.84
6.1	1.48	29.8	11.40	2.35	34.8	0.11	392	202	0.90

L (m^3/m^2*h)	u_G (m/s)	T_{corr} (℃)	$k_{OH-}*10^{-3}$ (m^3/kmol*s)	$D_{CO2}*10^9$ (m^2/s)	$H_{CO2}*10^{-5}$ (m^3*Pa/kmol)	[OH-] kmol/m^3	CO_2In ppm	CO_2 out ppm	a_f
12.2	1.48	29.8	11.36	2.35	34.8	0.11	392	193	0.97
24.4	1.48	29.3	11.07	2.32	34.4	0.11	392	184	1.06
36.7	1.48	29.2	10.98	2.31	34.3	0.11	392	178	1.12
48.9	1.48	29.2	10.96	2.31	34.2	0.10	392	173	1.17
61.1	1.49	27.1	9.63	2.19	32.3	0.10	404	181	1.29
73.4	1.48	27.0	9.57	2.18	32.3	0.10	404	173	1.29
36.6	1.98	30.4	11.71	2.39	35.2	0.09	399	219	1.15
36.7	2.31	29.1	10.84	2.31	34.0	0.09	392	227	1.23

RSR#0.7	SRP1102			Height	2.91 m				
6.1	0.59	27.2	9.67	2.19	32.4	0.10	401	167	0.88
12.2	0.59	27.1	9.64	2.19	32.4	0.10	401	149	1.00
24.4	0.59	27.0	9.57	2.18	32.3	0.10	401	136	1.10
36.7	0.59	27.1	9.62	2.19	32.3	0.10	401	129	1.15
48.9	0.59	27.0	9.56	2.18	32.2	0.10	401	124	1.20
61.1	0.59	27.0	9.57	2.19	32.3	0.10	401	119	1.25
73.3	0.59	27.1	9.59	2.19	32.3	0.10	401	115	1.29
6.1	0.99	28.1	10.22	2.25	33.2	0.10	393	222	0.93
12.2	0.99	28.1	10.21	2.25	33.2	0.10	393	209	1.03
24.5	0.99	27.8	10.08	2.24	33.0	0.10	393	195	1.16
36.7	0.99	27.7	9.98	2.23	32.9	0.10	393	189	1.22
48.9	0.99	27.6	9.91	2.22	32.8	0.10	393	184	1.27
61.1	0.99	27.6	9.93	2.22	32.8	0.10	393	177	1.34
73.3	0.99	27.7	9.97	2.23	32.8	0.10	393	172	1.39
6.1	1.49	31.2	12.25	2.45	35.9	0.09	387	259	0.99
12.2	1.48	32.3	13.12	2.52	36.9	0.10	387	244	1.06
24.5	1.48	31.5	12.52	2.47	36.2	0.10	387	234	1.19
36.7	1.48	31.3	12.33	2.45	36.0	0.10	387	228	1.26
48.9	1.48	31.1	12.18	2.44	35.8	0.09	387	225	1.31
61.1	1.48	31.1	12.17	2.44	35.8	0.09	387	221	1.36
73.3	1.48	30.9	12.06	2.43	35.6	0.09	387	215	1.43
36.7	1.98	30.6	11.80	2.41	35.3	0.09	387	260	1.33
36.7	2.31	30.4	11.70	2.40	35.1	0.09	387	273	1.38

A350Y	SRP1304			Height	3.04 m				
1.2	0.59	21.9	6.97	1.91	28.0	0.10	403	143	0.58
2.5	0.59	21.9	6.96	1.91	28.0	0.10	403	124	0.66
3.7	0.59	21.9	6.95	1.91	27.9	0.10	403	116	0.70
4.9	0.59	16.6	4.98	1.66	24.0	0.10	416	122	0.74
6.1	0.59	16.7	5.01	1.66	24.0	0.10	416	118	0.76
12.2	0.59	15.8	4.74	1.61	23.4	0.11	416	116	0.77
24.5	0.59	16.0	4.79	1.62	23.6	0.11	416	115	0.78

L (m^3/m^2*h)	u_G (m/s)	T_{corr} (℃)	$k_{OH-}*10^{-3}$ (m^3/kmol*s)	$D_{CO2}*10^9$ (m^2/s)	$H_{CO2}*10^{-5}$ (m^3*Pa/kmol)	[OH-] kmol/m^3	CO_2In ppm	CO_2 out ppm	a_f
36.7	0.59	16.1	4.83	1.63	23.7	0.11	416	115	0.77
48.9	0.59	16.4	4.91	1.64	23.8	0.10	416	128	0.71
61.1	0.59	16.6	4.96	1.65	23.9	0.10	416	134	0.68
1.2	0.99	16.1	4.82	1.62	23.6	0.11	415	233	0.59
2.5	0.99	16.1	4.83	1.62	23.6	0.10	415	217	0.66
3.7	0.99	16.2	4.83	1.62	23.6	0.10	415	207	0.72
4.9	0.99	16.0	4.79	1.62	23.5	0.10	415	203	0.75
6.1	0.99	15.8	4.72	1.61	23.4	0.10	415	202	0.75
12.2	0.99	15.6	4.65	1.60	23.2	0.10	415	200	0.77
24.5	0.99	15.4	4.59	1.60	23.1	0.10	415	198	0.79
36.7	0.99	15.4	4.57	1.60	23.0	0.10	415	197	0.80
48.9	0.99	15.4	4.57	1.60	23.0	0.09	415	197	0.81
1.2	1.48	14.4	4.29	1.54	22.4	0.10	400	278	0.58
2.5	1.49	14.5	4.34	1.55	22.5	0.10	400	265	0.66
3.7	1.48	14.7	4.37	1.56	22.6	0.10	400	255	0.72
4.9	1.48	14.2	4.24	1.54	22.2	0.10	400	249	0.77
6.1	1.48	13.7	4.09	1.52	21.9	0.10	400	247	0.80
12.2	1.48	12.9	3.88	1.49	21.3	0.10	400	246	0.83
24.5	1.48	12.7	3.83	1.49	21.2	0.09	400	249	0.81
36.7	1.48	12.9	3.88	1.49	21.3	0.10	400	247	0.79
24.5	1.82	16.8	5.07	1.66	24.2	0.11	416	258	0.85

B350X	SRP1303			Height	3.01 m				
1.3	0.59	20.8	6.47	1.85	27.1	0.09	390	185	0.44
2.4	0.59	20.9	6.53	1.86	27.2	0.09	390	163	0.52
3.7	0.59	21.0	6.59	1.87	27.3	0.10	390	153	0.55
4.9	0.59	21.3	6.70	1.88	27.5	0.10	390	147	0.56
6.1	0.59	21.5	6.79	1.89	27.7	0.10	390	139	0.59
12.2	0.59	21.7	6.87	1.90	27.8	0.10	390	132	0.62
24.4	0.60	21.6	6.87	1.89	27.8	0.10	390	124	0.64
36.7	0.59	21.6	6.84	1.89	27.8	0.10	390	119	0.67
48.9	0.59	21.7	6.90	1.90	27.9	0.10	390	112	0.70
61.1	0.59	20.2	6.25	1.83	26.6	0.09	390	140	0.61
73.3	0.59	21.8	6.93	1.90	27.9	0.10	390	140	0.58
1.2	0.99	21.1	6.65	1.87	27.4	0.10	385	251	0.40
2.5	0.99	21.2	6.67	1.87	27.4	0.10	385	224	0.50
3.7	0.99	21.3	6.72	1.87	27.5	0.10	385	213	0.54
4.9	0.99	21.4	6.77	1.88	27.6	0.10	385	207	0.57
6.1	0.99	21.6	6.85	1.89	27.8	0.11	385	198	0.60
12.2	0.99	21.8	6.94	1.90	27.9	0.11	385	187	0.65
24.4	0.99	23.5	7.75	1.98	29.4	0.11	385	174	0.67
36.7	0.99	22.6	7.33	1.94	28.7	0.11	385	169	0.71

L (m^3/m^2*h)	u_G (m/s)	T_{corr} (℃)	$k_{OH-}*10^{-3}$ (m^3/kmol*s)	$D_{CO2}*10^9$ (m^2/s)	$H_{CO2}*10^{-5}$ (m^3*Pa/kmol)	[OH-] kmol/m^3	CO_2In ppm	CO_2 out ppm	a_f
48.9	0.99	22.3	7.20	1.92	28.4	0.11	385	166	0.73
61.1	0.99	22.1	7.08	1.91	28.2	0.11	385	176	0.69
73.3	0.99	22.0	7.04	1.91	28.1	0.11	385	178	0.69
1.2	1.49	12.4	3.75	1.47	21.0	0.10	402	312	0.43
2.5	1.48	12.5	3.78	1.47	21.1	0.10	402	302	0.49
3.7	1.48	12.7	3.84	1.48	21.2	0.10	402	286	0.57
4.9	1.49	13.0	3.92	1.50	21.4	0.10	402	283	0.59
6.1	1.48	13.5	4.06	1.52	21.8	0.10	402	276	0.62
12.2	1.49	14.1	4.21	1.54	22.2	0.10	402	263	0.69
24.4	1.48	17.2	5.19	1.68	24.5	0.11	402	254	0.69
36.7	1.48	16.2	4.87	1.63	23.8	0.11	402	242	0.78
48.9	1.49	15.5	4.64	1.60	23.2	0.11	402	239	0.81
61.1	1.48	14.8	4.44	1.57	22.7	0.11	402	238	0.83
73.3	1.49	14.6	4.36	1.56	22.5	0.11	402	234	0.87
24.4	1.98	11.1	3.43	1.42	20.1	0.10	402	293	0.75
GTC350Y	SRP1201			Height	2.79 m				
6.1	0.59	27.6	9.97	2.21	32.9	0.11	395	107	0.67
12.2	0.59	27.7	10.04	2.22	33.0	0.11	395	99	0.72
24.4	0.59	27.8	10.06	2.23	33.0	0.10	395	93	0.76
36.7	0.59	28.9	10.67	2.29	33.8	0.09	395	88	0.80
48.9	0.59	26.2	9.05	2.15	31.4	0.08	395	107	0.80
61.1	0.59	26.5	9.16	2.16	31.6	0.08	395	106	0.81
73.3	0.59	26.9	9.39	2.19	31.9	0.08	395	97	0.87
6.1	0.99	28.3	10.41	2.26	33.5	0.11	395	183	0.66
12.2	0.99	28.4	10.41	2.26	33.5	0.10	395	171	0.73
24.5	0.99	28.0	10.20	2.24	33.2	0.10	395	162	0.78
36.7	0.99	28.3	10.37	2.26	33.4	0.10	395	159	0.81
48.9	0.99	28.4	10.42	2.27	33.5	0.10	395	156	0.83
61.1	0.99	24.7	8.30	2.06	30.3	0.09	395	154	0.90
6.1	1.49	34.0	14.65	2.61	38.8	0.12	395	213	0.67
12.2	1.48	33.9	14.52	2.60	38.6	0.11	395	203	0.72
24.5	1.49	29.3	10.94	2.32	34.2	0.09	395	213	0.84
36.7	1.49	29.1	10.81	2.31	34.0	0.09	395	206	0.88
48.9	1.48	27.2	9.74	2.20	32.6	0.11	395	195	0.89
24.4	1.65	32.7	13.47	2.52	37.4	0.10	388	216	0.77
MP250Y	SRP1201			Height	2.92 m				
6.1	0.59	17.5	5.27	1.69	24.6	0.10	410	174	0.74
12.2	0.59	17.5	5.26	1.69	24.6	0.10	410	168	0.78
24.5	0.59	17.3	5.21	1.68	24.5	0.10	410	153	0.87
36.7	0.59	17.2	5.16	1.68	24.4	0.10	410	145	0.92

L (m^3/m^2*h)	u_G (m/s)	T_{corr} (℃)	$k_{OH-}*10^{-3}$ (m^3/kmol*s)	$D_{CO2}*10^9$ (m^2/s)	$H_{CO2}*10^{-5}$ (m^3*Pa/kmol)	[OH-] kmol/m^3	CO_2In ppm	CO_2 out ppm	a_f
48.9	0.59	17.1	5.13	1.68	24.3	0.10	410	140	0.95
61.1	0.59	17.2	5.16	1.68	24.4	0.10	410	134	0.99
73.3	0.59	17.4	5.23	1.69	24.5	0.10	410	130	1.03
6.1	0.99	15.0	4.47	1.57	22.8	0.11	392	228	0.81
12.2	0.99	14.6	4.36	1.56	22.5	0.10	392	222	0.85
24.4	0.99	14.1	4.21	1.54	22.2	0.10	392	209	0.96
36.7	0.99	13.9	4.15	1.53	22.0	0.10	392	203	1.01
48.9	0.99	13.6	4.08	1.52	21.8	0.10	392	202	1.04
61.1	0.99	13.5	4.05	1.51	21.7	0.10	392	194	1.11
73.3	0.99	13.5	4.04	1.51	21.7	0.10	392	185	1.18
6.1	1.48	14.0	4.20	1.53	22.2	0.11	382	266	0.80
12.2	1.49	13.6	4.09	1.51	21.9	0.11	382	257	0.89
24.4	1.49	12.7	3.86	1.48	21.3	0.11	382	250	0.97
36.7	1.48	12.4	3.77	1.46	21.0	0.11	382	246	1.02
48.9	1.49	12.2	3.71	1.46	20.9	0.11	382	242	1.07
61.1	1.49	12.1	3.69	1.45	20.8	0.11	382	238	1.12
36.7	1.98	12.4	3.76	1.47	21.0	0.10	382	273	1.07
36.7	2.31	25.0	8.48	2.11	31.2	0.10	382	282	1.05

MP250X	SRP1104			Height	2.91 m				
6.2	0.59	15.6	4.68	1.60	23.3	0.11	415	170	0.77
12.2	0.59	15.5	4.66	1.60	23.3	0.11	415	166	0.79
24.5	0.59	15.2	4.54	1.58	23.0	0.11	415	155	0.86
36.7	0.59	15.0	4.51	1.58	22.9	0.11	415	147	0.91
48.9	0.59	15.0	4.49	1.58	22.9	0.11	415	148	0.91
61.1	0.59	15.0	4.49	1.58	22.9	0.11	415	147	0.92
73.3	0.59	15.1	4.51	1.58	22.9	0.11	415	139	0.98
6.1	0.99	15.1	4.52	1.58	22.9	0.11	406	254	0.69
12.2	0.99	15.0	4.50	1.58	22.9	0.11	406	239	0.79
24.5	0.99	14.4	4.32	1.55	22.5	0.11	406	228	0.87
36.7	0.99	14.1	4.21	1.54	22.2	0.10	406	221	0.92
48.9	0.99	13.8	4.15	1.53	22.0	0.10	406	215	0.98
61.1	0.99	13.7	4.11	1.52	21.9	0.10	406	210	1.02
73.3	0.99	13.6	4.07	1.52	21.8	0.10	406	204	1.07
5.8	1.48	17.2	5.19	1.67	24.5	0.11	403	278	0.78
12.2	1.49	16.9	5.11	1.66	24.3	0.11	403	271	0.84
24.5	1.49	16.3	4.91	1.63	23.8	0.11	403	264	0.91
36.7	1.49	16.0	4.79	1.62	23.6	0.11	403	259	0.96
48.9	1.48	15.9	4.75	1.61	23.5	0.11	403	253	1.02
61.1	1.49	15.7	4.69	1.61	23.3	0.11	403	247	1.08
73.3	1.48	15.6	4.66	1.60	23.3	0.11	403	238	1.16
36.7	1.98	15.3	4.56	1.59	23.0	0.10	403	289	1.00

L (m^3/m^2*h)	u_G (m/s)	T_{corr} (℃)	$k_{OH-}*10^{-3}$ (m^3/kmol*s)	$D_{CO2}*10^9$ (m^2/s)	$H_{CO2}*10^{-5}$ (m^3*Pa/kmol)	[OH-] kmol/m^3	CO_2In ppm	CO_2 out ppm	a_f
36.7	2.31	15.0	4.48	1.58	22.8	0.10	403	303	1.01
RSR#0.3	SRP1202			Height	2.94 m				
6.1	0.59	29.2	11.00	2.31	34.3	0.11	404	138	0.58
12.2	0.59	28.5	10.54	2.26	33.7	0.11	404	119	0.67
24.4	0.59	28.1	10.27	2.24	33.3	0.11	404	106	0.74
36.7	0.59	27.7	10.00	2.22	32.9	0.10	404	101	0.77
48.9	0.59	27.2	9.71	2.19	32.5	0.10	404	100	0.80
61.1	0.59	27.0	9.57	2.18	32.2	0.10	404	101	0.80
73.4	0.59	26.6	9.34	2.16	31.9	0.10	404	102	0.80
6.1	0.99	28.0	10.27	2.23	33.3	0.11	401	203	0.61
12.2	0.99	27.6	10.00	2.21	32.9	0.11	401	187	0.69
24.5	0.99	27.3	9.82	2.19	32.7	0.11	401	175	0.76
36.7	0.99	26.9	9.56	2.17	32.3	0.11	401	169	0.81
48.9	0.99	26.5	9.30	2.15	31.9	0.11	401	167	0.83
61.2	0.99	26.6	9.35	2.16	31.9	0.10	401	162	0.86
6.1	1.48	29.4	11.11	2.32	34.4	0.10	393	244	0.65
12.2	1.49	28.8	10.67	2.28	33.8	0.10	393	233	0.73
24.5	1.49	28.2	10.32	2.25	33.3	0.10	393	223	0.80
12.2	1.65	23.2	7.57	1.98	29.1	0.10	393	253	0.76
GTC500Y	SRP1307			Height	3.06 m				
6.1	0.59	33.8	14.35	2.60	38.4	0.11	411	61	0.56
12.2	0.59	33.7	14.27	2.59	38.3	0.10	411	53	0.60
24.4	0.59	33.6	14.17	2.58	38.2	0.10	411	47	0.64
36.7	0.59	33.6	14.22	2.59	38.2	0.10	411	42	0.68
48.9	0.59	33.7	14.29	2.60	38.3	0.10	411	40	0.70
61.1	0.59	33.7	14.22	2.59	38.2	0.10	411	41	0.69
73.4	0.59	33.0	13.65	2.55	37.6	0.09	411	48	0.67
6.1	0.99	28.9	10.82	2.28	34.1	0.12	409	144	0.54
12.2	0.99	28.8	10.73	2.27	34.0	0.12	409	134	0.58
24.5	0.99	28.8	10.72	2.28	33.9	0.11	409	121	0.64
36.7	0.99	28.9	10.81	2.28	34.1	0.11	409	115	0.66
48.9	0.99	29.1	10.93	2.30	34.2	0.11	409	110	0.69
6.1	1.49	29.7	11.34	2.34	34.7	0.11	409	209	0.53
12.2	1.49	29.7	11.28	2.33	34.7	0.11	409	198	0.58
MP125Y	SRP1316			Height	2.92 m				
12.2	0.59	22.8	7.44	1.95	28.9	0.11	412	223	0.93
24.4	0.59	22.9	7.47	1.95	28.9	0.11	412	210	1.03
36.9	0.59	23.0	7.50	1.96	29.0	0.11	412	202	1.08
48.9	0.59	23.0	7.51	1.96	29.0	0.11	412	195	1.14

L (m^3/m^2*h)	u_G (m/s)	T_{corr} (℃)	$k_{OH-}*10^{-3}$ (m^3/kmol*s)	$D_{CO2}*10^9$ (m^2/s)	$H_{CO2}*10^{-5}$ (m^3*Pa/kmol)	[OH-] kmol/m^3	CO_2In ppm	CO_2 out ppm	a_f
61.6	0.60	23.1	7.53	1.96	29.0	0.11	412	188	1.20
73.3	0.59	23.4	7.67	1.98	29.3	0.11	412	181	1.25
12.2	0.99	27.2	9.73	2.19	32.5	0.11	392	261	0.94
24.5	0.99	27.0	9.59	2.17	32.3	0.11	392	252	1.03
36.7	0.99	27.2	9.73	2.19	32.5	0.11	392	246	1.08
48.9	0.99	27.2	9.70	2.19	32.5	0.11	392	241	1.14
60.9	0.99	27.2	9.69	2.19	32.5	0.11	392	236	1.19
73.0	0.99	27.0	9.59	2.18	32.3	0.11	392	230	1.26
12.2	1.49	26.3	9.19	2.13	31.7	0.11	397	302	0.97
24.5	1.48	26.3	9.20	2.14	31.7	0.11	397	294	1.07
36.7	1.48	26.7	9.42	2.16	32.0	0.11	397	289	1.13
48.9	1.48	26.9	9.52	2.17	32.2	0.11	397	285	1.17
61.1	1.49	26.9	9.52	2.17	32.2	0.11	397	280	1.24
73.3	1.49	26.9	9.54	2.17	32.2	0.10	397	276	1.30
36.7	1.98	27.0	9.57	2.18	32.3	0.10	397	311	1.17
36.7	2.47	27.2	9.72	2.19	32.5	0.10	394	323	1.20

RSP200X	SRP1306			Height	3.05 m				
6.1	0.59	22.5	7.30	1.93	28.6	0.11	410	138	0.98
12.2	0.59	22.5	7.27	1.93	28.6	0.11	409	130	1.04
24.5	0.59	22.4	7.25	1.93	28.5	0.11	409	120	1.12
36.7	0.59	22.5	7.26	1.93	28.6	0.11	408	118	1.14
48.9	0.59	22.5	7.29	1.94	28.6	0.11	407	121	1.12
60.3	0.59	22.9	7.46	1.95	28.9	0.11	406	120	1.13
73.3	0.59	23.0	7.48	1.96	28.9	0.10	405	124	1.10
6.1	0.99	22.5	7.29	1.93	28.6	0.11	404	210	1.01
12.2	0.99	21.8	6.95	1.90	28.0	0.10	404	208	1.05
24.5	0.99	21.1	6.66	1.87	27.4	0.10	404	197	1.16
36.7	0.99	20.7	6.45	1.84	27.0	0.10	404	194	1.20
48.9	0.99	20.1	6.24	1.82	26.6	0.10	404	196	1.22
61.1	0.99	19.8	6.12	1.80	26.4	0.10	403	196	1.24
73.4	1.00	19.6	6.00	1.79	26.1	0.09	403	190	1.34
6.1	1.48	15.7	4.72	1.60	23.4	0.11	413	275	1.05
12.2	1.49	15.3	4.57	1.58	23.1	0.11	413	273	1.09
24.4	1.49	14.9	4.46	1.57	22.8	0.11	413	265	1.18
36.7	1.48	14.8	4.43	1.57	22.7	0.11	413	260	1.23
48.9	1.48	14.8	4.44	1.57	22.7	0.11	413	256	1.29
60.9	1.49	15.1	4.50	1.58	22.9	0.10	413	252	1.34
73.3	1.49	15.3	4.56	1.60	23.0	0.10	413	246	1.41
36.7	1.98	15.5	4.60	1.61	23.1	0.10	413	296	1.22
36.7	2.47	15.9	4.74	1.63	23.4	0.10	411	312	1.26

Table D.2. Detailed Liquid film mass transfer coefficient data (k_L).

L (m^3/m^2*h)	u_G (m/s)	Water in (℃)	Tol in (ppm)	Tol out (ppm)	NTU	HTU (m)	a_e (m^2/m^3)	k_L*10^5 (m/s)
MP2X	SRP1006		Height	1.77 m				
6.1	1.48	23.7	36.6	0.5	4.21	0.42	159	2.49
12.2	1.49	24.0	84.3	2.3	3.61	0.49	171	3.99
24.4	1.48	23.7	242.9	17.1	2.65	0.67	193	5.18
24.5	0.99	24.5	184.0	14.8	2.52	0.70	192	4.97
24.4	0.59	25.4	212.5	16.1	2.58	0.69	191	5.09
36.6	1.48	23.2	120.1	15.0	2.08	0.85	200	5.88
48.9	1.48	23.0	131.9	19.7	1.90	0.93	211	6.82
61.1	1.48	24.2	117.3	19.0	1.82	0.98	217	7.91
73.4	1.48	24.4	105.3	14.8	1.96	0.90	220	10.12
RSP250Y	SRP1103		Height	1.62 m				
6.2	0.99	28.8	21.1	0.2	4.84	0.33	216	2.35
12.2	0.99	28.3	91.9	0.3	5.77	0.28	238	5.03
24.3	0.59	22.9	64.4	0.9	4.32	0.37	253	7.03
24.5	0.99	20.0	79.1	1.4	4.00	0.40	259	6.41
24.4	1.48	18.3	82.9	1.2	4.23	0.38	275	6.37
36.6	0.99	17.2	100.3	4.0	3.23	0.50	271	7.39
48.9	0.99	22.9	138.9	5.4	3.25	0.50	272	9.92
60.6	0.99	25.2	131.3	5.6	3.16	0.51	265	12.22
64.2	0.99	27.5	128.5	4.3	3.40	0.48	293	12.64
73.3	0.99	28.8	110.7	4.2	3.28	0.49	293	13.90
36.7	0.99	29.0	113.5	1.9	4.07	0.40	271	9.33
12.3	0.99	27.8	94.1	0.4	5.36	0.30	238	4.68
RSR#0.7	SRP1102		Height	1.75 m				
6.1	0.99	24.8	100.5	0.3	5.90	0.30	168	3.39
12.2	0.99	24.8	94.3	0.8	4.75	0.37	186	4.90
24.5	0.99	24.9	353.0	10.3	3.54	0.49	208	6.52
36.7	0.99	24.2	144.0	7.2	2.99	0.58	220	7.85
48.9	0.99	24.3	151.5	10.2	2.70	0.65	229	9.05
61.1	0.99	24.4	134.9	10.6	2.55	0.69	241	10.17
73.3	0.99	24.8	103.0	9.3	2.41	0.73	250	11.08
MP250X	SRP1317		Height	1.78 m				
6.1	0.99	15.6	176.9	27.1	1.87	0.95	174	1.02
12.2	0.99	15.6	159.5	24.9	1.86	0.96	197	1.77
24.4	0.99	20.6	133.3	29.9	1.49	1.19	217	2.59
36.7	0.99	15.6	158.9	36.6	1.47	1.21	231	3.59
48.9	0.99	15.8	222.2	44.9	1.60	1.11	245	4.92
61.1	0.99	16.0	111.3	27.0	1.42	1.26	254	5.25

L (m^3/m^2*h)	u_G (m/s)	Water in (℃)	Tol in (ppm)	Tol out (ppm)	NTU	HTU (m)	a_e (m^2/m^3)	k_L*10^5 (m/s)
73.3	0.99	20.5	180.1	39.7	1.51	1.18	269	6.37
MP250Y	SRP1318			Height	1.87 m			
6.1	0.99	11.3	102.9	1.3	4.34	0.43	202	1.92
12.2	0.99	11.5	88.1	3.3	3.28	0.57	214	2.75
24.4	0.99	11.8	78.0	6.0	2.57	0.73	241	3.81
36.7	0.99	13.8	160.9	15.2	2.36	0.79	254	4.99
48.9	0.99	12.4	207.9	29.0	1.97	0.95	259	5.45
61.1	0.99	11.1	127.7	20.3	1.84	1.02	277	5.94
73.3	0.99	11.0	207.5	36.6	1.73	1.08	296	6.30
GTC500Y	SRP1307			Height	1.84 m			
6.1	0.99	27.3	39.6	0.1	6.04	0.30	269	2.04
12.2	0.99	28.1	98.6	0.2	6.22	0.30	289	3.92
12.2	1.48	27.4	91.6	0.2	6.25	0.29	301	3.78
24.4	0.99	25.4	311.8	1.9	5.11	0.36	318	5.85
24.4	0.59	25.3	130.5	1.2	4.69	0.39	322	5.30
36.6	0.99	25.3	123.8	1.5	4.41	0.42	332	7.24
48.8	0.99	25.5	124.9	2.3	4.00	0.46	345	8.43
61.1	0.59	28.3	141.0	3.3	3.75	0.49	347	9.82
73.4	0.59	28.8	112.6	3.8	3.38	0.54	333	11.10
MP125Y	SRP1316			Height	1.87 m			
12.2	0.99	18.4	149.9	3.3	3.81	0.49	118	5.77
24.5	0.99	18.5	121.6	4.8	3.24	0.58	128	9.03
36.6	0.99	20.5	158.5	9.1	2.86	0.66	136	11.31
48.9	0.99	19.8	234.2	20.5	2.44	0.77	142	12.29
36.7	0.59	20.5	187.1	9.3	3.00	0.62	135	11.92
36.7	1.49	20.1	159.0	8.5	2.93	0.64	141	11.16
61.1	0.99	20.0	180.8	21.3	2.14	0.88	149	12.84
73.3	0.99	19.5	143.4	19.4	2.00	0.94	157	13.66
RSP200X	SRP1306			Height	1.88 m			
36.6	0.59	21.6	109.8	5.6	2.97	0.63	229	2.12
36.7	1.48	21.3	169.1	4.9	3.55	0.53	247	2.35
36.7	0.99	21.1	186.8	7.3	3.24	0.58	241	2.19
48.9	0.99	17.4	200.4	12.4	2.78	0.68	244	2.48
61.1	0.99	21.2	312.4	22.4	2.64	0.71	247	2.90
73.3	0.99	17.9	202.4	20.1	2.31	0.81	268	2.81
24.4	0.99	17.0	51.9	1.8	3.34	0.56	232	1.56
12.2	0.99	18.1	116.1	2.6	3.81	0.49	211	0.98
6.1	0.99	21.3	188.8	0.5	5.93	0.32	202	0.80

L (m^3/m^2*h)	u_G (m/s)	Water in (℃)	Tol in (ppm)	Tol out (ppm)	NTU	HTU (m)	a_e (m^2/m^3)	k_L*10^5 (m/s)
A350Y	SRP1304		Height	3.04 m				
1.2	0.99	15.1	187.6	1.7	4.68	0.65	205	0.25
2.4	0.99	14.6	183.8	1.5	4.80	0.63	233	0.45
3.7	0.99	14.3	193.9	1.7	4.75	0.64	251	0.62
4.9	0.99	14.0	212.8	1.6	4.88	0.62	261	0.82
6.1	0.99	13.8	262.0	1.4	5.20	0.58	264	1.09
12.2	0.99	13.6	298.5	2.0	4.99	0.61	270	2.04
24.4	0.99	14.4	282.4	2.5	4.73	0.64	276	3.78
24.4	0.59	15.0	347.7	1.6	5.37	0.57	272	4.36
24.4	1.49	13.6	305.7	0.8	5.90	0.51	284	4.58
36.7	0.99	13.4	256.3	3.2	4.39	0.69	281	5.19
48.8	0.99	13.6	331.3	3.9	4.43	0.68	283	6.91
B350X	SRP1303		Height	2.87 m				
1.2	0.99	8.0	181.1	1.3	4.95	0.58	139	0.40
2.4	0.99	7.8	251.5	1.2	5.32	0.54	175	0.71
3.7	0.99	7.9	217.4	2.0	4.71	0.61	190	0.87
4.9	0.99	8.2	243.3	1.8	4.93	0.58	198	1.16
6.1	0.99	8.8	479.5	1.9	5.56	0.52	210	1.54
12.2	0.99	15.5	170.9	0.9	5.22	0.55	227	2.69
24.4	0.99	16.0	298.8	1.6	5.26	0.54	235	5.24
24.4	0.60	18.3	376.9	1.3	5.69	0.50	224	5.95
24.4	1.48	16.9	295.1	0.9	5.77	0.50	241	5.60
36.7	0.99	15.6	190.2	2.8	4.23	0.68	249	5.95
48.9	0.99	15.4	251.1	5.5	3.82	0.75	257	6.96
61.1	0.99	15.4	197.6	6.8	3.37	0.85	242	8.16
73.3	0.99	15.6	160.5	6.0	3.28	0.87	240	9.60
GTC350Y	SRP1201		Height	2.79 m				
5.8	0.99	15.2	194.2	2.0	4.59	0.19	231	1.13
12.2	0.99	15.3	159.3	0.5	5.76	0.15	256	2.71
24.5	0.99	15.4	162.5	1.6	4.63	0.18	272	4.09
36.7	0.99	17.5	265.8	4.2	4.14	0.21	282	5.28
48.9	0.99	16.6	371.8	10.3	3.59	0.24	290	5.94
61.1	0.99	15.9	198.6	7.9	3.23	0.26	315	6.15
36.7	0.59	19.5	404.1	4.6	4.48	0.19	281	5.73
36.7	1.48	18.3	272.0	2.7	4.62	0.18	307	5.42
12.2	1.49	15.3	169.3	0.5	5.82	0.15	256	2.74
24.5	0.59	15.4	152.5	1.6	4.57	0.19	272	4.03
RSR#0.3	SRP1202		Height	2.94 m				
6.1	0.99	17.8	227.9	0.3	6.70	0.44	187	2.04

L (m^3/m^2*h)	u_G (m/s)	Water in (℃)	Tol in (ppm)	Tol out (ppm)	NTU	HTU (m)	a_e (m^2/m^3)	k_L*10^5 (m/s)
12.2	0.99	17.7	248.3	0.3	6.70	0.44	213	3.60
24.4	0.99	19.9	299.8	0.4	6.69	0.44	234	6.52
36.7	0.99	19.2	139.0	0.6	5.45	0.54	248	7.52
48.9	0.99	18.7	267.2	1.7	5.07	0.58	255	9.06
60.9	0.99	18.2	371.5	4.6	4.38	0.67	265	9.43
24.4	0.60	22.7	214.0	0.4	6.31	0.47	227	6.35
24.4	1.48	20.8	190.2	0.3	6.44	0.46	247	5.96
36.6	0.99	19.6	406.2	2.9	4.95	0.59	248	6.82
48.9	0.99	18.8	264.9	1.7	5.04	0.58	255	9.00
GTC350Z	SRP1101		Height	2.79 m				
6.3	0.99	26.9	103.6	3.1	3.51	0.80	262	0.83
12.2	0.99	26.7	78.7	3.5	3.13	0.89	276	1.36
24.5	0.99	26.4	135.0	5.1	3.27	0.85	303	2.59
48.9	0.99	29.3	233.2	8.3	3.34	0.84	328	4.89
61.1	0.99	29.4	194.1	8.0	3.19	0.88	334	5.73
73.3	0.99	27.4	203.1	11.7	2.86	0.98	320	6.42
36.6	0.59	27.0	254.8	9.1	3.33	0.84	284	4.22
36.7	1.49	26.3	258.7	8.9	3.38	0.83	351	3.46

Table D.3. Detailed Gas film mass transfer coefficient data (k_G).

L (m^3/m^2*h)	u_G (m/s)	Air in (℃)	SO_2 in (ppm)	SO_2 out (ppb)	NTU	HTU*10 (m)	a_e (m^2/m^3)	k_G*10^2 (m/s)
MP2X	SRP1308		Height	0.448 m				
24.4	0.59	35.4	35.5	691	2.47	1.92	191	1.62
24.5	0.99	36.6	33.6	1332	1.86	2.54	192	2.03
24.5	1.48	38.5	28.0	1822	1.54	3.07	193	2.50
36.7	1.98	42.3	24.0	1315	1.38	3.43	200	2.88
36.7	2.48	44.7	22.5	1665	1.22	3.89	200	3.18
36.7	0.99	40.7	32.0	931	2.01	2.35	202	2.08
RSP250Y	SRP1310		Height	0.232 m				
48.9	0.59	38.5	71.3	850	2.61	0.89	251	2.67
48.9	0.99	39.0	65.4	1704	2.00	1.16	272	3.15
48.9	1.48	39.6	63.6	2180	1.91	1.22	290	4.22
48.9	1.98	41.2	66.1	2780	1.73	1.34	305	4.86
48.9	2.48	43.8	68.9	3720	1.70	1.36	305	5.95
RSR#0.7	SRP1309		Height	0.235 m				
24.5	0.59	38.3	58.0	1320	2.18	1.08	197	2.80
24.4	0.99	38.6	48.8	2299	1.46	1.61	208	2.94

L (m^3/m^2*h)	u_G (m/s)	Air in (℃)	SO_2 in (ppm)	SO_2 out (ppb)	NTU	HTU*10 (m)	a_e (m^2/m^3)	k_G*10^2 (m/s)
24.5	1.48	35.2	28.1	1672	1.22	1.92	214	3.61
24.5	1.98	42.9	45.8	3370	1.01	2.33	214	3.98
24.4	2.31	44.7	33.8	2370	1.06	2.22	214	4.87
36.7	0.99	31.7	60.2	1455	2.12	1.11	220	4.07
MP250X	SRP1104			Height	0.892 m			
36.7	0.59	25.4	65.8	26	6.46	1.38	227	1.89
36.7	0.99	26.0	57.6	69	5.36	1.66	231	2.57
36.7	1.49	26.7	51.1	172	4.33	2.06	241	2.99
36.6	1.98	27.9	53.0	344	3.68	2.43	250	3.27
36.7	2.48	28.9	53.0	538	3.23	2.76	252	3.55
48.9	1.48	26.1	50.7	177	4.29	2.08	254	2.81
MP250Y	SRP1201			Height	0.841 m			
36.7	0.59	21.7	62.9	23	6.30	1.34	229	1.94
36.7	0.99	21.7	58.6	31	5.92	1.42	254	2.74
36.7	1.48	22.8	51.3	60	5.12	1.64	256	3.53
36.7	1.98	23.4	52.4	115	4.49	1.87	268	3.95
36.7	2.31	24.3	55.1	143	4.32	1.95	262	4.53
48.9	1.49	13.3	51.4	56	5.19	1.62	268	3.42
GTC500Y	SRP1307			Height	0.21 m			
24.5	0.59	35.4	66.5	658	3.40	0.62	322	2.99
24.4	1.48	31.3	37.8	476	2.91	0.72	318	6.50
36.7	0.99	36.6	58.7	746	3.07	0.68	332	4.36
36.7	0.60	36.4	62.6	398	3.76	0.56	340	3.15
36.7	1.24	37.9	36.7	245	2.93	0.72	332	5.21
36.7	0.79	37.1	44.3	309	3.51	0.60	336	3.95
MP125Y	SRP1316			Height	1.87 m			
36.7	0.59	28.6	56.4	2072	1.75	2.39	135	1.84
36.7	0.99	28.2	21.8	1435	1.62	2.59	136	2.82
36.7	1.49	26.0	21.2	1963	1.28	3.27	141	3.22
36.7	1.98	27.6	18.1	1853	1.18	3.55	146	3.82
36.7	2.48	30.4	15.9	1636	1.17	3.57	149	4.64
RSP200X	SRP1306			Height	0.428 m			
36.7	0.59	31.7	70.0	2260	2.32	1.01	229	2.56
36.7	0.99	32.0	69.0	3980	1.88	1.25	241	3.29
36.7	1.48	33.4	69.3	4285	1.75	1.34	247	4.47
36.7	1.98	34.1	69.4	5740	1.53	1.53	243	5.31

L (m^3/m^2*h)	u_G (m/s)	Air in (℃)	SO_2 in (ppm)	SO_2 out (ppb)	NTU	HTU*10 (m)	a_e (m^2/m^3)	k_G*10^2 (m/s)
36.7	2.48	35.2	69.5	7880	1.17	2.00	253	4.90
A350Y	SRP1304			Height	0.406 m			
24.4	0.60	28.2	74.1	133	4.94	0.82	272	2.66
24.4	0.99	29.7	73.4	654	3.54	1.15	276	3.12
24.5	1.49	28.9	59.1	801	3.26	1.25	284	4.21
24.5	1.82	30.1	48.6	903	2.90	1.40	297	4.37
B350X	SRP1303			Height	2.87 m			
24.5	0.59	13.2	23.2	175	3.70	1.17	224	2.28
24.4	0.99	13.2	21.5	413	2.78	1.56	235	2.71
24.5	1.49	13.2	16.1	231	3.06	1.41	241	4.37
24.4	1.98	13.3	15.3	274	2.84	1.52	262	4.98
GTC350Y	SRP1201			Height	0.645 m			
24.4	0.59	34.4	77.4	14	7.11	0.91	265	2.46
24.5	0.99	36.4	79.6	22	6.69	0.96	272	3.77
24.4	1.49	37.3	79.0	73	5.49	1.17	294	4.30
24.4	1.65	37.1	62.5	83	5.12	1.26	270	4.85
12.2	0.99	35.6	80.1	57	5.75	1.12	256	3.45
36.7	0.99	35.9	76.4	31	6.32	1.02	282	3.43
24.4	0.99	36.4	79.0	39	6.12	1.05	272	3.45
RSR#0.3	SRP1202			Height	0.428 m			
12.2	0.60	14.1	99.9	46	6.88	1.03	205	2.83
12.2	1.00	14.3	99.3	68	6.49	1.10	213	4.31
12.2	1.49	14.2	67.0	52	6.37	1.12	224	5.94
12.2	1.65	14.2	59.7	51	6.26	1.14	234	6.22
GTC350Z	SRP1101			Height	0.428 m			
36.7	0.59	21.2	55.6	8	7.34	1.28	284	1.64
36.7	0.99	22.2	57.0	12	6.98	1.34	325	2.27
36.7	1.48	23.4	51.1	18	6.44	1.46	351	2.90
36.7	1.98	24.8	53.1	30	5.98	1.57	368	3.43
48.9	0.59	23.8	61.4	9	7.37	1.27	298	1.57

References

Akita K, Yoshida F. "Gas holdup and volumetric mass transfer coefficient in bubble columns: effects of liquid properties." *Industrial & Engineering Chemistry Process Design and Development.* 1973;12(1):76-80.

Billet R, Mackowiak J. "Recent progress in distillation design." *5th International Congress in Scandinavia on Chemical Engineering.* Copenhagen, Denmark. 1980.

Billet R, Schultes M. "Predicting mass transfer in packed column." *Chem. Eng. Technol.* 1996;16: 1-9.

Bird RB, Stewart WE, Lightfoot EN. *Transport Phenomena.* New York, John Wiley & Sons, Inc.: 2002.

Bravo JL, et al. "Mass Transfer in Gauze Packings." *Hydrocarbon Processing.* 1985; 91-95.

Bravo JL, Rocha JA, Fair JR. "A comprehensive model for the performance of columns containing structured packings." *ICHEME Symp. Ser.* 1992;128: 489-507.

Brunazzi E, Paglianti A. "Liquid-Film Mass-Transfer Coefficient in a Column Equipped with Structured Packings." *Ind. Eng. Chem. Res.* 1997; 36: 3792-3799.

Bureau of Labor Statistics. CPI Detailed Report (complete text and tables). February 2014.

Danckwerts PV., Kennedy AM., Roberts D. "Kinetics of CO2 absorption in alkaline solutions—II: Absorption in a packed column and tests of surface-renewal models." Chem. Eng. Sci. 1963:18:63–72.

Danckwerts PV. Gas-Liquid Reactions. McGraw-Hill Book Company, New York. 1970.

Danckwerts PV., Sharma MM. "Absorption of carbon dioxide into solutions of alkalis and amines." Chem Engr. 1966; 202: 244-280.

Dugas RE. *Carbon Dioxide Absorption, Desorption and Diffusion in Aqueous Piperazine and Monoethanolamine.* The University of Texas at Austin. Ph.D. Dissertation. 2009.

EIA. *Electric Power Monthly Report.* U.S. Energy Information Administration. 2013.

El-Behlil MA, El-Gezawi SM, Adma SA. "Volatile Organic Chemicals Removal from Contaminated Water using Air Stripping Low Profile Sieve Tray Towers." *Sixteenth International Water Technology Conference*, Istanbul, Turkey, 2012.

Fujita S, Sakuma S. "Wetted area of Raschig rings in packed columns." *Chem. Eng. (Japan).* 1954;18: 64-67.

Fair JR, Seibert AF, Behrens M, Saraber PP, Olujic Z. Structured Packing Performance-Experimental Evaluation of Two Predictive Models. *Ind. Eng. Chem. Res.* 2000;39(6):1788-1796.

Frailie P. "Process Economics of Amine Scrubbing Systems." *PSTC Fall Meeting*, Austin. 2013.

Freeman SA et al. "Density and viscosity of aqueous (piperazine + carbon dioxide) solutions." *Journal of Chemical and Engineering Data.* 2011;56(3): 574-581.

Henriques de Brito, et al. "Effective Mass-Transfer Area in a Pilot Plant Column Equipped with Structured Packings and with Ceramic Rings." *Ind. Eng. Chem. Res.* 1994;33(3):647-656.

Higbie, R. "The rate of absorption of a pure gas into a still liquid during short periods of exposure." *Trans. Am. Inst. Chem. Engrs.* 1935;31:365-383.

Johnstone HF, and Pigford RL. "Distillation in wetted-wall column." *Trans. Am. Inst. Chem. Engrs.* 1942;38:25-50.

JPI. *Air Stripping of VOCs from Water*. Houston, Texas, Jaeger Products Inc (JPI). 1996.

Kister Henry Z. Distillation design. McGraw-Hill, Inc. 1992

Kunesh JG, et al. "Sieve Tray Performances for Steam Stripping Toluene from Water in a 4-ft Diameter Column." *Ind. Eng. Chem. Res.* 1996; 35: 2660-2671.

Lin YJ, Madan T, Rochelle GT. "Regeneration with Rich Bypass of Aqueous Piperazine and Monoethanolamine for CO_2 Capture." *Ind. Eng. Chem. Res.* 2014; 53: 4067−4074.

Linek V, Moucha T, Rejl FJ. "Hydraulic and mass transfer characteristics of packings for absorption and distillation columns. Rauschert-Metall-Sattel-Rings." Trans IChemE. 2001;79: 725-732.

Linek V, Petericek P. "Effective interfacial area and liquid side mass transfer coefficients in aborption columns packed with hydrophilised and untreated plastic packings." *Chem Eng Res Des.* 1984;62:13-21.

Mangers RJ, Ponter AB. "Effect of viscosity on liquid film resistance to mass transfer in a packed column." *Ind. Eng. Chem. Process Des. Dev.* 1980;19: 530-537.

McCabe WL, Smith JC, Harriott P. Unit Operations of Chemical Engineering, Fifth Edition. McGraw-Hill, Inc. 1993.

Mehta VD, Sharma MM. "Effect of diffusivity on gas-side mass transfer coefficient." *Chemical Engineering Science.* 1966;21: 361-365.

Mouch T, Linek V, Prokopová E. "Effect of packing geometrical details influence of free tips on volumetric mass transfer coefficients of Intalox saddles." *Chem. Eng. Res. Des.* 2005;83:88-92.

Olujic Z, Kamerbeek AB, de Graauw J. "A Corrugation Geometry Based Model for Efficiency of Structured Distillation Packing." *Chem. Eng. Process.* 1999;38: 683-695.

Olujic Z, Seibert AF, Fair JR. Influence of corrugation geometry on the performance of structured packings: an experimental study. *Chem. Eng. Process* 2000;39(4):335-342.

Onda K, Sada E. "Liquid-side mass transfer coefficient packed towers." *AIChE Journal.* 1959;5:235-239.

Onda K, Takeuchi H, Okumoto Y. "Mass transfer coefficients between gas and liquid phases in packed columns." *Journal of Chemical Engineering of Japan.* 1968;1(1): 56-62.

Peters MS, Timmerhaus KD. *Plant Design and Economics for Chemical Engineers.* New York, McGraw-Hill, Inc.: 1991.

Perry RH, Green DW. Perry's Chemical Engineers' Hand Book, Eighth Edition. McGraw-Hill, Inc. 2008.

Pigford RL. *Counter-Diffusion in a Wetted Wall Column.* The University of Illinois at Urbana. Ph.D. Dissertation. 1941.

Razi N et al. "Cost and energy sensitivity analysis of absorber design in CO2 capture with MEA." *International Journal of Greenhouse Gas Control.* 2013;19: 331-339.

Rochelle GT, Fisher KS, Beitler C, Rueter C, Searcy K, Jassim M. "Integrating MEA Regeneration with CO_2 Compression and Peaking to Reduce CO_2 Capture Costs." Final Report for Trimeric Corp. (Subcontract of DOE Contract DE-FG02-04ER84111). June, 2005.

Rocha JA, Bravo JL, Fair JR. "Distillation Columns Containing Structured Packings: A Comprehensive Model for Their Performance. 1. Hydraulic Models." *Ind. Eng.Chem. Res.* 1993;32(4):641-651.

Rocha, JA, Bravo JL, Fair JR. "Distillation Columns Containing Structured Packings: A Comprehensive Model for Their Performance. 2. Mass-Transfer Models." *Ind. Eng. Chem. Res.* 1996; 35:1660.

Sahay BN, Sharma MM. "Effective interfacial area and liquid and gas side mass transfer coefficients in a packed column." *Chemical Engineering Science.* 1973;28:41-47.

Sharma MM, Danckwerts PV. "Chemical methods of measuring interfacial area and mass transfer coefficients in two-fluid systems." *British Chemical Engineering.* 1970;15(4): 522-528.

Sherwood, TK. et al., *Mass transfer*. McGraw-Hill, New York, 1975.

Shi MG, Mersmann A. "Effective Interfacial Area in Packed Columns." *Ger. Chem. Eng.*1985;8:87-96.

Song D, Seibert AF, Rochelle GT. "Effect of liquid viscosity on the liquid phase mass transfer coefficient of packing. " Energy Procedia.

Tsai R., Schultheiss P., et al. “Influence of Surface Tension on Effective Packing Area”. Ind. Eng. Chem. Res. 2008;47:1253-1260.

Tsai R. "Mass Transfer Area of Structured Packing". The University of Texas at Austin. Ph.D Dissertation. 2010.

Yaici W., Laurent A. "Determination of gas-side mass transfer coefficients in trickle-bed reactors in the presence of an aqueous or an organic liquid phase." International Chemical Engineering. 1988;28(2):299-305.

Wang C et al. "Packing characterization: Mass Transfer Properties. " *Energy Procedia.* 2012;23: 23-32.

Wang C et al. "Characterization of novel structured packing for CO2 capture." *Energy Procedia.* 2013;37: 2145-2153.

Xu Q. "Total pressure and CO_2 solubility at high temperature in aqueous amines." *Energy Procedia*. 2011;4: 117-124.

Vita

Chao Wang was born in Jiangxi, China in 1985 to Xiaozhou Wang and Ling Wang. He graduated from Ganzhou No.3 Middle School in 2002, and attended Tianjin University, PR China from 2002 to 2008. He earned a B.S. in Chemical Engineering in 2006 and M.S. in Chemical Engineering in 2008. While at Tianjin University, he worked in the Distillation Center laboratory of Dr. Peng Bai for his master thesis. After graduation he enrolled in Chemical Engineering program at The University of Texas at Austin, where he worked for Dr. Gary T. Rochelle and Dr. Frank Seibert.

Permanent e-mail: chaowang24@gmail.com

This dissertation was typed by the author.